

# **Fundamental Design and Application of an Acoustic Temperature Measurement System**

**Stephen Ireland**



**Department of Chemical and Process Engineering**

**1996-2002**

**University of Sheffield**

# **Fundamental Design and Application of an Acoustic Temperature Measurement System**

Stephen Ireland

## **Summary**

Temperature measurement is critical in virtually every industrial heating application in terms of product quality, process efficiency and environmental emission control. Acoustic pyrometry is a non-contact measurement technique based on the well-known compressible flow relationship between the speed of an isentropic sound wave in a gas and its internal temperature. The objective of the work was to investigate the fundamental components of an acoustic pyrometer both experimentally and through numerical analysis with the aim of designing, testing and commissioning a ruggedised version and applying it to a combustion system.

A key issue that the study addressed was the performance of the technique in the presence of invasive combustion and background noise levels present at most industrial plant. The noise levels were recorded at various kilns and furnaces in order that a measurement strategy was identified. A factor, which had also not been fully quantified to date, was the absolute accuracy of the acoustic technique given a typical combustion application where the exact gas composition along the line of flight is unknown. A comprehensive analysis indicated that the acoustic constant has a strong dependence on temperature but this can easily be taken account of in the measurement by using correction factors.

A number of transmitted acoustic signal types and processing methods were examined and the error associated with each technique quantified. Transmitted signals included pulses, pure frequencies, chirps, and pseudo random binary sequences (prbs), while processing involved edge detection and correlation. The operation of an instrument based on a prbs transmitted signal is described and test results under controlled noise conditions are presented. These confirm the value of the strategy and demonstrate that measurements can be made with signal to noise amplitude ratios down to 0.5.

# Table of Contents

Table of Contents .....	i
Index of Figures .....	iii
Index of Tables.....	vi
Nomenclature .....	vii
Summary .....	ix
<b>Chapter 1 .....</b>	<b>10</b>
Project Aims and Objectives .....	10
1.1 Aim of Project .....	10
1.2 Objectives .....	10
<b>Chapter 2 .....</b>	<b>13</b>
Literature Review .....	13
2.1 Introduction to Temperature Measurement.....	13
2.2 Current Measurement Techniques .....	13
2.3 Introduction to Acoustic Pyrometry .....	21
2.4 Conclusions.....	23
<b>Chapter 3 .....</b>	<b>25</b>
Fundamental Design Theory .....	25
3.1 Introduction to Acoustics .....	25
3.2 General Design Theory .....	29
3.3 Velocity of Sound in a Gas .....	30
<b>Chapter 4 .....</b>	<b>33</b>
Fundamental System Design .....	33
4.1 Introduction.....	33
4.2 System Design.....	33
4.2.3 Noise Generation.....	40
4.2.4 Signal Injection .....	41
4.2.5 System Protection .....	42
4.2.6 Receiver Properties .....	45
<b>Chapter 5 .....</b>	<b>49</b>
Investigation into system performance parameters .....	49
5.1 Introduction.....	49
5.2 Combustion noise.....	49
5.3 Filtering and noise elimination methods .....	57
5.4 Speed of sound .....	57
5.5 Particles in the gas.....	58
5.6 Gas composition.....	59
5.7 Gas velocity effects.....	64
5.8 Path Curvature.....	66
5.9 Temperature Gradients.....	67
5.10 Attenuation mechanisms .....	68
<b>Chapter 6 .....</b>	<b>78</b>
Signal Processing Methodology .....	78
6.1 Introduction.....	78
6.2 Signal Types.....	78
6.3 Signal Modulation.....	82
6.4 Signal Filtering.....	85

6.5 Software Design and Signal Processing Equipment .....	86
<b>Chapter 7 .....</b>	<b>92</b>
Signal Processing Performance Trials.....	92
7.1 Introduction.....	92
7.2 Calibration of the compression driver.....	93
7.3 Properties of the chirp signal.....	93
7.4 Properties of the PRBS signal .....	97
7.5 System resolution considerations.....	98
7.6 System performance in the presence of noise .....	99
7.7 Numerical investigation .....	104
<b>Chapter 8 .....</b>	<b>113</b>
Experimental Application.....	113
8.1 Introduction.....	113
8.2 Acoustic pyrometer performance trials .....	113
<b>Chapter 9 .....</b>	<b>120</b>
Discussion .....	120
<b>Chapter 10 .....</b>	<b>125</b>
Conclusions.....	125
<b>Chapter 11 .....</b>	<b>128</b>
Recommendations for Future Work.....	128
11.1 Reconstructing or Mapping a Temperature Field.....	128
11.1.2 Phase-Amplitude Imaging: Tomography .....	129
11.2 Emission Control: Volumetric Flow through a Stack .....	131
11.3 Gas Mixture Analysis.....	133
11.4 Application of PRN's with correlation to ultrasonic non-destructive testing.....	134
11.5 Specific Applications .....	134
<b>Figures .....</b>	<b>136</b>
<b>Publications and Presentations.....</b>	<b>214</b>
<b>References.....</b>	<b>215</b>
<b>Appendix</b>	

## Index of Figures

Figure 1: Schematic of system components .....	136
Figure 2: The Cavity Resonator .....	136
Figure 3: The Wedge Resonator.....	137
Figure 4: Diagram of the Hartmann generator (a) and principle of operation (b).....	137
Figure 5: Cross-sectional view of the 10kHz Hartmann Generator.....	138
Figure 6: Sound pressure level versus frequency response for a pressure of 6 bar applied to the 10kHz Hartmann generator ( $x=1m$ ).....	139
Figure 7: Output profile for a pressure of 6 bar applied to the 10kHz Hartmann generator with cavity movement relative to the generated instability zone ( $x=5m$ ) .....	140
Figure 8: Output profile for a pressure of 6 bar applied to the 40kHz Hartmann generator with various nozzle positions relative to the instability zone.....	141
Figure 9: Variation in response time of the 10kHz Hartmann generator (including solenoid response = 0.010 to 0.015 sec.).....	142
Figure 10: Raw output profiles of pink and white noise generated by the IVIE signal generator.....	143
Figure 11: Plot indicating the effects of sound pipe injection on the transmitted signal under anechoic conditions.....	144
Figure 12: Theoretical sound power loss versus differing sectional thickness calculated for several membrane materials .....	145
Figure 13: Theoretical sound power loss versus applied frequency calculated for several materials... 146	146
Figure 14: Theoretical and experimental sound transmission performance curves for various thickness of nylon nitrile membrane.....	147
Figure 15: Plot showing the response profile of the Bruel and Kjaer type 4166 microphone to a calibrated pistonphone output. ....	148
Figure 16: Combustion and background noise levels at various furnaces and kilns .....	149
Figure 17: Signal to Noise Ratio (SNR) versus frequency relationship for various furnaces and kilns150	150
Figure 18: Attenuation versus frequency relationship for various furnaces and kilns.....	151
Figure 19: The dependence of the acoustic constant on temperature for the products of complete combustion of methane in air for varying exhaust excess oxygen concentrations.....	152
Figure 20: The systematic error in the measurement of temperature in combustion products resulting from an unknown combustion mixture ratio between 0 and 12% $O_2$ vol. dry as a function of fuel molar h/c ratio with air as oxidant. ....	153
Figure 21: The systematic error in the measurement of temperature in methane combustion products resulting from an unknown combustion mixture ratio between 0 and 12% $O_2$ vol. dry as a function of oxidant composition .....	154
Figure 22: Schematic of acoustic flow measurement technique.....	155
Figure 23: Schematic diagram indicating possible transmission paths. ....	155
Figure 24: Positional considerations for two transceivers due to the influence of exhaust gas velocity at high temperature (1273K).....	156
Figure 25: Sound absorption in carbon dioxide at N.T.P. ....	157

Figure 26: Molecular absorption in pure CO<sub>2</sub> at various temperatures against signal frequency, with 4<sup>th</sup> order polynomial curve fits ..... 158

Figure 27: Plot of relaxation time against temperature for pure CO<sub>2</sub> with 2<sup>nd</sup> order power law curve fit ..... 159

Figure 28: Plot of the ratio of external to internal specific heat contributions for CO<sub>2</sub> at several temperatures with 2<sup>nd</sup> order logarithmic curve fit ..... 160

Figure 29: Derived absorption coefficient versus temperature curves for CO<sub>2</sub> at various frequencies 161

Figure 30: Calculated sound absorption levels due to molecular relaxation in CO<sub>2</sub> for a limited range of temperatures and various frequencies ..... 162

Figure 31: Calculated sound absorption for furnace \ kiln levels of CO<sub>2</sub> for a limited range of temperatures and various frequencies ..... 163

Figure 32: Unit Pulse Function,  $\Pi(t)$ ..... 164

Figure 33: Unit Triangle Function,  $\Lambda(t)$  ..... 164

Figure 34: Sinusoidal function,  $f(t)$  ..... 164

Figure 35: Shift register circuit for a 15 digit sequence ..... 165

Figure 36(a,b):Difference in phase of the sinusoidal signal at the receiver for two different temperatures ..... 165

Figure 37: Schematic of acoustic pyrometer test equipment..... 166

Figure 38: Compression driver frequency response profile to a calibrated white noise input signal measured at a standard separation distance of 1m under anechoic conditions..... 167

Figure 39: Variation in sound pressure level with directional variation of the transmitter relative to the receiver microphone..... 168

Figure 40: Calibrated pink and white direct input signals including the effects of the band pass filter 169

Figure 41: Compression driver frequency response profile to a calibrated white noise input signal measured at a standard separation distance of 1m under anechoic conditions including the band pass filter ..... 170

Figure 42: Constant frequency burst signal (a) & chirp signal (b). ..... 171

Figure 43: 1000 Hz(a) and 2000 Hz(b) range performance..... 172

Figure 44: Raw transmitted and received data. .... 173

Figure 45: Correlation curve with performance markers to gauge correlation level and ratio values.. 174

Figure 46: Correlation level performance for a constant duration chirp signal transmitted over a separation distance of 5.5m..... 175

Figure 47: Variation in correlation performance with change in chirp duration and frequency range. 176

Figure 48: Nylon nitrile membrane attenuation characteristics..... 177

Figure 49: PRBS profiles (upper signal) including clock frequency (lower signal)..... 178

Figure 50: Raw transmitted PRBS signal..... 179

Figure 51: PRBS correlation profile..... 180

Figure 52: Correlation function of a PRBS signal of period  $N\Delta t$ ..... 181

Figure 53:Sampling considerations for a 15 bit PRBS..... 182

Figure 54: Effect of reducing the PRBS period on the correlation profile. .... 183

Figure 55: Chirp correlation profile for low noise conditions. .... 184

Figure 56: Chirp correlation profiles of two signals under similar conditions. .... 185

Figure 57: Chirp correlation profiles for increasing noise levels. .... 186

Figure 58: PRBS correlation profiles for various levels of SNR..... 187

Figure 59(a,b): Oscilloscope traces of modulated and demodulated signals..... 188

Figure 60: a) FM signal in low noise & b) FM signal degradation for increasing noise ..... 189

Figure 61: Received chirp signal profiles in the presence of increasing noise levels..... 191

Figure 62: PRBS received signal profiles in the presence of increasing noise levels..... 193

Figure 63: Plot of the modulated signal at the amplifier output at maximum gain (zero modulation). 194

Figure 64: Plot of the modulated signal at the amplifier output at reduced gain (zero modulation) .... 195

Figure 65: Plot of the modulated signal at the amplifier output at maximum gain (zero modulation) with filter..... 196

Figure 66: Direct input raw PRBS input signal with demodulated output signal (low clock frequency) ..... 197

Figure 67: Direct input raw PRBS input signal with demodulated output signal to indicate circuit delay (low clock frequency) ..... 198

Figure 68: Direct input raw PRBS input signal with demodulated output signal (high clock frequency) ..... 199

Figure 69: Single shock pulse embedded in acoustic noise..... 200

Figure 70: Noise free correlation functions of transmitted signals of 3ms duration and sampled at 150 points: (a) single sequence 15 bit PRBS, (b) chirp function with frequency from 4 to 6 kHz. .... 201

Figure 71: Model used to estimate variance of the measured transit time due to background noise using the correlation method. .... 202

Figure 72: The relative performance error for edge, chirp and PRBS as function of noise/signal amplitude..... 203

Figure 73: Average combustion and background noise levels for the combustion of 1.0 kg/s propane at the fire rig test facility..... 204

Figure 74: Chirp flight time and correlation values measured at the exit of the compartment fire rig with combustion of 0.1kg/s propane (x=3.465m) ..... 205

Figure 75: Successful chirp correlation profile recorded at the exit of the compartment fire rig with combustion of 0.1kg/s propane (x=3.465m) ..... 206

Figure 76: Failure mode chirp correlation profile recorded at the exit of the compartment fire rig with combustion of 0.1kg/s propane (x=3.465m) ..... 207

Figure 77: Raw input and demodulated output PRBS signals for ambient conditions (x=3.027m)..... 208

Figure 78: Raw modulated output PRBS signal for ambient conditions at a separation distance of 3.14m ..... 209

Figure 79: Correlation profile of raw modulated input and raw modulated output PRBS signals under ambient conditions (x=3.027m) ..... 210

Figure 80: modulated PRBS output signal for combustion of 0.03kg/s mass flow rate of propane at a separation distance of 3.14m..... 211

Figure 81: Temperature measurements produced by thermocouples located at the compartment fire rig upper exit ..... 212

Figure 82: Stack gas velocity measurement system. .... 213

## **Index of Tables**

Table 1: Hartmann Generator Design Parameters .....	37
Table 2: Sound power loss calculations for various thicknesses of aluminium membrane. ....	44
Table 3: Sound power loss calculated values for various signal frequencies. ....	45
Table 4: Ultimate analysis of typical Sheffield municipal waste. ....	61
Table 5: Experimental results from Shields .....	72
Table 6: Approximate curve fits.....	73
Table 7: Relaxation times for several temperatures .....	73
Table 8: Energy contributions at various temperatures. ....	75
Table 9: Pseudo-Random Binary Sequences.....	81
Table 10: Properties of the experimental acoustic pyrometer system .....	91
Table 11: Effects of near-field disruption on correlation levels. ....	96
Table 12: Summary of model conditions for edge, chirp and PRBS signal processing .....	110

# Nomenclature

$A$	(-)	amplitude
$a$	m/s	adiabatic speed of sound
$a_1$	m	distance to the first interval of instability
$a_2$	m	end of the first interval of instability
$c$	m/s	velocity of sound
$C_e$	kJ/kg.K	external energy level specific heat contribution
$C_i$	kJ/kg.K	internal energy level specific heat contribution
$C_p$	kJ/kg.K	specific heat at constant pressure
$C_v$	kJ/kg.K	specific heat at constant volume
$C_w$	kJ/kg.K	dynamic specific heat
$d$	m	diameter
$d_{jet}$	m	diameter of a fluid jet
$d_{cavity}$	m	diameter of a cavity
$E$	J	energy
$f$	Hz	frequency
$f_m$	Hz	frequency of maximum absorption
$f_{rel}$	Hz	relaxation frequency
$I$	W/m <sup>2</sup>	sound intensity
$I_c$	W	power required to maintain a fluid jet
$I_o$	W	total radiation of acoustic power (total sound intensity)
$k$	kW/m <sup>2</sup> K <sup>4</sup>	Stefan-Boltzman constant
$l_{cavity}$	m	characteristic cavity length
$L_p$	dB	sound pressure level
$L_{p1}$	dB	received sound pressure level: cold transmission trial
$L_{p2}$	dB	received sound pressure level: combustion transmission trial
$L_{p3}$	dB	received sound pressure level: combustion \ background noise
$L_{pMAX}$	dB	maximum sound pressure level obtained
$L_w$	dB	sound power level at transmitter
$m(t)$		continuous time signal
$M$	Kg/kmol	molar mass
$p$	N/m <sup>2</sup>	pressure
$p_o$	N/m <sup>2</sup>	reference pressure level
$R, r$	J/kg.K	specific gas constant
$R_u$	kJ/kmol.K	universal gas constant (8.314 kJ/kmol.K)
$T$	K	temperature
$t$	s	time
$u$	m/s	RMS velocity
$\overline{U}_p$	m/s	average velocity over a path length
$v$	m/s	phase velocity
$v_o$	m/s	phase velocity for $\omega\tau \ll 1$ (i.e. $v_o = c$ )
$V$	V	voltage level (amplitude)
$\overline{V}$	m/s	average velocity
$W_o$	W	reference power level
$W$	W	source power
$x, r$	m	length, distance
$\tau$	s	relaxation time
$\alpha$	dB/m (or Nepers/m)	absorption coefficient of particle amplitude (NB: 1 Neper = 8.7 dB)
$\alpha_c$	dB/m	attenuation due to system components
$\alpha^*$	(-)	dimensionless absorption amplitude coefficient
$\gamma$	(-)	adiabatic index (ratio of specific heats)
$\theta$	deg.	angle

$\rho$	kg/m <sup>3</sup>	mass density
$\lambda$	m	wavelength
$\omega$	rad/s	angular (rotational) velocity
$\sigma$	(-)	Standard deviation
ACF		Auto-Correlation Function
AM		Amplitude Modulation
BG		Combustion\Background Noise Level
CARS		Coherent anti-Stokes spectroscopy (CARS)
CFD		Computer Fluid Dynamics
dB		Decibel
EMF		Electro-Magnetic Force
FDM		Frequency-Division Multiplexing
FEGT		Flue Exit Gas Temperature
FFT		Fast Fourier Transform
FM		Frequency Modulation
H/C		Hydrogen to Carbon ratio
HVB		High Velocity Burner
IR		Infra-Red
IRT		Infra-Red Thermocouple
LDV		Laser Doppler Velocimetry
NO <sub>x</sub>		Oxides of Nitrogen
NTP		Normal Temperature & Pressure
PAM		Pulse Amplitude Modulation
PM		Phase Modulation
PPM		Pulse Position Modulation
PRBS		Pseudo Random Binary Sequence
PWM		Pulse Width Modulation
QM		Quadrature Multiplexing
RMS		Root Mean Square
SN		Received, signal and combustion\background noise level
SNR		Signal to Noise Ratio
T/C		Thermocouple
TDM		Time Division Multiplexing
TOF		Time Of Flight (i.e. of transmitted signal)
UHC		Unburned Hydrocarbon
XM		Transmitted signal level 1 metre from the sound source

## Summary

Temperature measurement is critical in virtually every industrial heating application in terms of product quality, process efficiency and environmental emission control. Acoustic pyrometry is a non-contact measurement technique based on the well-known compressible flow relationship between the speed of an isentropic sound wave in a gas and its internal temperature. The objective of the work was to investigate the fundamental components of an acoustic pyrometer both experimentally and through numerical analysis with the aim of designing, testing and commissioning a ruggedised version and applying it to a combustion system.

A key issue that the study addressed was the performance of the technique in the presence of invasive combustion and background noise levels present at most industrial plant. The noise levels were recorded at various kilns and furnaces in order that a measurement strategy was identified. A factor, which had also not been fully quantified to date, was the absolute accuracy of the acoustic technique given a typical combustion application where the exact gas composition along the line of flight is unknown. A comprehensive analysis indicated that the acoustic constant has a strong dependence on temperature but this can easily be taken account of in the measurement by using correction factors.

A number of transmitted acoustic signal types and processing methods were examined and the error associated with each technique quantified. Transmitted signals included pulses, pure frequencies, chirps, and pseudo random binary sequences (PRBS), while processing involved edge detection and correlation. The operation of an instrument based on a PRBS transmitted signal is described and test results under both controlled and combustion plant noise conditions are presented. These confirm the value of the strategy and demonstrate that measurements can be made with signal to noise amplitude ratios down to 0.5.

# Chapter 1

## Project Aims and Objectives

### 1.1 Aim of Project

The aim of the project is to investigate the design and application of an acoustic temperature measuring system, utilising the relationship between the speed of sound in a gas and its internal temperature. The initial approach of the project is to be carried out at a fundamental level, producing a database of information to provide a solid foundation for continued research in this emerging and important area.

### 1.2 Objectives

- 1 To collect a number of samples of noise profiles from a wide variety of industrial combustion applications such as incinerators, kilns and furnaces to provide a valuable design tool for an acoustic temperature measuring system. The profiles should include the magnitude of sound levels measured and the corresponding frequency spectrum. The results should enable a optimum frequency “window” to be defined in an area of maximised signal to noise ratio for operation of an acoustic pyrometer system.
- 2 To investigate possible sound sources available that will provide sound transmission in conjunction with, and based on, the results of objective (1). The sound source (likely either to be electromagnetic or mechanical) must possess characteristics that enable it to operate in an industrial combustion plant environment and produce the required acoustical response, in terms of sound power level, frequency and repeatability. The characteristics of the sound source therefore must be carefully calibrated and monitored throughout the investigation.
- 3 Fundamental investigation will receive high priority in terms of the influence of :

- Sound transmission components: this includes such items as the sound-source and sound source housings and supporting equipment.
  - Sound receiving components: this includes such items as microphones and microphone housings and support equipment.
  - Introduction of the sound to the application environment: includes sound transmission piping characteristics as well as performance enhancing equipment such as acoustic horns.
  - Receiving the sound from the application environment: sound receiver transmission piping.
  - Protection of components from the application environment: the use of air-cooling or membrane protection of delicate electrical or mechanical components.
  - Identification and quantification of parameters affecting the sound under application conditions: characterisation of all processes present in the combustion environment or similar, which may lead to a reduction, degradation or performance loss of the transmitted sound signal.
  - Possible utilisation or control of echoes and reverberations: these may be present in the combustion environment and therefore an obstruction to the process, or be produced by the transmitted sound signal and therefore their presence may be controlled and possibly utilised.
  - Format of the sound signal used: with high specification signal generating software and hardware available, user defined signal formats can be designed to fulfil a desired application. Various different signal formats will be tested to identify those with transmission characteristics that match both the transmitter capabilities and the acoustic pyrometer performance.
  - Possible reduction methods of the influence of combustion and background noise: such as by the use of low, high or band pass filtering of the received signal.
4. To design, construct and test several transmitter units containing the different types of sound transmission identified in objective (2) both at a fundamental level,

objective (3), and on an industrial heat treatment facility to assess the possible performance available. One transmitter unit to be based on an ultrasonic mechanical generator using compressed air as an energy source.

5. Through the use of a software control program, assess the performance of various types of sound signal for an acoustic temperature measuring system under controlled conditions.
6. Apply the system to a high temperature facility to assess its performance and capabilities.
7. Apply the acoustic system to a pilot scale-soaking furnace for long term performance trials.
8. Investigate methods of reduction of measurement error by using signal processing techniques.
9. Modification of the software program to include “window time tracking” to reduce the possibility of correlating to an erroneous sound signal especially if a transceiver echo technique is used. This will also reduce computation time during operation.
10. Investigate the possible application of amplitude or frequency modulation in terms of protecting the sound signal from the effects of invasive noise present.
11. Carry out research into the possible validity and strategy for the design and application of tomographic signal processing techniques, and through this, the possibility of multiple senders and receivers creating multi-path analysis.

# Chapter 2

## Literature Review

### *2.1 Introduction to Temperature Measurement*

Temperature measurement is critical in virtually every industrial heating application in terms of product quality, process efficiency and environmental emission control. It is the most important parameter in terms of energy use, our most valuable commodity.

Energy in the form of power generation is based on the utilisation of coal, oil and gas. Due to the finite nature of these reserves and the increasing commitment to reducing emissions, the efficient use of and control of such processes has received much attention.

A primary cause of reduced process efficiency or reduction in product quality in high temperature applications is measurement error. Where gas temperature measurement is required this is of particular concern. The development of new sensors and sensing technology is seen as a key area in the Office of Science and Technology's Foresight Challenge document<sup>1</sup> and the sensing of temperature is no exception and requires high priority.

Important subjects of concern include continuous emission monitoring which has received much attention both in this country and abroad and improved methods of combustion and process control. Accurate temperature sensing techniques are vital to all these areas. However despite the importance on the various aspects of plant performance there are very few types of sensor available.

### *2.2 Current Measurement Techniques*

#### **2.2.1 Introduction**

The types<sup>2</sup> of temperature measurement systems available can effectively be divided into two areas, thermal contact and non-contact methods. The thermal contact category contains such devices as thermocouples and resistive temperature devices

(RTD's and thermistors), bimetallic devices, liquid expansion devices and change of state devices. The non-contact methods include radiation techniques such as radiation thermometers and infra-red imaging systems (optical pyrometers) such as infra-red spectroscopy.

### 2.2.2 Thermocouples

The application and use of thermocouples in industrial environments is well documented<sup>3,4</sup> as are the problems associated with them, namely convection, radiation and application error. A thermocouple uses an electromotive force (emf) generated between two thermo-elements that are in electrical contact to measure temperature. As the temperature increases, the output emf of the thermocouple rises, though not always linearly.

These elements are essentially two alloys joined together at one end and open at the other. At the output, (the end open to the measurement environment), the emf is a function of the temperature,  $T_1$  at the closed end. The open-end emf is a function of not only the closed-end temperature (i.e. the temperature at the point of measurement) but also the temperature at the open end  $T_2$ . Only by holding  $T_2$  at a standard temperature can the measured emf be considered a direct function of the change in  $T_1$ .

The industrially accepted standard for  $T_2$  is  $0^\circ\text{C}$ . Since  $T_2$  often varies, in industrial instrumentation the difference is usually corrected for electronically. This emf adjustment is referred to as the cold-junction adjustment. Often the thermocouple is located inside a metal or ceramic shield that protects it from harsh or corrosive environments. The materials used for the thermoelement define the type of thermocouple which are letter designated, B, S, R, N, K, T, J and E. For example type K has a chromel (Ni, Cr, Si) and an alumel (Ni, Si, Mn, Al) thermoelement. This is fairly commonly used and is often referred to as a "chromel-alumel" thermocouple. The equilibrium temperature of the hot junction of the thermocouple when inserted into a gas stream is a result of:

1. Heat transfer by convection between the thermocouple and the gas across a boundary layer,
2. Heat transfer by radiation,
3. Heat transfer by conduction along the thermocouple wires,

4. Transfer of kinetic energy of the gas to the thermal energy within the boundary layer.

Therefore in order to find the true temperature further refinements have to be made;

1. Apply a correction to the measured value by applying heat transfer correlations based on boundary layer theory such as for convective heat transfer. This may depend on the orientation of the probe, its physical shape, the gas flow characteristics (i.e. turbulent or laminar) and many more. Correction equations are also available for radiation effects, conduction effects and also the thermocouple response time,
2. Design the measurement system to minimise any possible errors i.e. size of the probe or insulation to reduce conduction error,
3. Use a suction pyrometer for which the temperature of the gas is measured under known conditions and a previously calibrated correction factor is applied to the measured temperature.

In its simplest form a concentric cylindrical radiation shield surrounds the suction pyrometer. Two simplifying assumptions are made;

1. The sheath and the radiation shield have the same emissivity characteristic as an oxidised metal surface,
2. The radiation shield is thin enough that conductive thermal resistance is negligible.

The combined elements of shield and sheath can be represented by a standard model of radiative heat transfer describing the relationship between the surfaces of concentric cylinders of the same axial length. From this the heat transfer from the sheath to the thermocouple and the radiation heat transfer from the shield to the walls may be derived and thus the temperature.

The suction pyrometer also uses “suction” to improve the convection heat transfer from the gas to the thermocouple, which also improves the measurement performance. Multiple shields and ceramic shields may also be used with increasing temperature to increase the performance. Even through these corrections and enhancements, thermocouples are still open to errors such as calibration drift, physical

failure (many applications require thermocouple replacement very regularly) and response errors that ensures that the true temperature of the gas remains out of reach.

### **2.2.3. RTD's and Thermistors**

Resistive temperature devices (RTDs) utilise the changes in electrical resistance of a material when introduced to temperature changes. RTDs rely on the resistance change in a metal with the resistance rising relatively linearly with temperature. A typical RTD consists of a fine platinum wire wrapped around a mandrel and covered with a protective coating normally glass or ceramic. The mean slope of the resistance versus temperature plot for an RTD is often referred to as the alpha value. The descriptor alpha stands for the temperature coefficient. The slope of the curve for a given sensor depends on the purity of the platinum in it.

Thermistors are based on the resistance change in a ceramic semiconductor. The resistance lowers non-linearly with temperature increase. This non-linearity poses a serious problem for engineers; however the thermistors are used in pairs in such a way that the non-linearities offset each other.

### **2.2.4 Bimetallic Devices**

Bimetallic devices utilise the difference in rate of expansion between different metals. When the two strips of metal are bonded together and heated, one side will expand more than the other. The resulting bending force is translated into a temperature reading by a mechanical coupling.

### **2.2.5 Fluid-Expansion Devices**

Fluid expansion devices come in two main classifications: the mercury type (widespread laboratory use) and the organic-liquid type. Versions employing gases (such as alcohol) are also available. Fluid-expansion devices do not require a power supply, do not pose explosion hazards and are stable after repeated use. However they do not generate data that is easily recorded or transmitted and cannot make point measurements.

### **2.2.6 Change of State Temperature Sensors**

These consist of labels, pellets, crayons, lacquers or liquid crystals whose appearance changes once a certain temperature is attained. Response time is often of the order of

several minutes or more, so these devices are restricted to non-transient changes. Except for the liquid-crystal technique the changes that occur are irreversible. Accuracy is also lower than other types of sensor. Main applications include confirmation that the temperature of a piece of equipment or material has not exceeded a certain level for technical or legal reasons, i.e. whilst in transit. For applications where a constant temperature profile is required the use of thermal paint can indicate the position of "hot spots" i.e. by conduction of the heat through a body shell or casing.

### **2.2.7 Radiation techniques**

Radiation techniques<sup>5</sup> include radiation thermometers and infrared (IR) imaging systems (optical pyrometers) like infra-red spectroscopy. Designs for an infrared thermometer (IRT), have existed since at least the late nineteenth century, and various concepts were featured by Charles Darling in his book "Pyrometry," published in 1911<sup>6</sup>. However it was not until the 1930's that the technology was available to turn these concepts into practical measuring instruments.

Most IRT sensors<sup>7</sup> operate with electromagnetic radiation whose wavelength is in the visible and infrared portions of the spectrum. Physical bodies (solids, liquids and gases) may emit electromagnetic radiation for a number of reasons. For sensing temperature, only radiation that is produced solely by temperature is required. The methods<sup>8</sup> use the measurement of emission<sup>9</sup> or absorption of radiation from the gas in comparison with a calibrated black body source to define the temperature.

A most basic design consists of a lens to focus the infrared (IR) energy on to a detector, which converts the energy to an electrical signal that can be displayed in units of temperature after being compensated for ambient temperature variation. This configuration facilitates temperature measurement from a distance without contact with the object to be measured.

In this way, the infrared thermometer is useful for measuring temperature under circumstances where thermocouples or other probe type sensors cannot be used or do not produce accurate data for a variety of reasons. Some typical circumstances are where the object to be measured is moving; where the object is surrounded by an EM field, as in induction heating; where the object is contained in a vacuum or other controlled atmosphere; or in applications where a fast response is required.

The measurement technique relies on a calibrated “black body”, which approximates an ideal thermal radiator. The body would absorb completely any radiation falling on it and for a given temperature, emit the maximum amount of thermal radiation possible. While the concept of a “black body” is abstract, physical bodies can be constructed to approximate closely blackbody behavior. Such radiation sources are needed for calibration of radiation thermometers and generally take the form of a blackened conical cavity of about 15 degree cone angle. The temperature is adjustable, automatically controlled to be constant, and measured accurately by a device such as a platinum resistance thermometer.

While it is possible to construct a nearly perfect “black body”, the body whose temperatures are to be measured with some radiation-type instrument often deviate from such ideal conditions. The deviation is expressed in terms of the emittance of the measured body. If a radiation thermometer has been calibrated against a “black body” source, knowledge of the appropriate emittance value allows correction of its readings for non-blackbody measurements.

Emittances are not simple material properties such as densities, but rather depend on size, shape, surface roughness, angle of viewing etc. This leads to uncertainties in the numerical values of emittances, which is one of the main problems associated with radiation temperature measurement.

A further source of error is the losses of energy in transmitting the radiation from the measured object to the radiation detector. Generally the optical path consists of some gas (i.e. atmospheric air) and various windows, lenses, or mirrors used to focus the radiation or protect sensitive elements from the environment. In atmospheric air the attenuation of radiation is due mainly to the resonance-absorption bands of water vapour, carbon dioxide and ozone, as well as the scattering effect of dust particles and water droplets. Since the absorption varies with wavelength, a radiation thermometer can be designed to respond within a certain frequency range or “window” making it insensitive to these effects.

The absorption also varies with thickness of the gas traversed by the radiation so the effect is not an instrument constant and thus cannot be calibrated out. IR instruments use lenses which must be made of special materials since normal glass is opaque to the required wavelengths utilised. The high levels of radiation present in many

furnaces often cause an overload to the spectroscopy system, this is quite a major obstacle to the technique.

### **2.2.8 Laser-Based Measurement Techniques**

Laser based temperature measurement systems have made significant progress but are still not available for practical use<sup>10</sup>. Instrumentation such as Laser Doppler Velocimetry (LDV)<sup>11</sup> and Coherent anti-Stokes spectroscopy (CARS)<sup>12</sup> have evolved from the specialised research laboratory into a practical engineering tool for combustion research. However due to its complex nature and required operational skills it has remained a research tool.

LDV tends to be restricted to measurements of particle size, flux, and concentration, as well as scalar-velocity correlations that have been used to produce small-scale temperature profiles of combustion applications. Probably the area that has been investigated most thoroughly by the CARS technique is laboratory scale flames based on temperature and species concentration measurements.

### **2.2.9 Fibre Optics**

The coupling of optical fibres to infrared detectors and signal processing electronics represents very recent progress in the field of non-contact temperature measurement and control. Fibre optics have become of widespread interest due to their ability to carry optical information signals over long distances and around obstacles with minimal attenuation.

As described in the section on radiation techniques, IR detectors are normally used in conjunction with conventional elements (lenses, mirrors and prisms). The method was excluded due to the opacity in the spectral region of the construction material (glass or plastic). Recent developments have led to the successful use of a silicon (glass) material; however plastic and glass are still available but normally for data transmission.

Most optical fibres produced consist of a light conducting core surrounded by a thin layer of glass cladding with a lower refractive index, to protect the core finish. All fibres used in IR instrumentation are made of glasses especially chosen for their ability to transmit the radiation comprised in the chosen spectral range. All rays entering the front surface that acquire an inclination smaller than the critical angle are

totally reflected inside the fibre core and keep propagating along the fibre length to the control system. The value of the critical angle is a function of the ratio between the refractive indices of the glass of which the core is made and the medium surrounding it.

The range of applications of this technique is extensive and includes monitoring of induction heating, continuous casting, metal die casting, flame cutting, flame hardening and control of metal-working lasers; the benefits in most cases are improved product quality and energy efficiency.

## **2.2.10 Discussion**

Each of the above temperature measuring devices has distinct advantages depending upon the application considered. For high temperatures and harsh conditions which would be encountered in a cement kiln or steel soaking furnace, RTDs although more stable than thermocouples, have a lower operating temperature range from -270 to 850°C and therefore must be rejected.

Thermistors have a more restrictive span, commonly from -40 to 150°C. Thermocouples on the other hand have a large temperature operating range of -270 to 2300°C. Disadvantages associated with thermocouples include relatively short life spans, calibration drift, slow response time and single point measurements.

IR methods, although relatively expensive, can be applied to higher temperatures, up to 3000°C, which exceed the range of any of the contact devices. However, strong emissions from the walls in a furnace environment often make the technique impossible to apply in such situations.

Laser-based and optical fibre technologies are making significant progress but as yet are not at a stage where they could be considered for industrial application.

**Acoustic pyrometry is a promising non-contact measurement technique that could address some of the problems associated with the current techniques especially for high temperature applications.**

## 2.3 Introduction to Acoustic Pyrometry

The idea of a temperature measurement system based on the speed of sound<sup>13</sup> was first outlined by Mayer<sup>14</sup> in 1873 but it was not until 1983 that it was put as a practical proposition by Green and Woodham<sup>15</sup> and also by Dadd<sup>16</sup>. The method is based on the well-known compressible flow relationship between the speed of an isentropic sound wave in a gas ( $a$ ) and its internal temperature ( $T$ ). The speed of sound is generally defined by equation (1.1):

$$a^2 = \left. \frac{\partial P}{\partial \rho} \right| \quad (1.1)$$

For an isentropic process, equation (1.2):

$$a = \left( \left. \frac{\partial P}{\partial \rho} \right|_s \right)^{1/2} = \left( \gamma \left. \frac{\partial P}{\partial \rho} \right|_T \right)^{1/2} = \left( \frac{\gamma P}{\rho} \right)^{1/2} \quad (1.2)$$

Using a perfect gas (pressure and density) relationship, equation (1.3):

$$a = (\gamma RT)^{1/2} \quad (1.3)$$

where  $\gamma$  is the ratio of specific heats of the gas mixture and  $R$  is the specific gas constant (kJ/kg.K). Through measurement of the time of flight ( $t$ ) of a sound wave over a known path length ( $x$ ) (i.e. from one side of the furnace to the other) the average gas temperature can be calculated, hence equation (1.4);

$$T = \frac{1}{\gamma R} \left( \frac{x}{t} \right)^2 \quad (1.4)$$

The technique has the following advantages:

1. It is a non-contact technique.
2. The measurement is an integral measurement across the line of flight, weighted slightly towards the cooler zones due to the non-linear relationship between speed of sound and temperature, equation (2).
3. The technique has the potential of excellent accuracy and resolution due to its dependence on the measurement of time.

4. Internal gas temperature is measured.

Even relatively simple microprocessors are able to measure time to accuracies better than  $\pm 1 \times 10^{-4}$  %. Referring to equation (1.4), this accuracy is translated directly to the measurement of temperature being doubled due to the squared dependence on time. Distance,  $x(m)$ , may also be measured very accurately (typically to within 0.5%). Calibration trials of the acoustic pyrometry system are also possible during plant shut down where gas composition and temperature are known.

Another advantage may be through the use of multiple paths by utilising multiple transmitters and receivers (or transceivers) to produce a reconstructed tomographic<sup>17</sup> 2D/3D measurement field.

An investigation by Green and Woodham<sup>15</sup> discussed the feasibility of acoustic pyrometry using high intensity spark gaps as acoustic sources and microphones as signal receivers. The arrival of an acoustic wave was measured using an oscilloscope. The oscilloscope X-axis sweep was triggered the instant an acoustic wave was generated and transmitted. The Y-axis was controlled by the received signal causing the waveform to also be captured on the screen. A visual inspection was used to determine when a given detection threshold or received signal level was reached and subsequently a time of flight for the acoustic wave was derived.

The detection point was not clearly defined and therefore the method could not be applied to continuous temperature measurement. The technique could not be automated and output information was not available in a useful format. Most current work has been produced by Kleppe et al.<sup>18</sup> and Nuspl et al.<sup>19</sup> who developed the method further to measure “furnace exit gas temperatures” (FEGT) in boilers during start-up, thus replacing conventional retractable thermoprobes. The system is also used when the boiler is on-line to measure temperature between the superheater banks and provides valuable real time furnace exit gas temperature data which, when utilised, can prevent tube fouling, furnace-wall slagging and secondary superheater slagging.

Modern digital signal processing techniques are utilised to significantly improve the system, resulting in a much simpler and safer configuration. Recently further acoustic systems<sup>20</sup> have entered the market primarily for use with cement kilns and in the incineration industries as well as in the combustion<sup>21</sup> and chemicals industry. The

success of these systems is still fairly limited due to the methods employed to overcome the noisy environments that they have to deal with.

To improve the technique a fundamental investigation is required into separating the sound signal from the combustion and background noise present in furnaces, kilns and incinerators. There is only a small amount of data available on noise levels<sup>22</sup> associated with furnaces, so a major issue is to build up a database of these measurements. The previous measurements carried out in the literature indicate that most of the combustion and background noise is limited to lower frequencies (< 2-3kHz) and therefore operating at a frequency above this zone has advantages in terms of signal discrimination. This requires the design and use of alternative sound sources, as well as looking at new types of sound signals and signal processing that may be available.

## *2.4 Conclusions*

The above review has highlighted many of the benefits of an acoustic temperature measurement system, the possible routes of investigation required for a design of such a system and included some of the problems that need to be overcome. The possible application of such a system is extremely wide, which necessitates the continued research carried out both in this investigation and by others.

Incineration of municipal and clinical waste has received much attention due to the location of incinerators and the content of the fuel. The temperatures associated with the burning waste on an incinerator grate are difficult to measure (mainly due to the uncertainty in the waste composition) and to date have been primarily measured using optical methods.

Several acoustic pyrometers, positioned just above the bed could produce important temperature data which, if linked to the control system could be utilised in, for example, the control of levels of primary air to the grate, thus ensuring complete combustion of the waste. This not only will produce important operating data for the operator but also will help ensure combustion efficiency and environmental targets are improved. Similarly, in industrial boilers and furnaces, benefits from the real time

response of such a system (e.g. in the control of levels of oxidant supplied to the fuel) could lead to significant cost savings.

Oxyfuels are utilised widely in the glass and ceramics industry with flame temperatures well exceeding 2000K, which is too high for invasive measurement techniques due to material restrictions. Acoustic pyrometry may prove useful in determining gas temperature data that is critical in deriving the heat transfer capabilities of the oxyfuel process. Hostile measurement conditions such, as those found in gas turbine combustors, (high pressures, temperatures and velocities) is another possible application area. A constant, controlled temperature profile at the combustor exhaust with minimised smoke and emissions is critical to commercial and military applications. Important validation data may also be provided for Computational Fluid Dynamic (CFD) modeling.

**The current work aims to overcome some of the inherent difficulties associated with the acoustic technique and establish the method as an accurate, non-contact, high temperature measurement procedure.**

# Chapter 3

## Fundamental Design Theory

### 3.1 Introduction to Acoustics

The most important properties of sound waves are the pressure variations which can be characterised in terms of size (amplitude) and the number of repetitions occurring in each second (frequency). Sound transmission begins with mechanical vibration of molecules next to a source. Each molecule is linked to an adjacent molecule by a complex array of forces. A vibrating object (e.g. loudspeaker diaphragm) causes adjacent molecules to vibrate and these movements are continued to successive molecules through to the receiver (e.g. microphone).

If the process is halted in successive time segments, it is evident that the molecules are compressed and then spread apart (rarefaction) along the propagation path. This is represented by a wave, with the pressure varying above and below atmospheric pressure. This range of response of the human ear to this variation in pressure is extremely large ( $2 \times 10^{-5} \text{ N/m}^2$  to  $100 \text{ N/m}^2$ ). Since the range is large, a more useable range has been defined which is a ratio based on the human threshold of hearing, called the Decibel (dB) range.

The energy content of a real acoustic pressure signal is related to the *Root Mean Square (RMS)* value of that signal resulting in, equation (3.1):

$$RMS = \sqrt{\frac{1}{t} \int_0^t p^2 dt} \quad (3.1)$$

The measurement type can define the duration of time, ( $t$ ) over which the above equation is integrated. There are standards available defining exponential and linear time weightings for different applications.

The passage of a sound wave is accompanied by a flow of sound energy. The power per unit area in the direction of travel is the intensity, ( $I$ ) equation (3.2):

$$I = up \cos \phi \quad (3.2)$$

Where  $u$  is the rms velocity,  $p$  = rms sound pressure and  $\phi$  is the phase difference between  $u$  and  $p$ . In a free field the rms velocity is related to the rms sound pressure by equation (3.3):

$$u = \frac{p}{\rho c} \quad (3.3)$$

Where  $\rho$  is the density ( $kg/m^3$ ) and  $c(m/s)$  is the speed of sound.

For a plane wave with  $p$  and  $u$  strictly in phase the  $\cos\phi = 1$  in equation (3.2). Substituting this result and equation (3.3) into (3.2) gives equation (3.4):

$$I = \frac{p^2}{\rho c} \quad (3.4)$$

In order to define the sound in terms of power, an imaginary sphere of radius,  $r$  surrounding a sound source in a free field, is defined. The area of a sphere is  $4\pi r^2$ , so the average sound intensity in the radial direction is provided by equation (3.5):

$$I_{av} = \frac{W}{4\pi r^2} \quad (3.5)$$

Similarly for an average squared sound pressure combining equations (3.4) and (3.5) produces equation (3.6):

$$I_{av} = \frac{W}{4\pi r^2} = \frac{p_{av}^2}{\rho c} \quad (3.6)$$

where  $I_{av}$  is the intensity ( $W/m^2$ ). The “sound power level ( $L_W$ )” produced by an acoustic source remains the same, whereas the “sound pressure level ( $L_p$ )” it creates varies, depending on the properties of the environment (i.e. acoustic impedance) it is passing through.

The sound pressure level, ( $L_p$ ) in decibels (dB), corresponding to a sound pressure,  $p$  is defined by equation (3.7):

$$L_p = 10 \log_{10} \left( \frac{p^2}{p_0^2} \right) = 20 \log_{10} \left( \frac{p}{p_0} \right) \quad (dB) \quad (3.7)$$

where  $p_0$  is  $2 \times 10^{-5}$  ( $N/m^2$ ).

Similarly for sound power level, ( $L_p$ ), equation (3.8):

$$L_w = 10 \log_{10} \left( \frac{W}{W_0} \right) \quad (dB) \quad (3.8)$$

where  $W_0 = 10^{-12}$  ( $W/m^2$ ).

To provide a relationship between sound pressure level, ( $L_p$ ) and sound power level, ( $L_w$ ), equations (3.6), (3.7) and (3.8) are combined to produce equation (3.9):

$$L_p = L_w - 20 \log_{10} \left( \frac{r}{r_0} \right) + 10 \log_{10} \left( \frac{\rho c}{407} \right) - 11 \quad (dB) \quad (3.9)$$

where the distance  $r$  is in metres and  $r_0$  is 1 metre. For calculations in air at normal temperature and pressure, the acoustic impedance,  $\rho c = 407$  ( $Ns/m^3$ ), hence equation (3.9) reduces to equation (3.10):

$$L_p = L_w - 20 \log_{10} r - 11 \quad (dB) \quad (3.10)$$

Equation (3.9) assumes a point source propagating noise over a spherical volume. For propagation over a hemispherical volume the area is halved from  $4\pi^2$  (sphere) to  $2\pi^2$  (hemisphere) in equation (3.5) and therefore equation (3.10) reduces by 3 dB to equation (3.11):

$$L_p = L_w - 20 \log_{10} r - 8 \quad (dB) \quad (3.11)$$

Most sound sources are located near a surface and hence the propagation is in the shape of a hemisphere, not a sphere. A similar expression to equation (3.11) can be derived for  $L_w$ . Generally in air at normal temperature and pressure, (NTP), the noise level decreases by 6 dB per doubling of distance. However in reality, sound loss (sound attenuation) is increased by many factors such as temperature, pressure, frequency, humidity and physical effects.

These particular expressions are highlighted since they are used in the investigation to indicate the performance of the system, i.e. the magnitude of background noise levels or the level of attenuation due to a specific mechanism.

The aim of the fundamental design work was to identify the elements required for an acoustic temperature measurement system and those parameters that would influence the performance of it.

The first elements required were a transmitter (source signal) and a receiver (signal recovery). The initial requirement of the transmitter was that it would have sufficient magnitude to overcome any combustion noise, background noise and attenuation associated with its industrial application. This required that the design of the transmitter go hand in hand with the investigation of the likely noise levels encountered in furnaces or kilns.

With these parameters identified the transmitter could be operated within an optimum frequency window where a high Signal to Noise Ratio (SNR) could be established i.e. the ratio of the transmitted signal to the combustion and background noise level is as high as possible. It was therefore necessary to measure the combustion and background noise at various furnaces and kilns. As discussed, the transmitter required a high sound power level not only to produce a high SNR but also to overcome transmission loss (sound attenuation) associated with the hot gas atmosphere and any other parameters which may have been of influence. Transmission tests were required to measure the SNR and sound attenuation levels.

The format of the transmitted signal was found to be an area of special interest and became an integral component of the design strategy. A study was carried out to produce a signal with properties that would allow accurate identification of the transmitted signal in the noisy environment with reducing SNR. A software control program was therefore required in order to achieve this.

Fundamental testing had to be carried out in a suitably controlled atmosphere. Therefore most of the initial work was carried out under anechoic conditions. This enabled detailed characterisation of the transmitter and receiver performance without the influence of invasive noise. Suitable measurement equipment had to be identified to ensure accurate and repeatable analysis of the required parameters.

## 3.2 General Design Theory

A general design structure was adopted in order to clarify the important constituent parameters involved in the acoustic pyrometer system.

1. Measurement of the invasive noise levels present including combustion noise and background (i.e. machinery) noise.
2. Measurement of signal performance during operation under controlled conditions.
3. Measurement of signal performance under full industrial operating conditions.
4. Identification and quantification of those parameters which influence system performance.

These performance criteria may be evaluated in terms of the attenuation of the transmitted signal over a separation distance (flight path length) and may include the effects of temperature, noise, system components etc.

In order to produce useful measurement data, the equations derived by Kleppe<sup>23</sup> were modified and used to describe the system transmission performance. The important parameters were defined as follows: -

- $L_{p1}$  = transmitted signal measured at a separation distance of 1 metre from the sound source.
- $L_{p2}$  = received signal (including combustion and background noise) measured at the receiver.
- $L_{p3}$  = combustion and background noise levels only

The attenuation level per metre,  $\alpha$  (dB/m) is a function of the furnace only and can be defined as the difference between the available received signal ( $L_{p2}$ ), with the background noise, ( $L_{p3}$ ) subtracted, and the transmitted signal, ( $L_{p1}$ ) recorded at the source. The difference represents the total attenuation of the transmitted signal. Division by the separation distance ( $x$ ) produces the signal attenuation per unit length, equation 3.13.

$$\alpha = \frac{L_{p1} - (L_{p2} - L_{p3})}{x} \quad (3.13)$$

If the magnitude of the received signal ( $L_{p2}$ ) is large compared with the background noise ( $L_{p3}$ ), (i.e. difference is greater than 10dB<sup>24</sup>), then the background noise can be assumed negligible and the attenuation is independent of the background noise.

The SNR can be defined in its simplest form as the transmitted signal at the source minus the background noise and attenuation over the path length, equation 3.14.

$$SNR = [L_{p1} - 20 \log(x) - 8] - \alpha - L_{p3} \quad (3.14)$$

The logarithmic term in the square brackets represents the general sound attenuation in air, for propagation over a hemispherical volume, for a separation distance (x). Where  $\alpha$  is the total attenuation, the logarithmic term is not required.

Care must be exercised when carrying out the calculations since the operations should be carried out where possible in terms of the 'raw' measured signals i.e. pressures if available and then converted into decibels for convenience. Where sound levels of similar magnitude are encountered, (i.e. background noise level,  $L_{p3}$ , is similar in magnitude to the received signal,  $L_{p2}$ ), special care should be taken when carrying out logarithmic operations.

The equations enable comparison between different measurements taken at the various furnaces and kilns. The attenuation indicates the level of sound transmission loss per metre over the entire path length. This value, therefore, includes all forms of sound loss such as attenuation mechanisms. The SNR indicates the level that the transmitted signal is above the combustion and background noise. Ideally, therefore, we would like to see low levels of sound attenuation and a high SNR.

### 3.3 Velocity of Sound in a Gas

The equation (1.4) relating the gas temperature to the speed of sound in a gas was derived based on the assumption that the pressure and density associated with a sound wave changes adiabatically (i.e. at constant entropy). No heat enters or leaves an element of fluid during its alternate warm and cold cycles. Using standard thermodynamic relations and assuming that the gas behaves like an ideal gas, the well known relationship for the velocity of sound in a gas is produced, equation (3.16):

$$c = \left( \frac{\gamma R_u T}{M} \right)^{1/2} \quad (m/s) \quad (3.16)$$

Where  $R_u$  is the universal gas constant and  $M$  is the molar mass (also called the molecular weight) of the gas. Two important factors must be considered if equation (3.16) is to be used as the basis of the acoustic temperature measurement concept.

The first is an area, which had not been fully explored to date, of the systematic error resulting from the unknown gas composition in a furnace. The critical property of the gas that must be considered is the product  $\gamma R$ , often referred to as the acoustic constant,  $C_a$ . This may be calculated for a gas mixture with knowledge of the volumetric fraction ( $\phi$ ), of the species present. In particular, equation (3.17):

$$\gamma_{mix} = \sum_{species\ i} \gamma_i \phi_i \quad R_{mix} = \sum_{species\ i} R_i \phi_i \quad (3.17)$$

The gas properties are solely functions of temperature<sup>25</sup>. The volume fractions of species present in the furnace depend on furnace equivalence ratio, air humidity and fuel and oxidant type.

In large-scale plant, the measurement of some exhaust components is common, for example excess  $O_2$  and  $CO_2$ . These may be used to infer the overall exhaust composition and, hence, an accurate evaluation of  $C_a$  is possible. There are many combustion applications where acoustic pyrometry is useful but in which there is limited knowledge of the exhaust composition. This may be due to lack of measurement (for example in smaller systems where feed forward control is used) or due to lack of information of fuel type (for example incineration systems with unknown waste composition). In this case, a value of  $C_a$  must be assumed and a systematic error is introduced. A detailed analysis of the chemical composition of the combustion products has been undertaken to quantify this error as a function of key furnace parameters.

The second important factor is related to the isentropic assumption in the derivation of equation (3.16). At higher frequencies, the density changes associated with the sound waves are too fast for equilibrium to be achieved. This leads to sound attenuation by a process termed molecular (or thermal) relaxation. This process is due to the unequal energy balance established between the external and internal degrees of freedom of

polyatomic molecules. This unequal energy state does not recover equilibrium due to the fast cycling time hence energy is lost. The relaxation process is highly complex and is not treated rigorously here. However some experimental and theoretical work was carried out to ascertain the effects of this valuable addition to the range of parameters associated with the acoustic pyrometer technique.

This section has introduced the subject of acoustics and the basic relations describing sound propagation in a gas. Further, the basic principles behind the fundamental design of a temperature measurement system utilising those relationships are given.

# Chapter 4

## Fundamental System Design

### *4.1 Introduction*

The stated objectives of this project were: to research, design and build a test rig to study the acoustic pyrometer concept in terms of the effects of sound frequency on the pyrometer performance; to assess the options available for noise reduction and to reduce the effect of reverberation and echoes; and to gather a database of information on plant background noise from a variety of industrial furnaces. To fulfill these objectives, an experimental system capable of sound generation, sound measurement and signal processing was required. The choices of components necessary for such a system are introduced as well as fundamental investigative work into their respective performance.

### *4.2 System Design*

A schematic of the basic components of a sound generation, measurement and processing system is shown on Figure 1.

#### **4.2.2 Transmitter design**

##### **4.2.2.1 Introduction**

Sound waves are generated by transducers, which transform electrical, mechanical or thermal energy into acoustic energy. There are several types<sup>26</sup> of transducer available falling into various categories;

1. Crystal oscillators which utilise the piezoelectric effect. This is a reversible transducer that can transform energy in both directions and has a wide frequency range. The piezoelectric effect occurs in crystals having non-axial symmetry. On subjecting a slab of the crystal to a mechanical stress, equal and opposite electric charges appear on the parallel surfaces. The magnitude of the electrical charge is directly proportional to the applied stress.

2. Electromagnetic transducers that include the widely used loudspeakers and microphones in the audio frequency range. These have the ability to provide high power but not at ultrasonic frequency levels, where the power is limited.
3. Magnetostrictive oscillators based on magnetostriction that occurs in ferromagnetic materials (nickel, iron and cobalt) and certain non-metals called ferrites. When the material is subjected to a magnetic field it experiences a change in length and hence, when a magnetic stress is applied to the material, this causes a change in the magnetic intensity. The oscillator may be used as a transmitter or receiver.
4. Mechanical Generators and Receivers such as whistles, sirens and cavity resonators.

Neither of the crystal or the magnetostrictive oscillators were considered for this particular application due to the low power levels and coupling difficulties associated with them.

#### **4.2.2.2 The compression driver**

Of the electromagnetic transducers available, compression drivers were selected for one of the acoustic pyrometer concepts. The compression drivers were used due to their excellent sound reproduction, resistance to fracturing due to fatigue, and freedom from distortion for a frequency range from 250Hz to 20kHz.

Two different sizes of compression driver were used during testing. The smaller driver offered 40 Watts nominal power handling through impedance of 8 ohms. The driver consisted of a titanium diaphragm allied to a lightweight polyimide former with a double layer, high temperature voice coil and driven by a large magnet system. A larger compression driver with a power rating of 300 Watts was also used for some trials. The larger compression driver had a mass of over 10kg and the smaller driver over 1 kg which had to be taken into account when designing the transmitter housing. They are also highly magnetic so a material such as aluminum must be used in housing constructions.

#### **4.2.2.3 Mechanical generators**

One aim of the project was to investigate operation of the acoustic system at ultrasonic frequencies, i.e. > 15 kHz, where combustion and background noise is significantly low. In this frequency region the power available from a compression

driver is reducing rapidly due to the relationship between its physical size and the frequency dependent power output.

The need to overcome the combustion and background noise was first attempted by using strong shocks, demonstrated for example in the work of Green and Woodham<sup>15</sup> and Stones and Webb<sup>27</sup> by use of spark discharge involving large capacitances. The energy levels produced by the discharges were in the range 140 – 400 J. These result in pulse pressure levels of 6 - 15 kN/m<sup>2</sup> (170dB) at the source, and therefore introduce corresponding deviations from Mach 1 operation of 6 - 15%. Whilst detection at such sound pressure levels against background noise becomes unambiguous, the error associated with the pressure dependent sound speed is difficult to quantify. The method was also difficult to reproduce constantly in terms of repeatability and accuracy. Therefore an ultrasonic mechanical generator was considered as a second concept to generate high sound power levels at high frequencies (10 kHz to 100 kHz) for this project.

Of the mechanical generators available in the literature, three are classified as ultrasonic whistles and the fourth is commonly known as the siren. The siren is capable of producing high power sound levels up to a frequency of about 30 kHz but requires a period of time to achieve this and is fairly complex in its construction. The ultrasonic whistles are much simpler in design and are capable of a greater range of ultrasonic frequencies.

The first type of whistle considered was the cavity resonator, Figure 2. This involves a high-pressure jet of fluid entering a cavity causing it to vibrate at its natural frequency. The frequency produced is a function of the physical characteristics of the cavity and the pressure of the jet. The maximum frequency obtainable with air is about 25 kHz though if a less dense fluid was used such as hydrogen the maximum frequency would be four times greater.

A wedge resonator, Figure 3, consisting of a solid plate with wedge-shaped edges is set into flexural vibrations when positioned in front of a supersonic jet. The wedge will resonate when one of its edges is positioned in an area of instability formed by the jet of fluid. The resonant frequency is a function of the material and physical properties of the wedge. Although high frequencies can be obtained, the power levels achieved are not large.

A vortex whistle<sup>28,29</sup> consists of a small cylindrical drum where air is introduced tangentially and follows a helical path through an adjoining tube of small diameter. Due to momentum conservation, there is an increase in rotational speed as the air passes from the larger to the smaller diameter and therefore an increase in frequency. This leads to sound wave propagation at the exit of the smaller tube, the frequency of which is a function of the applied air pressure. The sound power level and maximum frequency (15 kHz) obtainable is low.

The “Hartmann Generator<sup>30</sup>” was designed in 1927 by Hartmann and Trolle and is a whistle capable of high sound power levels at ultrasonic frequencies. The generator is similar in principle to the cavity resonator but produces higher power outputs and higher frequencies (>60kHz). The simple construction and operation of such a generator to produce a pre-determined frequency and the availability of compressed “shop” air at most plants established the Hartmann generator as the obvious candidate for an ultrasonic mechanical generator.

#### 4.2.2.4 The Hartmann Generator

The design work identified the possible use of a mechanical sound generator as well as a compression driver (loudspeaker) for the transmitter. The advantages of a mechanical generator are due to the removal of delicate electronic or mechanical parts often present in electromagnetic systems.

This therefore removes the necessity of protective membranes, or similar, which affect the magnitude of the transmitted signal. A mechanical generator is most commonly powered by air under pressure which can cause problems in some applications i.e. gas turbines where air to fuel ratio is critical. Several formats for a mechanical sound generator have been found in the literature but to meet the criteria of high sound power levels and the capability of producing ultrasonic frequencies, the Hartmann generator was identified as a suitable sound source.

Figure 4 shows a diagram of the Hartmann generator and the principle behind its operation. For the special case where the nozzle diameter equals the cavity diameter and the cavity depth, Hartmann derived the following, equation (4.1):

$$f = \frac{c}{4(l_{cav.} + 0.3d_{jet})} \quad (4.1)$$

where:  $d_{jet} = d_{cavity}$ ,  $f$  = frequency,  $c$  = sound velocity of the fluid. The nozzle is required to accelerate the fluid to supersonic flow, which requires in most cases a supply pressure minimum of 0.9 bar. Therefore, the frequency of the sound generated is a function of the dimensions of the jet and cavity and the power is a function of the pressure applied. Design calculations were carried out based on Hartmann's original analysis as shown on Table 1.

$N_{max}$ =	5000	10000	15000	20000	25000	30000	35000	40000	45000	50000	(Hz)
d	11.72	6.20	3.91	2.93	2.34	1.95	1.67	1.47	1.30	1.17	(mm)
R	20.0	20.0	20.0	20.0	20.0	20.0	20.0	20.0	20.0	20.0	(%)
p	3.13	3.13	3.13	3.13	3.13	3.13	3.13	3.13	3.13	3.13	(bar)
$a_1$	12.78	6.76	4.26	3.19	2.56	2.13	1.83	1.60	1.42	1.28	(mm)
$a_2$	18.59	9.84	6.20	4.65	3.72	3.10	2.66	2.32	2.07	1.86	(mm)
$I_0$	60.09	16.82	6.68	3.76	2.40	1.67	1.23	0.94	0.74	0.60	(kW)
$I_c$	1513.8	423.79	168.20	94.61	60.55	42.05	30.89	23.65	18.69	15.14	(kW)

**Table 1: Hartmann Generator Design Parameters**

Where:

$N_{max}$  = Maximum frequency obtained just inside the first interval of instability, (corresponding to the minimum wavelength).

d = Diameter of jet orifice = diameter of cavity = length of cavity

R = Percentage regulation.

p = Excess pressure

$a_1$  = Distance from nozzle to the entrance of the first interval of instability.

$a_2$  = Region of the first interval of instability. (interval of constant power)

$I_0$  = Total radiation of acoustic power

$I_c$  = Power required for the maintenance of the jet (theoretical)

Figure 5 shows a cross-sectional view of a Hartmann generator constructed to operate just below 10 kHz, a similar generator was also built to operate at 40 kHz. The diagram shows that the design allowed the cavity to be maneuvered into the zone of instability and hence produce the sound source at the required frequency. Tests were

carried out to establish the sound pressure levels available from the Hartmann generator. Initially compressed air was passed through 10mm diameter nylon piping through a water filter to the generator.

Figure 6 indicates the resulting sound pressure levels obtained against frequency. The results show a high sound pressure level of 131.42dB at approximately 8.7 kHz at a separation distance of 1 metre. This is a considerably higher sound pressure level than the levels possible with the compression drivers at this frequency as shown later in the report.

Figure 7 shows the effect of varying the position of the cavity in relation to the nozzle i.e. moving the cavity within the area of pressure instability defined by the parameters  $a_1$  and  $a_2$  in Table 1. The tests were carried out under anechoic conditions with both the generator and microphone receiver connected to 1 metre long, 3-inch diameter sound pipes. The sound pipes were connected using flanges to an anechoic chamber of length 5 metres. The results indicate that the Hartmann Generator may be activated over this region with little variation in frequency.

It is important to note that generators designed for higher frequencies have smaller instability zones. A 10 kHz generator has an instability zone of length 3 mm but for a 40 kHz generator the zone region reduces to 0.7 mm.

An investigation was also carried out to establish the effect of inlet pressure variation. The inlet pressure was increased from 3 to 6.4 bar. The results showed that 3 bar was sufficient to activate the generator producing high sound pressure levels. The increase in pressure from 3 to 6.4 bar led to a small increase in sound pressure level (approximately 6 dB).

A 40kHz Hartmann Generator was also constructed with the design specifications as outlined on Table 1 for a 40,000Hz generator. The diameter of the nozzle is considerably reduced (1.6mm) at this ultrasonic frequency and the length of the region of instability is also small (1.6 to 2.3mm).

Figure 8 shows a plot of amplitude versus frequency produced by the 40kHz Hartmann Generator and includes variation of the position of the cavity relative to the nozzle (i.e. movement of the cavity within the area of instability). A large variation in frequency and amplitude is indicated due to a small change in the position of the

cavity relative to the nozzle. The highest peak ( $\approx 30,000$  Hz) has a sound pressure level of approximately 90dB and it should be remembered that at these frequencies, the noise level in furnaces is low.

The results indicate the high sound pressure levels at high frequencies that the Hartmann Generator can produce. However, this is limited unless use can be made of its capabilities in the current investigation.

In order to obtain a time of flight measurement, we need to correlate between a point on the generated source signal at time=0 and the same point on the received signal at time=t(s). The most suitable point to do this is on the initial rise time of the signal, defined as when the signal reaches a certain magnitude above a reference level known as the threshold level. Therefore an investigation carried out to find characteristics of the Hartmann Generator, such as its response time, sharpness of initial rise time of the produced sound signal when the generator is operated, format of the signal and its repeatability. To operate the generator, a high-speed solenoid valve was required.

The response time of the valve had to be significantly faster than the response of the generator to avoid the activation time being characteristic of the solenoid, not the generator. Hence the activation time of the solenoid valve controlling the airflow to the generator had to be significantly faster than 10 kHz. A 10 kHz signal corresponds to a time period of 0.1 ms i.e. considerably quicker than any standard solenoid available. Specially designed, high-speed response, solenoid valves are available, but due to the expense, it was decided to use a standard solenoid for the initial trials. The solenoid used was an ASCO/JOUCAMATIC normally closed, direct operated valve for high-pressure fluids. The response time given by the manufacturers was between 5 and 25 ms (corresponding to 200 and 40 Hz respectively) depending on the orifice size chosen. A control unit was required, including a mechanical switch to energise the solenoid.

Initially a mechanical relay was used, but this had a response time of 10-15 ms and produced considerable noise fluctuation and hence was the likely limiting factor of the set-up. This was then replaced by a solid state relay with a quicker response time. This highlights the importance of the necessary evaluation steps required to find the limiting factor in the experimental set-up. A trigger from the computer was used to activate the solid state relay and hence energise the solenoid for a period of time that

could be user-defined. The solenoid when operated released a burst of air into the Hartmann Generator for a defined time period.

Figure 9 shows the variation in response time for a large number of activation trials. The response time varies from 0.022s (22ms) to 0.033s (33ms), a variation of about 10ms which is not constant. This variation is significant and poses a large drawback to the technique.

#### **4.2.2.5 Discussion**

The advantage of the Hartmann Generator is the extremely high sound pressure levels it achieves at ultrasonic frequency levels by a system that does not need protection from the furnace environment. It is clearly evident that the 40kHz Hartmann Generator can produce these high magnitudes in a frequency zone of very low noise levels. However, due to the limitations of the solenoid activation time compared with the characteristic frequency of the generator, the technique at this stage, cannot be applied to the acoustic temperature measuring method. However by utilising a different signal processing method, further progress may be made.

The compression driver is a low power, rugged device, with excellent sound response over a wide range of frequencies and is a suitable choice for the measurement system.

### ***4.2.3 Noise Generation***

#### **4.2.3.1 Pink and white noise**

In the analysis of sound, “harmonic” waves are often used, that is pressures which vary sinusoidally in both time and space. The variation in time leads to the concept of frequency ( $f$ ) and the variation in space is defined by the wavelength ( $\lambda$ ).

Sound in reality however is rarely monotonic; the sounds from a musical instrument consist of a fundamental frequency upon, which is superimposed, a series of higher harmonics having frequencies which are multiples of the base frequency. Noise from forms of machinery in an industrial workplace includes, sounds rich in higher harmonics and sounds without a harmonic connection. Other sound sources such as gas burners and jet engines, produce a total sound which contains a random and variable mixture of many frequencies. Such sounds are termed “noise.” If there is a uniform spread of sound energy over all frequencies, such noise is called “white

noise” (by analogy to white light). For all sounds other than those of extremely high intensity, the acoustic waveform is preserved as the wave spreads out.

It is therefore convenient to consider sounds as a superposition of harmonic components of different frequencies. An analysis in this way can be made by simple frequency filtering in narrow or broad bands. Broad octave bands are often used, however, much more accurately. A mathematical Fourier Analysis can be made which will rely on digital measurements and software in a computer. The octave band spectrum is found by summing the narrow band spectrum over intervals of one octave.

Further refinement can be achieved by dividing the band into smaller intervals such as thirds, eighths and twelfths etc. of an octave. Generating constant energy for each octave creates pink noise. The characteristic energy spectrum from a pink and white noise generator, Figure 10, provided a useful tool to establish the effects of the system components.

The generator used was an IVIE (Model IE-20B) portable pink and white noise generator, which through the use of digital techniques allow the generation of noise signals that are statistically well defined and very stable. Some of the features of the IE-20B sound generator are listed as follows:

- 10 Hz to 40 kHz 3 dB bandwidth,
- 20 Hz to 20 kHz  $\pm$  0.5 dB,
- Output level: Pink = 0 to 1.0 Volt RMS, White = 0 to 0.65 Volt RMS
- Output load: 600 Ohms or greater

One of the main features of the generator was the ability to step the output attenuator in 2 dB increments from 0 to -58 dB.

## ***4.2.4 Signal Injection***

### **4.2.4.1 Sound pipe effects**

In order to assess all the characteristics of the system, all components must be considered. Physical effects on the transmission that may be caused by the equipment,

such as the sound pipes used to inject the sound into, and receive from, the furnace, must be quantified. To achieve this, white noise was used by injecting it through the designed sound pipes in various configurations under anechoic conditions as shown in Figure 11. The configurations consisted of adding, removing and combining the transmitter and receiver sound pipes to isolate their effects on the sound transmission. The chamber was approximately 2.5m wide by 2.5m high and was 5m in length.

Two sets of sound pipes (receive and transmit) were produced of similar design but of differing section. One set was 3 inch B.S.P and the other 1 inch B.S.P., both sets with an angled bend of approximately 30 degrees. The reason for the bend was to avoid the driver or microphone looking directly at the furnace environment and hence in some cases, high levels of radiation. It is clear that the use of sound pipes has little affect on the sound signal in the range 1.0 to 3.0 kHz. However at frequencies above 3kHz variation in the signal magnitude is seen.

A picture of the transmitter, receiver and angled 1 inch BSP sound pipe attached to a mock furnace is shown in Appendix 3, Plate 1.

## ***4.2.5 System Protection***

### **4.2.5.1 The furnace environment and access considerations**

One aspect of the use of the sound pipes is protection of the delicate electronic components from radiation effects as well as the corrosive acid gases and water present in most industrial furnaces. Further protection will be required for a system that is in place over long periods thus requiring either an air purge system or the use of a protective membrane material. Purge systems are often rejected since they add excess air to the furnace or kiln. Therefore a membrane appears a better choice. The type of membrane material used must resist fairly high temperatures and corrosive gases over a reasonable operating period but allow passage of the required acoustic signal without high attenuation levels. Achieving an airtight seal around the membrane will ensure no air leakage that could cause significant damage via forced convection heat transfer processes.

#### 4.2.5.2 Membrane design theory

For a sound wave approaching a circular membrane, the level of transmission loss ( $\alpha_t$ ) is a function of the material and mechanical properties of the membrane as well as the medium properties either side of the membrane. The transmission loss<sup>26</sup> is given by equation (4.2), where  $l$  (m) is the thickness of the membrane material;

$$\alpha_t = \frac{4}{\left(4 \cos^2 k_m l\right) + \left(\frac{R_m}{R_a} + \frac{R_a}{R_m}\right)^2 \times \left(\sin^2 k_m l\right)} \quad (4.2)$$

$R_a$  and  $R_m$  are the acoustic impedance of the medium (air assumed) and the membrane respectively. The symbol  $k_m$  is the wave number for the membrane material and is given by equation (4.3a,b);

$$k_m = \frac{2\pi}{\lambda} \quad (m^{-1}) \quad (4.3a)$$

Where;

$$\lambda = \frac{c_m}{f} \quad (m) \quad (4.3b)$$

The speed of sound in a material is required to calculate the wave number as well as the acoustic impedance values for  $R_m$ . Assuming the main component of the sound wave through the membrane material is longitudinal, the speed of sound may be calculated from material property relations, equation (4.4);

$$c_m = \left[ \frac{K_m + \frac{4}{3}G_m}{\rho} \right]^{0.5} = \left[ \frac{Y_m(1 - \sigma_m)}{\rho(1 + \sigma_m)(1 - 2\sigma_m)} \right]^{0.5} \quad (4.4)$$

The parameter  $K$  = bulk modulus of elasticity ( $N/m^2$ ),  $E$  = Youngs modulus ( $N/m^2$ ),  $G$  = modulus of rigidity ( $N/m^2$ ) and  $\sigma$  = Poissons ratio. These values are readily available for a wide range of materials.<sup>31</sup>

The magnitude of sound power loss can then be calculated using equation (4.2), such that the power loss is found from equation (4.5):

$$L_{w,loss} = 10 \log(\alpha_t) \quad (dB) \quad (4.5)$$

### 4.2.5.3: Membrane performance

The following tables show typical calculated values for an aluminum membrane of various thicknesses, Table 2 and for various applied signal frequencies as shown on Table 3.

$l$	(mm)	1.00	0.50	0.25	0.10	0.05	0.01
$f$	(Hz)	10000	10000	10000	10000	10000	10000
$c$	(m/s)	6400	6400	6400	6400	6400	6400
$\lambda$	(m)	0.64	0.64	0.64	0.64	0.64	0.64
$k'$	( $m^{-1}$ )	9.81	9.81	9.81	9.81	9.81	9.81
$k'l$	(-)	0.00981	0.00491	0.00245	0.00098	0.00049	0.00010
$R_a$	( $kg/m^2s$ )	400	400	400	400	400	400
$R_m$	( $kg/m^2s$ )	17E+06	17E+06	17E+06	17E+06	17E+06	17E+06
$\alpha_1$	(-)	0.000023	0.000092	0.000368	0.002295	0.009116	0.186990
Loss	(dB)	-46.38	-40.36	-34.34	-26.39	-20.40	-7.28

**Table 2: Sound power loss calculations for various thicknesses of aluminium membrane.**

Figure 12 & Figure 13 indicate that the higher density solid materials tend to produce a higher sound power loss.

This is due to the higher acoustic impedance as well as the inelastic behaviour of these types of material. The material found to be most suitable in this case was a composite nylon nitrile rubber that combines good temperature and corrosion resistance with mechanical stiffness and availability in thin sections.

$f$	(Hz)	100	500	1000	5000	10000	50000
$l$	(mm)	0.5	0.5	0.5	0.5	0.5	0.5
$c$	(m/s)	6400	6400	6400	6400	6400	6400
$\lambda$	(m)	64.00	12.80	6.40	1.28	0.64	0.13
$k'$	( $m^{-1}$ )	0.098	0.491	0.981	4.906	9.813	49.063
$k'l$	(-)	0.00005	0.00025	0.00049	0.00245	0.00491	0.02453
$R_a$	( $kg/m^2s$ )	400	400	400	400	400	400
$R_m$	( $kg/m^2s$ )	17E+06	17E+06	17E+06	17E+06	17E+06	17E+06
$\alpha_t$	(-)	0.479164	0.035493	0.009116	0.000368	0.000092	0.000004
<i>Loss</i>	(dB)	-3.20	-14.50	-20.40	-34.34	-40.36	-54.34

**Table 3: Sound power loss calculated values for various signal frequencies.**

Figure 14 shows a plot of sound power loss versus frequency for various thickness of nylon nitrile membrane.

To validate the theoretical calculations, a sound signal of known power level was passed through the nylon nitrile membrane material and the sound power loss (attenuation level) was measured using a frequency analyser. Figure 14 indicates that the magnitude of the experimental transmission loss is in reasonable agreement with the theoretically calculated values. These are further validated using different signals later in the investigation. Note that the experimental curves include the compression driver output profile that accounts for the variation with frequency.

A picture showing nylon nitrile membranes that have been exposed to direct radiation is included in Appendix 3, Plate 2.

## 4.2.6 Receiver Properties

### 4.2.6.1 Introduction

To measure or analyse an acoustic waveform, it is usual to generate an electrical analogue of the pressure variation by means of a transducer. Transducers, which convert energy from one form to another, can be separated into two groups: input transducers or sensors (i.e. microphones) or output transducers (i.e. loudspeaker or

compression driver). There are three main types of microphone: capacitive, piezoelectric and electromagnetic. Capacitor microphones are the most common and are used for laboratory and industrial noise measurement and are an entirely suitable choice for this investigation.

The characteristics of the sound field to be measured are important when choosing the microphone. The high frequency response is influenced by the reflections and diffraction caused by its presence in the sound field, and to some extent, on the direction of the incident sound.

There are two main kinds of acoustic conditions: diffuse and free-field. We are primarily interested in free field where the sound comes predominantly from one direction, as opposed to diffuse, where the sound could come from any direction. A free-field microphone has a pressure/frequency response designed to give a flat response to the sound waves that would exist if the microphone were not present. (NB. A “pressure-field” microphone has a uniform response to the sound field as it exists, including all disturbances caused by the presence of the microphone). A microphone receives sound waves, converts the pressure variation into mechanical motion, and uses the motion to generate an electrical signal. A typical microphone can only extract a small amount of energy from the sound wave and even after amplification by a high-impedance amplifier, the peak voltage amplitude is of the order of a few volts.

Further considerations include the frequency content of the sound and its relation to the frequency response of the microphone. The sensitivity ( $S$ ) of a microphone is an important characteristic and in most cases a flat response is required over a large frequency range.

Once the electrical output has been obtained, it is necessary to carry out some form of analysis. In most cases this is in the form of spectral analysis in which the frequency content of the sound is calculated. Spectral analysis entails digitising the sound at regular intervals (thus producing a digital format for compatibility with computer hardware). Alternatively, analogue spectrum analysers are also used. These operate by measuring the energy transmitted by narrow band pass filters.

#### 4.2.6.2 Receiver instrumentation

Initial measurements were made with a Bruel and Kjaer type 4166 pressure-field, 0.5 inch microphone connected via a pre-amplifier to a sound frequency analyser provided by the Rutherford Laboratories<sup>32</sup> equipment pool.. The microphone provided measurement sensitivity of 50 mV/Pa over a frequency range of 2.6 Hz to 10 kHz. The Bruel and Kjaer type 2143 portable sound frequency analyser included the ability to carry out  $1/n$  octave analysis ( $n= 1, 3, 12, 24$ ) and real-time  $1/3$  octave operation. Up to 1000 spectra/second could be recorded and stored for further analysis. Due to its portable nature, this equipment was used for the combustion and background noise measurements at various industrial plants.

To enhance the laboratory measurements and to continue the remote experimental monitoring of combustion noise, further long term system components were required. An important addition was a Bruel and Kjaer “Nexus” signal conditioning amplifier to provide a versatile link between the transducer and the data acquisition system. This then allowed acquisition of the “raw” measured data from the microphone. Through use of an accurate digital gain control, the signal-conditioning amplifier could be used to vary the microphone sensitivity dependent on the amplitude of the incoming sound field.

The microphone was a Bruel and Kjaer type 4135 1/4-inch, free-field condenser cartridge with a sensitivity of 4 mV/Pa over a frequency range of 4 Hz to 100 kHz. This was connected to the conditioning amplifier via a Bruel and Kjaer “Falcon” range  $1/4$  inch microphone preamplifier type 2670. The system includes a Bruel and Kjaer charge injection calibration (CIC) technique that allows verification of the entire measurement set-up including the microphone, preamplifier and connecting cable. The output from the conditioning amplifier was fed to the data acquisition system which comprised of a computer and a Stanford Research Systems (SRS), Model SR760 FFT spectrum analyser. The spectrum analyser<sup>33</sup> is a useful device for computing the frequency spectrum of a time varying input signal. The operation of the analyser is based on Fourier’s basic theory that any waveform in the time domain can be represented by the weighted sum of pure sine waves of all frequencies. If the signal in the time domain is periodic, then its spectrum is likely to be dominated by a single frequency component. The spectrum analyser allows us to clearly represent the time domain signal by its component frequencies. Looking at noise analysis on an

oscilloscope would just produce a measurement of the total noise amplitude, whilst the spectrum analyser produces a measurement of noise as a function of its frequency components. The versatility of the spectrum analyser in terms of its speed of measurement, resolution and processing functions makes it an essential addition to the frequency domain analysis equipment.

#### **4.2.6.3 Receiver calibration**

Calibration is a necessary part of any process to ensure correct and accurate measurements are made, to verify the stability of the measurement equipment and to account for local measurement conditions. Calibration is carried out by using a Bruel and Kjaer piston-phone that produces a single tone at a prescribed amplitude.

Any variation in microphone performance from the calibration curves must be accounted for in any calculations. Figure 15 shows a plot of amplitude and sound pressure level versus frequency of the measured response of a type 4166 microphone. The single peak representing the calibrated piston-phone signal is clearly evident on the plot. Consideration has to be made of the ambient pressure variation and the influence of equipment such as signal attenuation in long cables. The copy of the calibration chart for the microphone is included in Appendix 1.

# Chapter 5

## Investigation into system performance parameters

### *5.1 Introduction*

In order to design a system based on the acoustic pyrometer concept it is essential to characterise all parameters and components associated with the technique in terms of their influence on performance. This then enables careful calibration of the system based on the contributions of each of the constituent elements, traceability of changes to performance levels and confidence in the reliability of results.

This section aims to investigate those parameters introduced by the environment in which the measurement technique is to be applied. The results from this section along with the fundamental design work on system components described in the previous chapter form an essential database of information for experimental design and application of the technique.

### *5.2 Combustion noise.*

#### **5.2.1 Introduction**

A crucial element in the implementation of a system utilising a transmitted signal into a noisy and attenuating environment is the ability to distinguish between the information bearing signal and the invasive noise present. The introduction of combustion to a flow field creates an increase in noise. Termed combustion noise (see comprehensive investigation by Bragg<sup>34</sup>), this may be a low frequency rumble or a resonating sound with a definite period.

The first, often defined as true noise, is produced by the random nature of turbulent combustion processes where the pressure fluctuations are quite irregular and un-repetitive. The latter, is the regular discrete-tone sound at a well defined frequency

produced by a periodic, combustion-driven oscillation<sup>35,36</sup> associated with rocket engines, tunnel burners and cyclic pulsation's in oil fired furnaces.

The levels of noise emission from turbulent flames, both premixed and of the diffusion type, increased through the use of compact, higher intensity burners, producing higher noise levels and unacceptable working conditions. Investigations<sup>37,38,39</sup> were carried out to find the effects of combustion on the noise levels which included limited experimental combustion noise measurements.

Gupta and Beer<sup>40</sup> investigated noise emissions from open turbulent methane-air diffusion flames. Peak noise levels in the range 250 Hz to 350 Hz were measured, of magnitude 75 dB to 90 dB depending on turbulence levels.

Green and Woodham<sup>41</sup> produced measurements for a pulverised coal furnace, using  $\frac{1}{3}$  octave analysis. Sound pressure levels on average of 95 dB at 300 Hz to 1000 Hz, reducing to 85 dB at 5000 Hz were presented. Reported attenuation levels for the coal furnace (on load) were 1 dB/m at 1000 Hz rising to 4 dB/m at 5000 Hz.

Kleppe et al.<sup>42</sup> reports similar attenuation levels for a frequency range of 500 Hz to 2500 Hz measured inside a 250 MW pulverised coal-fired utility boiler. Signal to noise ratio values are also given. Measurements of furnace noise were carried out by Young et al.<sup>43</sup> on a small gas fired furnace. The resulting frequency spectrum showed higher levels of noise at frequencies less than 2000 Hz.

More recently Ryzhov et al.<sup>44</sup> carried out measurements in furnaces and boilers of various capacities for a frequency range of 250 to 10,000 Hz. The result was that the noise levels were high in the range 1500 Hz to 6000 Hz but did not exceed 90 dB and tended to decrease at higher frequencies.

Further combustion noise measurements of a wider range of industrial plant such as incinerators and cement kilns as well as more resolute data on gas fired furnaces and boilers, is required for a more comprehensive database.

### **5.2.2 Combustion noise measurement technique.**

The preliminary combustion and background noise measurements were carried out using the Bruel and Kjaer, type 2143, portable sound frequency analyser with a type 4166, pressure field, 0.5 inch microphone. The microphone was mounted on one end

of a 1m long sound tube with 37° bend during each measurement period. The other end of the sound tube was fixed to an open inspection hatch. Each measurement consisted of recording the noise level with linear averaging over a period of time using different levels of octave analysis.

When operating a sound frequency analyser, increasing the frequency resolution by reducing the filter bandwidth (i.e. increasing from  $\frac{1}{3}$  octave analysis to  $\frac{1}{8}$  octave analysis) reduces the frequency measurement range. This can be addressed by making several measurement passes across the frequency range (i.e. 2 passes, measuring 50% of the frequencies on the first run and the other 50% on the second) but this is time consuming especially at higher frequencies. In most cases the measurement time was restricted due to the possibility of damage to the measurement equipment by “puffing” of hot gases from the furnace along the sound tube toward the microphone.

### **5.2.3 Sound transmission measurements**

In order to account for the absorption encountered along the path traveled by the transmitted signal, a set of further tests<sup>45</sup> was carried out in which a calibrated sound source was introduced into the furnace through a second inspection hatch opposite to the first.

Calibration of the sound source was carried out in order that the full characteristics of the transmitted signal would be known under controlled conditions. This ensured that under test conditions the effect of variation in the acoustic measurement technique such as operating at different frequencies, using alternative transducers or indeed the effect of the transmission medium could be characterised by comparison with the calibrated results. The sound sources and associated equipment were calibrated under anechoic conditions as well as a limited number of tests carried out in a cold ‘mock’ furnace constructed from plywood to evaluate the effect of reflections.

The aim of tests carried out under anechoic conditions was to quantify the response of the transducers and associated components such as sound pipes to a range of signals and conditions. The range of signals included single tone frequencies (square, triangle and sinusoidal signals) as well as multi-frequency chirp signals, pulses and prbs. The range of conditions looked at the effects of differently sized sound pipes, separation distance, transducer alignment, obstacles in the line of flight and controlled temperature changes on the transmitted signal under known conditions. By taking this

approach the performance characteristics of the transmitter and associated components were known and hence the effect associated with a change in operating regime of the acoustic technique under test conditions could be validated. The effects of components associated with the receiver were also characterised in this way.

The aim of tests carried out in the mock 'cold' furnace was to evaluate both the potential of utilising reflected signals for the acoustic technique as well as determining the effect of 'secondary' reflections of the transmitted signal on the accuracy of the acoustic technique. It was evident that 'rogue' reflections could lead to spurious results if care was not taken in ensuring that for example the correlation method carried out was achieved with the correct 'primary' transmitted signal.

Initial sound transmission trials used a compression driver generating a range of single tone frequencies from 1 kHz to 12 kHz through use of a frequency generator. Later trials used the compression driver driven by the pink and white noise generator as a calibrated sound source. Synchronously as the driver was transmitting the signal ( $Lp_1$ ) into the furnace, the receiver was recording the output ( $Lp_3$ ), which included the signal and combustion noise ( $Lp_1$  &  $Lp_3$ ). Hence from equation (3.13) and (3.14) the total attenuation ( $\alpha$ ) and SNR of the signal could be calculated respectively.

## 5.2.4 Experimental Method

### 5.2.4.1 Plant location and operating conditions

Test were carried out at several locations including:

- Cement kiln (Full scale plant trials)
- Municipal solid waste (MSW) incinerator (Full scale plant trials)
- Experimental soaking furnace (Pilot scale plant trials)
- 27 kW gas fired furnace (Laboratory scale trials)

### 5.2.4.2 Cement kiln trials

The experimental trials were carried on one of two 70 metre long rotating kilns used to heat raw meal principally consisting of limestone and shale. The process consists of the raw meal passing down a pre-heater tower where the powder is heated by warm kiln exhaust gases that rise up through the tower. The preheated raw meal then enters the high temperatures of the kiln, which is heated by a flame fuelled by pulverised coal. As the kiln slowly rotates, the raw meal moves down it to reach the 'burning

zone' where it is heated at up to 1,450 degrees Celsius. At this temperature the meal is converted to nodules of clinker.

The measurement of temperature in the 'burning zone' presents significant difficulties due to the hostile nature of the combustion process and the presence of high levels of particulate in the gases. However it is critical that the temperature is accurately measured in order to control the conversion of the meal into clinker with the correct material properties.

In order to carry out the trials a site induction was required and full personal protective equipment (PPE) was required. The trials were carried out at the end of one of the 70 metre kilns at close proximity to the coal burner and therefore within the burning zone. The plant was running at full rating and therefore calibration of the equipment at ambient temperature was not possible. The 3.5-inch BSP (with bend) sound pipes were attached to inspection hatches located either side of the kiln with a direct line of sight. The diameter of the kiln at the burning zone was approximately 2.8 metres. Care was taken during installation of the measurement equipment and during the actual measurements since intermittent 'puffing' of hot gases through the sound pipes occurred. Equally, the exterior surfaces of the kiln as well as the local surfaces and flooring were hot to the touch. Careful support of the equipment was necessary, as was protection from the high levels of dust present. As often as possible the receiver instrumentation was removed and the sound pipe sealed off with a 'blanked' flange in order to prevent damage to the receiver transducer.

The aim of the trials was to measure the combustion and background noise and to carry out sound transmission tests using a calibrated sound generator. Hence the tests carried out were as follows:

- Measure the background noise at the plant
- Measure the combustion noise produced in the burning zone (this measurement will therefore also include background noise).
- Carry out sound transmission tests at various frequencies to ascertain attenuation values and Signal to Noise Ratios.

During the tests the hostile nature of the process was experienced and the need for 'soot blowers' to remove the build-up of particles on transmitter and receiver surfaces was established.

A visit to the process central control room was also carried out in order to establish how an acoustic temperature measurement technique could be integrated with the kiln control strategy in order to improve the heating process.

(Trials courtesy of, **Blue Circle Cement**, Hope Works, Hope Valley, S33 6RP, U.K.)

#### **5.2.4.3 MSW Incinerator trials**

One of the principal difficulties associated with the incineration of MSW is due to the variable composition of the fuel. It is essential that during the incineration process that the waste is converted to a harmless product. This is most often achieved by thermal treatment using combustion techniques. The difficulty lies in supplying the correct amount of oxidant to the process to control the combustion and hence to minimise the release of any unwanted emissions.

Incineration was identified as a suitable application for the acoustic measurement technique since, for example, the transducers could be located above the moving refuse bed and by measurement of the gas temperature control the supply of primary (or underfire) or secondary air.

The tests were carried out on a fully operational MSW incinerator which generates 12.9 MW of electricity and supplies process heat to a local company. The plant consists of a set of moving grate beds where thermal treatment of the waste takes place. The transducers were located approximately two metres above the bed towards the top of the moving grate. The grate was angled downwards as is typical of most conventional roller type MSW incinerators.

Although the incinerator was operating at a negative pressure to minimise the release of odours, regular ‘puffing’ of hot products through the sound pipes was experienced. The 3.5-inch BSP pipes (with bend) were attached to inspection hatches on the furnace wall. The path length between transducers was approximately 5.7 metres including the length of the sound pipes. As with previous tests, characterisation of the combustion and background noise, and transmission measurements were carried out.

(Trials courtesy of **Coventry & Solihull Waste Disposal Co**, Bar Road, Whittle, Coventry, CV3 4AN, U.K. and **CODEL International Ltd**, Station Building, Station Road, Bakewell, Derbyshire DE45 1GE, U.K.)

#### 5.2.4.4 Pilot scale soaking furnace trials

The trials were carried out on a pilot scale 'soaking' furnace used to trial new burners for steel treatment processes. The furnace was approximately 5 metres long by 3 metres wide with 0.3 metre thickness refractory firebricks. Access to the furnace was by removal of the top section. A set of regenerative burners had been installed, one at either end of the furnace operating alternately with a cycle time of approximately 5 minutes. The burners used produced traditional diffusion flames during the heating cycle. This type of regenerative process is used where several tonnes of material need to be held at high temperature for many hours, in particular, in heat treatment furnaces in the steel industry. The regenerative burners fired alternately through a 4-inch quarl during the start up cycle until a temperature of 850<sup>0</sup> Celsius is reached. The burners operate at high velocities (~150m/s) during the start-up cycle, this has repercussions for the acoustic technique in terms of velocity gradient. When 850<sup>0</sup> Celsius is reached the control system switches to injecting pure gasoil through a set of 2-inch diameter ports located either side of the quarl.

There was a significant amount of instrumentation attached to the pilot scale furnace including thermocouples located on the refractory wall at positions along the length of the furnace as well as gas monitoring equipment for oxygen (O<sub>2</sub>) and carbon monoxide (CO). Further thermocouples were mounted inside steel billets that were located on the soaking furnace floor. Access to the furnace was available for the 1-inch BSP sound pipes (with bend) and these were located centrally along the furnace length and at a position of half the furnace height. Due to the experimental nature of the pilot scale soaking furnace, access was available to calibrate the acoustic technique at ambient conditions prior to combustion trials. The separation distance (path length) was calculated at 2.658m at NTP. The distance from the nearest installed thermocouple to the line of sight of the acoustic instrumentation was 0.245m.

Initial trials indicated that the bend in the sound pipe protected the instrumentation from radiation effects and therefore on the transmission side a membrane was not required. However for the purposes of protecting the delicate microphone components it was decided that a membrane should remain on the receiver side. As with the cement kiln, tests of combustion and background noise were carried out, as were sound transmission trials.

(Trials courtesy of Mr D. Hibberd & Mr J. Massingham of **CORUS** (Previously **British Steel**), Swinden Technology Centre, Moorgate, Rotherham, S60 3AR, U.K.)

#### **5.2.4.5 Natural Gas Fired Furnace Trials**

Tests were also carried out on a laboratory scale gas fired furnace. These tests were mainly to test the performance of the equipment since the path length was too short for analysis of the signal performance. However as with the other plant items combustion noise measurements and transmission tests were carried out. The furnace dimensions were approximately 1.5 metre in length and 1 metre diameter. The tests were carried out across the diameter of the furnace that also included a layer of refractory material.

It should be noted that all of the combustion noise and sound transmission measurements were carried out at the very early stages of the investigation prior to an appropriate acoustic signal type being identified for the acoustic technique.

### **5.2.5 Results and discussion**

Figure 16, shows a plot of combustion and background noise level, ( $L_p$ ) as a function of frequency ( $f$ ) for the various plants. It can be seen that each curve has distinct maxima and minima allowing selection of a frequency “window” of maximised SNR. In general, the highest levels of noise are located towards the lower frequency range (<4kHz).

The tests of background noise, however, do not provide sufficient information to determine the optimum frequency window. Figure 17 shows the generic relationship between SNR and frequency, which includes all absorption effects. In order to determine the SNR for a particular application, the characteristics of the transmission system alone need to be measured and imposed on the above data.

Figure 18 is a plot of attenuation per metre versus frequency calculated from the transmission tests. The level of attenuation can be seen to vary at each location. However the path length of the gas fired furnace is considerably shorter than either the municipal incinerator or the oil fired soaking furnace. It is evident from Figure 17 and Figure 18 that operating at higher frequencies where the noise levels are lower has potential benefits. The levels of attenuation at very high (ultrasonic) frequencies must be considered due to attenuation mechanisms described later in this section.

### ***5.3 Filtering and noise elimination methods***

When operating a system over a certain frequency range or “window”, it is often good practice to filter out invasive noise levels which fall outside that window to reduce their possible influence on the system performance.

One method of achieving this on the current system is to include a band pass filter between the receiver and the software. A band pass filter will only allow passage of the signal between a set of frequency bands. In this case the upper and lower limit of 1 kHz and 10 kHz respectively were chosen. However this bandwidth was variable. It was important however to ascertain any effects that the band pass filter introduces in terms of the calibration of the system.

Testing revealed that the filter caused a small time delay of 0.1 milli-seconds. This could cause a problem if, for example, the receiver is positioned near to an obstacle or physical dimension change (near to an area of “near field effects”) where the time delay is enough to cause the system to miss part of the signal. In the case of a chirp signal this may cause correlation to an erroneous secondary peak, missing the primary peak. The filter also causes a small reduction in the magnitude of signals included in the frequency band. However this value is small. The main concern when using a filter is its effects on signal properties such as phase. This may be more critical when modulation of the signal is required.

### ***5.4 Speed of sound***

The range of temperatures experienced in industrial furnaces is from 500K to at least 2000K. This corresponds to speed of sound magnitudes of approximately 450 m/s to 900 m/s respectively. The sound pulse flight time must be resolved to a fraction of one wavelength in order to obtain a practical temperature resolution and system accuracy.

The work of Kleppe<sup>18</sup> suggests an operating frequency range of 500 Hz to 2000 Hz, which corresponds to wavelengths of the order of 1 metre over the above temperature range. Due to the improved signal processing methodology, the current work aims to increase the operating frequency in the range 3000 Hz to 5000 Hz at least, working with wavelengths down to one tenth of a metre. Using sampling rates of 50000 Hz

and upward provides the resolution required for the lower wavelengths. The errors associated with high amplitude pulses exceeding Mach 1<sup>46</sup> can be neglected due to the lower amplitude signals used, as can the errors associated with variable directional speed propagation of a shock wave emerging from a tube into a much larger area Green and Woodham<sup>8</sup>.

## 5.5 Particles in the gas

The effects of particles in the gas stream are of particular importance for applications such as those associated with coal, oil or cement kilns. The effects may be characterised by the weight percentage of the particles. Wallis<sup>47</sup> gives an approximation for the change in speed of the sound pulse due to these particles, equation 5.1:

$$c = \sqrt{\frac{\gamma_p R_p T}{M}} \quad (5.1)$$

where,

$$R_p = R/(1+m_a) \text{ (kJ/kmol.K)}$$

$$R = \text{universal gas constant (kJ/kmol.K)}$$

$$m_a = \text{mass concentration of particles in the furnace (kg/kmol)}$$

$$T = \text{temperature, (K)}$$

$$M = \text{molecular weight of the gas (kg/kmol)}$$

and equation (5.2):

$$\gamma_p = \left( \gamma + \frac{C_a m_a}{C_v} \right) / \left( 1 + \frac{C_a m_a}{C_v} \right) \quad (5.2)$$

where  $C_a$  is the specific heat of the particles and  $C_v$  is the specific heat of the gas at constant volume. Assuming standard deviations of 20% in  $C_a$ ,  $m_a$  and  $C_v$  and noting that  $C_a$  is approximately equal to the specific heat at constant pressure of the gas, results in a standard deviation in  $R_p$  of about 0.2 percent. The standard deviation in  $\gamma_p$  is approximately equal to that in  $\gamma$ . The main source of error is likely to be  $m_a$

resulting in a maximum standard deviation of approximately 0.2% in  $R_p$ , i.e. the particles have a small effect.

## 5.6 Gas composition

### 5.6.1 Introduction

A factor which had not been fully quantified to date is the absolute accuracy of the measurement of temperature given a typical combustion application where the exact gas composition along the line of flight is unknown. Even relatively simple microprocessors are able to measure time to accuracy's better than  $\pm 1 \times 10^{-4}$  %.

Referring to Equation (1.4), this accuracy is translated directly to the measurement of temperature being doubled due to the squared dependence on time. Distance ( $x$ ), may also be measured very accurately (typically to within 0.5%). Calibration trials of the acoustic pyrometry system are also possible during plant shut down where gas composition and temperature are known.

However, an area which has not been fully explored to date is the systematic error resulting from the unknown gas composition in a furnace. The critical properties of the gas which must be considered is the product,  $\gamma R$ , often referred to as the acoustic constant  $C_a$ . This may be calculated for a gas mixture with knowledge of the volumetric fraction,  $\phi$  of the species present, equation (3.11).

The gas properties are solely functions of temperature<sup>48</sup>. The volume fractions of species present in the furnace depend on furnace equivalence ratio, air humidity and fuel and oxidant type. In large-scale plant the measurement of some exhaust components is common, for example, excess  $O_2$  and  $CO_2$ . These may be used to infer the overall exhaust composition and, hence, an accurate evaluation of  $C_a$  is possible.

However, there are many combustion applications where acoustic pyrometry is also useful but in which there is limited knowledge of the exhaust composition, either due to lack of measurement (for example in smaller systems where feed forward control is used) or due to lack of information of fuel type (for example incineration systems with unknown waste composition). In this case, a value of  $C_a$  must be assumed and a systematic error is introduced. A detailed analysis of the chemical composition of the

combustion products has been undertaken to quantify this error as a function of key furnace parameters. These are considered separately below.

### 5.6.2 Dependence on fuel type

In terms of chemical composition, one of the most useful parameters to distinguish fuels is the Hydrogen to Carbon molar ratio. Considering first methane, which has a H/C ratio of 4, shown in Figure 19 is the dependence of the acoustic constant on temperature and exhaust excess oxygen concentration, a standard measure of furnace mixture ratio.

Two important features emerge from this data: first, the relatively strong dependence of  $C_a$  with temperature and second, the weak dependence on exhaust excess oxygen.

The variation of the acoustic constant with temperature is of order 10% over the range of 300 - 2000 K and clearly compromises measurement accuracy. However, since it is temperature that is being measured, it is trivial to construct a corrected sound-speed vs. temperature relationship (cf. equation 1.4) to completely eliminate this error. A quadratic polynomial fit is sufficient to cover the full range above with an accuracy of better than  $\pm 3$  K. If a narrower range of temperatures is chosen, a linear fit is adequate.

The variation of the acoustic constant with mixture ratio, however, may not be taken into account in the absence of information on the gas mixture. For methane gas (Figure 20), it is found that the variation of  $C_a$  with mixture for a given temperature is extremely small over a very wide range of exhaust excess oxygen concentrations between 0 and 12%  $O_2$  vol.dry. In this case, it is limited to only  $\pm 0.6\%$  at 300K and  $\pm 0.3\%$  at 2000K. Thus, the effect of furnace mixture ratio may be completely ignored whilst still maintaining a temperature measurement accuracy of better than  $\pm 6$ K across the temperature range 300-2000K.

Further investigation reveals that this independence of  $C_a$  on furnace mixture is a function of the H/C molar ratio of the fuel. The presence of  $H_2O$  and  $CO_2$  in the products of combustion have opposing effects to lower or raise the value of  $C_a$  respectively. When both are present, as is normally the case, their effects tend to cancel each other out.

The overall effect is quantified in Figure 20, which illustrates the absolute error in the measurement of temperature associated with assuming no dependence of  $C_a$  on mixture ratio (for exhaust excess oxygen concentrations between 0 and 12%). The systematic error is limited to  $\pm 3\%$  at the extreme where the fuel contains little hydrogen, for example cokes, chars and anthracitic coals. For most fuels, however, the error is significantly less than this with a minimised error occurring when the H/C molar ratio is 2.7. This value is also influenced to some extent by the humidity in the air.

Another chemical species to have a major effect on the systematic error is the oxygen. This is found in coals, CO gas and wastes. The effect depends on the level of oxygen in the fuel and its H/C ratio but, in general, tends to increase the systematic error.

For bituminous coals, municipal and clinical wastes the systematic error remains less than  $\pm 1.7\%$ . For CO, however, there is a far stronger effect,  $\pm 10\%$ , making the technique unsuitable for this fuel without the additional measurement of mixture ratio. Other minor chemical species present in the fuel, such as sulphur or nitrogen have a very minimal effect on the error due to their low levels. For example, the effect of varying sulphur content in a No.6 heavy fuel oil from 0% to 3.5% by mass is in the third decimal place of percentage in increased error. The same may also be said for minor pollutant products in the exhaust such as CO, UHC's, and NOx.

The other important fuel parameter to play a part is moisture. This is normally only found in significant quantity in solid fuels and wastes. For example municipal and clinical wastes may have moisture contents of up to 30% by mass. In addition to this, water may also be injected into the incineration chamber to moderate temperatures in order to prevent glass fusion. Values as high as 0.7 kgH<sub>2</sub>O / kg waste are common in clinical incinerators.

Element	Percentage by weight (dry, ash free)
Carbon	51.5 %
Hydrogen	6.4 %
Oxygen	41.1 %

**Table 4: Ultimate analysis of typical Sheffield municipal waste.**

The effect of the moisture is to adjust the H/C ratio of the fuel towards larger values. This may be quantified exactly if the moisture content is known, but realistically where it is not, it acts to increase the uncertainty in the measurement of temperature. For a typical municipal waste, Table 4, if we assume no dependence of  $C_a$  on fuel moisture and mixture ratio, the resulting error in the temperature measurement is  $\pm 1.93\%$ . This is for moisture content between 0 and  $30\%_{\text{mass}}$  and mixture ratio between 0 and  $12\% \text{ O}_2 \text{ vol.dry}$ . This value must be compared with the value of  $\pm 1.19\%$  if moisture content is known.

### 5.6.3 Dependence on oxidant type

Current trends in the glass industry are towards using oxygen enrichment in burners to increase flame temperatures and heat transfer rates. The effect of oxygen concentration is therefore of relevance to the current study. The same analysis as above was undertaken to assess the degree to which  $C_a$  varies with mixture ratio for different oxidant compositions.

Again the range of excess oxygen concentrations considered was between 0 and  $12\% \text{ vol.dry}$ . The systematic error resulting from ignoring the mixture ratio is shown in Figure 21. This is for the combustion products of methane combustion in an oxidant in which the percentage nitrogen (balance oxygen) is varied from 0% (pure oxygen) to 79% (air). The systematic error reduces from  $\pm 0.67\%$  for air to  $\pm 0.35\%$  for pure oxygen.

This is explained by the removal of nitrogen in the oxidant which greatly reduces its volume and hence its influence on the combustion products. The results reported are limited to methane fuel, but similar trends are seen with any fuel. This is an especially important result since the measurement of gas temperature in oxygen fired furnaces poses particular problems to contact probes due to the extreme temperatures present.

In applications fired with air, there is an additional factor to consider - the humidity. Again, if humidity is monitored then this information may be fed back into the sensor system and corrections may be made accordingly. However, if ignored, this will result in a systematic error in the measurement of temperature, the level of which depends on the moisture content in the air and the furnace mixture ratio.

This error is estimated by considering a UK worst case of 100% relative humidity (RH) at 20°C<sub>dry bulb</sub> (water content 0.0148 kg / kg dry air). Again, if we assume no dependence of  $C_a$  on fuel moisture and mixture ratio, the resulting error in the temperature measurement for methane fuel is  $\pm 0.976\%$ . This is for humidities in the range of 0 - 100% RH and mixtures in the range of 0 - 12 % O<sub>2 vol dry</sub> and should be compared with a value of  $\pm 0.64\%$  if humidity is known.

#### 5.6.4 Discussion

Acoustic pyrometry has the potential for great accuracy and fine resolution but this is limited by the dependence of the technique on the acoustic constant,  $\gamma R$ , which is a function of gas composition. A study has been undertaken into the variation of the acoustic constant with the products of combustion for a wide range of mixtures, temperatures and fuel and oxidant compositions.

A strong dependence of  $C_a$  is seen with temperature, which may be easily taken into account using a modified speed of sound vs. temperature relationship. A far lesser effect is seen with variations in mixture ratio. For the majority of fuels having H/C molar ratios of greater than unity, the variation of,  $C_a$  is less than  $\pm 1\%$  for furnace excess oxygen concentrations between 0 and 12%vol.dry.

This equates directly to a systematic error in temperature measurement if no dependence is assumed. The effect is found to be a function of the H/C molar ratio and minor chemical species in the fuel, such as sulphur and nitrogen have very little additional effect. However, other major species do. These include oxygen and moisture that are found in solid fuels. They have the effect of increasing the systematic error, but for most fuels, this is still below  $\pm 2\%$ .

Oxidant composition is also shown not to have a strong effect. Enrichment of the air with additional oxygen results in a reduction in the deviation of  $C_a$  with mixture and hence an improved systematic error.

Humidity in air fired systems does increase systematic error but only marginally.

## 5.7 Gas velocity effects

### 5.7.1 Application to a high velocity system.

In most cases the effect of gas velocity on the acoustic technique can be assumed negligible. However when considering applications such as measurements associated with a turbine combustor or high velocity burner (HVB), further investigation is needed.

The main difficulty associated with applying the acoustic temperature measurement technique to a turbine combustor is; (1) resolution considerations for such a short pathlength, (2) the effects on the technique due to large velocity components along the axis of the exhaust.

For a 200 mm diameter exhaust, the total path length (for a reflected signal) is 400mm (or 0.4m). For typical temperatures in the range 1073K TO 1273K the time of flight magnitudes are calculated at 0.6ms and 0.55ms respectively. At 300K the time of flight would be 1.15ms. This is quite a restrictive time 'segment' to produce a sufficient number of data points to achieve good resolution for measurement purposes. However it is not prohibitive.

There are several effects due to the axial velocity component. The first is due to the likely need to use a reflection technique (or echo method) since it would not always be possible to achieve a direct line of flight measurement. In most applications, the ratio of the velocity of sound of the transmitted signal from the acoustic transmitter to the velocity of the combustion gases is large, hence the velocity component from the combustion gases is considered negligible.

In a turbine combustor or HVB the velocity component (main flow) reaches magnitudes of over 100m/s and is therefore approaching 20% of the magnitude of the sound velocity of the gas (assuming the gas is at a typical exhaust temperature). Therefore the main flow velocity component cannot be assumed negligible. Figure 39 shows the influence of the main flow velocity on the transmitted signal in terms of the time-derived measurement (due to change in velocity) produced by the acoustic technique.

The calculations are based on an exhaust temperature of 1273K. Figure 39 also includes the corresponding effect on the acoustic pyrometer temperature measurement due to the change in velocity. It is clear that it is important to take into account the axial flow velocity when making the acoustic measurements. One method of overcoming the problem is to use the acoustic pyrometer to make flow measurements as well as gas temperature measurements. Flow measurement using acoustic transceivers has been discussed in various papers for use in industrial stacks and pipelines but not, as of yet, with high flow velocities.

Figure 22 shows a possible format of the velocity \ gas temperature acoustic measurement system. Where average flow velocity is required we need two transceivers at a variable distance (x) apart. Transmit velocity component is given by equation (5.4):

$$V_{T1} = \frac{d}{t_1} \quad (5.4)$$

where  $t_1$  is the time of flight from  $T_{R1}$  to the reflection point (R). From the reflection point (R) to  $T_{R2}$  the velocity component is equation (5.5):

$$V_{T2} = \frac{d}{t_2} \quad (5.5)$$

Correspondingly the equations describing the transmit velocity components from  $T_{R2}$  to R to  $T_{R1}$  are as follows, equations (5.6):

$$V_{T3} = \frac{d}{t_3} \quad \& \quad V_{T4} = \frac{d}{t_4} \quad (5.6)$$

The average velocity ( $\bar{V}$ ) is proportional to the difference between the time of flight from  $T_{R1}$  to  $T_{R2}$  and  $T_{R2}$  to  $T_{R1}$ . Hence equation (5.7):

$$\bar{V} = \left( \frac{d}{t_1} + \frac{d}{t_2} \right) - \left( \frac{d}{t_3} + \frac{d}{t_4} \right) \quad (5.7)$$

Since  $t_1 = t_2$  and  $t_3 = t_4$ , equation (5.8) reduces to:

$$\bar{V} = d \left( \frac{1}{t_1} - \frac{1}{t_3} \right) \quad (5.8)$$

In the case shown in

Figure 22, the signal is transmitted at angle ( $\theta$ ) with respect to the flow direction, hence equation (5.8) becomes:

$$\bar{V} = \frac{x}{\cos\theta} \left( \frac{1}{t_1} - \frac{1}{t_3} \right) \quad (5.9)$$

Gas temperature could then be calculated using the average velocity value ( $\bar{V}$ ) in the following form, equation (5.10):

$$T = \frac{(\bar{V})^2}{\gamma R} \quad (5.10)$$

where  $\gamma$  is the ratio of specific heats and  $R$  is the gas constant.

Figure 22 shows the change in separation distance between Transceiver 1 and Transceiver 2 due to the influence of the exhaust gas flow velocity. This is important since the transmitted signal must be accurately captured.

The directional influence has to be accounted for over the whole of the signal path as highlighted in Figure 23. In CASE 1, if the acoustic signal is transmitted perpendicular to the exhaust flow velocity, the resulting change in angle of the signal over the entire path length is  $2\theta$ . In CASE 2, a transmit angle of  $3\theta$  against the flow direction must be set up at  $T_{R2}$  so that the reflection at  $R_2$  is to reach  $T_{R1}$ . Measurements over a full range of operating conditions would be, therefore, more difficult unless one of the transceivers could move relative to the other or change the angle of transmission (i.e.  $T_{R1}$  transmits at an angle  $\theta$  in the negative x-direction).

Defining equations are therefore:

$$\bar{V} = d \left( \frac{1}{t_1} - \frac{1}{t_3} \right) \quad (m/s) \quad (5.8)$$

$$T = \frac{(\bar{V})^2}{\gamma R} \quad (K) \quad (5.10)$$

$$\theta = \tan^{-1} \left( \frac{V}{V_T} \right) \quad (-) \quad (5.11)$$

## 5.8 Path Curvature

As described in the following section, thermal gradients in high temperature applications will lead to distortion of the acoustic line of flight. However the error due

to the effect of the variable temperature field and thermal gradients at the wall should produce a path length error of less than 1% for most applications.

Temperature gradients in the thermal boundary layer close to the furnace walls can be very high, typically over 1000 K/m. Beyond 0.5m from the wall, temperature gradients are of the order of 100 K/m or less. Acoustic paths crossing such gradients will be distorted. The measured times will represent transit along the distorted paths and will be shorter than transit along the straight paths required for deconvolution. The error in the path length due to the boundary layer would be approximately 3.55 percent worst case and approximately 0.2 percent for more typical paths. An average temperature gradient away from the boundary layer of 80K/m, with a mean temperature of 1500K, would produce a maximum deflection of 0.75m in a typical path, of length 15m, giving a path length error of about 0.65 percent<sup>42</sup>.

## 5.9 Temperature Gradients

There is an important thermal coupling consideration to be accounted for as the signal passes along the soundpipes and meets the high temperature gases or passes through the high temperature gradients found at the walls of furnaces and kilns. Where there is a flow of hot gases past the end of the pipe from which the transmitted signal emanates, the problem is exacerbated and this occurrence should be avoided or minimised.

In the current work moving the pipe output outside the hot gas flow field (see fire rig experiments) provided considerable improvement to the coupling and hence the results.

One method (Kleppe)<sup>9</sup> of estimating the thermal gradient is by calculating the error in flight time due to the addition of the average temperature in the furnace wall to the gas temperature calculation. Measurements are required of the wall temperature as well as knowledge of the wall thickness.

## 5.10 Attenuation mechanisms

### 5.10.1 Introduction

One important area of investigation was identified through the design of the acoustic system to operate at ultrasonic frequencies. Most of the mechanical generators described operate in this frequency range. An important benefit of working at ultrasonic<sup>49</sup> frequencies is the very low levels of combustion and background noise anticipated in this range. However the level of sound signal transmission loss (sound attenuation<sup>50</sup>) greatly increases at ultrasonic frequencies.

When a sound wave passes through a fluid, the density, pressure and temperature of an element of the fluid varies periodically with time. With the approximation that these variations occur adiabatically and reversibly, a plane harmonic wave travels through the medium unattenuated and its velocity is determined from the thermodynamic equation of state of the fluid.

These assumptions may be categorised as (1) the fluid possesses no viscosity; (2) no heat enters or leaves an element of the fluid during its cycling due to the sound waves; and (3) the state of an element of fluid can be described by just two independent local thermodynamic parameters. If any of these restrictions is removed the pressure-density cycle is irreversible and in each cycle some of the sound energy is transferred to the fluid. Hence the cause of both absorption and dispersion of sound.

The variation of the velocity of sound in an ideal gas with frequency (dispersion) is small except in the case of such high frequencies that the wavelength of the sound wave is smaller than the mean free path of the molecules. However, in contrast, the absorption is both very temperature and frequency dependent. Hence in the following analysis we will consider the frequency and the nature of the medium (temperature, pressure, degrees of freedom etc.).

The main process which causes this attenuation is termed sound absorption and can be separated into two categories, classical absorption and absorption due to molecular relaxation<sup>51,52</sup>. Classical absorption is due to the heating (heat flow to or from an element of fluid, due either to heat conduction or radiation) and viscous effects of the fluid medium, but can be neglected except for extremely high frequencies.

Molecular relaxation was revealed when Herzfeld and Rice<sup>53</sup> (1928) discovered absorption levels far higher than those predicted by classical absorption theory in polyatomic gases such as carbon dioxide. Figure 25 shows a plot of dimensionless absorption coefficient ( $\alpha^*$ ) versus frequency/pressure ( $\nu/P$ ) for carbon dioxide at normal temperature and pressure. The plot indicates that absorption due to molecular relaxation affects ultrasonic frequency sound propagation, the curve maxima at a frequency of about 0.03 Mhz (30 kHz) for a pressure of 1 atmosphere. Classical absorption is also indicated on the graph affecting very high frequency sound propagation. The dimensionless absorption coefficient ( $\alpha^*$ ) is related to the frequency by the equation (5.12):

$$\alpha^* = \alpha\lambda \quad (5.12)$$

Where  $\lambda$  is the sound wavelength and  $\alpha$  is the absorption coefficient (*Neper/m*).

In order to convert to sound pressure levels note that 1 Neper = 8.7 dB. The frequency ( $f$ ) is related to the wavelength by:

$$f = \frac{c}{\lambda} \quad (\text{Hz}) \quad (5.13)$$

where  $c$  is the speed of sound in the fluid (*m/s*).

The absorption coefficient  $\alpha$ , is a function of the frequency, the relaxation time and the contributions made by the internal and external degrees of freedom.

Herzfeld and Rice<sup>20</sup> attempted to describe this by applying thermodynamic relations but as pointed out by Markham, Beyer and Lindsay<sup>54</sup> (1951), thermodynamic relations, ignore the non-equilibrium aspects of the process, which play an essential role. They outlined a full analysis including various experimental results to describe the process in a review that is still a benchmark work in the field today.

The polyatomic gases that require investigation for the purposes of this project are the products of combustion such as carbon dioxide and water (including humidity effects<sup>55,56,57</sup>) at temperatures up to 1400K minimum. An investigation by Shields<sup>58</sup> (1970) has identified the relaxation time and absorption coefficient for carbon dioxide for a range of frequencies, but for temperatures only up to 600K.

Since the project is concerned primarily only with the magnitude of absorption, a full quantitative analysis of molecular relaxation is not required. However a basic analysis in order to gain some insight into the parameters involved was undertaken and, through some of the tests carried out during the investigation the sound absorption levels can be calculated. By comparing the transmission of sound through a controlled environment with that of a furnace of known gas composition, the level of sound absorption may be calculated.

### 5.10.2 Molecular (thermal) relaxation

The reason that polyatomic gases are of prime interest (as opposed to simpler gases i.e. monatomic) is due to the total energy of the molecules being distributed among their translational (or external) degrees of freedom and partly among their rotational and vibrational (or internal) degrees of freedom. The time taken for this redistribution of energy is of the order of the collision time  $\tau_c$ . The establishment of thermal equilibrium between the translational and internal degrees of freedom is in general much slower than  $\tau_c$  and is termed the relaxation time  $\tau$ . As a consequence there is an instantaneous lack of thermal equilibrium between the external and internal levels, which gives rise to an additional absorption of sound in polyatomic gases.

Changes in the translational energy  $\Delta E$  of 1 kg of gas is related to changes in temperature  $\Delta T$  by the equation (5.14);

$$\Delta E = 3(0.5R\Delta T) \quad (5.14)$$

where  $R$  is the gas constant. This equation is in accordance with the classical law of equipartition of energy. The law states that on the average each mechanical degree of freedom of a gas molecule will carry the same amount of energy,  $kT/2$ , where  $k$  is the Boltzmann constant and is related to  $R$  by the equation  $R=nk$ . The symbol  $n$  represents the number of molecules per kilogram of the gas.

However for polyatomic gases we must also consider the internal energies of rotation and vibration of the molecules. When a polyatomic gas is compressed, the work done is not immediately equipartitioned amongst the various degrees of freedom. The delay is fairly short and may be taken into consideration by:

$$c_v = c_e + c_i(1 - e^{-t/\tau}) \quad (5.15)$$

where:

$c_e$  = the specific heat contribution that remains in phase with the pressure changes.

$c_i$  = part delayed by a fraction  $1/e$  from reaching its ultimate value in a molecular relaxation time  $\tau$ .

For low frequencies:  $\omega\tau \ll 1$   $c_w = c_e + c_i = c_v$

i.e. the dynamic specific heat = equilibrium specific heat.

For high frequencies:  $\omega\tau \gg 1$ ,  $c_w = c_e$ .

By use of the relationship (5.16):

$$\gamma = \frac{c_p}{c_v} = \frac{c_v + R}{c_v} = 1 + \frac{R}{c_v} \quad (5.16)$$

The attenuation constant is equation (5.17):

$$\alpha = \frac{\omega}{2c} \frac{Rc_i}{c_e(c_e + R)} \frac{\omega\tau}{(1 + \omega^2\tau^2)} \quad (5.17)$$

and for the phase velocity, equation (5.18):

$$v = \frac{c}{\sqrt{\gamma}} \left[ 1 + \frac{R[c_i + c_e(1 + \omega^2\tau^2)]}{c_v^2 + c_e^2\omega^2\tau^2} \right]^{1/2} \quad (5.18)$$

The dependence of phase velocity on frequency indicates that the relaxation behavior of sound waves associated with the properties of the medium not only produce attenuation in amplitude but also in dispersion in velocity of propagation. For  $\omega\tau \ll 1$ , equation (5.18) simplifies to:

$$v_o = \frac{c}{\sqrt{\gamma}} \left[ 1 + \frac{R(c_i + c_e)}{c_v^2} \right] = \frac{c}{\sqrt{\gamma}} \left[ 1 + \frac{R}{c_v} \right]^{1/2} = c \quad (5.19)$$

The following derivation of equations is for a single relaxation time for the internal degrees of freedom. However, where there is more than a single relaxation time, for internal degrees of freedom including vibrational and rotational degrees of freedom, further derivation is required which is not given here. As the frequency increases,  $\alpha$  increases and rises to a maximum and then decreases to zero proportionately to  $\omega^{-1}$ ,

see Figure 25. The maximum value of absorption per wavelength is found when the period of that sound wave is of the same order of magnitude as the relaxation time.

In carbon dioxide at standard temperature and pressure the relaxation time ( $\tau$ ) is approximately  $10^{-5}$ sec, whereas the collision time  $\tau_c$  is approximately  $10^{-10}$  sec. Hence the relaxation time corresponds to a frequency of 10 kHz.

### 5.10.3 Investigation for Carbon Dioxide (CO<sub>2</sub>)

Using the results of Shields<sup>26</sup>,

Table 5, a plot of dimensionless absorption coefficient ( $2\alpha^*$ ) versus frequency ( $f$ ) for four different temperatures (303.5K, 371.7K, 468K and 578K) an accurate copy was made on a spreadsheet of the data.

T(K)	303.5	371.7	468	578
F(kHz)	$2\alpha^*$	$2\alpha^*$	$2\alpha^*$	$2\alpha^*$
10	0.15	0.135	0.12	0.07
15	0.205	0.2	0.17	0.14
20	0.24	0.25	0.22	0.19
25	0.26	0.28	0.26	0.22
30	0.265	0.295	0.29	0.24
35	0.265	0.32	0.33	0.295
40	0.26	0.325	0.355	0.325
50	0.24	0.325	0.385	0.37
60	0.22	0.32	0.395	0.405
70	0.205	0.305	0.395	0.425
80	0.18	0.285	0.385	0.44
100	0.15	0.25	0.365	0.43
150	-	-	-	0.33

**Table 5: Experimental results from Shields**

Polynomial curve fits were then fitted to the data points as shown in Figure 26. The resulting polynomial equations approximating the curves are given on Table 6:

T(K)	Polynomial curve fits to Shields experimental data
303.5	$y = -0.000000023357x^4 + 0.000006276891x^3 - 0.000603513948x^2 + 0.022631579779x - 0.019914162701$
371.7	$y = 0.000001157710x^3 - 0.000255911198x^2 + 0.016506632637x + 0.003327778905$
468	$y = 0.000000673561x^3 - 0.000185322169x^2 + 0.015665854515x - 0.023422192507$
578	$y = 0.000000246293x^3 - 0.000106542002x^2 + 0.012901792706x - 0.039426871153$

**Table 6: Approximate curve fits.**

From the absorption coefficient ( $\alpha^*$ ) versus frequency data, the maximum frequency of absorption for each temperature could be found at each of the curves maxima. The maximum frequency of absorption (relaxation frequency) is related to the relaxation time, Equation (5.20):

$$f_m = \frac{1}{2\pi\tau} \quad (5.20)$$

The relaxation time could therefore be calculated and plotted for each of the temperatures as shown on,

Table 7 and Figure 27.

T (K)	$f_m$ (kHz)	$t$ (s)	$w_m$ (rad/s)	$\alpha/w_m$
303.5	32.8	4.85E-06	205984	0.00008340
371.7	47.7	3.34E-06	299556	0.00009251
468	66.1	2.41E-06	415108	0.00009395
578	86.5	1.84E-06	543220	0.00009674

**Table 7: Relaxation times for several temperatures**

The curve in Figure 27 is described by the power law equation indicated. Previous authors have stated that the relationship between the temperature and relaxation time is that of a power law and that relaxation time should decrease with increasing temperature. The above values for relaxation times are in good agreement with those reviewed by Herzfield and Litovitz<sup>51</sup>.

The next step was to calculate values for the internal and external contributions to the specific heat at constant volume ( $C_v$ ), i.e.  $C_i$  and  $C_e$ . Using equations (5.21) and (5.22):

$$\left(\frac{\alpha}{\omega_m}\right) = \frac{RC_i}{4cC_e(C_e + R)} \quad (5.21), \quad C_v = C_e + C_i \quad (5.22)$$

We have two unknowns ( $C_i$  and  $C_e$ ) and two equations. Substituting  $C_e = C_v - C_i$  into equation (5.21) and rearranging, a quadratic equation is produced as shown by equation (5.23) and (5.24):

$$\text{Let } \left(\frac{\alpha}{\omega}\right)_1 = A_1 \text{ for } T_1:$$

$$\therefore A_1 = \frac{RC_i}{4c_1(C_e + r)C_e} \quad (5.23)$$

$$C_e^2 + C_e R - \frac{rC_i}{A_1 4c_1} = 0 \quad (5.24)$$

$$\text{Let } C_e = C_v - C_i; \quad (5.25)$$

Substituting equation (5.25) into equation (5.24):

$$(C_v - C_i)^2 + (C_v - C_i)R - \frac{rC_i}{A_1 4c_1} = 0 \quad (5.26)$$

Hence rearranging (5.26):

$$C_i^2 + C_i \left( R + \frac{R}{A_1 4c_1} + 2C_v \right) - C_v^2 - C_v R = 0 \quad (5.27)$$

A quadratic equation in  $C_i$  where  $C_v$  and  $R$  can be found in tables,  $c_1$  ( $m/s$ ) can be calculated from compressible flow relations.  $A_1$  can be calculated using relaxation times  $\tau$  (s) from the relations derived from Figure 27. Using quadratic formulae this could be solved to give the relationship between  $C_i$  and  $C_e$ , Table (5.5):

	T <sub>1</sub> (K)	T <sub>2</sub> (K)	T <sub>3</sub> (K)	T <sub>4</sub> (K)
	303.5	371.7	468	568
C <sub>i</sub>	149.684	187.048	225.181	263.704
C <sub>e</sub>	510.038	534.973	573.014	606.258
C <sub>i</sub> /C <sub>e</sub>	0.293	0.350	0.393	0.435
C <sub>v</sub>	657	788	805	872

**Table 8: Energy contributions at various temperatures.**

Figure 28 shows the relationship between C<sub>i</sub> and C<sub>e</sub>.

We now have values for C<sub>i</sub>, C<sub>e</sub> and  $\tau$  that can be used to calculate the attenuation constant from the equation (5.17) and:

$$\alpha^* = \alpha\lambda \quad (5.28)$$

Figure 29 is of absorption coefficient versus temperature for various frequencies shown on the legend for pure CO<sub>2</sub>. The curves represent lines of constant frequency and agree well with the experimental results of Shields (26) for the temperature range 0 to 600K.

More usefully Figure 30 shows the attenuation constant in decibels per metre against temperature for various ultrasonic frequencies. Note that 1 *neper/metre* = 8.7 *decibels/metre* (dB/m).

With respect to the current work the volumetric levels of CO<sub>2</sub> are likely to be reasonably well known or measured in most cases, hence the mass fraction in the products can be calculated. This enables estimation of the likely attenuation levels as indicated in Figure 31 for a mass fraction of 16.91% resulting from reacting propane (C<sub>3</sub>H<sub>8</sub>) and air with an equivalence ratio ( $\phi$ ) of 0.866.

The plot indicates the higher signal loss occurring due to molecular relaxation at frequencies greater than 10 kHz. Note, however, that the attenuation level is reducing with increasing temperature for most of the frequencies shown. This result is produced to aid comparison with experimental results in the following sections.

### 5.10.4 Discussion

Consider equation (5.17) in the calculation of the attenuation constant  $\alpha$ : The equation was effectively split into three parts.

$$1) \frac{\omega}{2c} \quad 2) \frac{Rc_i}{c_e(c_e + R)} \quad 3) \frac{\omega\tau}{(1 + \omega^2\tau^2)}$$

The first part of the equation (1) relates the sound velocity( $c$ ) to the angular frequency ( $\omega$ ). The angular frequency at ultrasonic sound frequencies, however, is much greater than the sound velocity in all cases. ( $\omega \approx 100c$  to  $1000c$ ).

The second part of the equation (2) relates the internal energy contributions ( $c_i$ ) to the external translational energy levels ( $c_e$ ). The relationship between them was derived from the experimental data of Shields<sup>26</sup> (26) by locating the maximum frequency of absorption ( $f_m$ ) for four different temperatures, with which the relaxation time ( $\tau$ ) could be calculated. This then allowed us to calculate  $c_i$  and  $c_e$  at the four different temperatures and estimate a relationship between them. Hence the relationship between  $c_i$  and  $c_e$  is a function of the relaxation time.

The third part of the equation (3) includes the relaxation time and the angular velocity. For the lower range of ultrasonic frequencies the denominator of equation (3) can be approximated to one for the range of likely relaxation time magnitudes.

Only at the higher frequencies (and higher temperatures where the relaxation times reduce) does the denominator terms start to increase and become significant. The numerator terms play a more significant role, the relaxation time decreasing with increasing temperature from approximately  $5.00e^{-06}$  seconds towards  $1.00e^{-06}$  seconds. A relaxation time for internal energy contributions found in the text<sup>52</sup> for CO<sub>2</sub> at normal temperature and pressure is  $6.20e^{-06}$  seconds. Buschmann and Schafer are reported<sup>52</sup> as having obtained relaxation times of  $1.53e^{-06}$  and  $6.9e^{-06}$  seconds for CO<sub>2</sub> at normal temperature and pressure. These values for relaxation time are in comparison with the collision time ( $\tau_c$ ) for which values of the order of  $1.00e^{-10}$  are found for CO<sub>2</sub> at normal temperature and pressure.

The usefulness of these very approximate calculations may seem limited at this stage since, from previous work it is evident that the frequency range of an acoustic pyrometer is likely to be limited below ultrasonic levels due to the molecular relaxation phenomena. However, the contributions of the various attenuation mechanisms have not been fully quantified and may yet provide a useful property as

in the case of interferometry which, to date, has limited high temperature experimental data.

# Chapter 6

## Signal Processing Methodology

### 6.1 Introduction

Previously in this report, the important characteristics required by the transmitter were highlighted in terms of signal amplitude levels at various frequencies required to overcome combustion and background noise levels. It is essential, however, to consider the constituent properties of the transmitted signal from which the critical time of flight calculation, and hence temperature, is calculated. Investigation of various types of signal and signal processing techniques was seen as an important area in which to enhance the performance of the acoustic system in terms of improving the signal capture and also the accuracy and resolution of the system. The following section reviews the types of signals available and the processing techniques required for their application to the present investigation.

### 6.2 Signal Types

#### 6.2.1 Introduction

Signals and systems are closely related concepts, though each one can be studied separately. The relationship may be understood by considering how the system (i.e. furnace) modifies the input (transmit) signal as it propagates through the system. In order to properly design an input signal it is important to envisage how the system may change the signal so that the effects of the distortion introduced can be minimised.

It is important at this stage to differentiate between the two types of signal available with respect to their concept of time. A signal may be defined as a function that describes a physical variable as it evolves with time. The first signal concept is termed “continuous time” where time is modeled using real numbers. The second concept is “discrete-time” which is modeled only using integers.

These signals, therefore, effectively become sequences. There are many examples of test signals used in process control. Often termed forcing functions, these include pulses, steps, sinusoids and pseudo-random binary sequences (PRBS). Step and pulse functions are the most utilised forms of input signals previously used in combustion studies, whereas PRBS is established and widely used in the field of process control and is regarded as a useful and powerful signal. Although these differing types of signal will produce the same information, it is the format of the output in terms of resolution and accuracy that is of interest here.

### 6.2.2 Simple test signal functions

There are many simple functions such as impulse, step, ramp, pulse, triangle, exponential and logarithmic functions available<sup>59</sup>. Most of these are easily generated and their properties are well known. With regard to the current application, only the pulse and triangle function is defined here.

The Unit Pulse Function,  $\Pi(t)$  and the Unit Triangle Function,  $\Lambda(t)$  are shown on Figure 32 and Figure 33 respectively.

### 6.2.3 Sinusoids

The simplest alternating waveform is sine-wave voltage or current, which varies sinusoidally with time. A sinusoidal waveform is generated by the variation of the vertical component of a vector rotating counterclockwise with a uniform angular velocity. One complete revolution is termed a *cycle* and the time interval required for one cycle is called the *period*. Since there are  $2\pi$  radians in one complete revolution and this requires ' $t$ ' seconds, the angular velocity ( $\omega$ ) is  $2\pi f$ . If the length of the rotating vector is ' $A$ ' the instantaneous value at any time ' $t$ ' is  $A \sin(\omega t)$  where ' $A$ ' is the *maximum* or *peak amplitude* of the sine wave. Two sinusoidal waveforms that have the same frequency but pass through zero at different times is said to be out of *phase*, and the angle between the two rotating vectors is called the *phase angle*.

A sine wave is completely described by its frequency and amplitude unless it is compared with another signal of the same frequency. In this case the most general equation for the sine wave must include the phase angle, equation (6.1):

$$f(t) = A \sin(\omega t + \phi) \quad (6.1)$$

The Sinusoidal function is shown on, Figure 34.

### 6.2.4 Pseudo-Random Number Sequences (PRNS)

As an introduction, there are two methods<sup>60</sup> that are most commonly used for generating uniformly distributed random sequences. The first type is known as the “linear congruential” method (or minimal length sequences) which forms the basis for a major proportion of present day program sensors, and makes use of the recurrence relation, equation (6.2):

$$X_k = A_{k-1} + C(\text{mod } R) \quad k = 1, 2, 3, \dots, \quad (6.2)$$

Where A, C & R are constants. ( $X_0 > 0, A > 0, C \geq 0, R \geq X_0, R > A, R > C$ ).

The method is limited to one-dimensional problems and is computationally expensive due to the operations required in each generator cycle.

The second method is most often used in hardware pseudo-random sensors and computer units and is called an *M-sequence*. The method consists of obtaining a linear binary sequence by means of the recurrence relation, equation (6.3):

$$a_i = \sum_{k=1}^m \alpha_k a_{k-1} \quad i = 0, 1, 2, 3, \dots, \quad (6.3)$$

where  $i$  = clock number,  $a_i \in \{0, 1\}$  are output sequence digits;  $\alpha_k \in \{0, 1\}$  are constant coefficients; and the summation sign represents modulo-2 addition. By choosing the number of  $\{\alpha_k\}$  coefficients, the generated number sequence has the maximal (for a given  $m$ ) length of period.

A major advantage of the maximal-length PR-sequence generation method is how simple it is to implement. The hardware comprises only of a  $m$ -bit shift register and a set of modulo-2 adders in the feedback circuit, Figure 35.

In operation, the shift register stores the preceding bits of the sequence and shifts them right, and the adders in the feedback circuit compute the values of successive bits that are sequentially written to the left-most portion of the register. The number of stages, sequence period and feedback connections are shown in Table 9. The properties of maximal-length sequences are as follows;

1. The sequence may be started with any non-zero value in one or more of the registers.
2. “m” registers provide a sequence period of  $2^m - 1$ . These maximal-length sequences are only generated in the case when the characteristic (generating) polynomial,  $\varphi(x)$ , is primitive and irreducible (i.e. not divisible by any other polynomial with a lesser power of ‘x’).  $m = \deg \varphi(x)$
3. For the specified irreducible primitive polynomial there exists “L” distinct m-sequences which are shifts of each other.
4. Over an m-sequence there are  $2^m - 1$  ones and  $2^m - 1$  zeros.
5. The m-sequence auto-correlation function (ACF) is defined by equation (6.4):

$$R_a(\tau) = \begin{cases} 1 & \text{for } \tau = 0 \pmod{L} \\ -1/L & \text{for } \tau \neq 0 \pmod{L} \end{cases} \quad (6.4)$$

The techniques utilising PRBS have been applied by various methods to several industrial processes, such as plant modeling and control techniques in the chemical and nuclear industries, as well as others. Its application here is relatively simple since we are only considering the time-shift properties and not encompassing or stimulating whole systems. For a more detailed approach to PRBS applications to process systems, please refer to Godfrey<sup>61</sup>, Williams *et al.*<sup>62</sup> and Turan *et al.*<sup>63</sup>

Number of shift register stages $m$	Period of sequence	Feedback to first stage modulo 2 sum of output of stages
2	3	1,2
3	7	2,3
4	15	3,4
5	31	3,5
6	63	5,6
7	127	4,7

**Table 9: Pseudo-Random Binary Sequences**

### **6.2.5 Discussion**

The above section has identified several important signal functions whose suitability will be investigated for application to the acoustic pyrometer technique. The criteria for success will depend on several factors, including transmission performance, the ability to derive time of flight information and the accuracy and resolution of that information.

The form of each of the signal functions has been reviewed. However the method of transmission and the method of extracting the time-shift information is also important. Modulation is a technique whereby variations of a baseband signal are made to occur within the same bandwidth but in a different part of the spectrum. This has useful properties if we wish to use the properties of a type of signal (i.e. low frequency, 500 Hz) but wish to transmit the signal at a different level (i.e low combustion noise window, 5000 Hz).

## ***6.3 Signal Modulation***

### **6.3.1 Introduction**

Modulation translates the information-containing signal (referred to as the message signal) to a new spectral location. Taking as an example radio, the human voice has a frequency range standardised as between, 300Hz and 3400Hz which is required to be broadcasted (transmitted) over large distance to a receiver (i.e. radio).

However, it is not viable to transmit such low frequencies since, due to atmospheric attenuation and physical barriers, the signal would not get very far. However if the signal contained significantly higher frequencies (i.e. 625kHz), this problem would be overcome. Hence a “carrier signal” is applied to the information signal prior to transmission, modifying its properties such as frequency or amplitude. A process of “demodulation” is therefore also required at the receiver to extrapolate the information signal from its modulated form.

There are many types of modulation<sup>64</sup> including “linear modulation” which contains “amplitude modulation (AM),” “frequency modulation (FM),” and “phase modulation (PM).”

### 6.3.2 Frequency Modulation

Frequency modulation (FM) occurs when the carrier frequency is made to vary about its unmodulated value,  $f_c$ , in such a way that the instantaneous deviation is directly proportional to the instantaneous amplitude of the modulating signal. The rate at which the carrier frequency varies is identical to the frequency information of the message. Hence, as opposed to amplitude modulation (AM) where the amplitude varies as a function of the modulating signal, in FM the carrier amplitude can be kept constant.

Consider the application of FM to a very low frequency sinusoidal signal, for example 50 Hz. The period of the signal is therefore 20ms. If we consider a furnace of length 5 metres containing hot gases of temperature in the range 300K to 2400K the time of flight for the signal would vary from 14ms to 5ms respectively, less than the period of the sinusoidal signal.

Consider a 50Hz sinusoidal signal  $m(t)$  of amplitude  $A$  such that, equation (6.5):

$$m(t) = A \sin(\omega t) \quad (6.5)$$

where  $\omega$  (*rad/s*) is the angular velocity and  $t$  (*s*) is the time.

At 300K the sinusoidal waveform would only be able to complete approximately three-quarters of its period in the 5 metre furnace as shown in Figure 36(a) since the time of flight is only 14ms. Similarly at 2400K, Figure 36(b), the sinusoidal waveform travels the furnace in a time of 5ms and in the above example, only completes a quarter of a period.

If we consider the signal in terms of its phase( $\phi$ ), however, we see that as the temperature increases, the sinusoidal signal arrives at a different point of instantaneous phase. The signal at 300K arrives at the receiver at  $t_1$  with the phase at a maximum corresponding to  $-\pi$ , the signal at 2400K arrives at  $\pi$  at  $t_2$ .

The difference in the phase of the arriving signal from a calibrated baseline signal (i.e. at 300K) allows the speed of sound to be calculated and hence the temperature may be derived.

It is however impractical to use a 50Hz signal due to the size of the transmitter required to produce such a low sound level and the fact that high levels of noise are

present at this low frequency. However, by utilising frequency modulation (FM) a high frequency carrier signal ( $>$  noise level frequencies) can be used for the transmission. After demodulation the original 50Hz signal is retrieved and any phase difference can be identified.

The various components for a modulation system are fairly straightforward. A carrier signal is required to modify the information signal and this may be produced using the current signal processing software. For demodulation of a continuous signal such as a sinusoid, a simple low pass filter can be used, its properties defined by calculation using readily available software.

This is just one possible example of signal modulation applied to the acoustic technique. More complex modulation methods, such as pulse modulation and multiplexing, also warrant investigation. In the above example, a 50Hz continuous sinusoid signal was used which could be represented by a sequence of discrete samples if a high enough sampling rate were used.

Modulation of a pulse signal is slightly different due to the abrupt discontinuities between each pulse interval. Again there are various types of pulse modulation such as Pulse Amplitude Modulation (PAM), Pulse Width Modulation (PWM) and Pulse Position Modulation (PPM).

Multiplexing is the transmission of a large number of signals simultaneously using a single communication channel. The process may be of interest if we wish to transmit more than one form of signal. The techniques include Frequency-Division Multiplexing (FDM), Quadrature Multiplexing (QM) and Time-Division Multiplexing (TDM).

### 6.3.3 Correlation

This function describes the general dependence of one set of data on another, i.e. in this case, the similarity of a signal with a time-shifted version of itself. The cross correlation function,  $Corr(\tau)$ , between two signals  $i(t)$  and  $j(t)$ , whose statistical properties (i.e. mean level, mean squared amplitude) remain constant with time, is defined as, equation (6.6):

$$Corr(\tau) = \lim_{T \rightarrow \infty} \frac{1}{T} \int_0^T i(t)j(t - \tau)dt \quad (6.6)$$

In terms of application, long portions of the signals  $i(t)$  and  $j(t)$  are recorded, and  $j(t)$  is shifted by an amount  $\tau$  (proportional to the time of flight) with respect to  $i(t)$ . The signals  $i(t)$  and  $j(t+\tau)$  are then multiplied together and the integral of this multiplication determined. The result is then divided by the time over which the integration was carried out.

Since the transmitted signal is free from background noise it can be correlated to the received signal (plus background noise) and defined in terms of a “best” fit. Hence a qualifier can be defined between 0.0 and 1.0, indicating the level of correlation, the position of the maximum, enabling accurate estimation of the flight time of the signal.

## 6.4 Signal Filtering

There are several types of filter used in the current investigation:

- Low-pass filter
- High-pass filter
- Band-pass filter

The low-pass filter in its most basic form relies on the series combination of a resistor (R) and an inductor (L). If the RL filter is connected to a source of sinusoidal voltage an expression can be produced, equation (6.7):

$$v_i = I_p \sqrt{R^2 + (\omega L)^2} \sin(\omega t + \phi) \quad (6.7)$$

where:

$$\phi = \arctan \frac{\omega L}{R} \quad (6.8)$$

$I_p$  = current amplitude.

If the voltage drop across R is considered to be an output voltage of the circuit then the instantaneous voltage is, equation (6.9),

$$v_0 = R I_p \sin \omega t \quad (6.9)$$

The ratio of the *rms* output voltage to the *rms* input voltage is defined as, equation (6.10):

$$\frac{V_o}{V_i} = \frac{1}{\sqrt{1 + (\omega L/R)^2}} \quad (6.10)$$

At low frequencies where  $\omega L/R \rightarrow 0$ , the output voltage is equal to the input voltage. At high frequencies the output voltage is smaller than the input voltage. Thus the above circuit is a 'RL low-pass filter'.

A similar circuit employs a capacitor and resistor connected in series. An expression for the ratio of the *rms* output voltage to the *rms* input voltage is defined as, equation (6.11):

$$\frac{V_o}{V_i} = \frac{1}{\sqrt{1 + 1/(\omega RC)^2}} \quad (6.11)$$

where 'C' represents the capacitance.

In this case the output voltage 'V<sub>o</sub>' is very small at low frequencies and is equal to the input voltage at high frequencies. Since low frequencies are attenuated while high frequencies are not, this circuit is called a 'RC high-pass filter'.

A band-pass filter relies on a combination of the above circuits. For a full derivation of equations (6.7) to (6.11) and information of the band-pass filter an appropriate reference is provided<sup>59</sup>.

In the current investigation a range of filters (low-pass, high-pass and band-pass) were evaluated as described in a later section (cf. Section 7.2).

## 6.5 Software Design and Signal Processing Equipment

The aim of the software control program was as follows:

- Digital generation of the required signal,
- Communication with the datalogger boards in order to transmit and receive signals,

- Comparison and analysis of the transmitted and received signal in terms of threshold or correlation calculations,
- Visual display of results for on-site setup and analysis.

A portable computer was utilised with the datalogger boards (DAS 1600 and DAS 1200) installed in spare internal slots. The function of the datalogger boards was to provide digital to analogue conversion and vice versa where required. The software could therefore be used to digitally define a signal, such as a chirp, and through the use of the digital to analogue converter, change the signal into a suitable form for transmission by the compression driver. This allowed simple functions (that can be produced using digital techniques) such as sinusoids to be generated with easily variable properties.

For more complex signals, such as impulse, triangle and PRBS a separate generator was required. For impulse (square) and triangular waves a standard laboratory signal generator was available for which the frequency and amplitude could be varied. Care had to be taken when using such a signal generator since the direct input of a signal with a sharp edge (square wave) can cause damage to a compression driver compared to the 'softer' or more 'gradual' changes experienced with a sinusoid.

In order to provide Frequency Modulation (FM) and PRBS capability separate electronic circuits were produced courtesy of Kingfield Electronics Ltd. The FM circuit specification included the ability to utilise the properties of a high frequency carrier signal and that the frequency characteristics of that the carrier signal could be varied. Frequency shift keying (FSK) was used to concentrate the pulse spectrum within a particular band pass, (i.e. range of frequencies) due to in this case the physical limitations of the transmission medium.

A set of pictures of the FM circuit and the PRBS generation circuit is included in Appendix 3, Plate 3 and 4.

The specification for the FM circuit included the ability to define the carrier 'centre' frequency and the modulation depth about that frequency. The modulation depth defines the range of frequencies about the centre frequency over which the signal is modulated. A higher modulation depth improved signal capture in the case of the PRBS since the difference between the zero modulated value and positive modulated

value is at a maximum. The carrier frequency and modulation depth also had to be matched to the band pass filter curve and the compression driver characteristics.

The PRBS generation circuit had the following specification:

- Choice of sequence length of PRBS
- Variation of the period of the PRBS sequence
- Variation of the characteristic clock frequency of the PRBS signal
- The use of triangular or impulse PRBS signals.

A schematic diagram of the experimental equipment is shown on Figure 37. The diagram includes the system control (computer), PRBS generator, amplifiers, transducers, and analysers. Typical signal characteristics and equipment properties are shown on Table 10.

The software control programs were compiled in the commercially available 'QuickBasic' (version 2) since this was appropriate to the datalogger boards at the time. Several programs were written for various applications:

- CHIRP software program: MASTER7.EXE/BAS (Initially written by Dr. K.J. Young<sup>1</sup> and modified by the current author)
- PRBS software program: PRBS2.EXE/BAS (Written by the current author)

A copy of each of the programs is included in Appendix 2. The portable computer with the control software running is shown in Appendix 3, Plate 5

The control software was structured to allow the transmit and receive properties to be defined before entering an operating mode where analysis of the captured signal information was carried out. The initial main program screen offered the following options:

- Define properties of the transmitted signal
- Define properties of the received signal
- Run an analysis

---

<sup>1</sup> Initial project supervisor, currently Combustion Projects Team Leader, Rolls Royce Plc., Derby, U.K.

- Exit the program.

Depending on the input choice the appropriate subroutine was called.

The “TransmitSetup” subroutine allows a trigger, square wave or chirp signal to be defined. The trigger and square wave functions were used in trials to investigate the performance of simple functions at ambient conditions.

The chirp signal was defined by three input properties,

- Chirp start and stop frequency (Hz)
- Chirp duration (ms)

These properties therefore define the characteristic frequencies and period of the chirp function. The inputs are also used by the software to define test properties such as sampling rates, sampling duration, and transmit time. Since the PRBS was generated externally from the control software the transmit option was not applicable in the PRBS control program.

The “ReceiveSetup” subroutine dictates the method of analysis appropriate for the types of transmit signal. The type of analysis function includes threshold level and cross correlation.

The ‘Threshold’ function simply estimates the arrival time of a pulse by analysing the first occurrence of that signal above a set trigger level. The correlation function has been described in Section (6.3.3) and is used primarily in conjunction with the chirp and PRBS signal. The PRBS signal was analysed in a slightly different way due to the effective continuous nature of the generated signal. It was important to ensure that the start of the PRBS sequence is triggered at a positive clock pulse rise. This is carried out at the data collection (DA datalogger board) and controlled by the software.

The inputs required for the subroutine include the path length and estimated time range expected. In reality the path length is calibrated at ambient conditions and will be modified with increase in the plant temperature and medium properties. The estimated time range has to encompass the total change in flight time with temperature. Hence the sampling duration and rate must also be considered so as not to compromise memory capacity of the analysing equipment. The computer had an available memory size for an array of 32,000 bytes, which was equally split between,

transmit and receive arrays. This was in order that the transmit and receive data could be compared.

After inputting the required information for the transmit setup the user is directed back to the main program screen where the 'run program' option is available with the following subroutines:

- Dummy run
- Datalogger run
- Recall old data
- Return to main menu

The 'DummyRun' subroutine is available for the chirp function to check the format of the signal and to estimate if the input properties are appropriate and within the capabilities of the system. Hence, for a dummy run no signal is transmitted and the received signal is an offset function of the transmit signal. The subroutine is useful for defining chirp signals with different properties and estimating their potential. The 'ReadData' subroutine allows previously stored results to be read by the software and plotted on screen.

The choice of 'Datalogger run' causes a subroutine called 'das1600init' to be called. The subroutine initialises the datalogger boards for handling the data and carrying out the AD or DA operations. In order to achieve this the correct frame (AD or DA), memory allocation, channel, gain etc have to be initialised. In addition operations such as start, stop, synchronous start/stop, memory locations, read/write and error routes have to be set. Once the datalogger boards have been initialised and a check has been carried out to ensure that the memory buffers are clear from the previous analysis (Subroutine ClearVariables), a second part of the main program loop is entered and the analysis display screen is generated (Subroutine 'DrawRunScreen').

The subroutine uses the input data such as sample numbers and estimated range of flight times to generate a plot of amplitude versus time. The plot is refreshed each time a signal is analysed (i.e. transmitted and received).

The system is now in 'run' mode (Subroutine DataCapture) and is continuously transmitting and receiving unless placed in the 'hold' position. Each time a run cycle

is called the screen is refreshed (Subroutine Refresh), a correlation is carried out between the transmitted and received signal (Subroutine Correlation) and the results are displayed on screen (Subroutine Plotdata). If the data is to be stored for further analysis, then the system operation is manually controlled and the required parameters written to a file using the write function (Subroutine WriteData).

Property	Range	Typical value	Control \ Parameter
Chirp frequency	500 – 10 kHz	5 kHz – 7 kHz	Software
Chirp duration	0 – 10 ms	1 ms	Software
FM carrier frequency	1 kHz– 10 kHz	5 kHz	FM Circuit
FM modulation depth	1 kHz – 10 kHz	3.2 kHz	FM Circuit
PRBS sequence	7,15,31, 63 & 127	15	PRBS Circuit
PRBS clock frequency	20 Hz – 1.5 kHz	140 Hz	PRBS Circuit
Sampling rate	1 Hz – 100 kHz	50,000 Hz	Memory capacity
Sample number	0 – 32,000	16,000/channel	Memory capacity
Band pass filter	1 kHz – 10 kHz	-	Filter circuit
Low pass filter	< 1 kHz	-	Filter circuit
High pass filter	> 20 kHz	-	Filter circuit

**Table 10: Properties of the experimental acoustic pyrometer system**

# Chapter 7

## Signal Processing Performance Trials

### 7.1 Introduction

To understand and develop an acoustic temperature-measuring instrument, it was necessary to carry out trials under a range of controlled conditions to fundamentally evaluate the system performance characteristics. Several key areas were identified for investigation for each signal type:

1. The performance of the transmitter (compression driver).
2. The influence of the sound injection method on sound transmission (cf. 4.2.4).
3. The influence of physical barriers, such as walls or supports, on sound transmission.
4. The effects of protective components, such as membranes on sound transmission (cf. 4.2.5).
5. The effects of signal processing components, such as filters (cf. 5.3).
6. The performance of each signal type in the presence of a calibrated noise source.
7. Calibration of the measurement system under controlled conditions.
8. Numerical analysis of the measurement technique.

The trials were carried out under various conditions. When careful calibration of system characteristics was required (such as sound output power of a source and perhaps its directionality) the tests were carried out under anechoic conditions. This is a chamber with perfectly absorbing walls (in principle) which therefore simulates an open space (no reflections).

To represent the physical attributes of a furnace, a large “cold furnace” was constructed to aid investigation into possible influences of echoes, reflections and physical obstacles. The basic construction of the “cold furnace” allowed simple physical alterations to be made easily, such as the inclusion of extra testing ports on any part of the furnace wall, variation in directionality or relative position between transmitter and receiver.

## ***7.2 Calibration of the compression driver***

As described in a previous section (4.2.3.1), the characteristic energy spectrum from a pink and white noise generator is a useful method of testing the response of system components. The Figure 38 shows the frequency response of the 40-Watt compression driver to a white noise input.

The measurements were made at a separation distance of 1 metre using the Bruel and Kjaer sound measurement equipment and the SRS spectrum analyser. The resulting data (averaged over time) is plotted both in raw amplitude format, as well as in sound pressure level according to equation (3.5), to highlight the difference in profile due to the logarithmic relationship. The variable amplitude versus frequency response of the “mechanical” compression driver is evident from the curves.

It is important in terms of producing the transmitted signal to consider the above profiles. The Figure 39 shows the variation in sound pressure level of a continuous 1 kHz signal (separation 1 metre) with variation in the angle of the transmitter relative to the receiver, carried out under anechoic conditions. It is important that the variation in sound pressure level (5 dB, or  $0.025 \text{ mN/m}^2$  pressure) due to directionality is monitored when calibrating a system. In most cases however a direct line of sight should be achievable.

The frequency range encompassed by the band pass filter (cf. 5.3) is shown on Figure 40 and indicates a maximum at approximately 4kHz. However the curves indicate a response to a direct input signal of white and pink noise. In reality, the compression driver output profile is applied to the curves as shown in Figure 41. It is important to account for this variation in signal throughput for optimum performance of the system.

## ***7.3 Properties of the chirp signal.***

Initial calibration of the compression driver was by use of a single frequency transmitted “burst” signal over a set time period followed by an incremental increase in frequency and the procedure repeated. A calibrated frequency analyser recorded each “burst” signal in order to produce a frequency profile for the compression driver.

The “burst” signal is simply generated by using a succession of sinewave signals of the correct frequency.

A “chirp” signal is similarly generated, though instead of a succession of constant frequency components, it contains a variation in frequency, for example 4000 Hz to 6000 Hz over a period of time. This, therefore, provides more information for the correlation procedure between the transmitted and received signals. Figure 42(a) and Figure 42(b) show an example of each type of signal.

It was important to ensure that the chirp signal used was designed to operate both in a frequency window of low combustion noise and good compression driver transmission response, as well as in conjunction with protective components.. To isolate the most suitable chirp frequency range, a series of tests was carried out to measure the peak sound pressure levels produced by a variety of signals under different conditions. Figure 43(a) and Figure 43(b) show the peak sound pressure levels achieved by chirp signals (constant time duration) containing a frequency range of 1000 Hz and 2000 Hz respectively. Comparing the chirp performance with the compression driver frequency response curves indicates good performance in the range 2000-3000 and 4000-6000 Hz.

Figure 44 shows a plot containing a transmitted and received chirp signal. The chirp signal contained a frequency range of 3500 to 4500 Hz over 2ms and was sampled at 100 kHz. Note the small time shift ( $t$ ) between the two signals. This constant time shift is due to the signal generation time (i.e. electronics) of the hardware and is included here as an example. It is a similar (but larger) time shift which produces the time of flight and hence the gas temperature during operation by, in this case, utilising a correlation method as described in section (6.3.3).

The corresponding correlation profile is indicated on Figure 45. The maximum peak corresponds to a time shift of 0.21ms with a magnitude (correlation level) of 1.0. Substituting this value into equation (1.4) and for a known separation distance (path length) the temperature can be evaluated.

The correlation level is an indicator of the closeness of comparison between the transmitted and received signal. The level of correlation is defined between 0 and 1 where  $< 0.5$  is deemed a failed correlation, 0.5 is reasonable, 0.5 to 0.6 is good and

anything  $> 0.7$  is very good. The point of maximum correlation identifies the time shift.

A second indicator identifies the correlation ratio. This is achieved by first identifying the correlation maxima (or positive domain turning points) and then the correlation minima (or negative domain turning points) neighboring those maxima. The correlation ratio is then defined as the ratio of the peak amplitude to the neighboring minima. The maximum value of correlation ratio is therefore designated the best correlation position and therefore defines the time shift.

On the Figure 45, the maxima labeled (B) has neighboring minima (A) and (C), whilst the maxima (D) has corresponding minima (C) and (E). The ratio for the first correlation peak (B) is calculated from equation (7.1):

$$CorrRatio, B = \frac{2 \times [Maxima(B) + 1]}{[(Minima(A) + 1) + (Minima(C) + 1)]} = \frac{2 \times [(1.0) + 1]}{((-0.9) + 1) + ((-0.9) + 1)} = 20 \quad (7.1)$$

Correspondingly equation (7.2) calculates the ratio for the second correlation peak:

$$CorrRatio, B^* = \frac{2 \times [Maxima(D) + 1]}{[(Minima(C) + 1) + (Minima(E) + 1)]} = \frac{2 \times [(0.7) + 1]}{((-0.9) + 1) + ((-0.5) + 1)} = 5.6 \quad (7.2)$$

The correlation ratio calculations are carried out on all the data within the correlation range. Note that  $CorrRatio, B \gg CorrRatio, B^*$  in this case. As we shall see later in the experimental work the influence of noise, reflections and other parameters reduces the correlation ratio to levels where  $CorrRatio, B^* > CorrRatio, B$  and hence the wrong correlation peak is used to calculate the time shift and an erroneous gas temperature calculated.

With these indicators defined, the chirp signal was further evaluated by simple trials to isolate the best frequencies to produce good correlation levels and ratios. Figure 46 shows the correlation levels achieved for a range of constant duration (5 ms) chirp signals transmitted over a distance of 5.5 metres in ambient conditions. It is evident from the plot that a frequency range of 1500Hz (4400 to 6100 Hz) gives the highest correlation level performance.

The duration of the chirp was also investigated since this limited the number of periods available for the correlation method. It is clear from Figure 47 that a shorter duration chirp provides a better correlation level under ambient conditions.

A 1ms chirp signal containing a frequency range of 4000-6000 Hz contains only a few periods and, therefore, is in effect very simple for the correlation method to handle. With the duration increased, there are a greater number of periods available and, hence, there may be a higher risk of error in making the correlation due to the increased complexity. Importantly, though, as invasive noise levels are introduced in a real system, the use of more complex signals with increased information carrying capabilities may become more critical for the correlation level, since a more simple signal may be more easily disrupted.

Figure 48 indicates the effect on transmission of the chirp signal when the protective nylon nitrile membrane is introduced. The curves indicate a fairly constant transmission loss of approximately 15dB per membrane in the frequency range 1000 to 10,000 Hz. Note that the theory breaks down at higher frequencies due to the effect of the membrane stiffness.

The receiver housing was initially constructed to hold the membrane immediately in front of the microphone head. With only a small distance available, near-field effects generated by the membrane, causing substantial degradation of the correlation procedure, disrupted the received signal at the microphone. A simple re-design to increase the separation distance between the microphone and membrane was completed in line with the results shown on Table 11.

Separation distance (mic->membrane)	Correlation level
< 0.01m	0.21
0.02m	0.61
0.12m	0.68
0.24m	0.75
0.48m	0.75

**Table 11: Effects of near-field disruption on correlation levels.**

Corresponding effects were also seen at the transmission side. If a membrane is placed within close proximity to the loudspeaker diaphragm, the sound signal is disrupted due to the near-field effects and, therefore, a small separation distance is required.

To avoid the problem, the membrane should be located at a minimum distance of twice the characteristic dimension of the sound source (i.e. compression driver diaphragm diameter) away from that sound source. It is also critical to ensure that the minimum separation distance is greater than the distance traveled in twice the characteristic time length of the signal. This ensures that any echo returning from the membrane does not modify the remaining signal during transmission.

## 7.4 Properties of the PRBS signal

The methodology used to derive a PRBS was introduced in a previous section (6.2.4) and in this section the performance of this useful and powerful signal will be described. The PRBS profile for  $m=3,4,5,6$ , and 7 (where  $m$  = number of shift register stages) is shown on Figure 49. The profile for  $m=4$  is shown on Figure 50. The sequence period ( $N$ ) is correspondingly 7,15,31,63 and 127 according to the equation  $N = 2^m - 1$ . Each PRBS includes a sequence pulse of length equal to  $m$  clock pulses. This is the largest sequence “chunk” and is clearly evident on each of the plots. Figure 51 shows the auto-correlation for a single ( $m=4$ ) PRBS transmitted under ambient conditions and received at a separation distance of approximately 1 metre.

The PRBS shown is based on a 1500 Hz clock frequency ( $f_c$ ) but was frequency modulated to 5000 Hz ( $f_m$ ) prior to transmission. The received signal was sampled at 50 kHz for a sample size of 4000 providing a sample period of 80ms. The correlation peak is very clearly defined above the noise floor and shifted along the time axis.

The correlation profiles generated contain useful characteristics that may be used to check the validity of the results. As indicated on the profile as time period  $2\Delta t$ , the width of the peak as it crosses the  $y=0$  is equal to  $2t_c$ , where  $t_c$  is the characteristic period of the PRBS, (clock period). Hence, for a clock frequency of 1500Hz,  $2t_c = 1.33\text{ms}$ . The total period ( $t_{\text{seq}}$ ) for each PRBS is equal to  $(N \times t_c)$ , which, in this example, is  $t_{\text{seq}}=10\text{ms}$ , means that 8 sequences are sampled during the sample period (80ms). Since a correlation peak is generated for each PRBS period, the resulting profile for the total sample time is shown on Figure 52.

The auto-correlation function of a PRBS therefore consists of a set of “peaks” or “spikes” of width  $2\Delta t$  spaced by the signal period ( $t_{seq}$ ). Note the reduction in magnitude of each subsequent correlation peak after the initial peak. If necessary these secondary correlation peaks may supply important information in locating the main correlation peak which provides the required time shift data. It is important to note that the correlation function is symmetrical about the  $t=0$  axis although this makes no difference in the convolution.

### ***7.5 System resolution considerations.***

For every technique there are limiting factors that determine, for instance, accuracy and repeatability of a measurement method. These limiting factors may derive from the process being measured or the equipment used for the analysis. In the case of the current work there are several important factors to consider when investigating the accuracy of a measurement made, based on the resolution achievable.

The maximum sample rate available was 100 kHz, which when considering two sets of data (received and transmitted), was reduced in this case to 50 kHz. This represents a data point being recorded every 0.02 ms (20  $\mu$ s). As the temperature increases, the speed of sound in the gas correspondingly increases and therefore the signal effectively travels further in 0.02ms at higher temperatures than it does at ambient conditions. It is important to ensure that enough detail is captured from the signals to produce an accurate correlation. This includes critical points such as turning points (Chirp) or sharp changes in amplitude (PRBS). A reduction in resolution of the correlation profile will cause errors in the time-shift measurement that in turn introduces significant error to the temperature calculation.

A large number of samples is, therefore, collected (limited by the storage array size) to assist this process. In order to increase calculation efficiency, a correlation window could be used where appropriate. By simple calculation the approximate flight times for the likely gas temperatures encountered could be predicted. The required correlation calculations need only take place within this time window, thus saving considerable computer time.

To ensure that the required detail was captured from the PRBS, some simple analysis was carried out. Figure 53 shows the number of samples per PRBS bit against clock frequency for various sampling rates. It is evident that as the PRBS clock frequency increases, higher sampling rates are required to achieve a resolution of even 10 samples per bit.

The importance of increasing the clock frequency is to reduce the base width of the correlation peak, Figure 54, producing a more sharply defined peak.

This enables an increase in the accuracy of the method due to the improved definition of the peak maximum (cf. Figure 54) and hence the time-shift measurement. Note that the amplitude of the correlation peak is also reduced. The maximum clock frequency was limited by the hardware in this case.

## ***7.6 System performance in the presence of noise***

### **7.6.1 Experimental procedure**

The uses of various important types of signal is investigated during these trials to ascertain a level of comparison in terms of the accuracy of the extracted received signal in the presence of various levels of generated noise. The use of anechoic conditions restricts the levels of reflections and reverberations present during the analysis, producing an environment more associated with a furnace or kiln.

Most of the experiments were carried out at a constant reference separation distance of 1 metre between the transmitter and the receiver. Small temperature fluctuations were experienced over the experimental time period. However these may be neglected.

A pink noise generator connected to an amplifier driving two transmitters provided the background noise. The transmitters were located perpendicular to the line of transmission at a distance of 1 metre.. The pink noise generator has a 60dB range via steps of 2dB. Hence in each experiment the transmitted test signal amplitude was kept constant and the background noise level varied. The transmitter of the test signals was a 40W compression driver driven by a constant 0.5V RMS from a Denon 50 Watt per channel amplifier. The receiver was a calibrated Bruel and Kjaer Type 4135, 0.25

inch free-field microphone connected via a Bruel and Kjaer Type 2670, 0.25 inch microphone pre-amplifier to a Bruel and Kjaer Nexus conditioning amplifier.

The conditioning amplifier provided a calibrated output with digital gain control to the computer for software analysis and to a SRS spectrum analyser. The SRS spectrum analyser was used to accurately measure signal amplitude versus frequency data from the receiver that could then be downloaded to a spreadsheet and converted into sound pressure data. An “in-house” written software program was used to process the different types of signals used.

A digital oscilloscope was also used as a source of reference of time dependent measurements, complimenting the spectrum analyser. The trials also provided an opportunity to calibrate each type of system. This is achieved by calculating the error associated with each step in the process. In all cases these errors are reported at each stage but are not accounted for in the software analysis.

## 7.6.2 Chirp signal performance results

Figure 55 shows a chirp capture profile of correlation level against time. This example was measured with a low level of background noise present. The highest peak is located just before  $t = 3\text{ms}$  with several peaks following, reducing in amplitude. The first peak (at 2.91ms) is the point at which the correlation is made.

The influence of the background noise level is evident on the plots, as well as the effect of secondary reflections of the chirp signal as seen at  $t = 4.7\text{ms}$ . The reflection has an amplitude of only 10% less than that of the primary correlation.

Figure 56 identifies this as a major source of difficulty associated with the chirp signal technique. The plot shows two chirp capture profiles plotted against time, both recorded in similar high levels of background noise. One signal correlation is made at 2.9ms with a magnitude of 0.62, the second signal correlation is made at 3.1ms with a magnitude of 0.66. At normal temperature and pressure, the temperature measurement error between the two correlation results is greater than 30K. However, with increasing temperature, the error would increase to >60K at 1000K and >130K at 2000K. Clearly this effect is due to noise effects and this error is seen throughout the performance trials.

Figure 57 indicates the effect of increasing noise on the magnitude of the primary correlation. For each 10dB increase there is a 10% reduction in the correlation level.

### 7.6.3 PRBS signal performance results

Figure 58 shows a plot of PRBS correlation level versus time for various Signal to Noise Ratio (SNR). The SNR qualifier in this case is the ratio of the average signal magnitude of a discrete set of measured data in the frequency range 4000 to 6000Hz to the corresponding average noise magnitude in the same frequency range. The qualifier is therefore based on the ratio of two sets of averaged magnitude data within a chosen frequency range. The curves exhibit very clear maxima that are displaced from zero along the timescale by a value proportional to the time of flight of the transmitted signal. For the range of SNR from 2.22 to 0.15 the time displacement varied by only the sample resolution of 0.02ms, (3.42ms to 3.44ms). As the SNR decreases further, the correlation is lost due to the noise levels. The position of displacement was also measured on a digital oscilloscope and was found to be a constant 3.2ms until the signal could not be visually distinguished from the recorded noise data.

Checking the width of the base of the triangular “spike” validated the correlation function of the PRBS shown above. The width of the base of the “spike” should be equal to twice the period of the characteristic transmitted signal ( $\Delta t_c$ ). Hence the period of the 1500Hz transmitted signal is twice the inverse of the frequency which is equal to 1.32ms. From the experimental auto-correlation data the base interval is 1.30ms.

### 7.6.4: FM square wave performance results

A 100Hz signal (modulated at 5 kHz) was included as a test signal to investigate the performance of a simply generated low frequency signal and to look at the method of “edge detection” as a measurement method. Figure 59(a&b) shows an example oscilloscope capture trace of the transmitted (unmodulated) signal (a) and the received (demodulated) signal (b). The time delay between the two signals is shown more clearly on Figure 59(b).

Note that the position that the measurement of the time delay is made on the rise time of the demodulated signal has to be carefully monitored.

Figure 60(a) shows the transmitted and received signal sampled by the software under low noise conditions. The time delay between the two signals is clearly evident. As the background noise level is increased it has a greater influence on the received signal causing degradation of the rise time of the squarewave or noise spikes as can be seen on Figure 60(b). This disruption causes time of flight measurement errors that cause a large reduction in the accuracy of the method.

The received FM square wave signal was unrecognisable due to noise effects at a SNR of 1.37 and, therefore, can quickly be rejected as a suitable signal method when compared with the much better performance of the chirp and PRBS. The performance of edge detection as opposed to the correlation method is discussed in a later section.

### **7.6.5: Signal and noise profiles**

For each trial a capture was made of the received signal in order to ascertain the statistical levels of noise at which the signal was unobtainable from the noise. Considering Figure 61 for the chirp signal, we can see initially in the first few milliseconds of the time axis the amplitude of the noise before the chirp signal is captured. This is then followed afterward by noise and reflections. As we scan through the plots, we can see the noise amplitude increasing but the higher frequency chirp signal is always visible until the correlation level begins to drop indicating that the signal is starting to be lost.

The received data plots for the PRBS, Figure 62, appear different in format due to the continuous nature of the signal. Unlike the chirp plots, a snapshot of the noise level present for each test is not seen, only its influence on the PRBS is visible. It does appear to be evident that the lower frequency PRBS components suffer disruption earlier in terms of SNR (cf. pressure level profiles). However the remaining higher frequency components still allow a correlation to be made.

The influence of the lower frequency components of the PRBS on the compression driver performance for an unmodulated system was also found to be critical, hence this may be the most important factor. This “m” sized sequence “chunk” corresponds to a frequency of 400Hz in this case and in a low valued sequence (in this case 15), may have significant influence. Of course increasing the number sequence and clock frequency will reduce its influence on the PRBS length and move its “characteristic” frequency up the frequency scale. To ascertain its particular influence in the current

tests would require investigating the format of the modulated signal as it is transmitted. This may be possible in a simple test.

For a full range of signal profiles in increasing noise see plates (8) and (9).

### **7.6.6: Influence of system components**

Initial calibration trials were carried out under ambient conditions to gauge the response of the system, with the addition of wind effects and reflections from nearby obstacles, for a range of PRBS signals. These included various clock frequencies ( $f_c$ ) and modulation centre frequencies ( $f_t$ ).

It was at this stage that the stability of the received (demodulated) signal appeared to be variable even under ambient conditions. This was also represented by fluctuation in the sound pressure level profile of the PRBS signal constituent parts ( $f_o$  and  $f_h$ ). It was therefore necessary to isolate the cause of the deterioration by investigating each stage of the experimental process, initially prior to signal transmission.

Attention was focused on the performance of the amplifier, the signal of which passes directly to the compression driver. With zero modulation (i.e. basic sinewave) the output of the amplifier was monitored and revealed the introduction of higher frequency noise components to the signal at maximum amplification, Figure 63. At lower amplification levels however the effect is much reduced, Figure 64. This, although simply resolved, was present during previous calibration and performance trials. A 300-pF capacitor was applied across the amplifier output to filter out the high frequency noise, Figure 65. An optimum value can be calculated for future work based on closer inspection of the amplifier output performance.

Introduction of noise to the system at this stage has important consequences for the demodulation of the signal, effectively degrading the profile of the received signal further, making it more difficult to extract the required data. The modulation/demodulation process itself was of concern, since it is an extra system component, when compared with the chirp method and, hence, there is an extra element of possible error introduced

### **7.6.7: Further sources of measurement error**

Every system is reliant on the performance of each subsystem or component within it, and to calibrate the whole system, a careful investigation of each part should be carried out. In this case an important source of error is time delays caused by system components, which cause an increase in the time of flight value utilised in the technique. One method used to verify the performance of many systems is to form a closed loop between the output and input, and to look at system performance. In the context of this report the method has been termed “direct input” and an example is shown in Figure 66.

For a perfect system the delay between the input and output signal should be zero for a closed loop. If a “chunk” of the direct input “PRBS” is isolated, as indicated on Figure 67, the delay due to the rise time of the demodulated output signal is evident.

The rise time in this case is of the order of 0.5 ms, which would cause a very large temperature error if not accounted for. As the clock frequency is increased towards the limit of performance of the signal generation system, the error becomes more difficult to obtain accurately due to the reduction in quality of the demodulated signal, Figure 68.

Similar delays are seen for the chirp and squarewave signals. Since the delay is constant, and as long as it is accurately quantified, the delay can be deducted from the total time without reducing the accuracy of the technique. The difficulty is in qualitatively defining the delay prior to any signal processing occurring.

## ***7.7 Numerical investigation***

It is clearly evident that the design strategy required to overcome problems arising from background acoustic noise levels is a key element in the performance of the measurement technique. This has a significant influence on the feasibility of the technique for particular applications and determines both the scale of sound generation equipment that must be used and the likely relative error in temperature that underlies the measurement.

### 7.7.1: Measurement strategies<sup>65</sup>

Two general approaches to the measurement of “flight time” of a sound signal involve (i) edge detection of the arrival of a transmitted pulse and (ii) cross correlation of transmitted and received waveforms. Sub-sections (6.2.2) through (6.2.4) have identified a typical range of functions that may be used.

Edge detection is characterised by the transmission of a shock front, often from a spark discharge, and may be repeated an arbitrary number of times to provide an average. The need to overcome background noise by using strong shocks has been demonstrated, for example, in the work of Green and Woodham<sup>15</sup> and Stones and Webb<sup>66</sup>, where spark discharges with energies in the range 140 - 400 J have been used. These result in pulse pressure levels of 6 - 15 kN/m<sup>2</sup> and therefore introduce corresponding deviations from Mach 1 operation of 6 - 15%. Whilst detection at such sound pressure levels against background noise becomes unambiguous, the error associated with the pressure dependent sound speed is difficult to quantify.

The effect of reduction in signal/noise levels on mean error, therefore, becomes of interest for this strategy in relation to other signal generation and processing methods.

Correlation may involve a wide range of functions and is represented by the three main types of (i) a pure frequency, (ii) a chirp waveform and (iii) a low frequency envelope, modulated by a carrier and demodulated at the receiver. In the case of a periodic function, the correlation function will have a maximum at successive time-shifts corresponding to the period of the signal. For short period functions, which are desirable due to their associated time resolution, the time window which can be used will be less than this period due to the ambiguity which would otherwise arise. This is often inconvenient when knowledge of system temperature does not permit the use of such a narrow acceptance window and for this reason, pulses with short period internal structure, such as a pure sine wave, are of limited value. The chirp represents a better strategy, since the frequency variation across its time domain removes the internal periodicity but retains the time resolution, and this is indicated by the steep decrease in the function around the main maximum.

### 7.7.2: Multiple sampling and mean errors

The usefulness of the range of transmitted signals and processing strategies will depend on the average errors in the measured time of flight which result for any chosen SNR. The requirement for a large SNR has a direct impact on the scale of the acoustic driver equipment or spark discharge source. Large acoustic sources are more ruggedised, less accurate and require careful use and application due to problems such as electromagnetic field generation. For all methods, this may also result in wave amplitudes that are above the permissible pressure limit of a Mach 1 wave, leading to interpretation difficulties. In this context, an upper limit of 150 dB would give a speed deviation of 1%.

In the case of the chirp, the suppression of the secondary maximum is an important requirement for successful operation in noisy environments and this is improved as the upper and lower frequency difference increases. However, as the SNR is reduced, it is anticipated (sect.7.6.2) that these secondary maxima will be a source of error due to their occasional rise above the principal maximum and consequent misinterpretation of the flight time.

An alternative function is that of the Pseudo-Random Binary Sequence. This may have an internal frequency structure comparable with the chirp or be represented by a more slowly varying waveform that is transmitted by a higher frequency carrier. The properties of this function which have value for this application were detailed in (sect.7.6.3). The nature of the PRBS function is such that any secondary maxima in the correlation function are suppressed, providing the potential for better resistance to noise arising from misinterpretation of 'true maxima'. The separation between maxima can be chosen independently through the definition of sequence length, and even for a 15 bit sequence, would be long enough to avoid any ambiguity in interpretation. The representation of measurement error due to acoustic noise is examined below for edge detection and for the correlation methods applied to chirps and PRBS.

### 7.7.3: Error analysis

#### 7.7.3.1: Edge detection

It is assumed that a detection and measurement algorithm will be applied which interprets the highest amplitude signal within the prescribed time window as the correct signal, and uses the associated time for this to calculate the flight time.

This is depicted in Figure 69, where a single shock pulse is embedded in background acoustic noise.

In the presence of such noise, and depending on the signal/noise amplitude ratios, this may give rise to error. If the noise amplitude is taken to be normally distributed then the signal amplitude and the maximum noise amplitude determines the probability of any instantaneous measurement exceeding the signal. Since a number of samples are taken within the time window in order to resolve the signal arrival with adequate resolution, the probability of noise interpretation will be proportionately increased, assuming that the noise bandwidth is greater than the sampling rate.

The variance  $\sigma_t^2$  for the measured flight time will depend on the number of measurements,  $N$  included in the average i.e. the number of attempts to measure an individual signal arrival. The  $N$  measurements can be represented by a binomial distribution chosen from noise detection and signal detection possibilities, each with its characteristic probability of selection. If the probability of signal detection is  $p_{sig}$  and that of noise detection is  $p_n$  then this can be calculated from its normal amplitude distribution with variance  $\sigma_n^2$ , using the signal amplitude,  $a_{sig}$  as the threshold for detection, i.e.

$$p_n = \frac{m \left[ 1 - \Phi\left(\frac{a_{sig}}{\sigma_n}\right) \right]}{1 + m \left[ 1 - \Phi\left(\frac{a_{sig}}{\sigma_n}\right) \right]} = 1 - p_{sig} \quad (7.3)$$

where;  $\Phi(x)$  is the cumulative distribution function of the normal distribution and  $m$  is the number of sampled points within the time window. Each of the  $N+1$  distinct arrangements of noise and signal detection combinations contributes its own variance to the time of flight and this is related to the number of noise contributions within each set of samples and the variance of the flight time associated with the chosen time

window  $\Delta t$ . The distribution of noise detection within this acceptance window is rectangular and hence its variance ( $\sigma_{nw}^2$ ) is given by:

$$\sigma_{nw}^2 = \frac{\Delta t^2}{3} \quad (7.4)$$

Considering only the variance contribution from the noise detection, then for a set of  $N$  measurements containing  $j$  signal detections, the variance contribution from the noise detections is given by:

$$\sigma_{nw}^2 \frac{(N - j)}{N^2} \quad (7.5)$$

Considering the contributions from the full range of possible noise and signal combinations, the variance of the distribution of flight times for  $N$  averaged measurements is  $\sigma_t$  where,

$$\sigma_t^2 = \sum_{j=0}^N \binom{N}{j} p_{sig}^j (1 - p_{sig})^{N-j} \sigma_{nw}^2 \frac{(N-j)}{N^2} \quad (7.6)$$

where the coefficient of the variance term is the binomial coefficient.

### 7.7.3.2: Correlation function

For a discrete representation of two acoustic waveforms,  $x(p)$  and  $y(p)$ , the cross correlation function is described by equation(7.7),

$$R_{xy}(s) = \frac{1}{m} \sum_{p=1}^m x(p) y(p + s) \quad (7.7)$$

where  $m$  is the number of sampling points and  $s$  is a displacement of one waveform relative to the other corresponding to the time shift,  $\tau = s/f$ , with  $f$  equal to the waveform sampling rate. (Note that equation (7.7) is the same as equation (6.5) only with different notation).

Recognising that  $y(p)$  and  $x(p)$  are the transmitted and received waveforms respectively, then in the presence of background acoustic noise  $n(p)$ , the correlation can be represented by

$$R_{xy}(s) = \frac{1}{m} \sum_{p=1}^m [y(p) + n(p)] y(p+s)$$

$$= \frac{1}{m} \sum_{p=1}^m y(p)y(p+s) + \frac{1}{m} \sum_{p=1}^m n(p)y(p+s) \quad (7.8)$$

The first term corresponds to the correlation function in the absence of noise, whilst the second is the instantaneous contribution due to the noise correlated with the waveform. The mean values of  $n(p)$  and  $y(p)$  are zero and in the limit of large samples the second term will tend to zero. For finite samples however, it retains a finite variance around the zero mean and will instantaneously act to modify the average cross correlation. Since the noise and the acoustic waveform are un-correlated, the variance of this term, the 'correlation variance'  $\sigma^2$ , can be related to the mean square value of the wave amplitude,  $\bar{y}^2$  and the variance of the noise source,  $\sigma_n^2$  according to

$$\sigma^2 = \frac{1}{m} \bar{y}^2 \sigma_n^2 \quad (7.9)$$

This variance applies at each point of the correlation function causing local fluctuations, which may give rise to a mis-interpretation of the correct position of the main maximum corresponding to the correct time shift. The mean value of this time shift is thus associated with a distribution function, whose standard deviation will depend on the shape of the underlying correlation function and the relative magnitude of the above 'correlation variance'.

### 7.7.3.3: Estimation of standard deviations

For comparisons to be made between the different types of signals used for correlation analysis, transmitted pulses of 3 ms duration are considered. The received waveforms are acquired with 150 samples, representing  $m$  in the above equations. The acoustic noise amplitude is taken to be normally distributed and, for a fixed unit amplitude of transmitted signal, this noise amplitude is varied to represent different signal/noise amplitude ratios and in each case is used to calculate the correlation variance of equation (7.9). From this variance, the standard deviation  $\sigma$  is then used to represent the limits of fluctuation that the correlation function can undergo locally. Since the correlation maximum is the point of interest, a fluctuation band of  $\pm 3.5\sigma$  above and below this value is taken as the range over which the maximum may deviate. If other points on the correlation function are able to deviate above the lower level of the band then statistically they can contribute error. Each point on the correlation function is therefore assessed to determine its weighted contribution to the

error in the following way. The fluctuation band is divided into 100 amplitude levels, as depicted in Figure 71, and for each level, the probability of attaining this level is established for each point on the correlation function based on a normal distribution around the local mean level for that point.

The probability for each point is cumulative as the whole fluctuation band is traversed. The final weighting factors,  $w(p)$  for each point  $p$  are obtained on normalising the resultant probability function. The variance of the measured time shift is then given by

$$\sigma_t^2 = \sum_{p=1}^m w(p) \left( \frac{p - \bar{p}}{f} \right)^2 \quad (7.10)$$

where  $\bar{p}$  is the index value corresponding to the mean time shift.

#### 7.7.4: Discussion

The above analyses have been applied to the three types of measurement involving edge detection, chirp and PRBS correlation. The parameters associated with the analyses are summarised in Table 12. The quoted amplitude values would refer to those measured at the detector in its normal receiving position rather than at a specified distance from the sound source.

	Edge	CHIRP	PRBS
Number of sample points	150	150	150
Pulse duration – (ms)	-	3	3
Acceptance time window – (ms)	± 1.25	-	-
Carrier frequency – (kHz)	-	4 - 6	-
Clock frequency – (kHz)	-	-	5
Signal amplitude	1	1	1
No. of bits	-	-	15
Noise maximum amplitude	0.5 - 4	0.5 - 4	0.5 - 4
Number of measurements	20	1	1

**Table 12: Summary of model conditions for edge, chirp and PRBS signal processing**

The calculation of measurement variance does not depend on the absolute value of the mean flight time. However since the time window associated with the edge detection is likely to be related to flight time, a typical value equal to 5 ms has been chosen for the latter and applied to the three cases. The time window for edge detection is thus set at  $\pm 1/4$  of the flight time.

The “noise free” correlations for chirp and PRBS are shown in Figure 70. These are given for zero time delay and therefore correspond to autocorrelations.

The numerical assessment of the behaviour of correlation indicates that the general form of these functions is retained even for noise/signal amplitude ratios as high as 4.

For low noise amplitude, spurious detection is only possible for points around the main maximum and hence the variance of the measurement will be low.

However, as the maximum noise amplitude rises, the degradation of the function increasingly causes spurious detection at points further from the main peak, contributing larger variances.

The behaviour of  $\sigma_t / t$ , where  $t$  is the mean flight time, is shown in Figure 72 for the three cases as a function of noise/signal amplitude. The noise amplitude is taken to be the maximum amplitude present in the distribution.

For edge detection, the finite charging time for capacitors associated with spark discharges is likely to place an upper limit on the number of measurements, which can reasonably be incorporated into the average of equation (7.6), since this will limit the temperature sampling rate. For this case therefore, the variance has been calculated from equation (7.6), based on 20 measurements ( $N = 20$ ). Equation (7.3) indicates that the probability of noise detection over signal detection will increase with the number of samples that are taken to represent the received signal. This is due to a greater number of chances that the instantaneous noise amplitude will exceed the signal threshold. When better knowledge exists about the flight time, then the time window can be reduced, which will reduce the variance contributed by the window width, equation (7.4), and the number of samples,  $m$ , for a fixed sampling rate.

Figure 72 indicates that the relative error for edge detection begins to rise rapidly for a noise/signal amplitude ratio around 1.

This is consistent with the normal amplitude distribution assigned to the noise, since at this ratio  $a_{\text{sig}} \sim 3\sigma_n$ . The rate of rise above this ratio will be influenced by number of samples  $\underline{m}$  and number of measurements  $\underline{N}$  in the average. The relative error will limit at the value set by the window width.

The PRBS shows superior performance compared with the chirp for noise/signal ratios above 2, which arises from the suppression of correlation maxima adjacent to the main peak. For the chirp, these will contribute into the acceptance band at lower noise amplitude levels. The chirp, however, remains a good option whilst the lower level of the acceptance band remains  $2\sigma$  or more above the second maximum, where  $\sigma$  is the correlation variance. This occurs for noise/signal amplitude ratios of around 1.5. The slightly better performance of the chirp over the PRBS at noise/signal ratios below 2 is due to the relative widths of the correlation peaks, with the chirp having a baseline width of 1/4 that of the PRBS for the same underlying frequencies.

# Chapter 8

## Experimental Application

### 8.1 Introduction

To evaluate the performance of the pyrometer system it was necessary to find a high temperature rig that provided a reasonably uniform temperature profile over a path length of at least several metres. It would also be beneficial to make some comparisons with measurements made by standard methods such as thermocouples, hence an experimental “compartment fire” rig was chosen, based at the departments test facility.

### 8.2 Acoustic pyrometer performance trials

#### 8.2.1 Experimental rig and pyrometer installation

The rig was initially constructed for an investigation into experimental and modelling studies of compartment jet fire suppression by using water spray. The jet fire is fuelled by propane emerging from a 1.5cm diameter vertical nozzle at a variable mass flow rate, (though primarily 0.1 kg/s), into a large metal compartment measuring 6×2.4×2.4m. The compartment has two exits at one end, at the base and at the top, both measuring approximately 2.4×0.3m.

Whilst cooler ambient air is entrained at the lower exit, the hot combustion gases escape through the upper exit giving a fairly constant temperature profile over the width of the outlet. It is over this region (a path length of over 3 metres), that the prototype acoustic pyrometer system was to be evaluated. A grid of shielded thermocouples were in position over both exits to provide temperature comparisons, whilst gas analysers were utilised to provide levels of propane (C<sub>3</sub>H<sub>8</sub>), carbon dioxide (CO<sub>2</sub>), water (H<sub>2</sub>O) and oxygen (O<sub>2</sub>).

The system was run slightly lean, producing levels of 10 - 12 % CO<sub>2</sub>, 3 % O<sub>2</sub> and 2 - 5 % CO by volume in the exhaust products. Using standard balances for exhaust

concentrations of O<sub>2</sub> and CO<sub>2</sub> gives an actual Air Fuel Ratio (AFR) of between 18:1 and 19.2:1, compared with the stoichiometric AFR of 15.6:1, and an equivalence ratio of 0.81 to 0.86. Comparing these levels of combustion products with those that are calculated by equilibrium methods, we find reasonable agreement. Slight differences are due to incomplete combustion, environmental (wind effects) and measurement (gas analysis error) variability.

This variability however is not critical with respect to the acoustic performance trials since the dependence of the acoustic constant has been proved to be small or accountable for unknown combustion products. However some composition data for the products is of use for signal attenuation calculations.

The transmitter and receiver were attached either side of the upper compartment exit, at half the vertical exit height. Initially the soundpipe ends were located within the hot gases during combustion but this presented coupling problems at the receiver due to the hot gas flow / soundpipe entrance gradient. With the receiver soundpipe entrance retracted from the main flow, better signal transmission was achieved. This new position is still representative of the setup at an industrial furnace.

Initial measurements quantified the combustion and background noise levels and calibration of the system. The second set of trials used the chirp signal followed by some simple signal loss measurements. Finally the PRBS signal evaluation was carried out to complete the results.

A picture of the compartment fire rig during combustion of 0.1 kg/s propane is shown in Appendix 3, Plate 6.

### **8.2.2 Combustion noise measurements**

A plot of the average combustion and background noise level is given in Figure 73. The data indicates a similar trend to that of noise measurements carried out earlier in the project, (Figure 16), at various plants. The higher noise levels are located at the lower frequency levels (<2kHz), but the fluctuating nature of the combustion producing variability in the noise magnitude is not accounted for.

Comparison of combustion noise captured with and without the PRBS signal initiated indicate that the transmitted signal is available above the noise level during

combustion and it is the performance of the receiving strategy which is the limiting factor of the technique.

It was also important to capture the variance in the noise since the levels varied above and below an average level. To achieve this, a number of manual noise captures were carried out and their statistical properties evaluated. At lower frequencies the noise level oscillates, with the fluctuating combustion process, and with environmental effects such as wind. At higher frequencies the oscillatory effect is much less. Note also that several maximums were found located at 2000, 6000 and 10,000 Hz which are not visible after averaging.

The important statistical derivations from the captured profiles are a standard deviation calculated for each sample ranging from 5.71 to 7.25 and a variance of 30 to 50. The critical variation for the purposes of this investigation are in the chosen frequency operating window which at this stage was still in the region 4000 to 6000 Hz and from Figure 73 this remains a reasonable choice.

### **8.2.3 Chirp signal performance**

With the pyrometer setup as described in the previous section a 2ms-duration chirp signal of frequency range 3500 to 4500 Hz was used with no membrane protection on either transmitter or receiver.

Due to the bend in the sound pipe (radiation protection) and its length (minimisation of conduction along the pipe and convection at the microphone diaphragm mesh), a membrane was not required. This allowed a longer duration chirp containing a greater number of cycles. Commissioning trials at various kilns indicate this may be possible at most industrial plant with careful design.

A set of time of flight measurements is shown in Figure 74 with the corresponding correlation level for each test. The jet fire in the compartment was initially running at 0.05kg/s which was increased to 0.1kg/s at the beginning of the data capture log run, and this is evident from time of flight samples (1) to (4) in Figure 74. At 0.1 kg/s a temperature of approximately 1000 Celsius is predicted from previous investigations. However a slightly higher temperature was expected during the trials due to high ambient temperatures and minimal wind disruption to the flow. Expected time of flight values was in the range 4.7 to 4.8ms.

It is evident from Figure 74 that a large number of samples give a time of flight below this range but consistently at approximately 4.5 ms.

Data point (33) represents the last measurement made prior to flame extinction and the remaining data points indicate the corresponding reduction in gas temperature. For each sample shown, a correlation profile capture was also recorded to investigate any correlation failure properties.

Due to the spread of data on Figure 74, the correlation profiles for each flight time measurement were examined. For example, data points (10), (14), (17), (20), (23), (25) and (29) were checked against their corresponding correlation profiles and all exhibited the same failure mechanism as described in section (7.6.2). Figure 75 gives the correlation capture profile for data point (9) and Figure 76 for data point (10) respectively on Figure 74. The correct correlation is made on Figure 75 but not on Figure 76 and this is also the case for most of the other data points mentioned above, (10), (14).....(29). Measurements represented by data capture points (4) through (9) failed during combustion startup procedures.

## **8.2.4 PRBS signal performance**

### **8.2.4.1: Ambient conditions**

The implementation of the PRBS technique provided a range of further obstacles under both ambient and hot conditions. Due to the continuous nature of the signal, any physical effects such as reflections introduced during signal transmission can cause severe signal degradation. Care was taken to establish a reasonable line of sight for transmission reducing the effects of physical obstacles as much as possible. Under industrial application conditions most furnaces are enclosed and fairly anechoic, hence this did not invalidate the experimental premise.

Deterioration of the soundpipe bend also initialised reflections so these pipes were also removed and replaced with direct line of sight piping, which was not a problem due to the low radiation levels at this position of the fire rig.

The problems associated with the demodulation of the received signal with noise were evident with installation of the system to the fire-rig. Even under ambient conditions the performance was poor, Figure 77, due to the inability of the demodulator circuit to cope with even wind generated noise on the received signal. The noise is clearly

visible on the low clock frequency (<100Hz) received signal. As the clock frequency is increased the demodulator performance reduces further. The signal was unstable under ambient conditions, at lower clock frequencies, with continuously fluctuating properties that produced, in some cases, the loss of entire signal sequences. At higher clock frequencies the signal is more stable but the effectiveness of the demodulator is reducing. The signal is completely lost with the initiation of combustion and hence no result is possible.

Investigation into the performance of the demodulator led to an analysis of the raw modulated received signal, a profile of which is shown in Figure 78. From the plot it is evident (as opposed to the demodulated output on the previous plot), that this signal is very “clean” of noise and therefore would provide a very good correlation result. The important components are the high and low frequency parts of the profile which represent the high and zero level of the PRBS respectively. The two different frequency levels are clearly defined and should present no difficulties to a demodulator.

An important issue relating to the profile is the difference in amplitude between the high and zero frequency levels of the modulated PRBS signal. The higher frequency PRBS components are reduced compared to that of the lower frequency. This may be due to the mechanical limitations of the compression driver at the higher frequency or performance loss associated with the modulation circuit. It is evident that the modulating circuit has difficulty achieving an equal balance at its output.

The properties of the demodulated output signal is further promoted by a correlation with the modulated input signal that provides a high quality correlation. The results of which are illustrated on Figure 79, which is similar in profile to that of the chirp signal correlation profile. The quality of the correlation indicates that the constituent signals involved should easily provide enough information for a high-resolution measurement and hence the problem is restricted to the demodulator in this case.

It was therefore concluded that the raw modulated output signal should be recorded and demodulation applied separately, the most likely method being via software processing.

### 8.2.4.2: Combustion conditions

A typical result, showing the modulated output signal from a hot test running 0.03 kg/s mass flow rate of propane, is shown on Figure 80. The separation distance between the point of transmission and the receiver was 3.14 metres relative to ambient conditions. The centre transmit frequency was reduced to 3.88 kHz to allow for the introduction of the band pass filter which was essential to the method. Due to time restrictions, a higher centre frequency band pass filter could not be obtained. The transmitted frequencies were therefore reduced to 3.0 kHz and 4.2 kHz for  $f_0$  and  $f_h$  respectively. The clock frequency was 1.5 kHz.

The plot clearly indicates the structure of the PRBS with areas of lower frequency signal and more limited areas of higher frequency signal in between. The level of higher frequency component available is significantly reduced compared to the ambient tests, but the lower frequency component appears relatively unaffected. As with the ambient trials, the higher frequency component amplitude is reduced in magnitude in comparison with the lower frequency constituent.

To improve the performance, the centre frequency should be higher, as indicated by the combustion noise and signal evaluation trials. During the experimental investigation the transmitted PRBS signal was clearly available above the combustion noise, especially at higher frequencies ( $> 4\text{kHz}$ ). Ideal operation would take place at frequencies over 5 kHz possibly even approaching 10 kHz. The current experiments were frequency limited due to the limitations of the modulating circuit.

The performance of the modulated signal components is related to the compression driver output profile and the modulation depth on the frequency modulating circuit. The circuitry is a limiting factor in the performance of the technique, when the modulation depth is low, the low frequency component of the PRBS dominates the signal whilst the high amplitude component is reduced. When the modulation depth is increased, the domination is switched over to the higher frequency component. Due to the nature of the circuit it was impossible to achieve an equal balance between the two and hence the process suffered.

### **8.2.5 SNR and attenuation measurements**

Attenuation levels were recorded at the transmitted signal frequency only. In most cases this was 5kHz. The results show an overall signal loss of approximately 20 dB over the path length of 3.4 metres. This corresponds to an attenuation level of just over 6 dB per metre. The level of signal reduction indicates that the influence of the thermal (molecular) relaxation processes is negligible at this frequency and is in agreement with the calculated values given in section (5.10).

### **8.2.6 Thermocouple temperature measurements**

Figure 81 shows a temperature versus time profile measured at the upper exit of the compartment fire rig using a row of thermocouples parallel to the pyrometer “line of flight”. The measurements were taken for a mass flow rate of 0.1 kg/s propane. These measurements can be used to validate the pyrometer results and are in good agreement with the chirp signal performance. A carefully calibrated set of trials would be useful to enable comparison of the differing methods.

## Chapter 9

### Discussion

A review of current temperature measurement methods indicates the need for continued innovative research into new techniques. A combustion system is a difficult environment to deal with due to primary parameters such as density, velocity and temperature, as well as more complex mechanisms such as turbulence and heat transfer. Thermocouples are heavily relied on in many industries and until a cost effective alternative is produced this will continue. Optical techniques are making significant progress but suffer drawbacks, (including cost), that an acoustic based measurement system can address. Where high radiation levels and large path lengths are present the acoustic pyrometer may play an important role.

The samples of combustion and background noise, recorded at various furnaces and kilns, formed the initial start point of the project and clearly identified the sound pressure level versus frequency relationship present at most plant. In each case the higher levels of noise were restricted to the lower end of the frequency spectrum. This supported investigation of the performance of a higher frequency transmission signal. The experimental results compared favourably with other experimental work. However, longer-term trials would be a useful addition to the database. The derived parameters such as SNR and attenuation levels allowed estimation of the likely requirements for an acoustic measurement technique but did not divulge a clearly defined frequency operating window.

The choice of a suitable sound source was investigated with the aim of identifying both a novel component operating on a freely available energy source at most plant, and a more standard electromagnetic device.

The Hartmann Generator initially proved to be an exciting choice due to its excellent output levels and reasonable frequency control capabilities. The major drawback proved to be the performance of the driving mechanism for the generator, the solenoid. With current improvements in fluid control devices, (such as fluidic switches with no moving parts), the application of the generator may yet be possible. However the reliance of signal processes such as the PRBS correlation method on

faster and faster clock rates for more clearly defined correlation profiles, means that the Hartmann Generator as a contender for the measurement method is unlikely.

The compression driver proved to be a high quality, rugged device, which stood up to punishing temperatures, acid gases and vibration under industrial conditions. Due to its mechanically influenced output, the required transmitted signal had to be carefully adjusted or coordinated in line with the output profile. Care had to be taken to avoid disturbance to the delicate system circuitry from the compression driver due to the lack of electromagnetic shielding. Many compression drivers are available with shielding and are therefore recommended for future applications.

With the use of improved signal processing to overcome combustion and background noise, rather than using a much higher amplitude signal to force the sound across the system this will allow the choice of smaller compression drivers of lower power which occupy less space. The microphone used provided suitable performance over the operating range but due to its delicate construction, care had always to be taken. A more ruggedised component would be an improvement, or alternatively, a differing protection method might be found. The use of air-cooling would be suitable but the addition of extra air to a system is never welcome by combustion control.

The introduction of horns did not enhance the sound transmission, most likely due to the higher frequency signals used, which have a wavelength that is small compared with the characteristic dimension of the horn.

The implementation of a pink and white noise generator provided a variable, calibrated sound source, which was particularly useful for comparative experiments at various locations and environments. The generator was used to measure the performance of important system elements such as the transmitter, membrane, injection method and attenuation levels.

The investigation into the use of membrane protection produced some useful results. The main influences on the sound transmission were the thickness and density of the material. With decreasing sectional thickness, the level of sound loss reduces and with careful choice of density, as well as the physical properties of the material, a suitable choice may be identified. In this case a composite nylon nitrile material proved to have the correct properties such as acid resistance, high temperature resistance, low average density and thin section availability. The signal loss of 10-15dB due to the

membrane could not be improved on and since some systems may require protection on both transmitter and receiver, this is a severe drawback.

Creating an airtight seal to avoid convective heat transfer, and placing an angle in the receiver and transmitter piping to counteract the effects of radiation means that the main problem will stem only from conduction and acid gases. This proved to be the case at several high temperature applications (1300C, HVB soaking pit) as well as at the fire-rig trials.

An important result of the membrane investigation was the effect of position of the protective component relative the sound source or receiver. The “near field effects” generated due to poor positioning can cause extreme degradation to the transmitted signal format.

The abolition of a membrane type protection system is further promoted due to the requirements of the signal processing. The membrane, especially for higher frequencies, can modify the signal such that for more complex signals such as PRBS (especially since it is a continuous signal), the result is to disturb the signal components. Hence continuous signals are not suitable for membrane type transmission. Where membranes are present the transmitted signal should be of short duration where possible.

There are many parameters present in a combustion environment that affect the transmission of a sound signal through it. The work by Kleppe<sup>18</sup> has identified the effects of primary combustion parameters such as velocity and temperature gradients as well as particles in the gas<sup>46</sup>. The present work has accurately quantified the effects of unknown gas composition on the acoustic technique and this investigation in conjunction with an analysis of attenuation mechanisms now provides an improved database for future pyrometer design.

The calculations for attenuation due to the molecular relaxation mechanism were in good agreement with the experimental results recorded during the fire-rig trials indicating that the frequency operating window for such a measurement method is not restricted to lower frequencies (<3kHz), as suggested by Kleppe et al. This is supported by the combustion and background noise measurements that re-enforce the argument for operating at higher frequencies. With modern control methods and

microprocessor technology, the resolution at higher frequencies due to data collection capabilities and microprocessor speed are no longer limited.

The format of the transmitted signal became an important issue as the project progressed. The chirp signal was initially a prime candidate due to its efficient generation and cross correlation performance. Early trials indicated that the signal was not affected by local equipment and excellent transmission was seen under ambient conditions. As noise was introduced to the system the correlation performance was reduced at higher SNR due to the increasing magnitude of secondary correlation peaks. However at lower SNR the method remained of high quality.

The introduction of PRBS saw a shift to a continuous form of transmitted signal that required not only a different type of software capture but also necessitated careful system design. Care had to be taken with a continuous signal, since physical obstacles placed in the signal path will cause disruptive reflections which are carried on to the receiver. The generation of a PRBS type signal is quite simple; however the software processing is more computationally expensive when compared to the chirp signal due to the larger arrays generated whilst capturing a stream of signal over a correlation window. This is necessary to achieve a high level of resolution in the cross correlation process and hence produce an accurate measurement

As the process is simplified and with simple machine code programming used for any design system the calculation time will be reduced from 30-60s to much lower. The chirp signal correlation for a similar correlation window of about 6-8ms takes only several seconds.

With the introduction of “window tracking” where the system will assume that the temperature variance will be small between each measurement period, the computational time can be reduced further until we are much closer to real time measurement. However, during start-up when the temperature variations are large this would not be appropriate.

The comparative investigation into the performance of the different types of signal, PRBS, chirp and pulse, with the various processing methods, edge detection and correlation, provided a valuable benchmark for future applications involving signals in noise. The experimental work highlighted errors due to the misinterpretation of the

positions of edge arrival or correlation peaks due to instantaneous deviations caused by noise and these become more severe as signal to noise amplitude ratios decrease.

Population errors in the “mean time of flight” are estimated for the different measurement strategies, and it is concluded that the PRBS, combined with correlation, can provide the lowest errors when operating in high noise environments. A detailed examination of the source of error for each of the detection strategies has shown that PRBS is better resistant to high noise levels and is capable of remaining within a prescribed 0.5% error level for noise deviations which take the noise/signal amplitude ratio as high as 3.5.

# Chapter 10

## Conclusions

### *Transmitter and receiver design.*

The Hartmann Generator was found to be a suitable mechanical sound generator for possible application to an acoustic temperature measurement system. Two generators were designed and constructed to operate at 10kHz and 40kHz. An evaluation of their performance produced high sound pressure levels in excess of that possible with standard compression drivers. Due to the availability of shop (compressed) air at most plants and no need for membrane protection the Hartmann Generator establishes itself as an exciting possibility for various functions. However, application will depend on the ability to drive the generator at high switching rates that at the moment are limited to levels below those required.

### *Combustion and background noise measurements.*

A number of samples of noise profiles (combustion and background noise levels) have been measured at a variety of combustion applications (incinerator, soaking furnace, cement kiln and gas fired furnace). The profiles indicate regions of low noise allowing selection of a frequency “window” of maximised signal to noise (SNR) ratio. In general the highest levels of noise are located towards the lower frequency range (<4kHz). The tests however do not provide sufficient information to determine an optimum frequency window.

### *Sound transmission measurements.*

Tests were carried out in which a source signal from a calibrated sound source (compression driver) was transmitted through the combustion environment via an inspection hatch to a calibrated receiver (microphone). In this way a generic SNR vs. frequency relationship was established, which included transmission effects present. The levels of attenuation found highlighted the importance of an investigation into the parameters affecting transmission. Hence when assessing the characteristics of the

system, all components must be considered, this includes any protective membranes used to shield electronics from the corrosive gases. The effect of thin membrane materials such as nylon nitrile on the sound transmission over a range of frequencies was quantified.

### *Parameters affecting sound transmission.*

The work in this section attempted to quantify the attenuation parameters that affect the transmission of the source signal through the combustion environment. The overall levels of attenuation in various combustion systems were shown in the previous section, however the levels at high (ultrasonic) frequencies must be considered due to the process of molecular relaxation. An investigation was carried out to identify the likely attenuation levels present using the small amount of data available. The results indicate that the levels of absorption rapidly increases at frequencies far greater than 10kHz. The experimental work indicates that signal attenuation due to thermal relaxation is negligible whilst operating with the current design range of frequencies (<10kHz).

Errors associated with the acoustic technique due to gas composition uncertainty arising from fuel variation or post-combustion mixing in combustion systems have been quantified. The likely errors in calculated temperature due to incorrect assumptions on H/C ratio and local oxygen levels are around 0.5%.

The effects of high velocities present at a turbine combustor exhaust or high velocity burner were also investigated and the results indicate that in these situations any modified velocity component must be accounted for. This may require modification of the acoustic technique to measure the main axial velocity component whilst calculating the temperature.

The effects of the attenuation mechanism “molecular relaxation” were approximated by a simple theoretical analysis based on the polyatomic gas, carbon dioxide. The calculations indicate that the signal loss will be small in the frequency range < 10kHz. For frequencies > 10kHz the level of absorption increases rapidly. The experimental results from the fire-rig trials indicate total levels of signal loss per metre of 5-10 dB, which produce levels of attenuation due to the relaxation mechanism of 2-7 dB per metre which is significant.

### *Signal processing performance trials.*

Several signal types were identified for application to the acoustic, technique including a simple pulse (i.e. squarewave), a chirp (i.e. sinewave) and a pseudo-random number sequence (i.e. PRBS). Further signal processing was used, via the application of signal modulation, edge detection and correlation methods, to increase the performance of the technique. Each type of signal was evaluated in the numerical analysis in terms of their ability to reject noise. The PRBS was found to be a better signal at higher noise levels (lower SNR), whilst the chirp was a suitable choice at lower noise levels.

### *Experimental application*

For combustion conditions at a level similar to that found in industrial furnaces and kilns the signal was successfully transmitted through the measurement environment and collected at the receiver. The format of the received signal in its raw modulated form indicated a similar structure to the modulated transmitted signal even when transmitted at a non-optimum frequency position.

The conclusions therefore drawn, are that an improvement in performance would be seen by designing a band pass filter, so that transmission can take place at an optimum frequency window of 4-5kHz or higher, followed by carefully designed demodulation or software demodulation where possible.

Further advantages are envisaged with removal of the modulation altogether thus reducing the complexity of the system by one stage. This step requires either a suitable sound source being found capable of handling the PRBS constituent profiles or designing a pseudo-random number based signal, using a different type of profile such as triangle waves. This capability was available on an early PRBS circuit signal generator.

# Chapter 11

## Recommendations for Future Work

### *11.1 Reconstructing or Mapping a Temperature Field*

#### **11.1.1 Introduction**

One important issue related to the current work is the use of signal processing techniques to reconstruct temperature fields within a combustion system utilising measurements made by an acoustic pyrometer. The availability of such maps are important in the design of boilers and furnaces since they can highlight “hot spots”, areas of higher temperature where, for example, nitrogen oxides (NO<sub>x</sub>) may be formed.

The use of acoustic energy to produce images is not new. In nature, bats and dolphins have remarkable acoustical imaging systems far beyond those available to the engineer today. Modern applications make full use of the digital computer such as real time diagnostic equipment in hospitals (ultrasound, X-ray) and acoustical flaw detection systems for containment vessels in the nuclear industry.

In general three types of acoustical imaging systems<sup>67</sup> have been developed:

1. Intensity Mapping Orthographic Systems
2. Pulse Echo Systems
3. Phase-Amplitude Approaches

The first method is perhaps the simplest. The system essentially produces a two dimensional map of the transmission of sound through an object. The sound is attenuated as it passes through the body and the intensity of the sound on the other side is measured as a function of lateral position. The resulting intensity map is the image. This method is the basis for the scanning acoustic microscope (SAM) which is commercially available.

The second method (pulse-echo) has found applications in ultrasonic flaw detection for weld inspection and nuclear power plant containment vessels, as well as many clinical applications. In most cases the timing of return echo's to match the location of a scattering point in relation to an electronically controlled reference array, produces a two dimensional image of the subject. In both of these methods the image produced utilises the amplitude (intensity) and/or time of flight of a sound signal.

The third method, phase-amplitude approach, is most applicable to the current work. Some of the phase-amplitude systems developed operate similarly to intensity mapping methods, while others make use of transducer arrays and fast Fourier transform (FFT) signal processing to produce images. Hybrid pulse-echo and holographic techniques have also been developed. Relevant to the current work is acoustical tomography that combines holographic imaging with multiple projections. Acoustical tomography forms the ultimate in data acquisition and signal processing complexity for acoustical imaging.

Each method is based on a fundamental algorithm, which ranges in complexity from fairly simple in the intensity mapping and pulse echo systems, to highly complex in the phase-amplitude systems. It is the process of determining how best to acquire and process data that forms much of the basis of current work on the subject.

### 11.1.2 Phase-Amplitude Imaging: Tomography<sup>68</sup>

The difference between phase-amplitude imaging and other methods is due to the measurement and use of *phase* as well as *amplitude* and *time of flight* information. The key property of the acoustical transducer that makes it useful for phase measurement is the fact that its electrical-acoustical, input-output relationship is linear. Therefore it is possible to directly measure the complex amplitude of an acoustical signal as a function of spatial location and time. Hence for the acoustic pyrometer method a number of measurements of phase, amplitude and time of flight are made by several transducers located around the perimeter of a combustion system to encompass a cross sectional area. The collected measured data from all the transducers at their various locations is converted from analogue to digital and fed into the digital computer. The second task is to reconstruct the temperature field from this data. The reconstruction method is based on approximating a solution to the wave

equation for the acoustic field and also the relationship between the Fourier transforms of the transmitted signal and the tomogram to be reconstructed. There are many problems associated with the reconstruction method due to the approximations made and choosing the correct type of algorithm, as well as problems caused by noise, diffraction and resolution.

It is important to resolve the issue as to whether tomographic signal processing is suitable for the acoustic pyrometer method in terms of the overall accuracy obtainable with a differing number of transmitters and receivers (transceivers), for a multi-path system. In order to set up a multi-path system, a minimum number of transceivers will be required and these must be located around the perimeter of the combustion system. This significantly increases the cost and complexity of the system in terms of component costs as well as modification to existing combustion systems, in order to apply the multi-path pyrometer. It is important to look at the application of tomographic imaging at a fundamental level before getting into the complexities of the actual reconstruction method, by answering the following questions;

1. How many transceivers are required to produce a sufficiently accurate temperature reconstruction?
2. Is the number of transceivers required realistic in terms of application to real furnaces?
3. How much extra information is a multi-path system going to produce compared with using one or more single path systems?
4. What is the likely stability of the tomographic reconstruction method based on its foundation of approximations and complex algorithms?
5. Will the method be easily transportable to different combustion systems?

Previous work carried out has attempted to answer some of the above questions. The investigation by Ryzhov et al.<sup>69</sup> used a Fourier series to construct the temperature field from the measured time it took for sound waves to travel over different paths. Validation of the system was attempted by constructing and solving for an arbitrarily specified temperature profile. This shows how the number of paths and the number of terms in the truncated Fourier series influenced the accuracy of reconstructing the

temperature field. The work highlighted the large number of paths required (in this case 36) to achieve a reasonable temperature profile and the difficulty in achieving this number, due to the limited number of available sight holes in which the acoustic transmitters and receivers could be located. The work of Bramanti et al.<sup>70</sup> presented two classes of reconstruction algorithms based on the acoustic pyrometry method. The authors were restricted due to small amounts of experimental time of flight data from combustion systems on which they could base their analysis; an area which this current work aims to further.

The results of the current work may be used to improve the time of flight information from transceivers located around a furnace or boiler, but this is only one step in the tomographic process due to the need for improved reconstruction algorithms. The move toward low power transceivers resulting from the numerical investigation in the current work means that the size of the transceivers may be substantially reduced, hence improving the accessibility possibilities, which is restricted at most furnaces. The application of the technique may be attempted on furnaces where high radiation is present. This is an area where similarly emerging techniques utilising optical or laser technologies are often restricted. Results would provide a useful comparison to CFD modeling results.

## ***11.2 Emission Control: Volumetric Flow through a Stack***

A major challenge of emission control regulations is the continuous real time measurement of the flue gas volumetric flow rate and moisture content. These regulations not only apply to large-scale power generation plants but also to smaller scale activities, such as municipal incinerators. Measurement of volumetric flow is important in many industries for example flow through pipelines in the process industries so the technique may have more general applications.

If two transceivers were placed as shown on Figure (11.1), the transceiver (1) would generate a sound wave that would travel with the gas flow to transceiver (2). Alternatively the signal from transceiver (2) would travel against the stack flow to transceiver (1). Hence the signal from transceiver (1) would include the velocity component from the flowing gas and the signal from transceiver (2) would have the addition of a similar but negative component. Thus the average velocity of the

gaseous medium may be calculated as follows, starting with the velocity components in opposing directions from the transceivers, equations (11.1):

$$c_1 = \frac{d}{t_1}, \quad c_2 = \frac{d}{t_2} \quad (11.1)$$

Where  $c$  is the velocity (m/s),  $d$  is the path length in metres and  $t$  is the time of flight(s). The average velocity is therefore over the path length is therefore;

$$\bar{U}_p = c_2 - c_1 = d \left( \frac{1}{t_1} - \frac{1}{t_2} \right) = \frac{x}{2 \cos \theta} \left( \frac{t_2 - t_1}{t_2 t_1} \right) \quad (11.2)$$

Where;

$\bar{U}_p$  = path average velocity

$d$  = distance between transceivers

$\theta$  = angle in degrees

$t_1$  = flight time of the sound with the gas flow

$t_2$  = flight time of the sound against the gas flow

Equation (11.2) gives the average path velocity and not the desired volumetric average flow velocity unless the profile is perfectly uniform. The profile will, however, never be totally uniform due to viscosity at the stack walls. This is therefore an error that must be accounted for or accommodated, by a second instrument. A second drawback is that the transducers must face each other at an angle to the stack wall, the lower transducer being exposed to moisture. The instruments must be located far enough away from the duct inlet so that the velocity profile of the stack gases is fully formed (20 to 25 diameters) i.e. require plugged flow conditions. Rectangular ducts require multiple senders. Current system uses transceivers in conjunction with a pitot tube and thermocouple technology.

The Hartmann Generator identified during the current investigation seems to suit this type of application, due to meeting the following criteria;

1. Suitable frequency range identified as approximately 5kHz, however the Hartmann Generator can operate at higher frequencies if necessary.

2. Due to its simple design, the Hartmann Generator can be constructed from anti-corrosive materials such as aluminium which will resist attack from moisture or any similar gases or liquids present. This also makes it a lightweight construction.
3. It is effectively self-cleaning.
4. Requires a relatively low activation inlet pressure that would certainly be available at most plant.

Similar technologies use acoustic transceivers to measure the height of grain in storage hoppers up to distances of 30 metres. Fast acting valves are now available that run at over 10 kHz cycles time ( $<0.1\text{ms}$ ) and the cost is reducing. Hence the Hartmann Generator may find a suitable application.

### ***11.3 Gas Mixture Analysis***

The aim throughout the current work was to produce a working temperature measurement system utilising the relationship between the speed of sound in a gas and the temperature of that gas. However as noted earlier in the report, the products of combustion in a furnace environment consist of many gases, such as carbon dioxide, nitrogen and water. The effect of the different gases on the performance of an acoustic temperature measuring system has been fully evaluated in terms of the systematic errors associated with an unknown gas composition. A simple investigation for carbon dioxide has also indicated the effects on the transmitted signal.

The results leads to the consideration of effectively using the acoustic pyrometer system to estimate the mixture ratio by using the acoustic temperature measurements and speed of sound values to calculate back to the acoustic constant, and hence estimating the composition of the gas.

Use of this data to control a combustion system through an accurate estimation of the mixture ratio of the combustion products, by matching acoustically measured temperatures to the composition curves, could lead to fuel savings and higher combustion efficiency.

## ***11.4 Application of PRN's with correlation to ultrasonic non-destructive testing.***

Recent research<sup>71</sup> into the use of different signals for signal power optimisation in ultrasonic non-destructive testing has led to a movement away from using chirp pulse compression, (signal correlation technique that uses frequency modulated pulses), to using a non-linear frequency modulated chirp. One reason for the non-linear modulation scheme is to reduce the side-lobe level produced by the compression pulses. However, moving from linear amplified sine wave chirps to frequency modulated square waves improves the energy of the transmitted signal, as the fundamental of a square wave has a higher amplitude than a sine wave. The amount of hardware is also reduced since fast digital to analogue converters is not required.

A further advantage may be found via the use of Pseudo-Random Number (PRN's) sequences using a similar process to that of the current work. A previous section (6.2.4) has described the use of frequency modulated PRBS and the advantages of its correlation profile over that of a chirp signal. These properties should also be applicable in ultrasonic non-destructive testing in terms of reducing systematic error and, hence, improving the accuracy of the measurement method.

## ***11.5 Specific Applications***

### **Fossil fuel-fired power stations**

Due to the deregulation of the U.K electricity market the major utilities have had to make significant changes to the way that they operate. With changes in the supply requirements to the national grid, power stations have had to react much more quickly to feed fluctuating grid demands and the effect of this is carried right back to the station infrastructure. Many of the older coal fired stations in the U.K. were built in the early 1960s and therefore have passed their predicted life span. Many now have a projected life expectancy up to 2020 and have to compete with gas-fired combined cycle power stations as well as newer, renewable technologies.

The pf-fired boilers have seen many modifications due to increasing emissions legislation and renewable obligations. These include, for example, the introduction of low NOx burners, air or fuel staging, flue gas recirculation, fuel reburn techniques and

in some cases co-firing of alternative fuels. Each modification will in some way change the operating profile of the boiler. Knowledge of the temperature and pressure profiles within a boiler is essential in order to ensure efficient operation. Changes in the temperature distribution can lead to damage to superheater or boiler tubes due to heat transfer levels greater than the critical heat flux. This then requires maintenance time and whilst this is occurring the boiler is not reacting to the electricity demands and a significant loss in revenue is entailed. Most stations use thermocouples located at various positions within the boiler and radiation pyrometers to check flame temperatures. Acoustic pyrometry appears a suitable candidate for application to this type of boiler due its ability to resolve over the path lengths and the technique could be integrated with the soot blowing systems. The benefits to the station would be a much more accurate knowledge of the temperature profile at various positions throughout the boiler. Transducers can be placed local to the burners as well as monitoring the effects of overfire air, reburning and flue gas recirculation. Higher in the boiler temperatures local to superheater tubes or positions where chemical addition takes place for Selective Catalytic Reduction (SCR) or Selective Non-Catalytic Reduction (SNCR) takes place. Both SCR and SNCR are critically temperature dependent and accurate temperature measurement within the boiler may ensure that these techniques have less variable performance.

# Figures

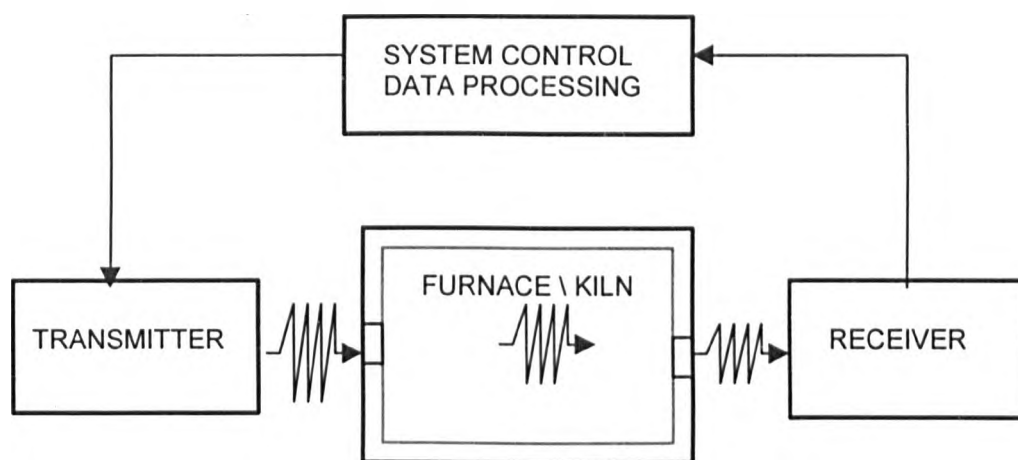


**Figure 1: Schematic of system components.**

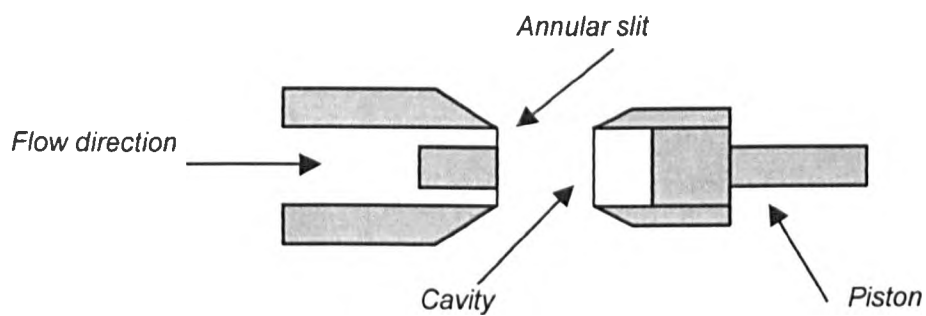


**Figure 2: The Cavity Resonator**

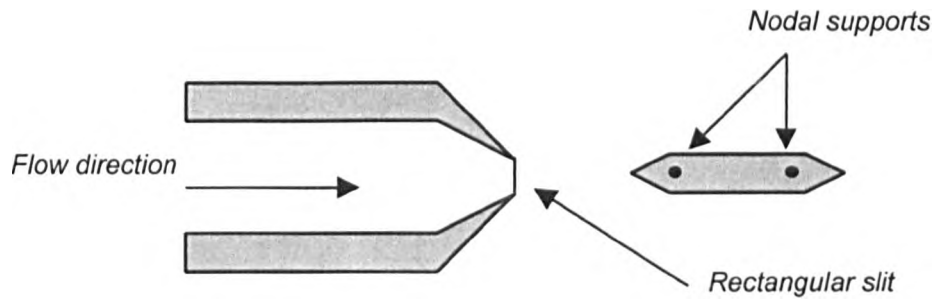


**Figure 3: The Wedge Resonator**

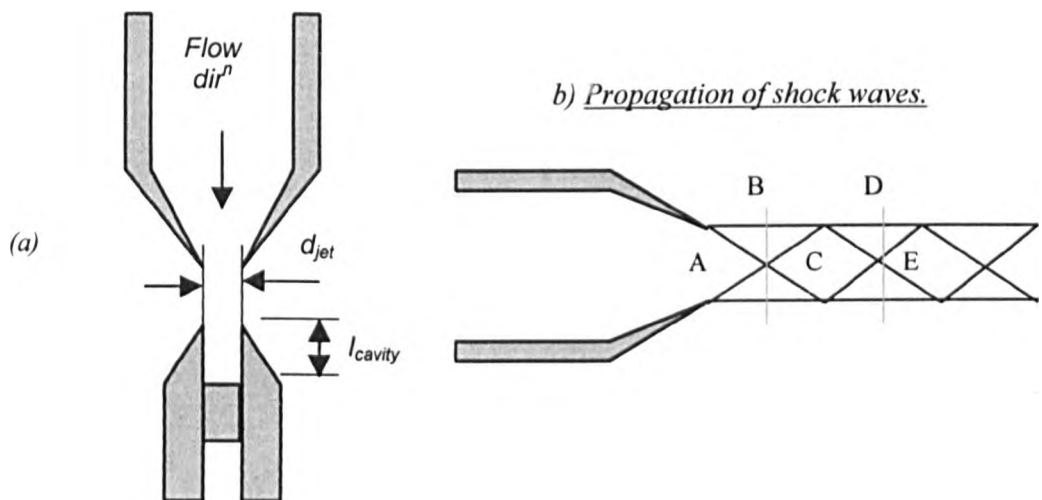


**Figure 4: Diagram of the Hartmann generator (a) and principle of operation (b)**



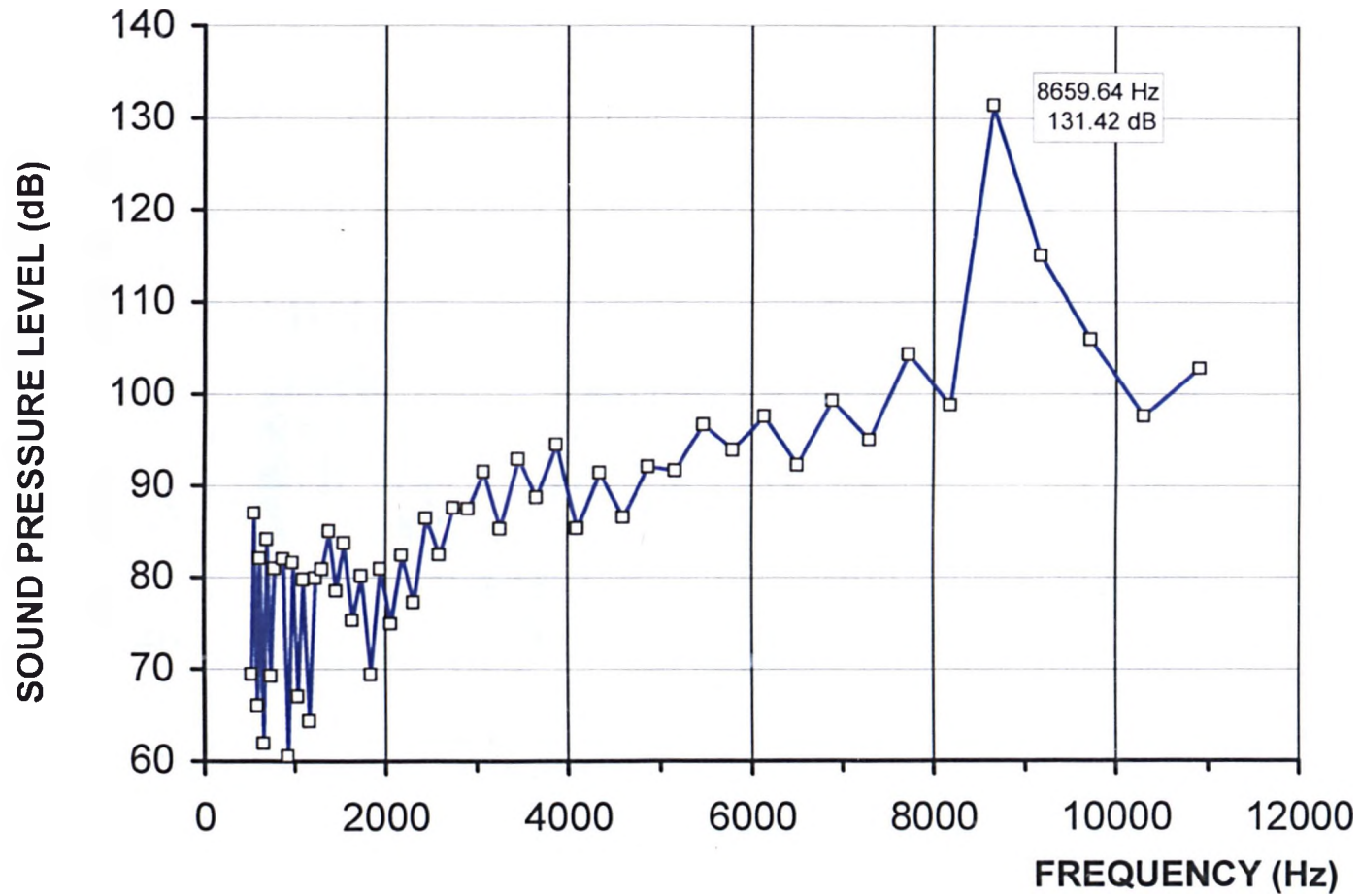


Figure 6: Sound pressure level versus frequency response for a pressure of 6 bar applied to the 10kHz Hartmann generator (x=1m)

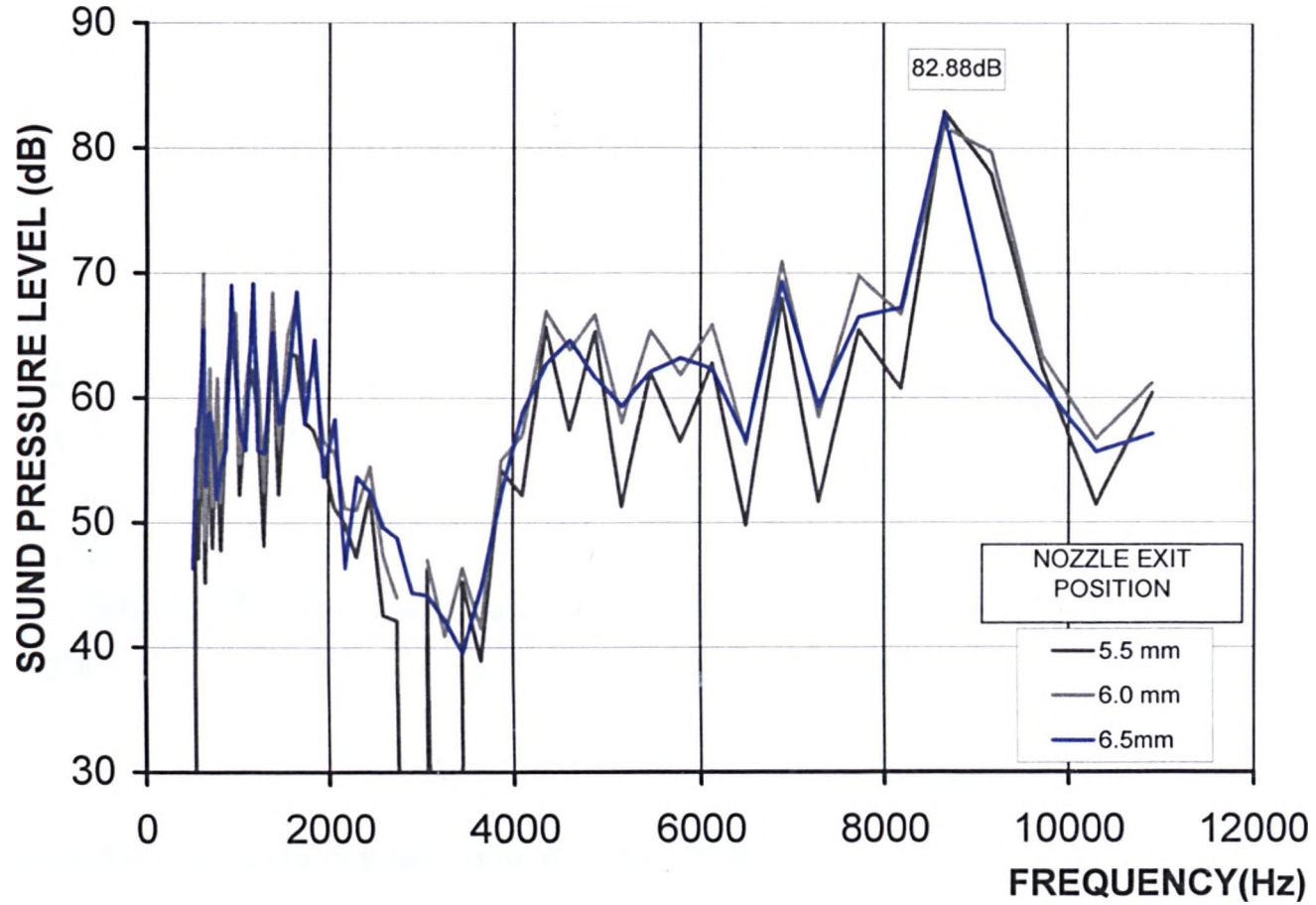


Figure 7: Output profile for a pressure of 6 bar applied to the 10kHz Hartmann generator with cavity movement relative to the generated instability zone ( $x=5m$ )

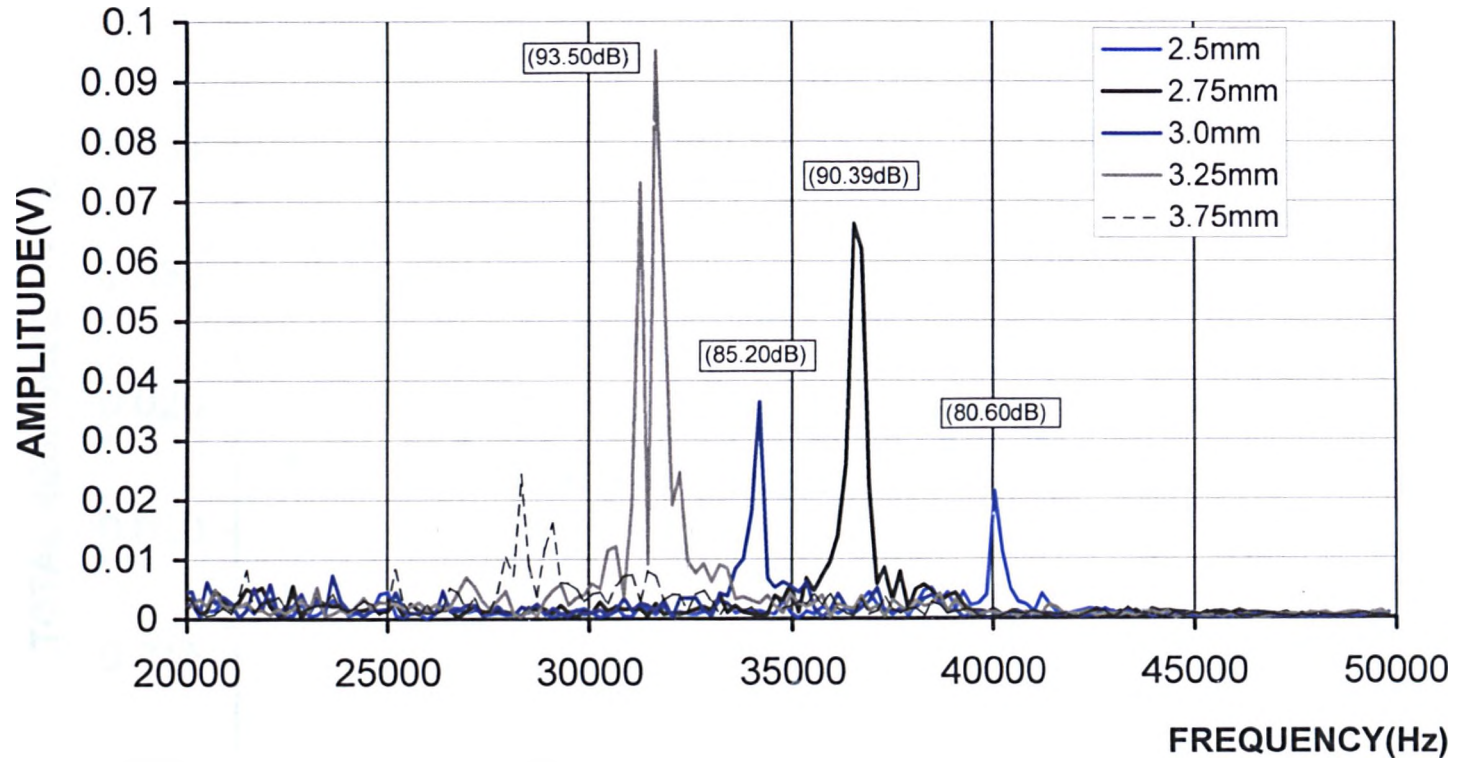


Figure 8: Output profile for a pressure of 6 bar applied to the 40kHz Hartmann generator with various nozzle positions relative to the instability zone

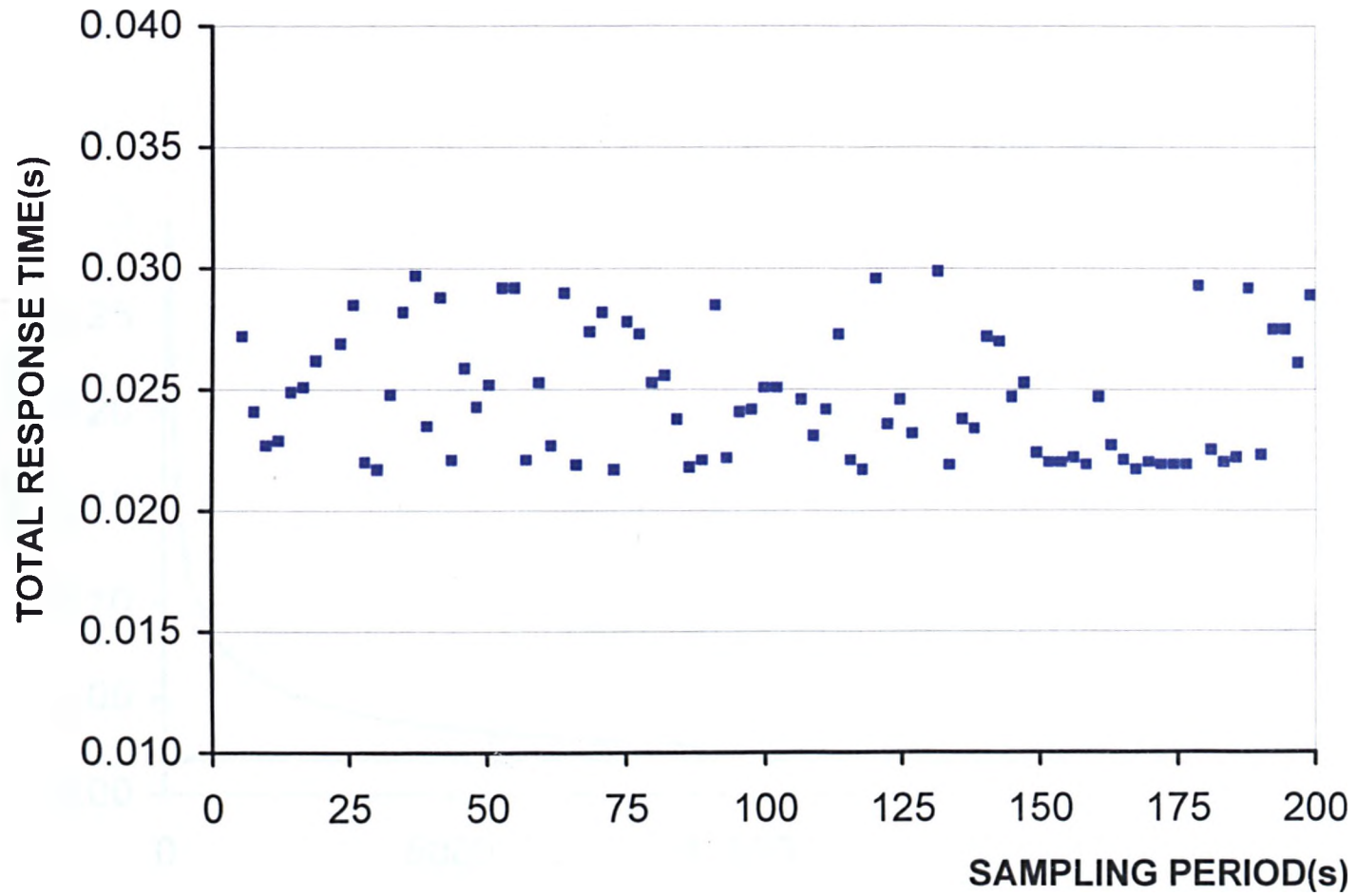


Figure 9: Variation in response time of the 10kHz Hartmann generator (including solenoid response = 0.010 to 0.015 sec.)

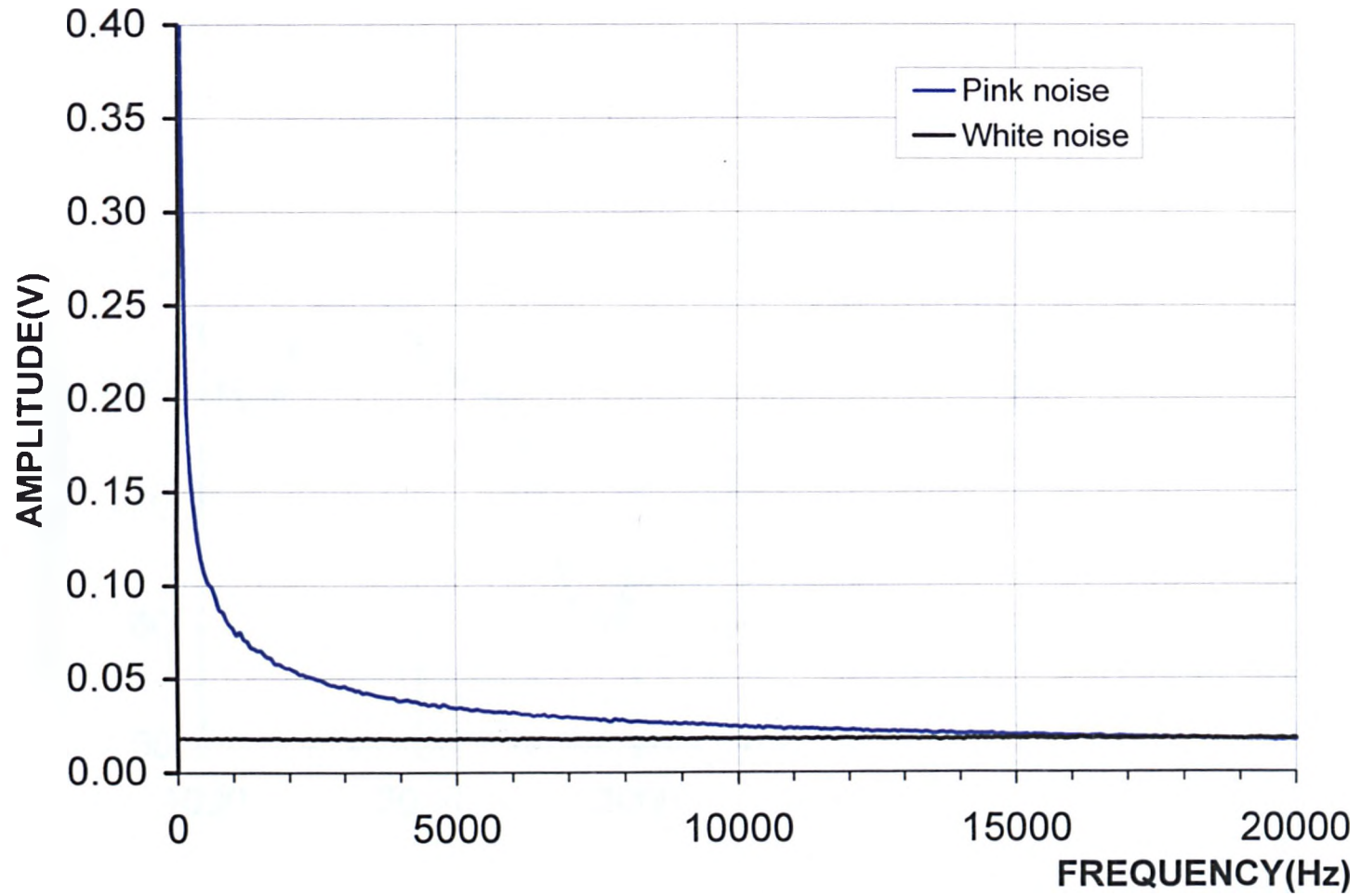


Figure 10: Raw output profiles of pink and white noise generated by the IVIE signal generator

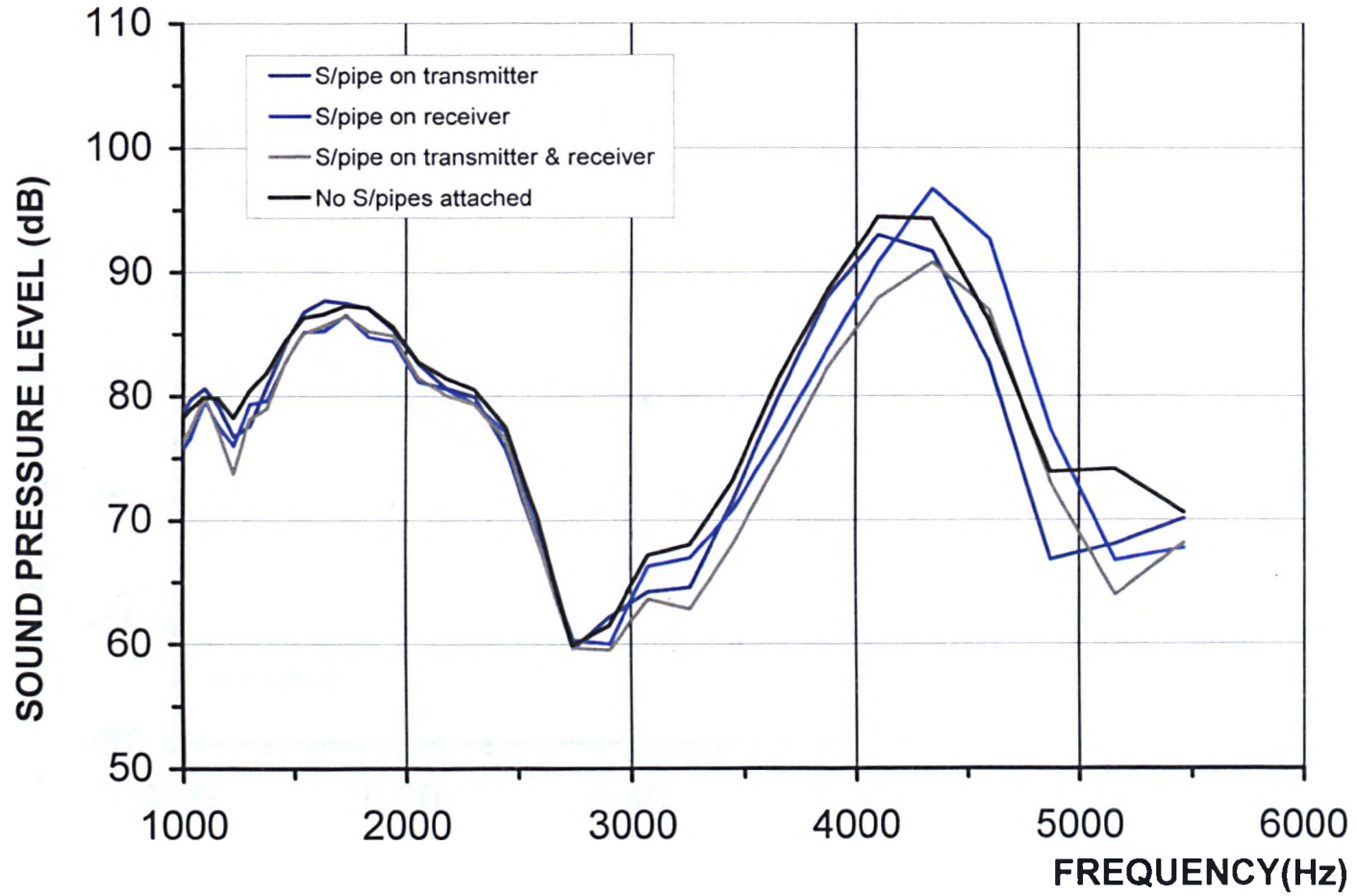


Figure 11: Plot indicating the effects of sound pipe injection on the transmitted signal under anechoic conditions

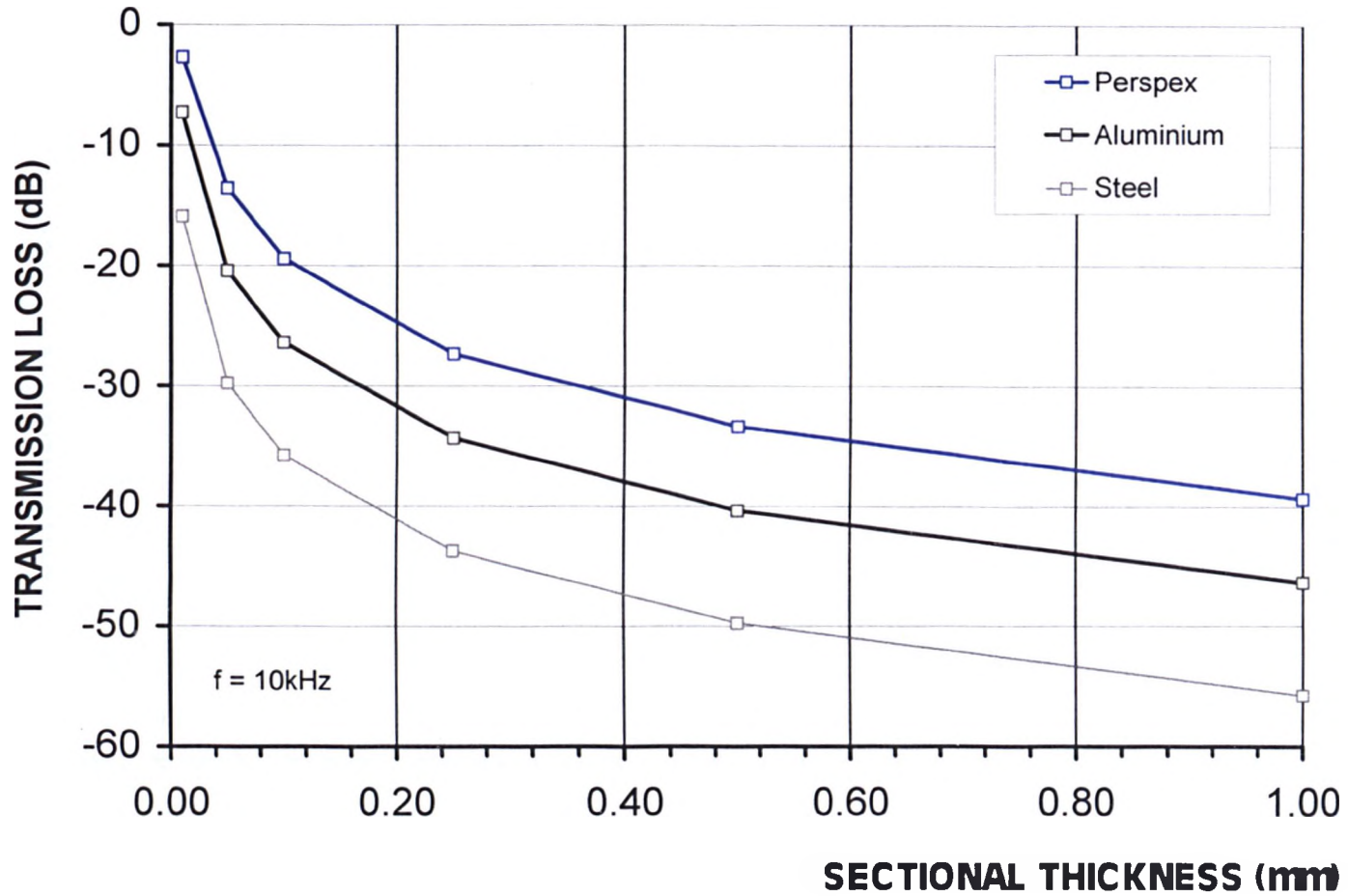


Figure 12: Theoretical sound power loss versus differing sectional thickness calculated for several membrane materials

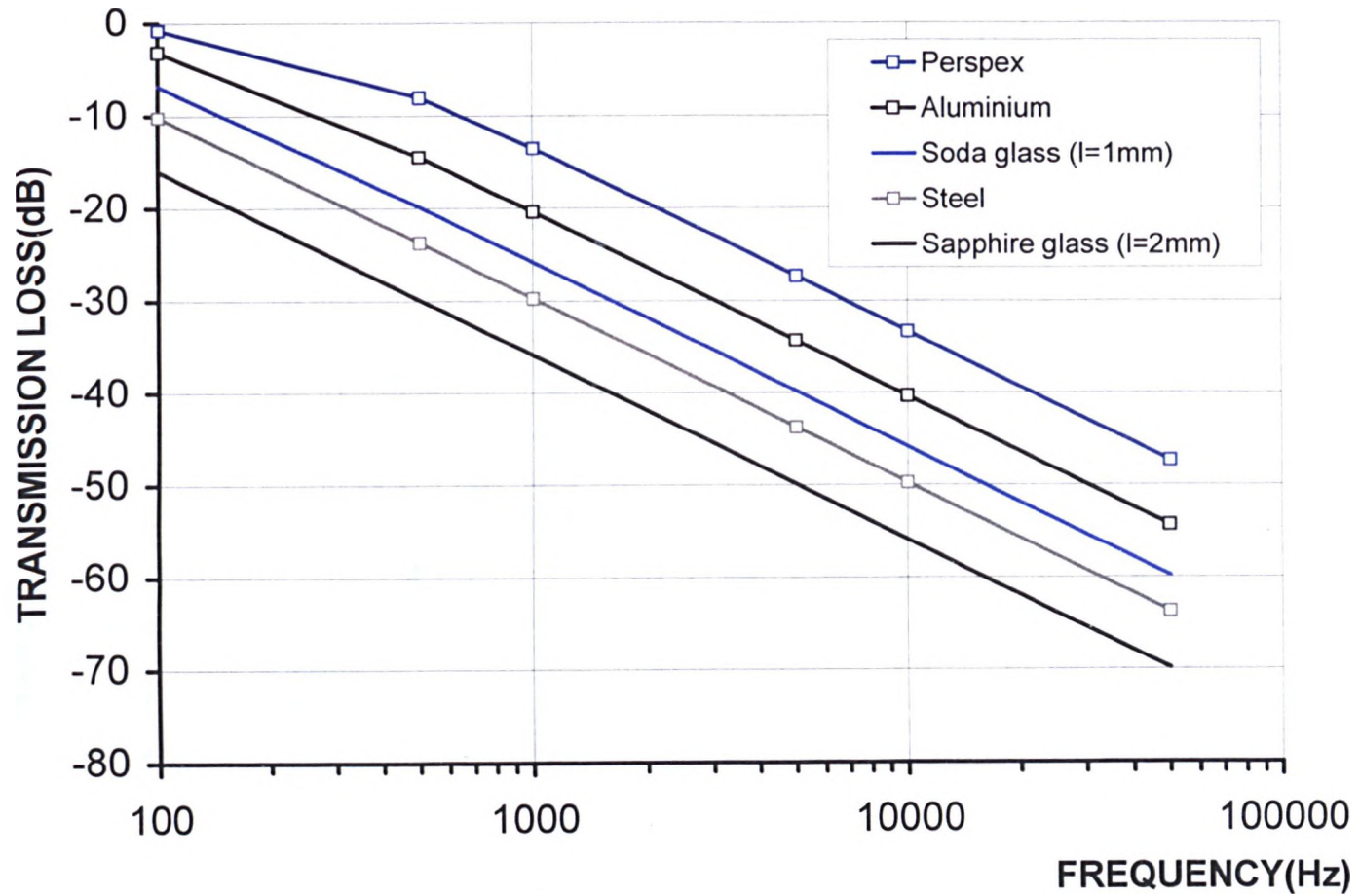


Figure 13: Theoretical sound power loss versus applied frequency calculated for several materials

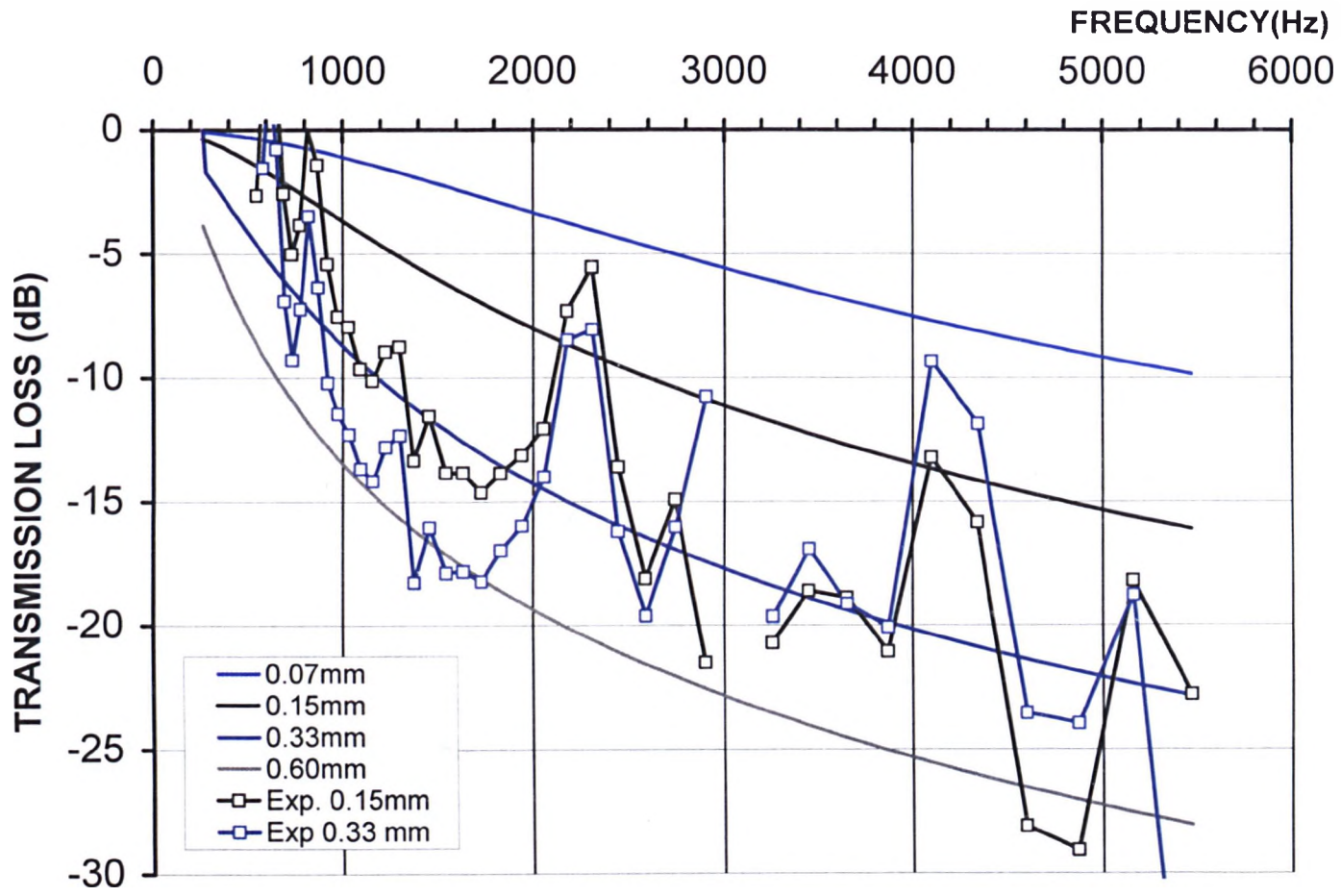


Figure 14: Theoretical and experimental sound transmission performance curves for various thickness of nylon nitrile membrane.

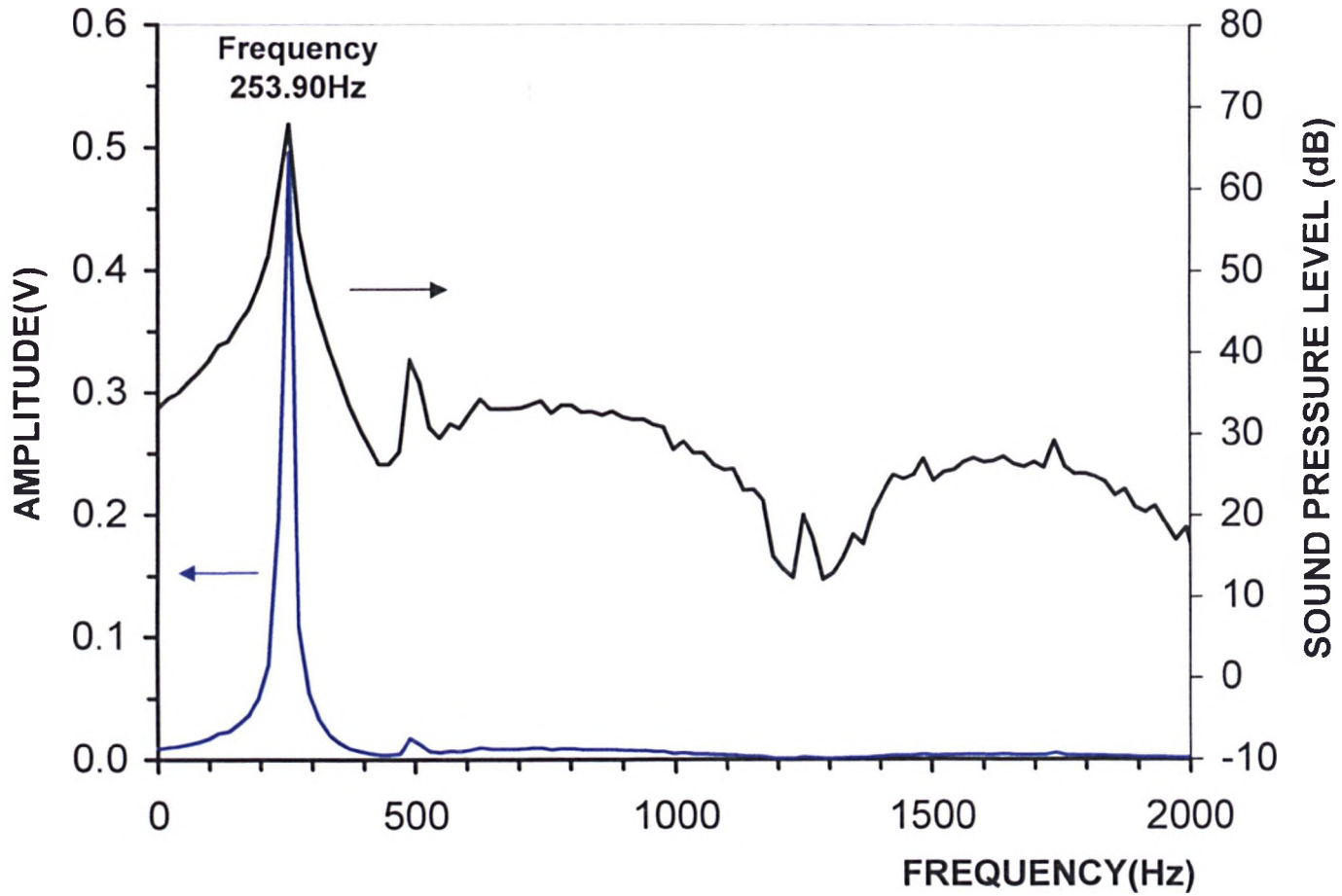


Figure 15: Plot showing the response profile of the Bruel and Kjaer type 4166 microphone to a calibrated pistonphone output.

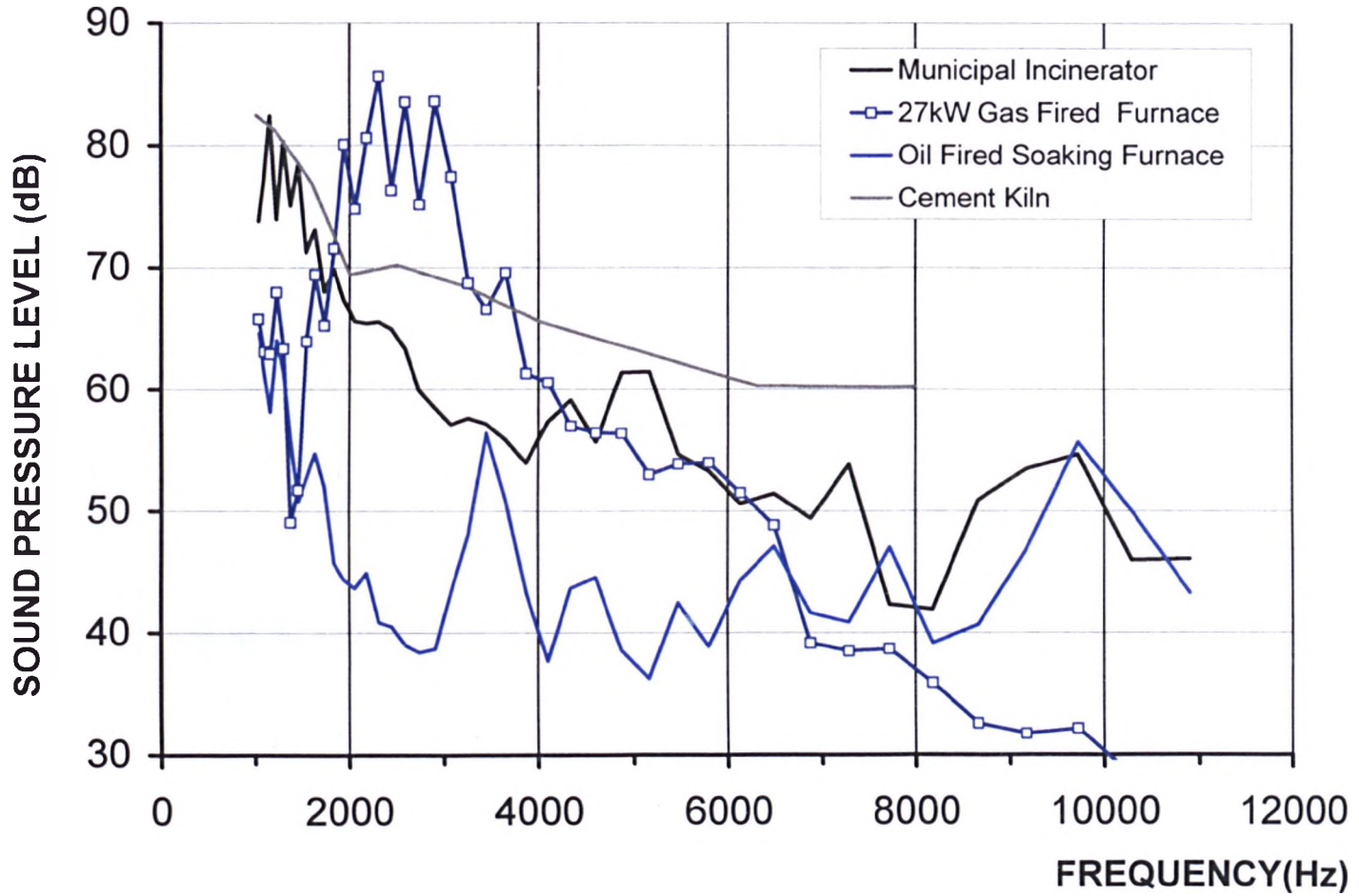


Figure 16: Combustion and background noise levels at various furnaces and kilns

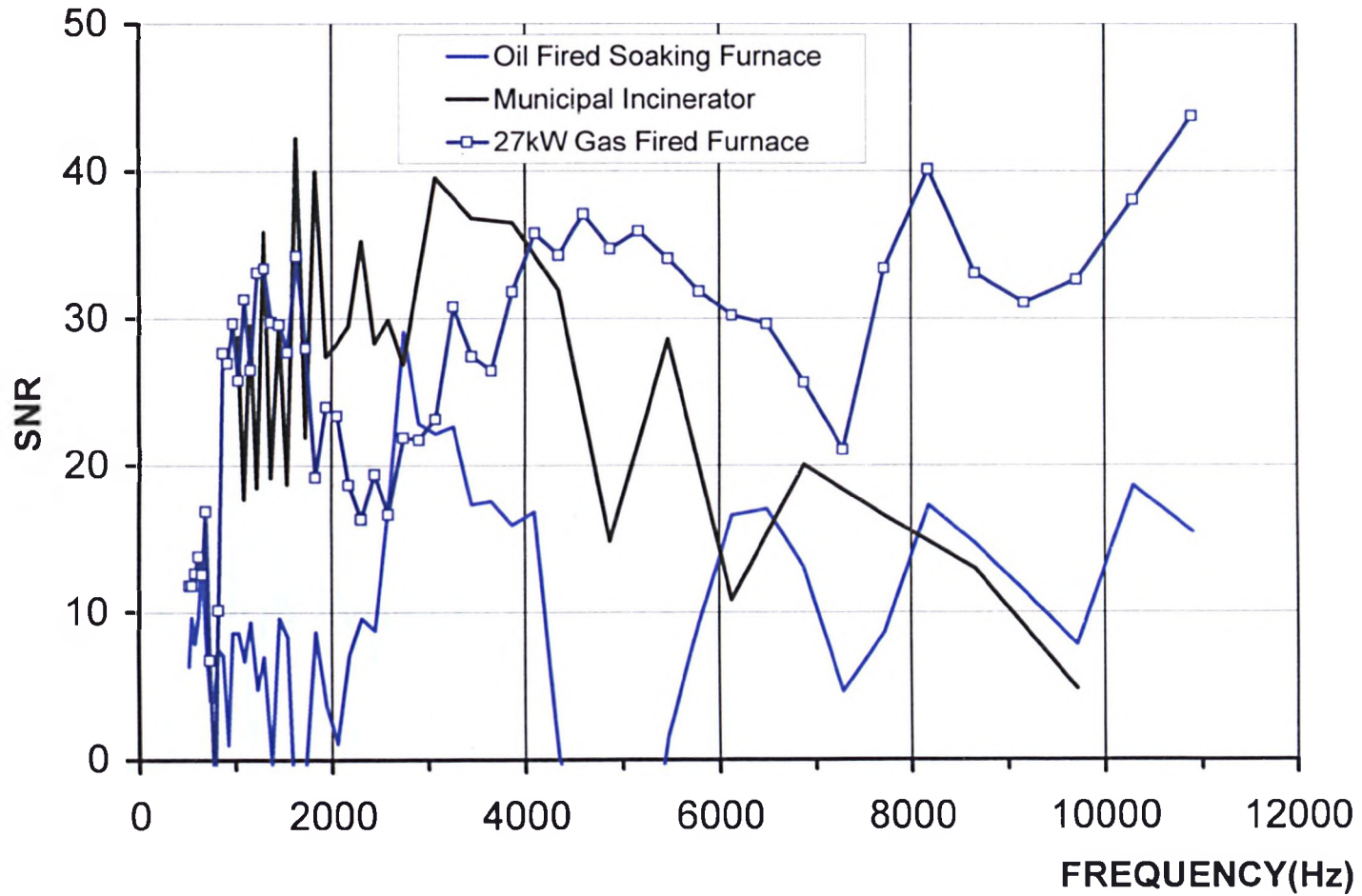


Figure 17: Signal to Noise Ratio (SNR) versus frequency relationship for various furnaces and kilns

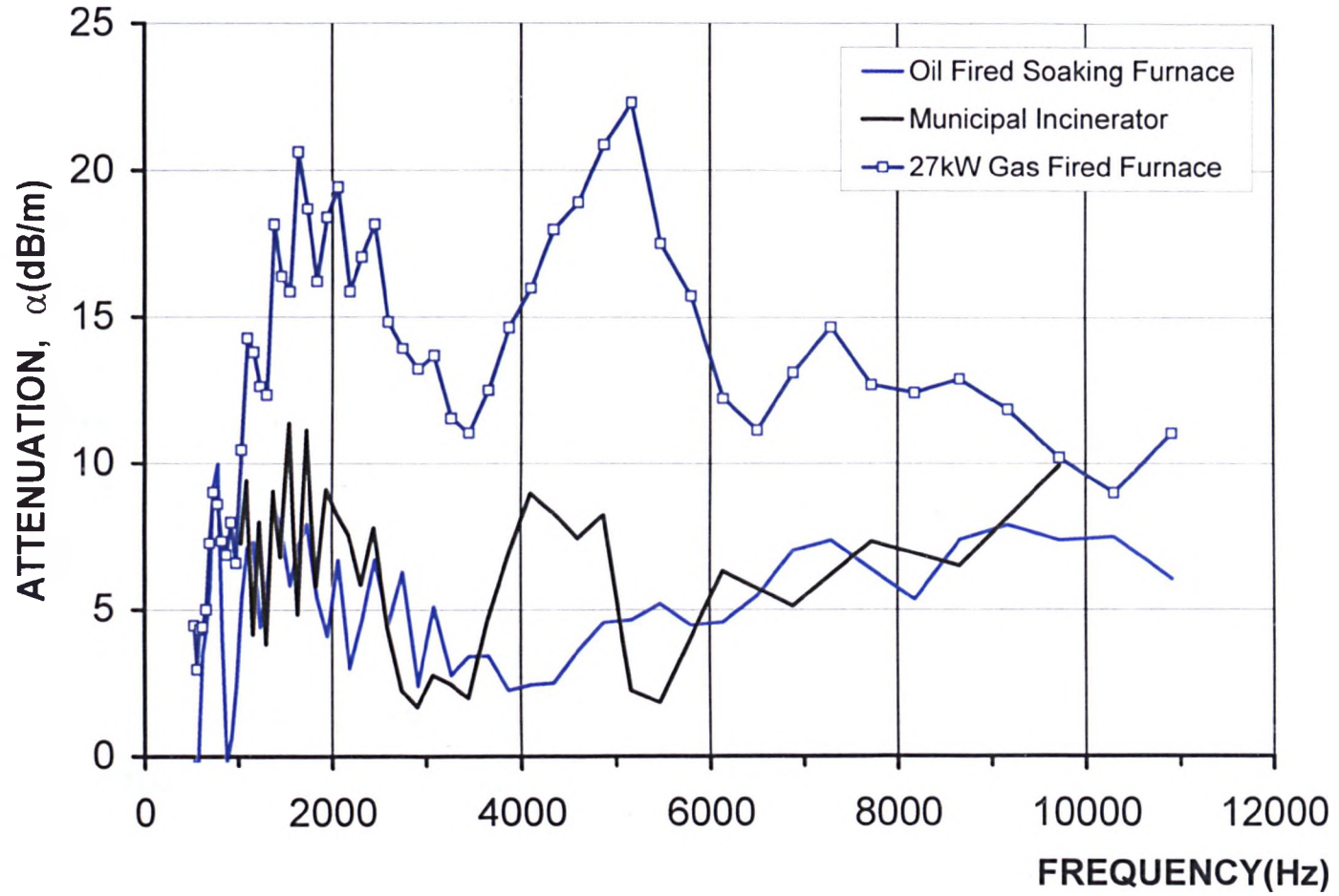


Figure 18: Attenuation versus frequency relationship for various furnaces and kilns

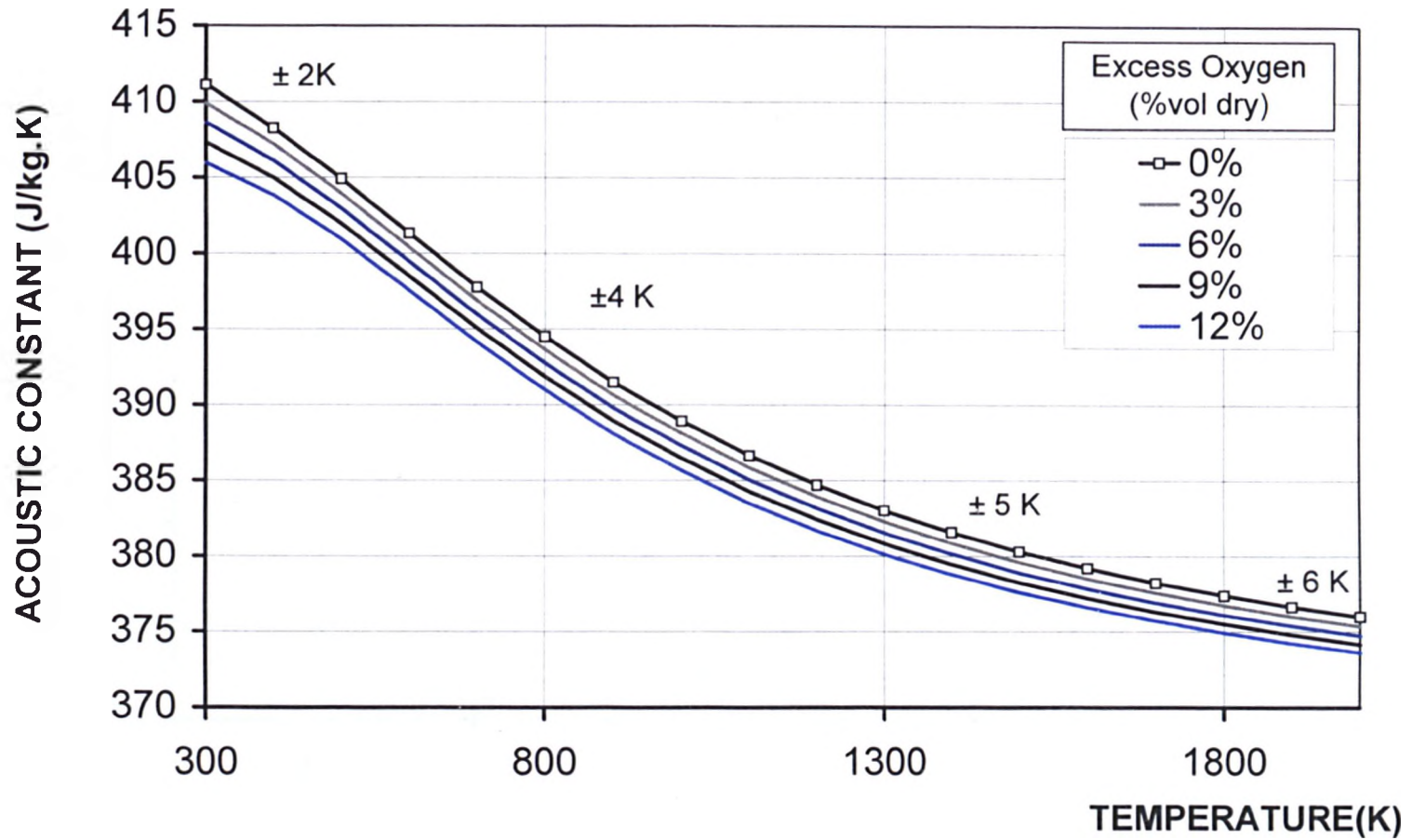


Figure 19: The dependence of the acoustic constant on temperature for the products of complete combustion of methane in air for varying exhaust excess oxygen concentrations.

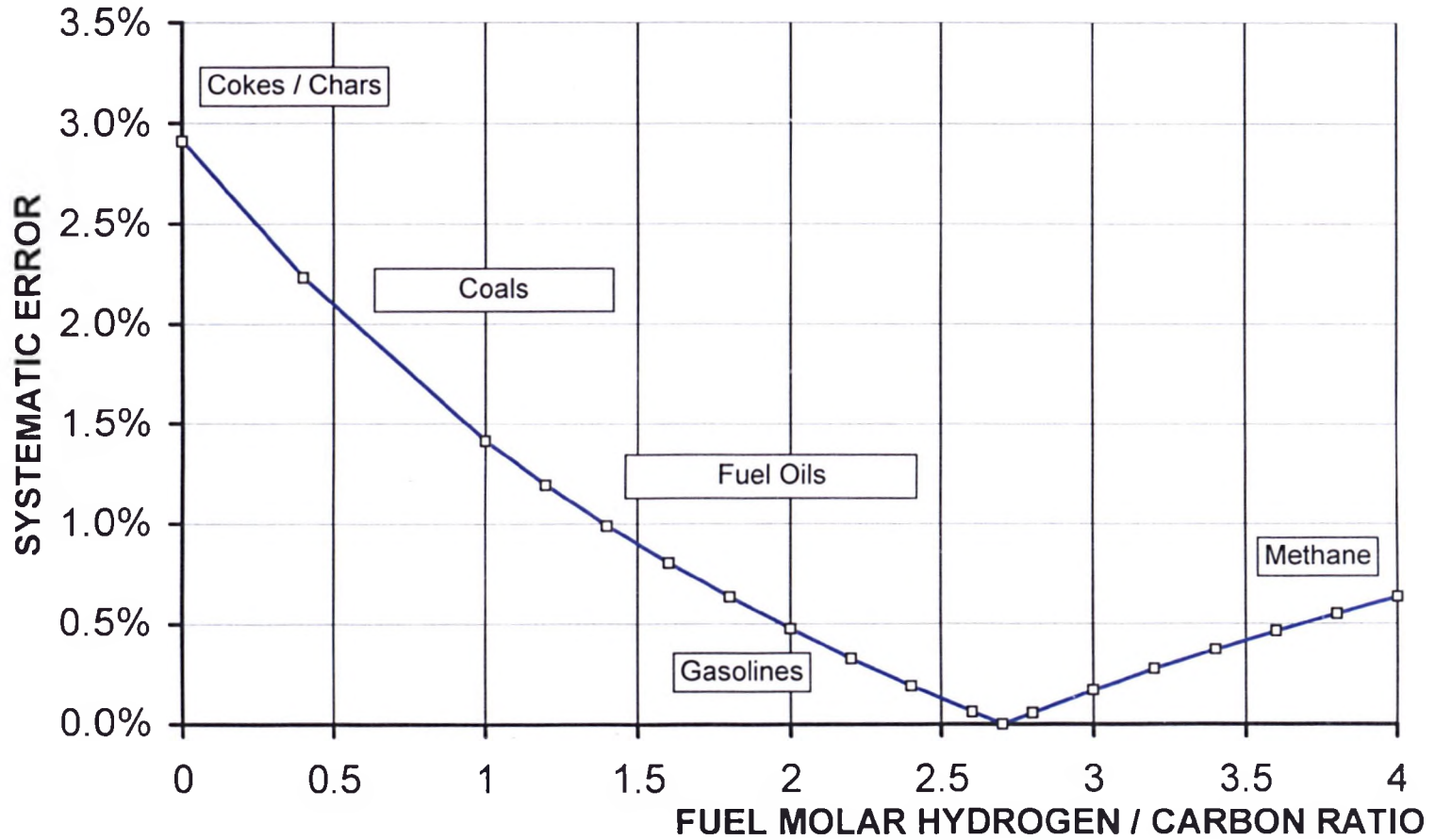
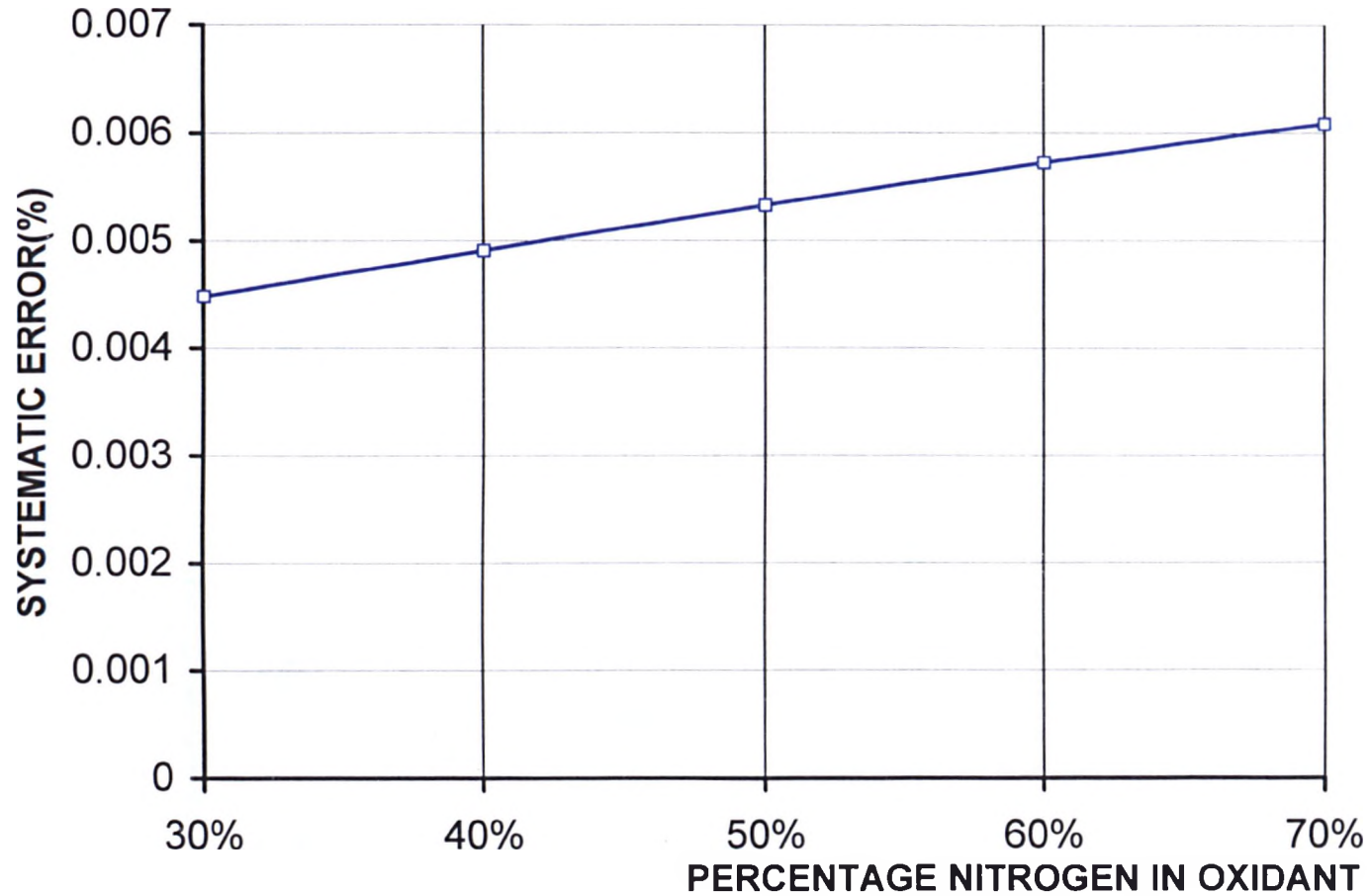


Figure 20: The systematic error in the measurement of temperature in combustion products resulting from an unknown combustion mixture ratio between 0 and 12% o<sub>2</sub> vol. dry as a function of fuel molar h/c ratio with air as oxidant.



**Figure 21: The systematic error in the measurement of temperature in methane combustion products resulting from an unknown combustion mixture ratio between 0 and 12% o<sub>2</sub> vol. dry as a function of oxidant composition**

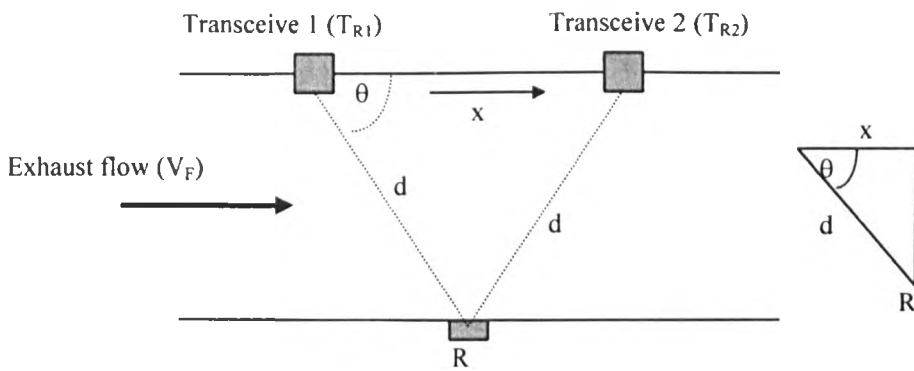


Figure 22: Schematic of acoustic flow measurement technique.

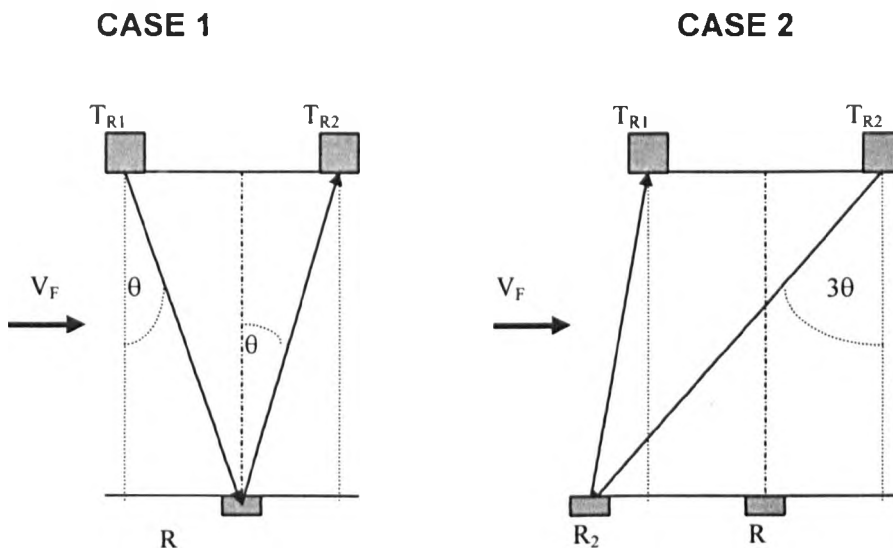


Figure 23: Schematic diagram indicating possible transmission paths.

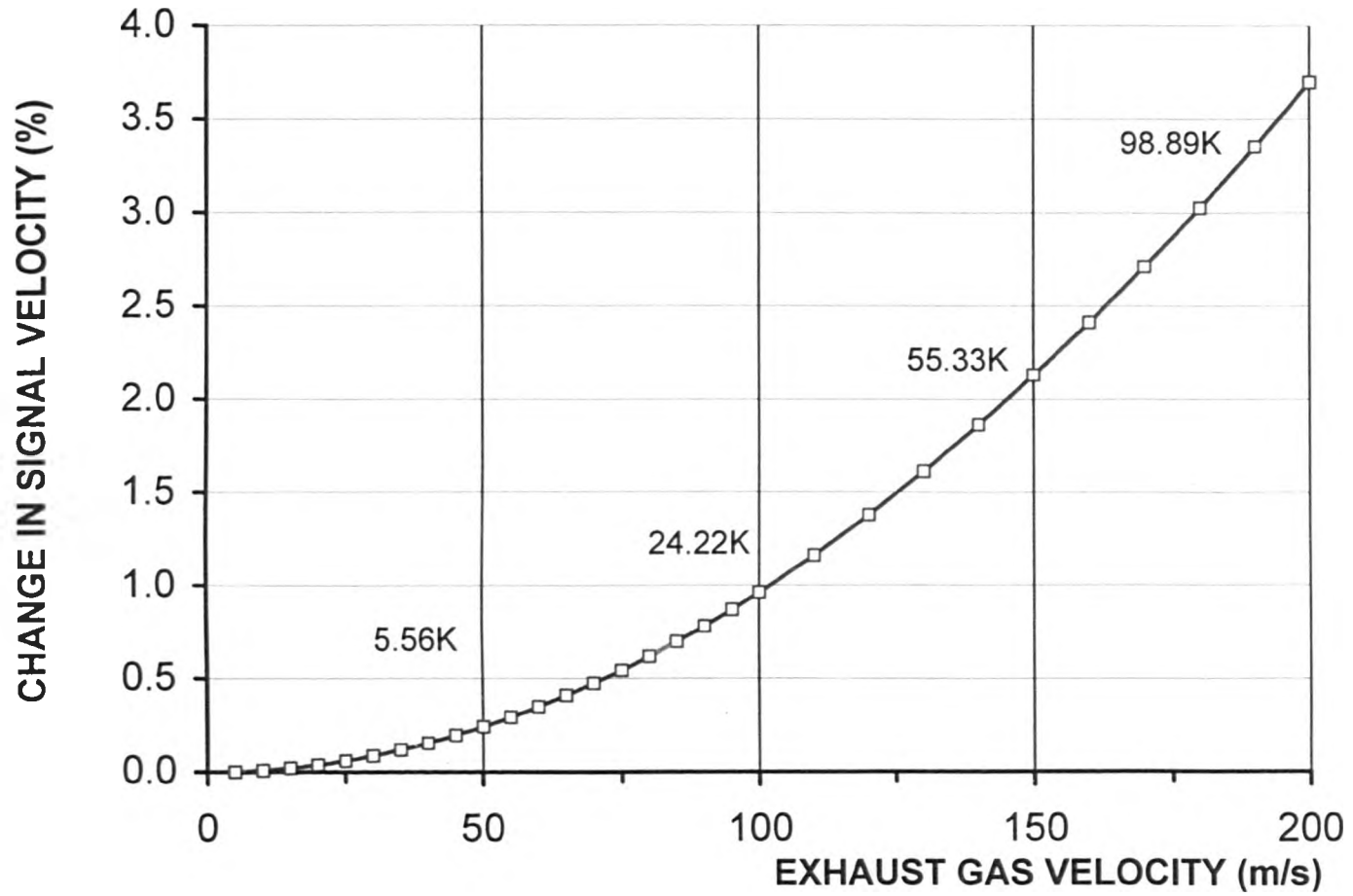


Figure 24: Positional considerations for two transceivers due to the influence of exhaust gas velocity at high temperature (1273K)

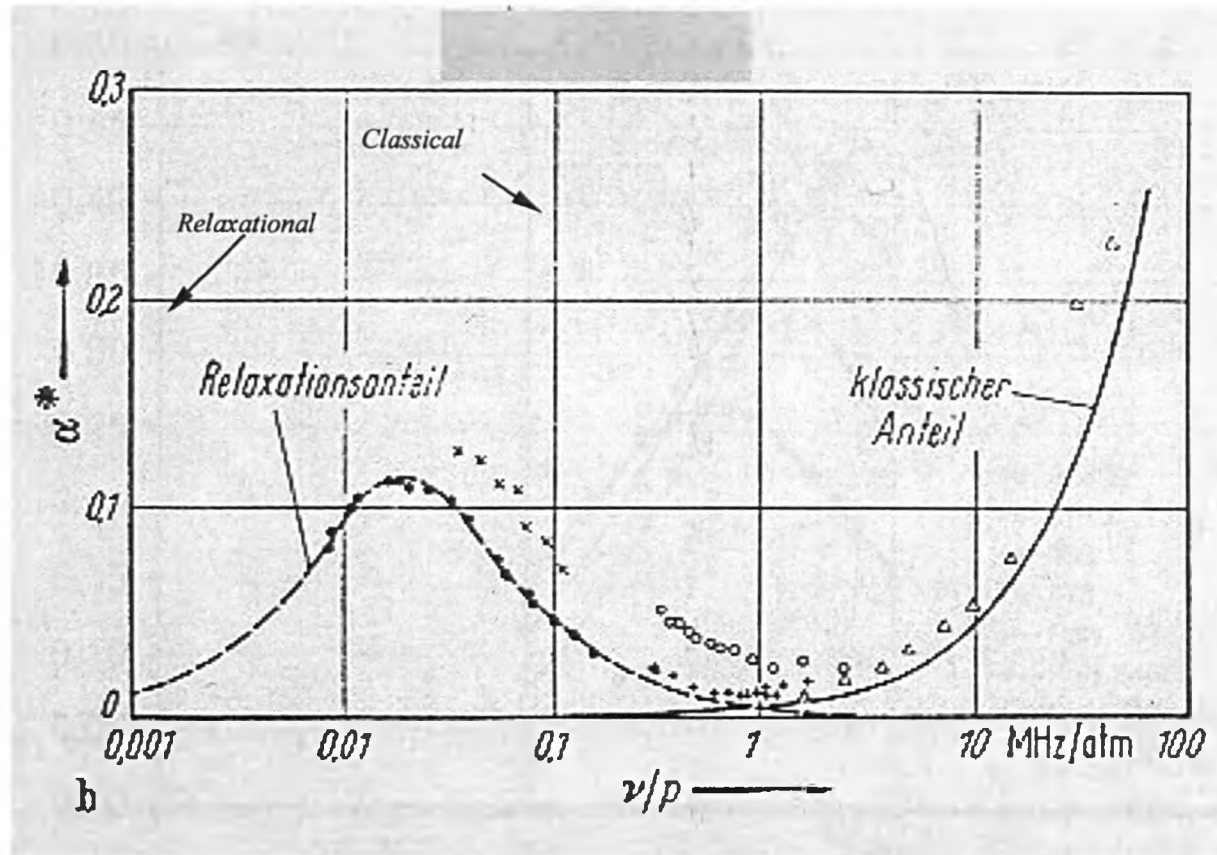


Figure 25: Sound absorption in carbon dioxide at N.T.P.<sup>72</sup>.

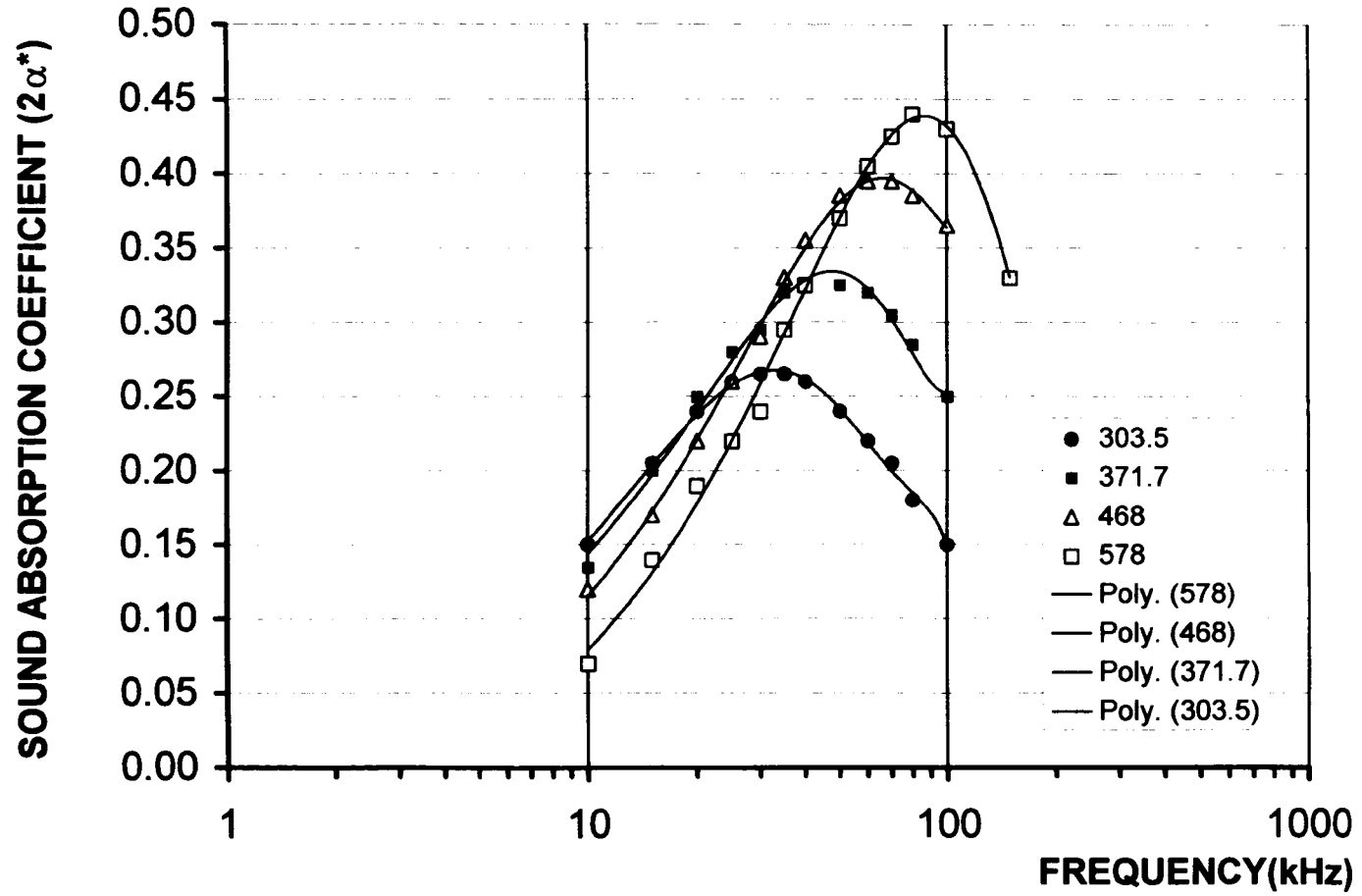


Figure 26: Molecular absorption in pure CO<sub>2</sub> at various temperatures against signal frequency, with 4<sup>th</sup> order polynomial curve fits

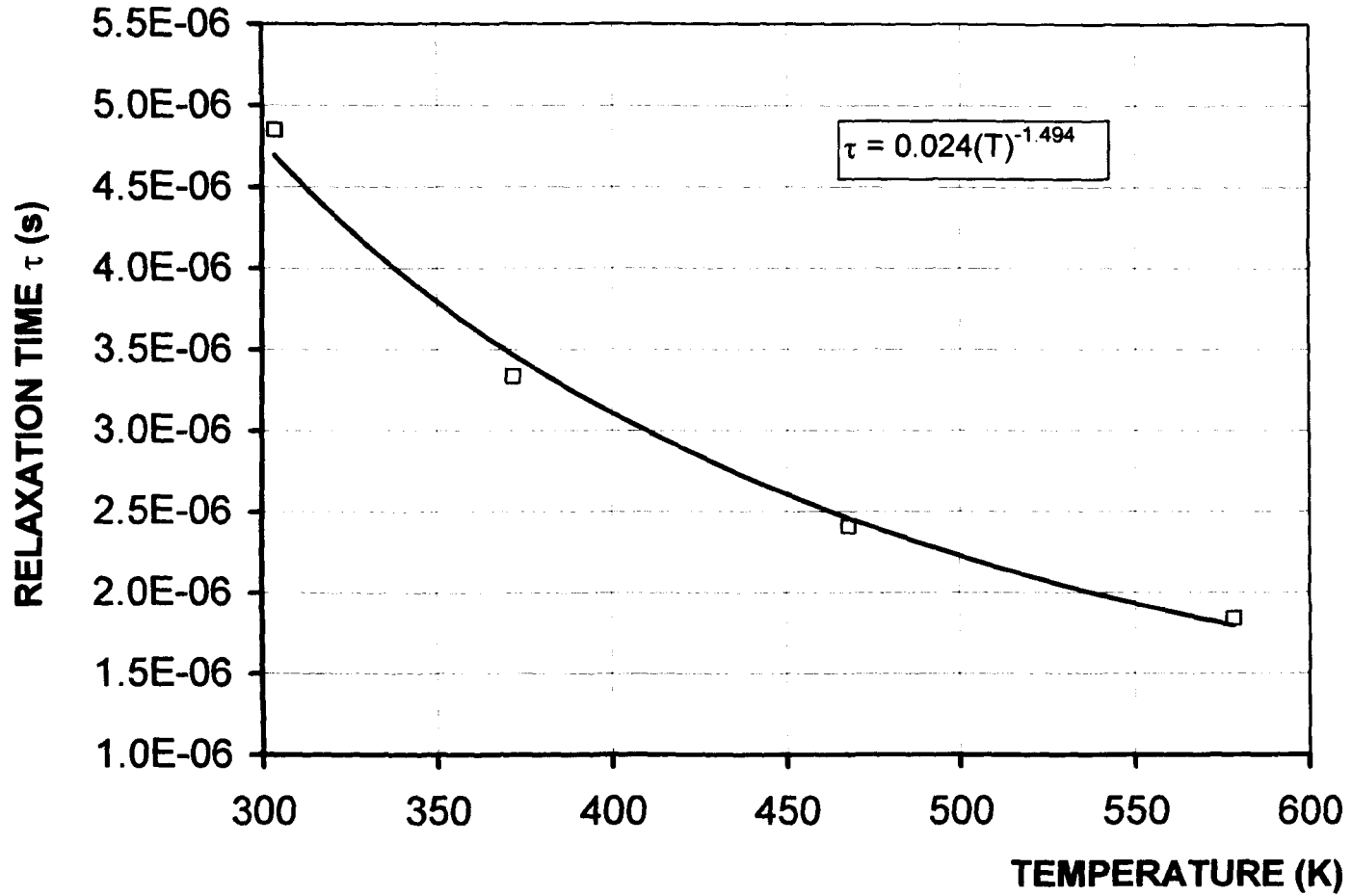


Figure 27: Plot of relaxation time against temperature for pure CO<sub>2</sub> with 2<sup>nd</sup> order power law curve fit

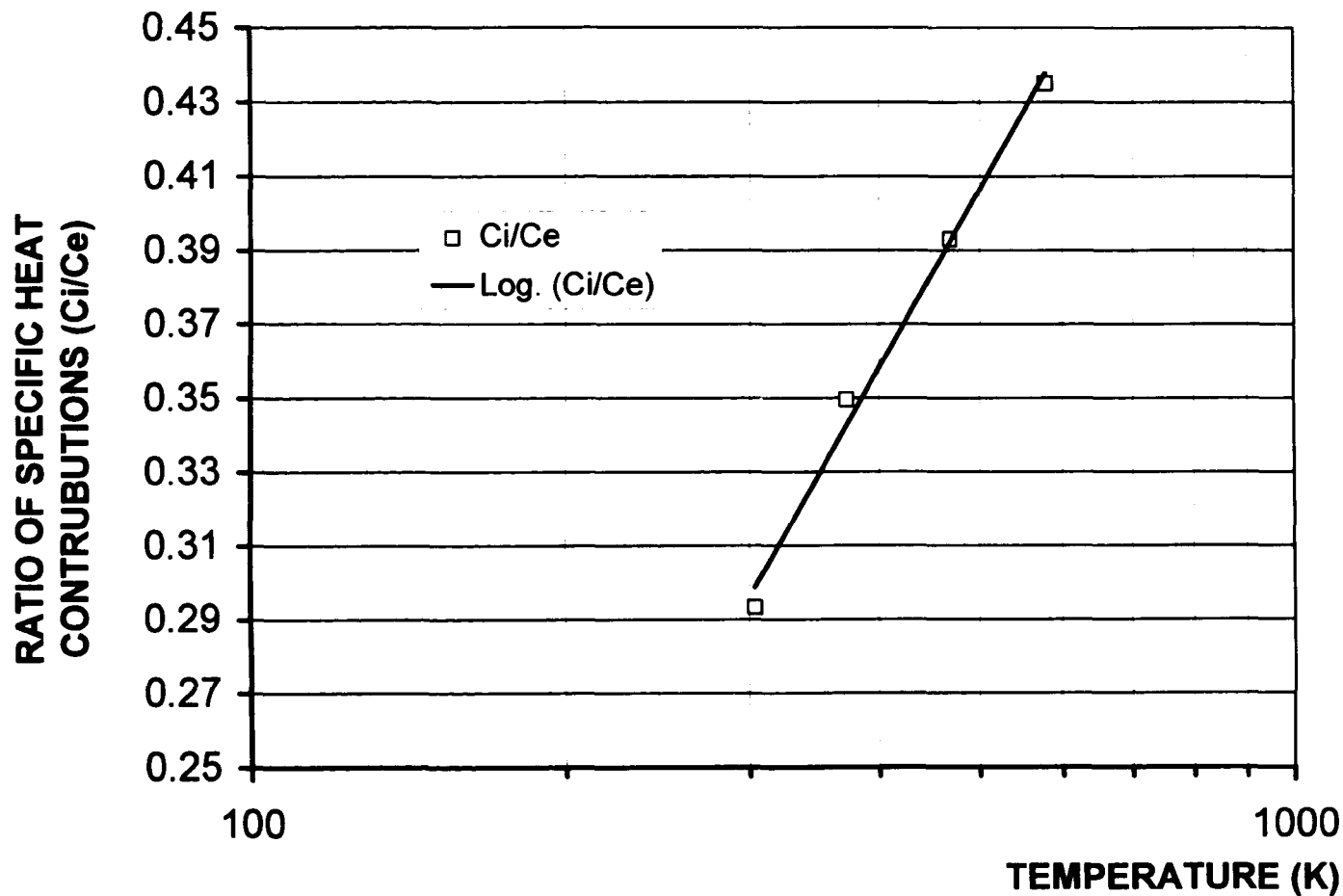


Figure 28: Plot of the ratio of external to internal specific heat contributions for  $CO_2$  at several temperatures with 2<sup>nd</sup> order logarithmic curve fit

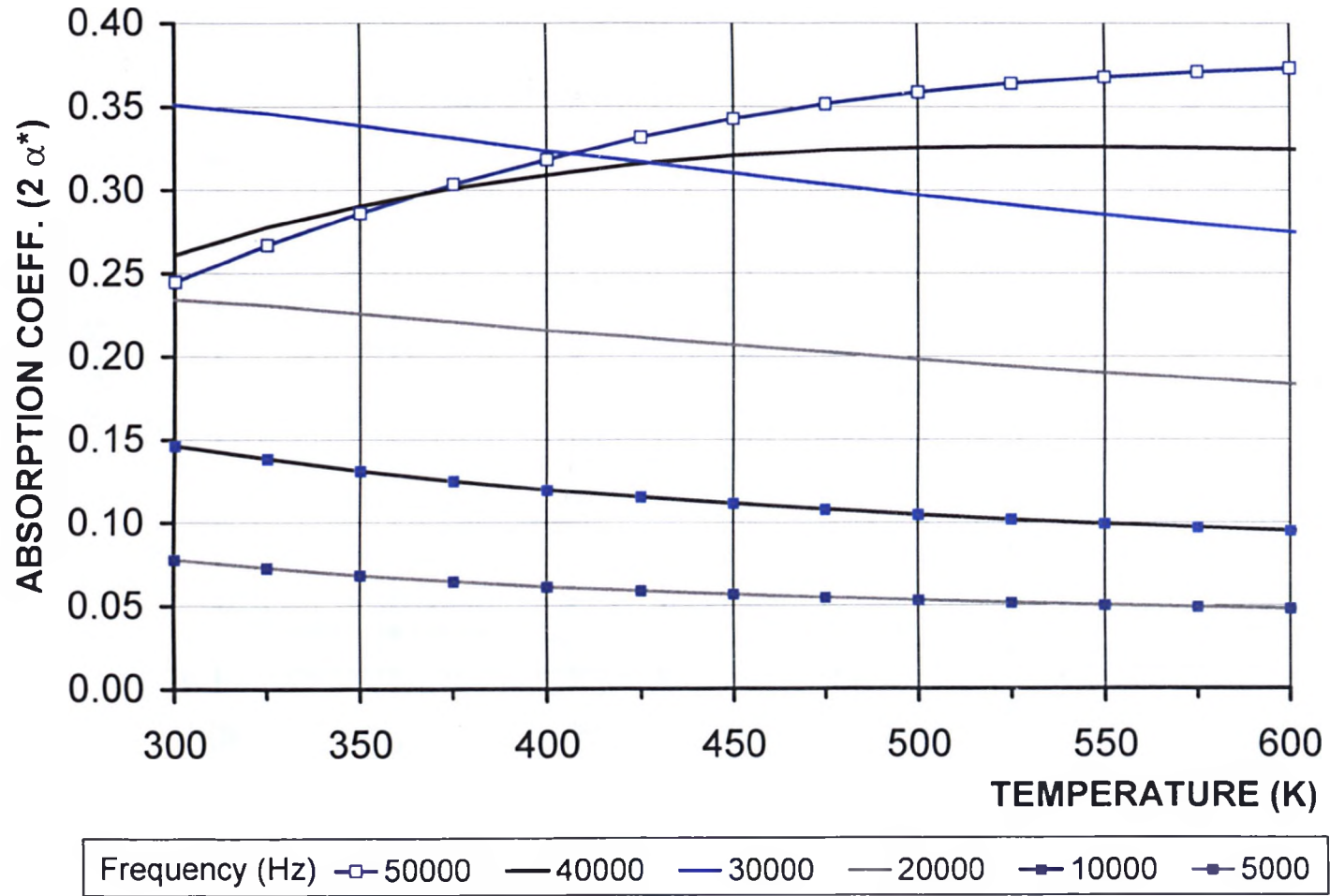


Figure 29: Derived absorption coefficient versus temperature curves for CO<sub>2</sub> at various frequencies

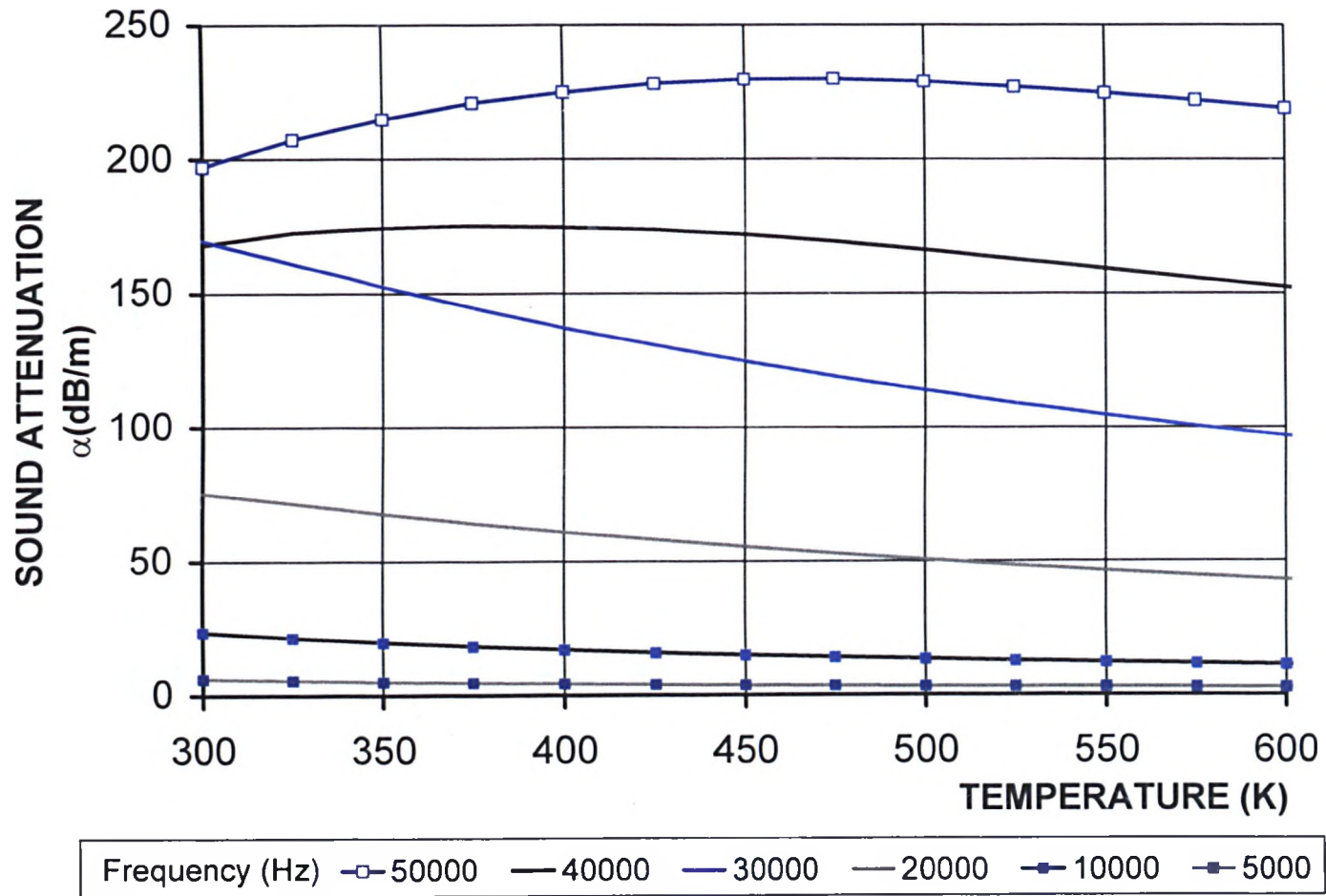


Figure 30: Calculated sound absorption levels due to molecular relaxation in CO<sub>2</sub> for a limited range of temperatures and various frequencies

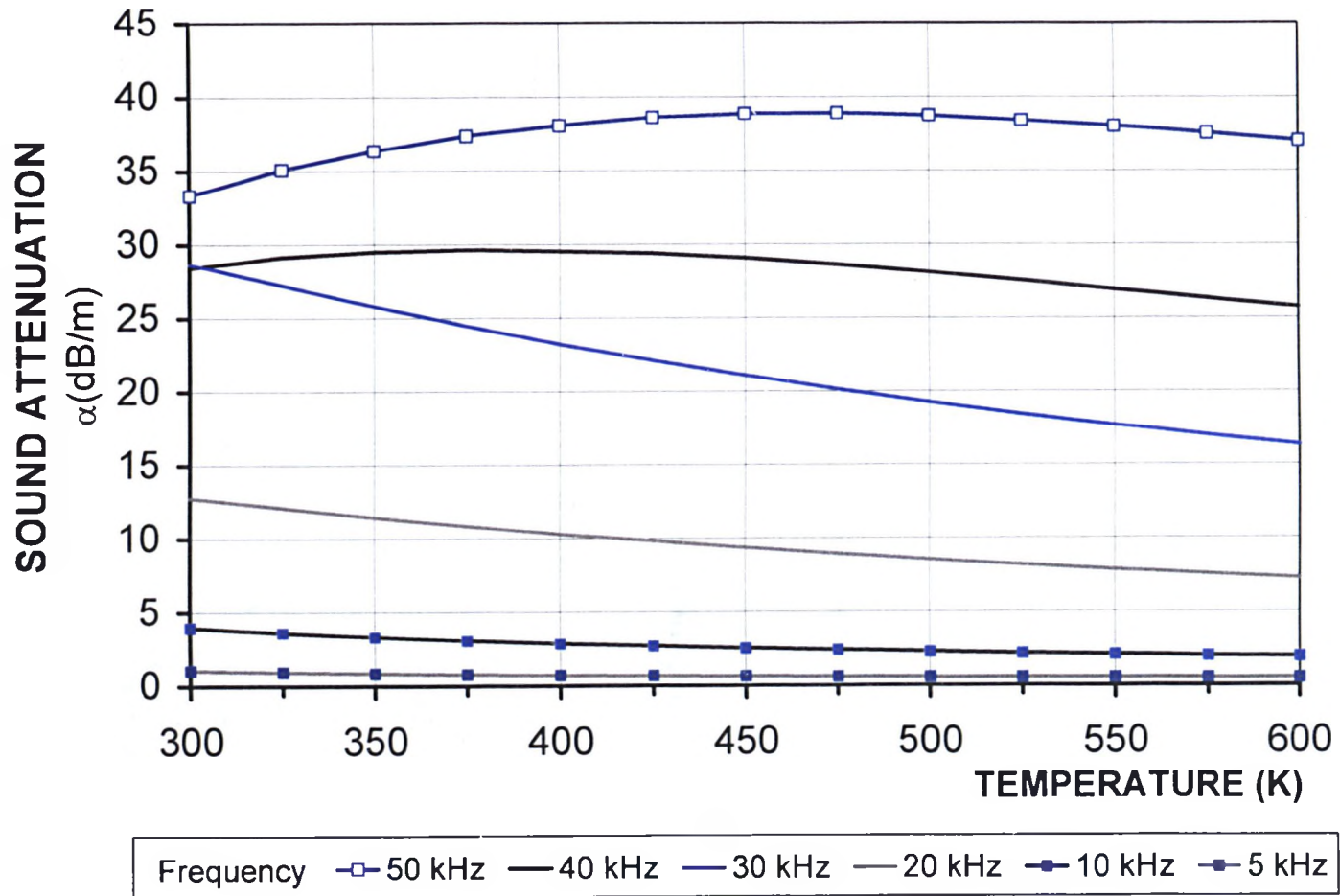
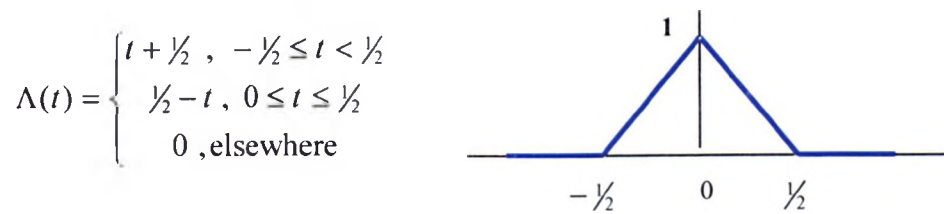


Figure 31: Calculated sound absorption for furnace \ kiln levels of CO<sub>2</sub> for a limited range of temperatures and various frequencies



**Figure 32: Unit Pulse Function,  $\Pi(t)$**



**Figure 33: Unit Triangle Function,  $\Lambda(t)$**

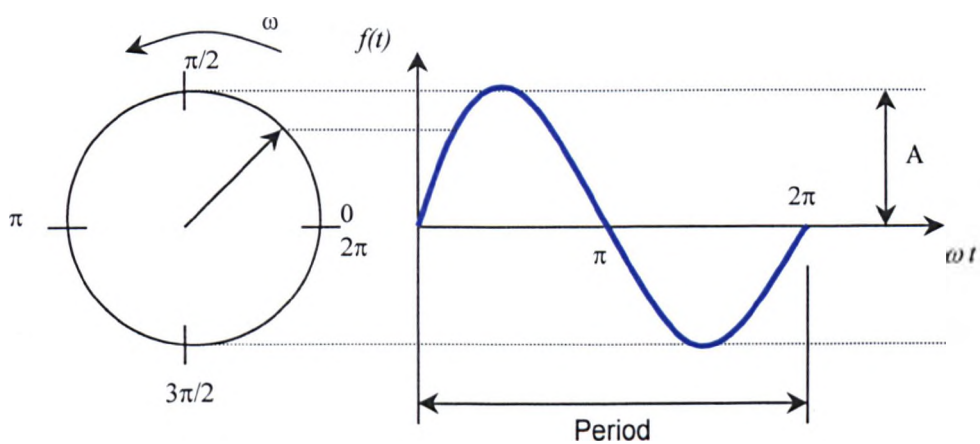


**Figure 34: Sinusoidal function,  $f(t)$**

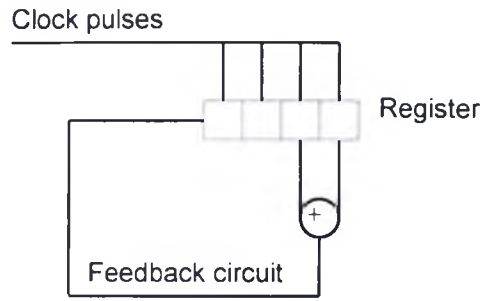


**Figure 35: Shift register circuit for a 15 digit sequence**

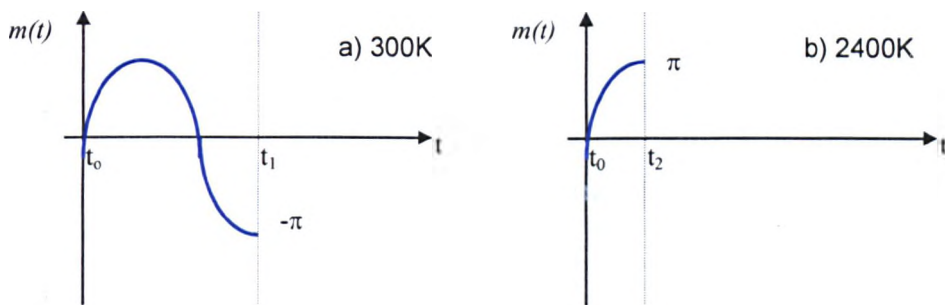


**Figure 36(a,b): Difference in phase of the sinusoidal signal at the receiver for two different temperatures**

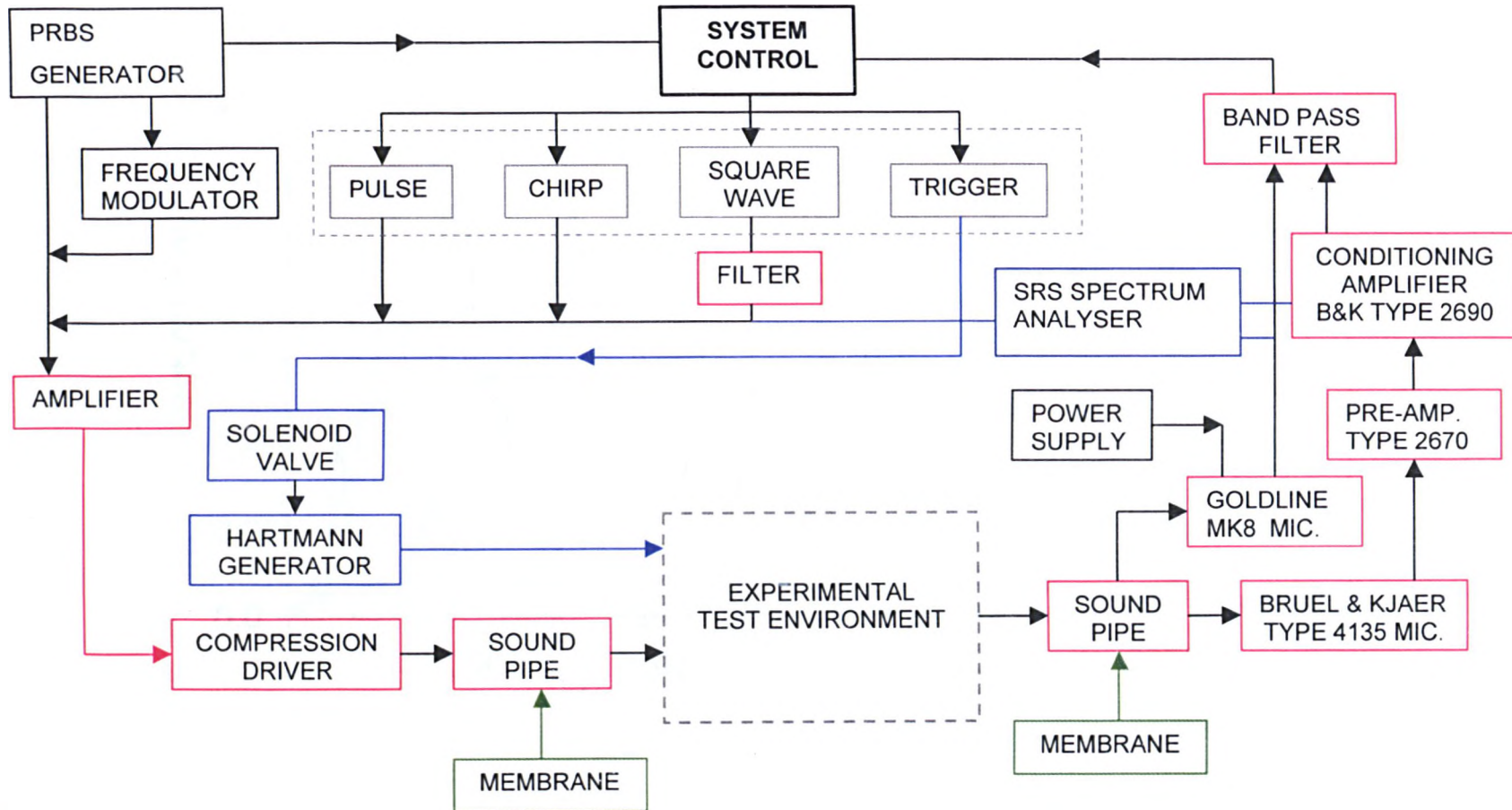
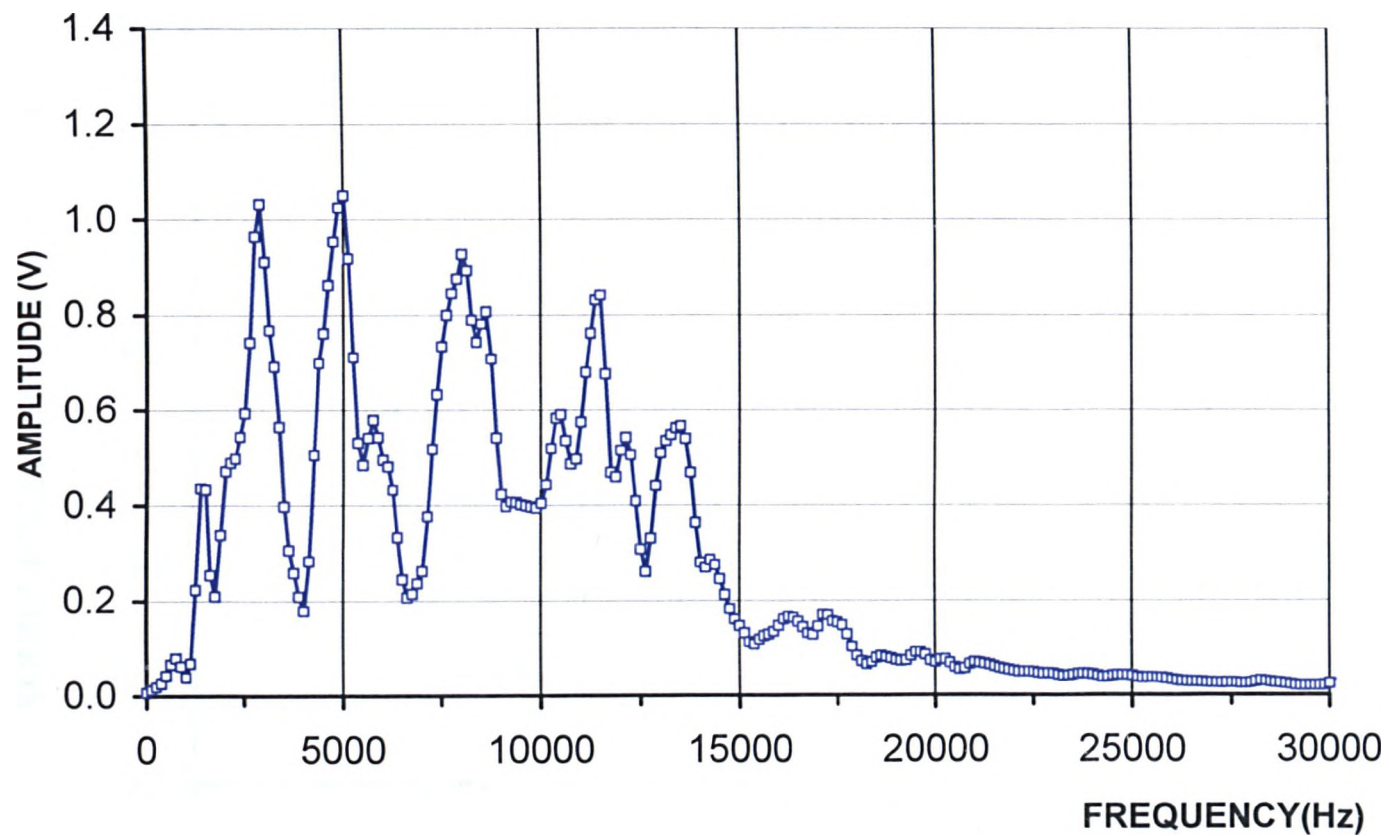


Figure 37: Schematic of acoustic pyrometer test equipment



**Figure 38: Compression driver frequency response profile to a calibrated white noise input signal measured at a standard separation distance of 1m under anechoic conditions**

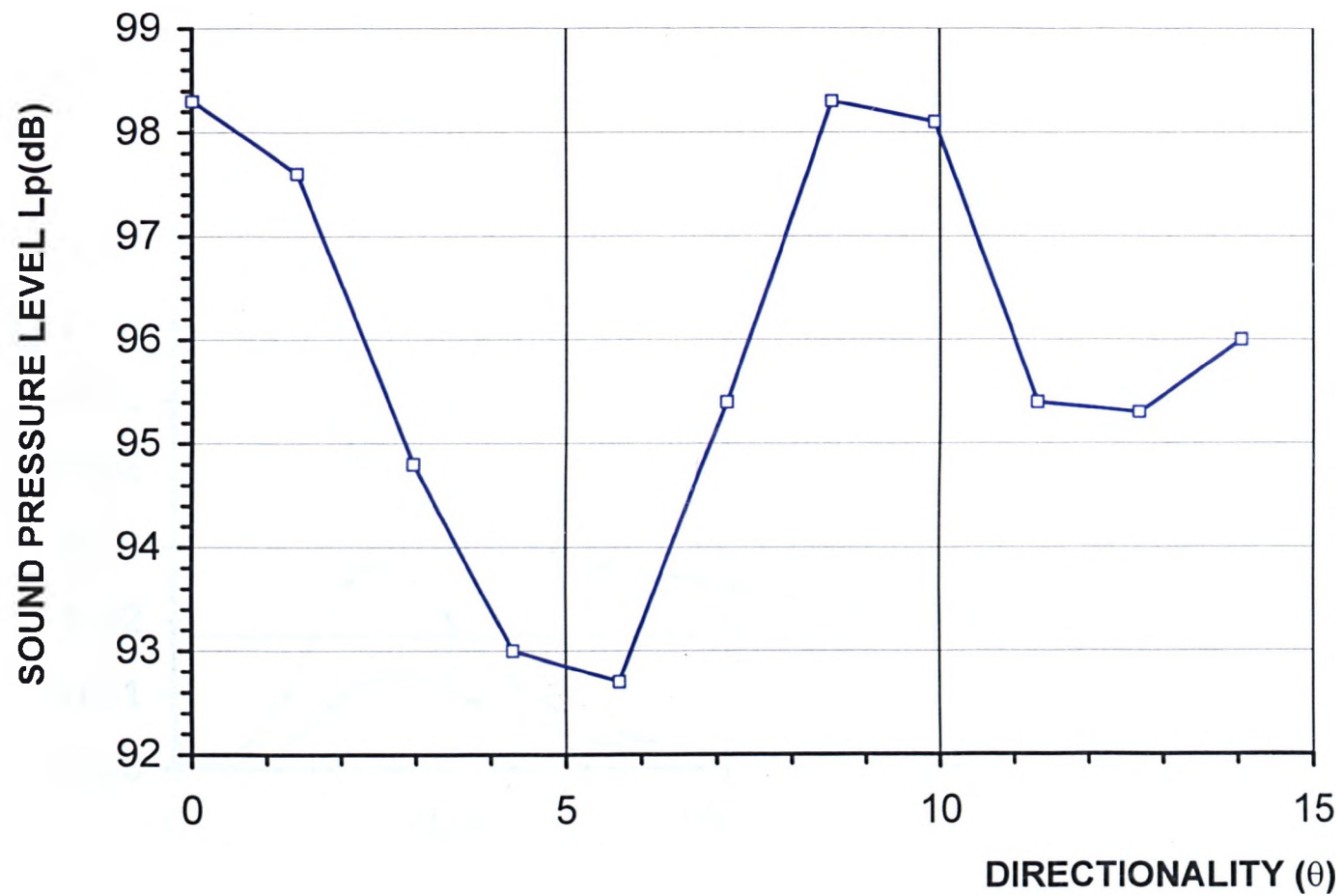


Figure 39: Variation in sound pressure level with directional variation of the transmitter relative to the receiver microphone

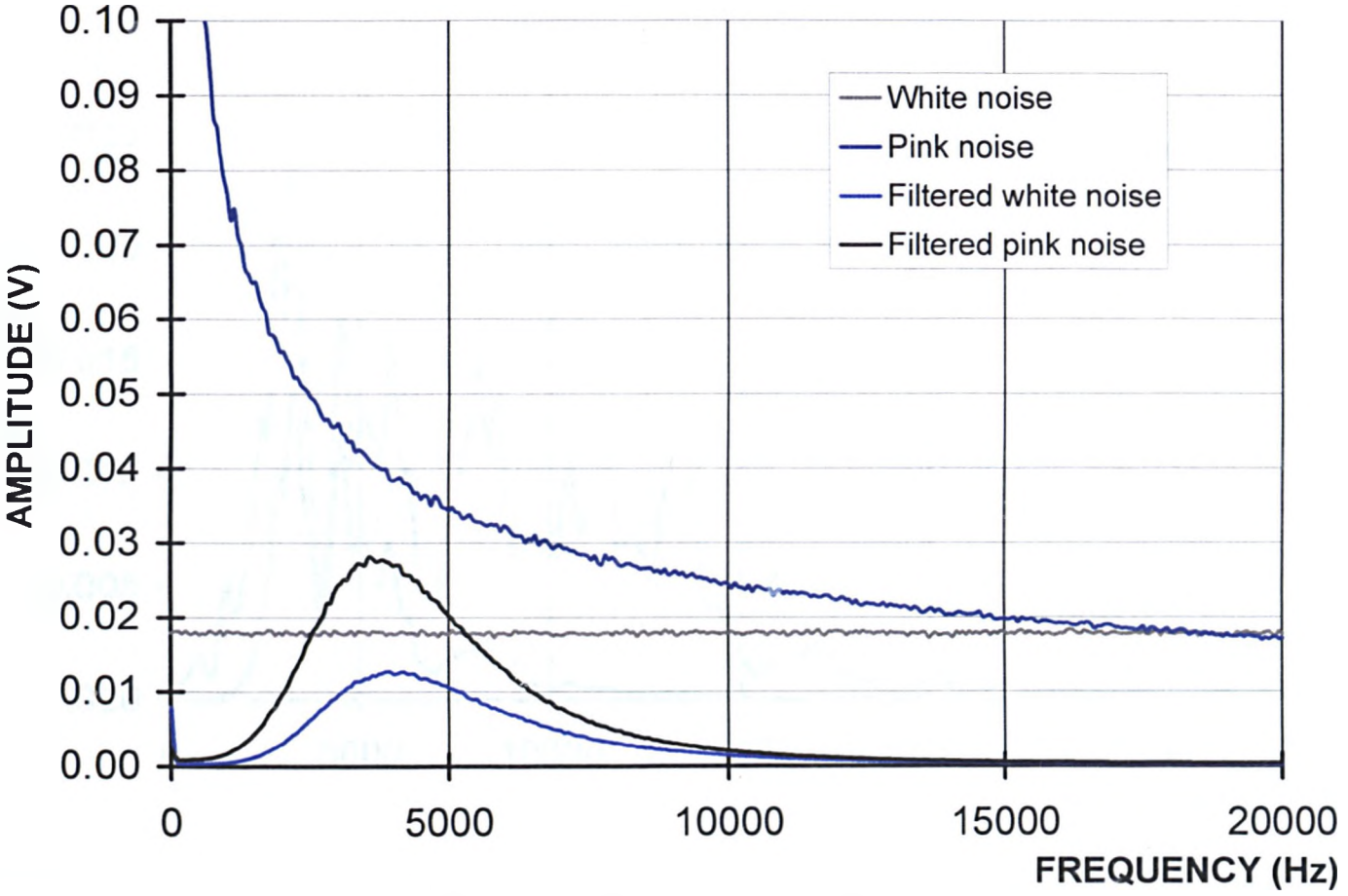
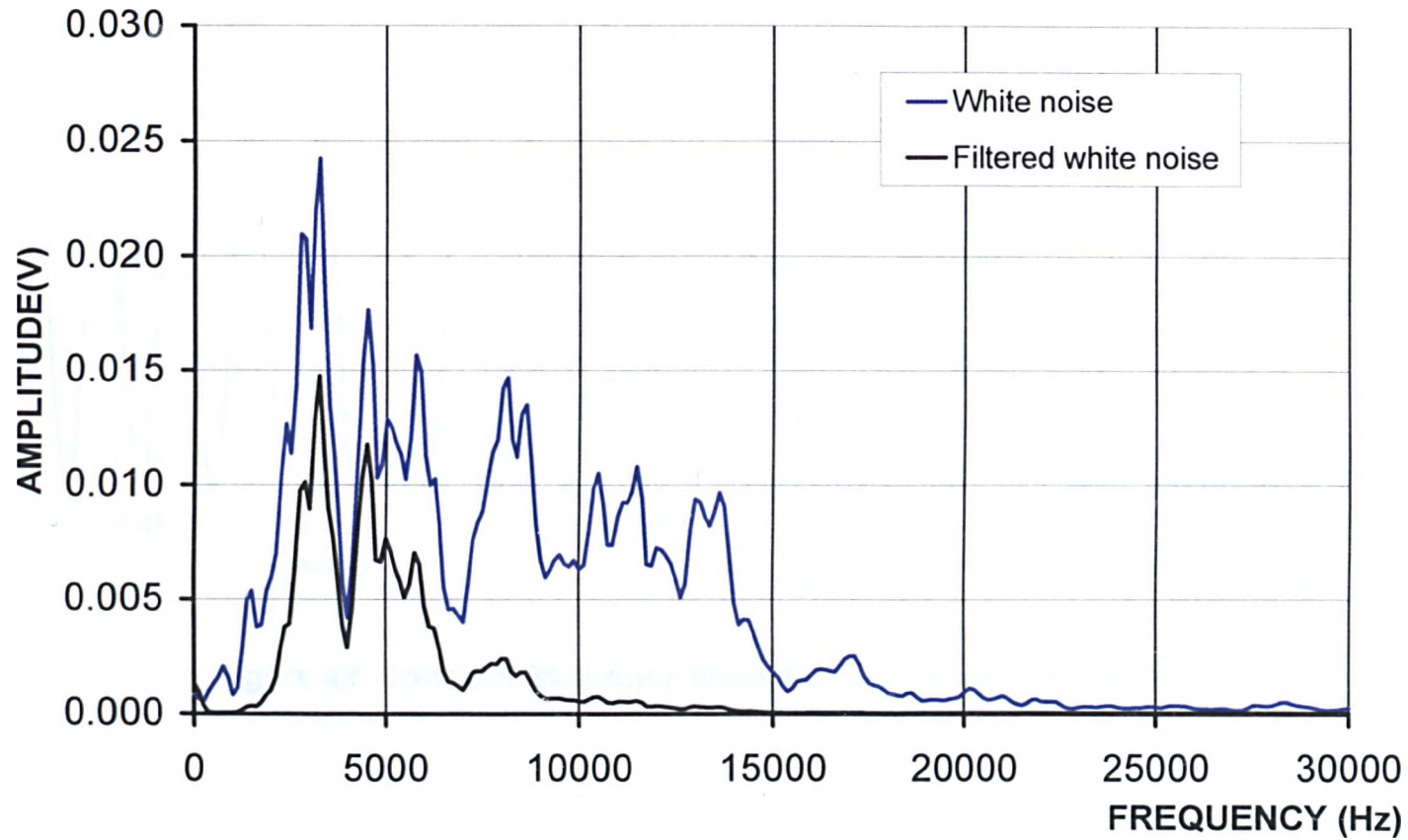
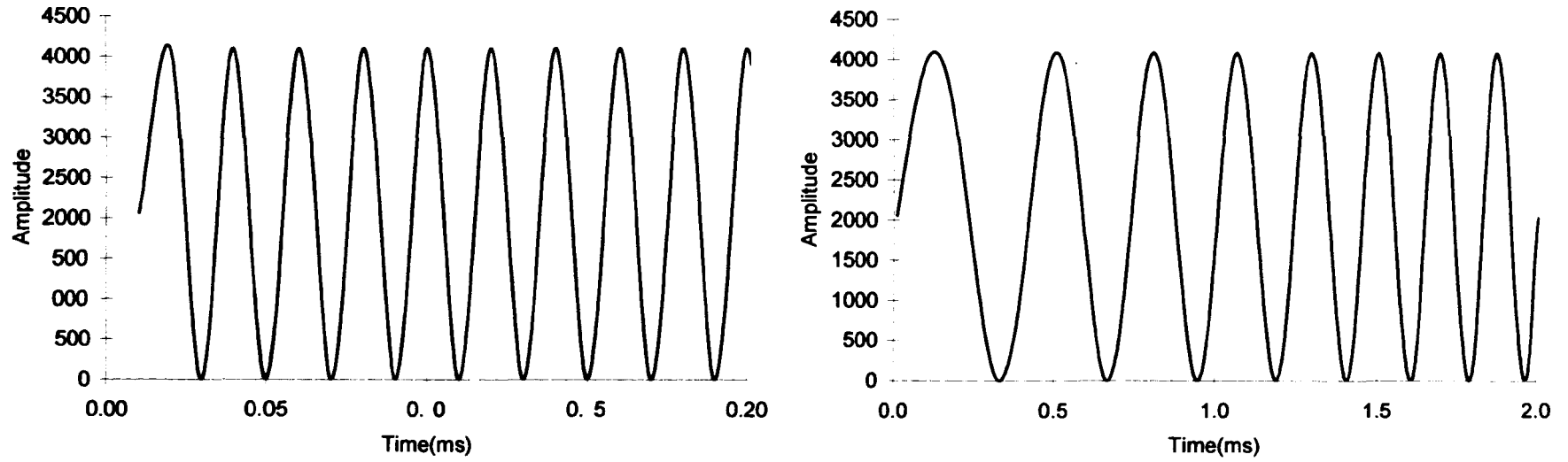


Figure 40: Calibrated pink and white direct input signals including the effects of the band pass filter



**Figure 41: Compression driver frequency response profile to a calibrated white noise input signal measured at a standard separation distance of 1m under anechoic conditions including the band pass filter**



**Figure 42: Constant frequency burst signal (a) & chirp signal (b).**

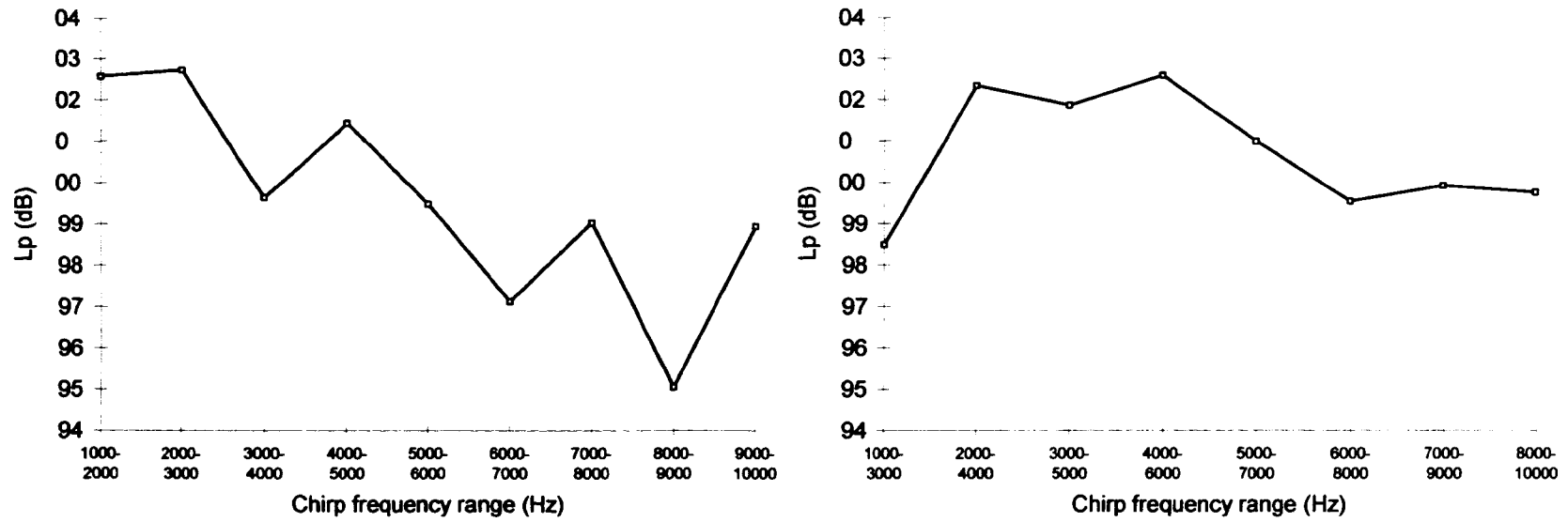


**Figure 43: 1000 Hz(a) and 2000 Hz(b) range performance**

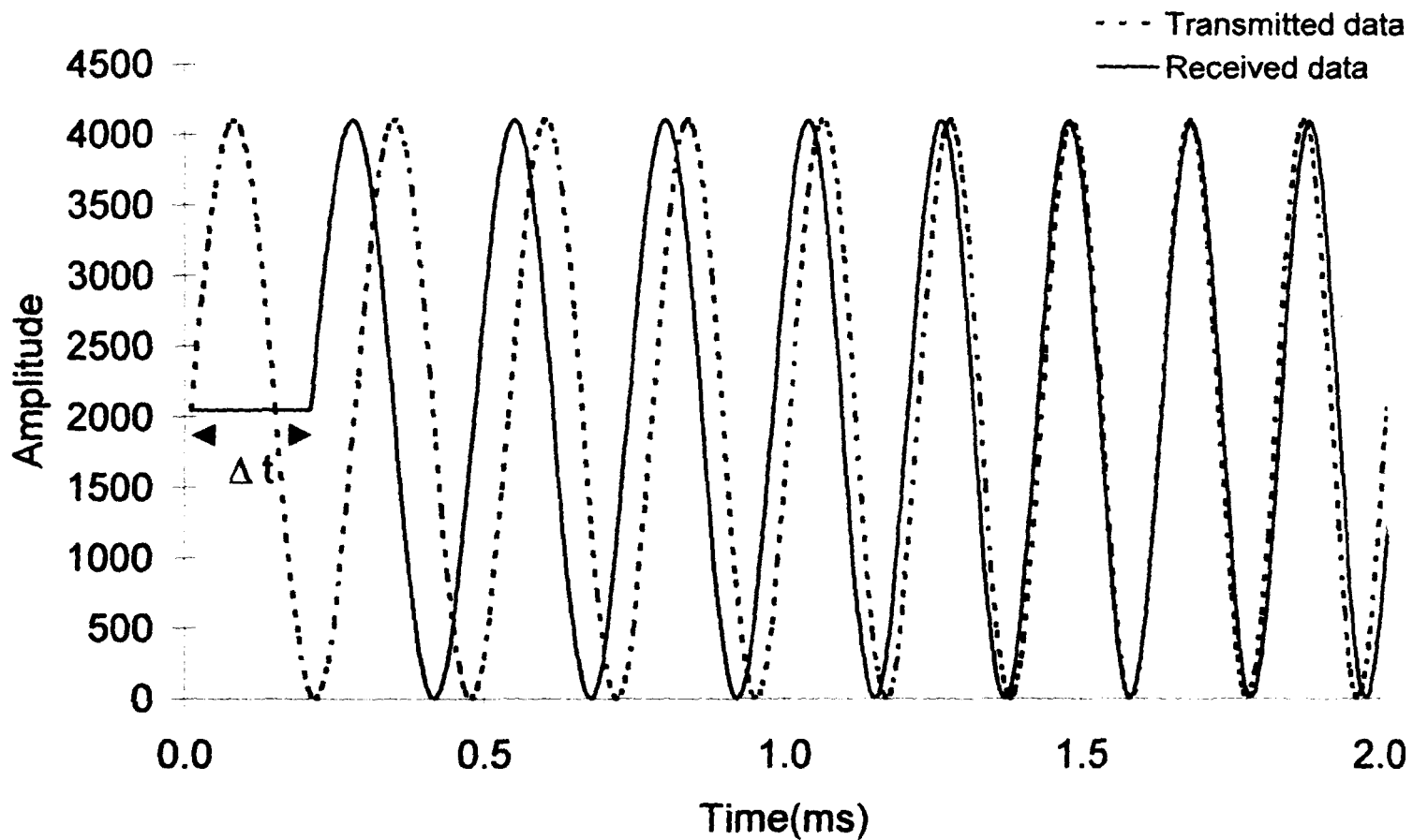


Figure 44: Raw transmitted and received data.

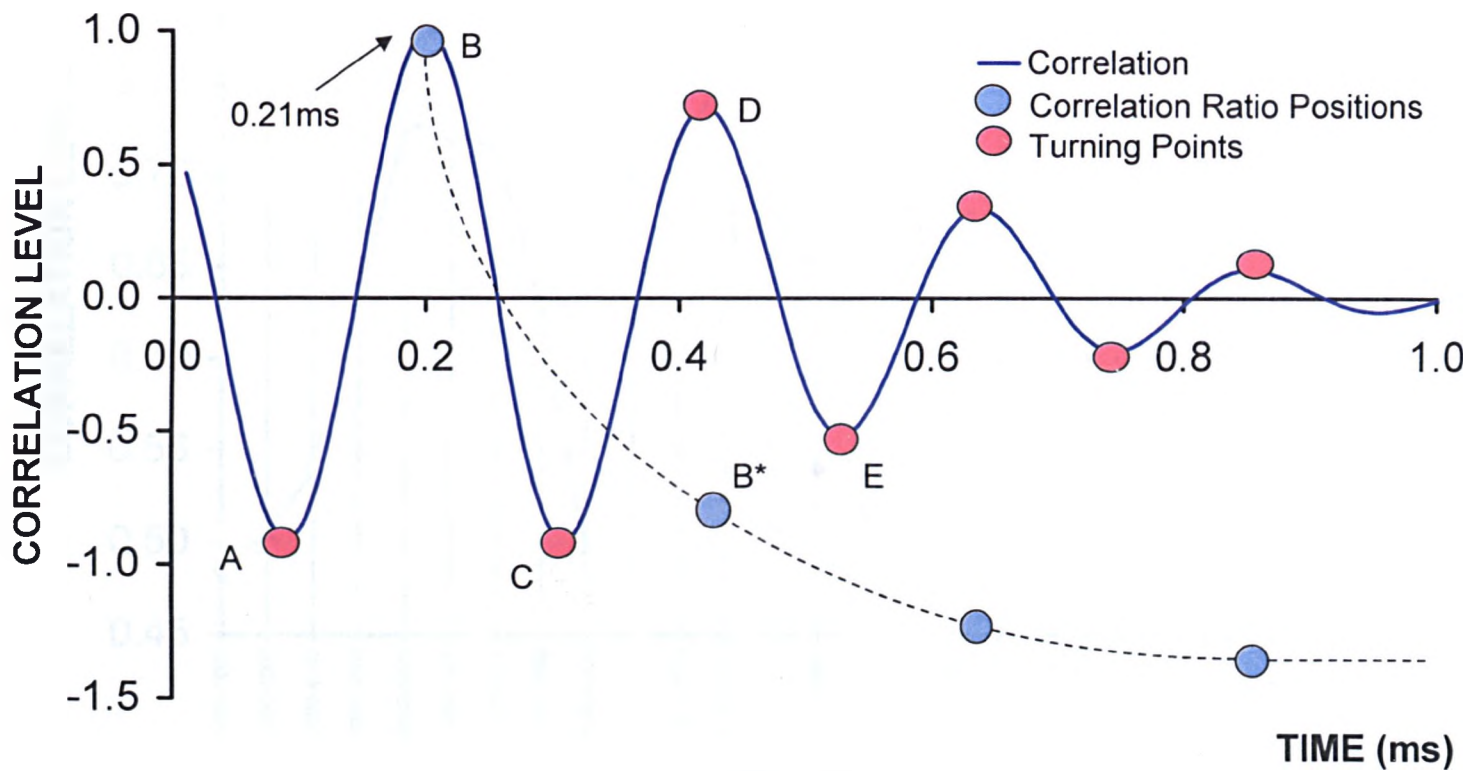


Figure 45: Correlation curve with performance markers to gauge correlation level and ratio values

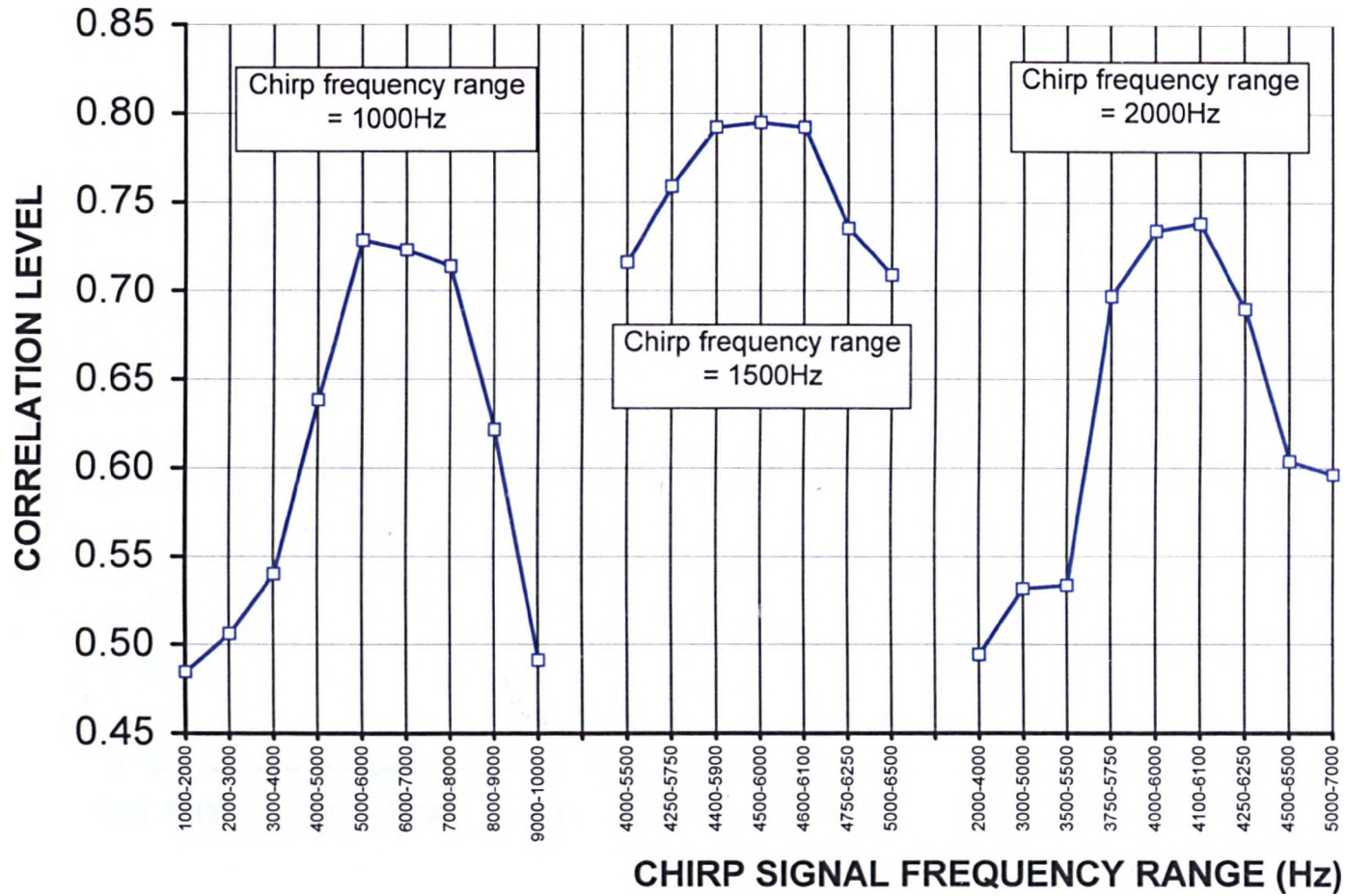


Figure 46: Correlation level performance for a constant duration chirp signal transmitted over a separation distance of 5.5m

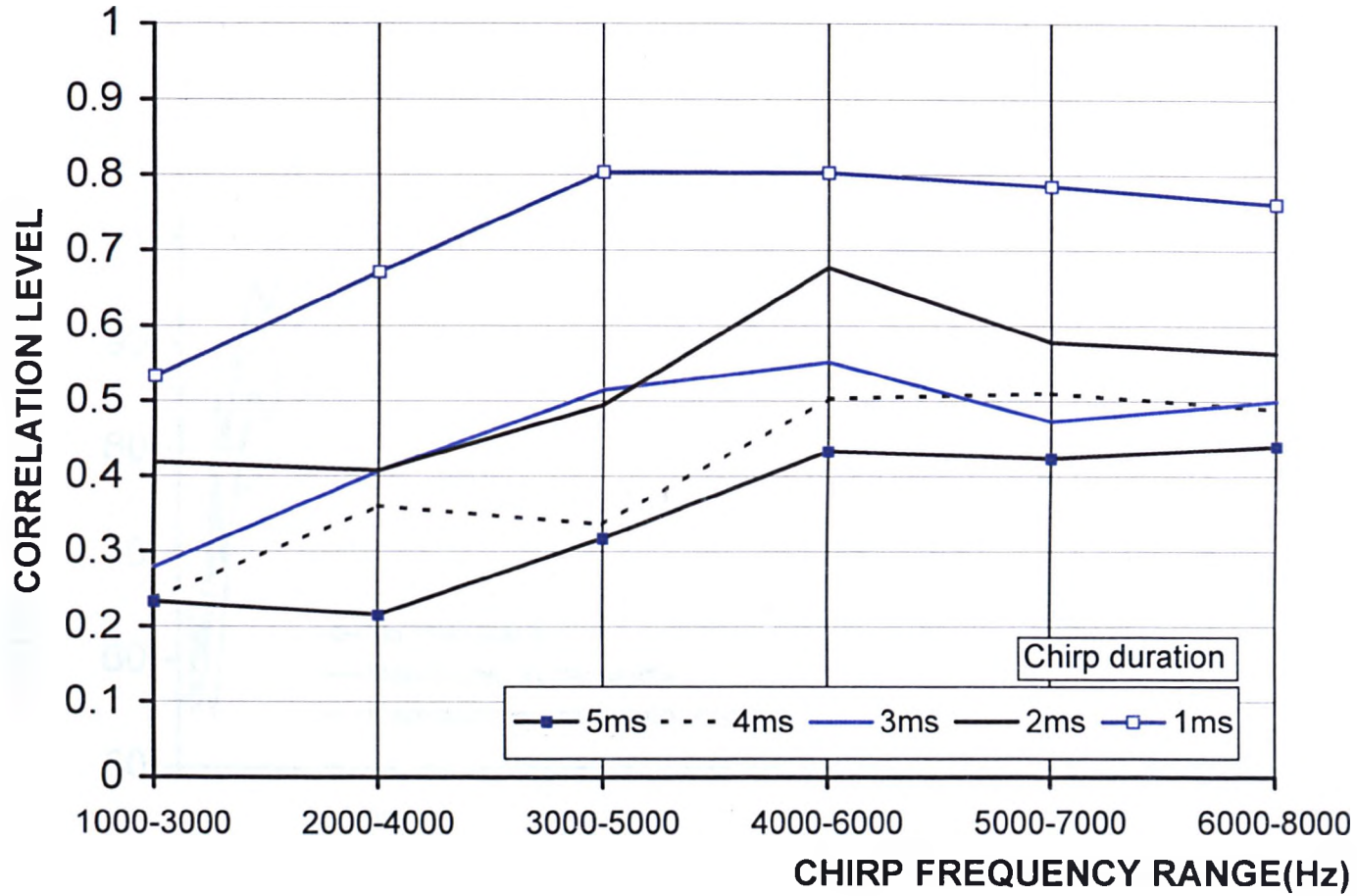


Figure 47: Variation in correlation performance with change in chirp duration and frequency range

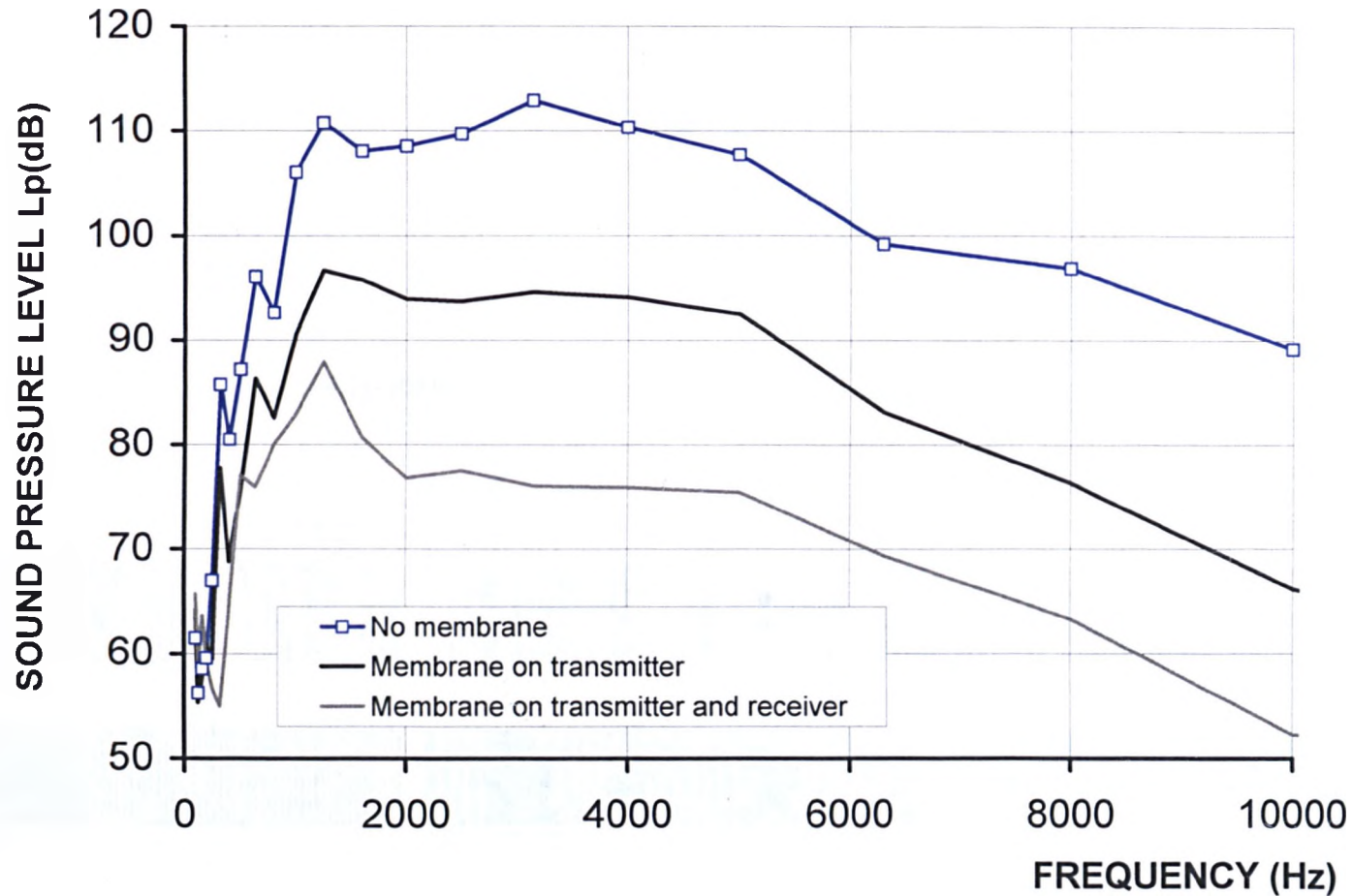
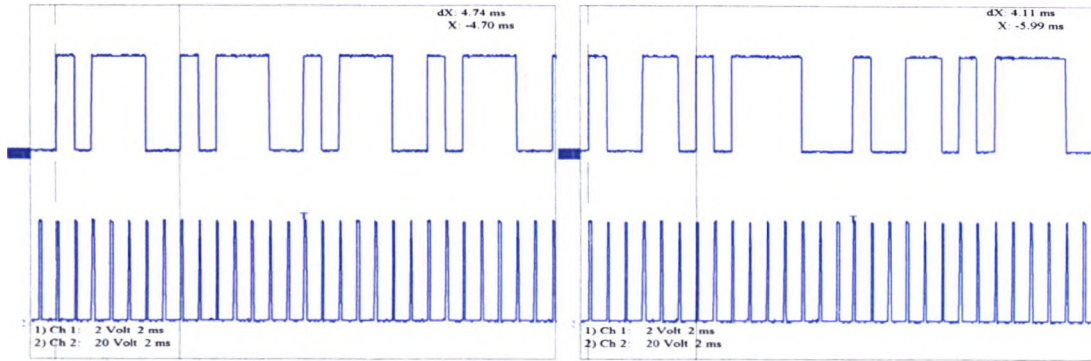
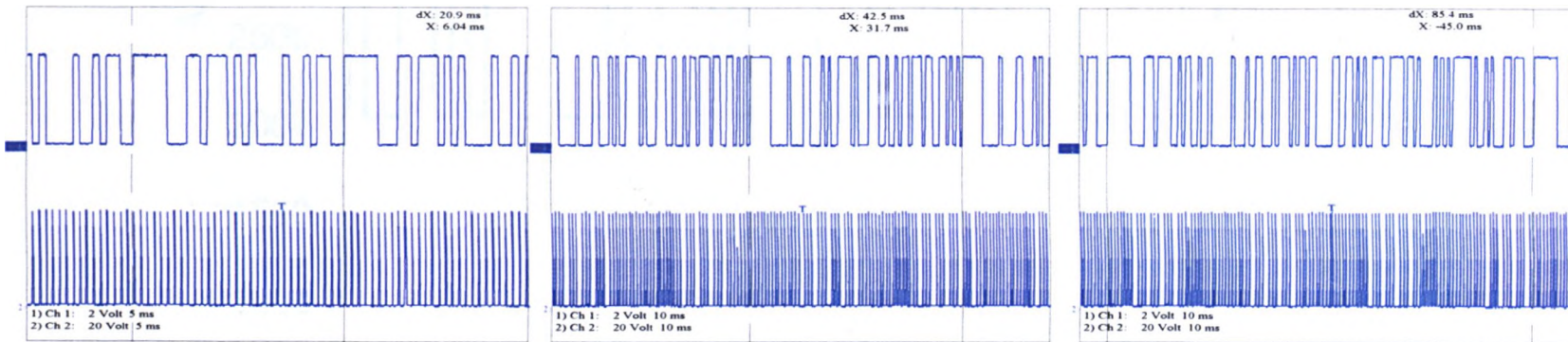


Figure 48: Nylon nitrile membrane attenuation characteristics



7 Step PRBS

15 Step PRBS



31 Step PRBS

63 Step PRBS

127 Step PRBS

Figure 49: PRBS profiles (upper signal) including clock frequency (lower signal)

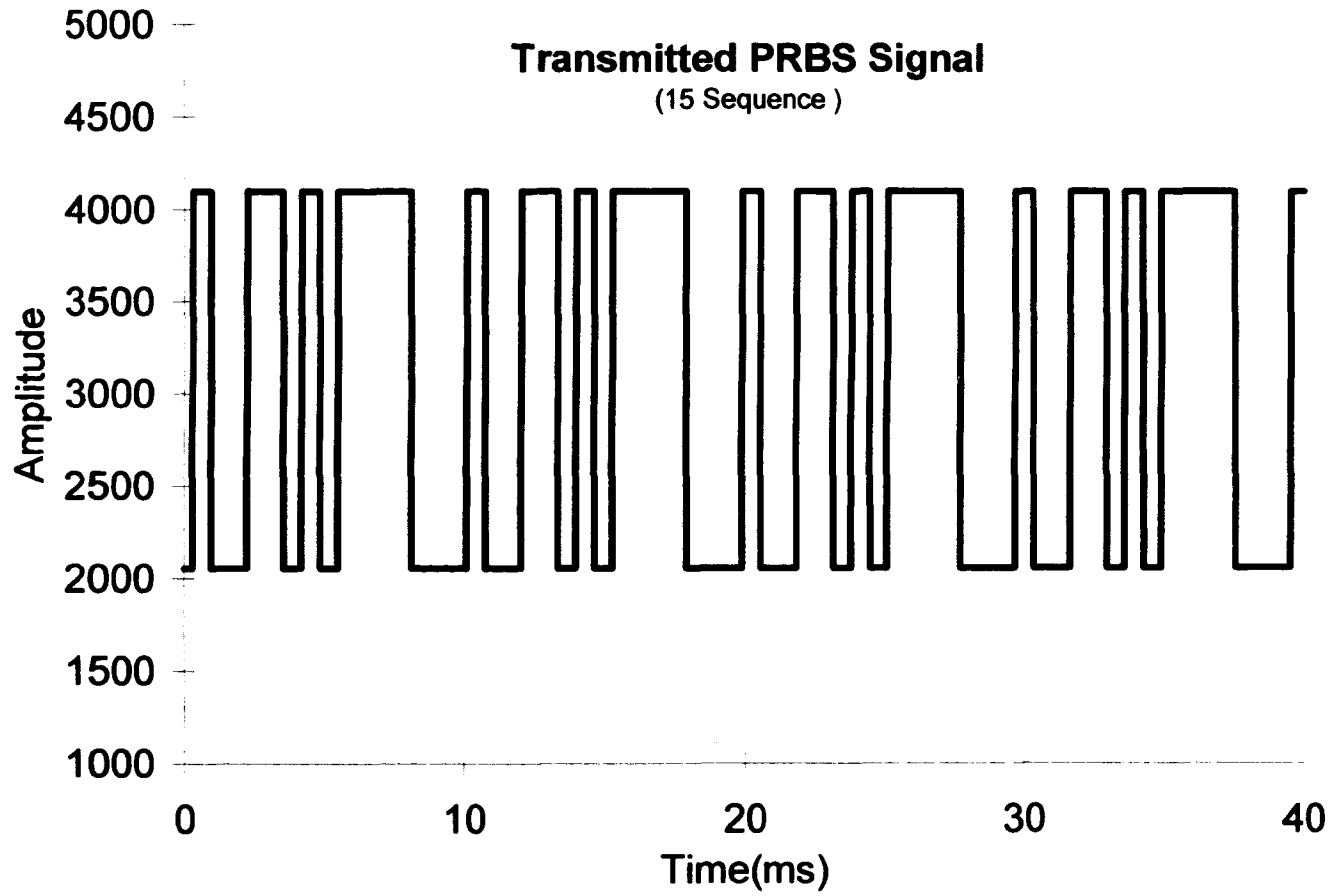


Figure 50: Raw transmitted PRBS signal.

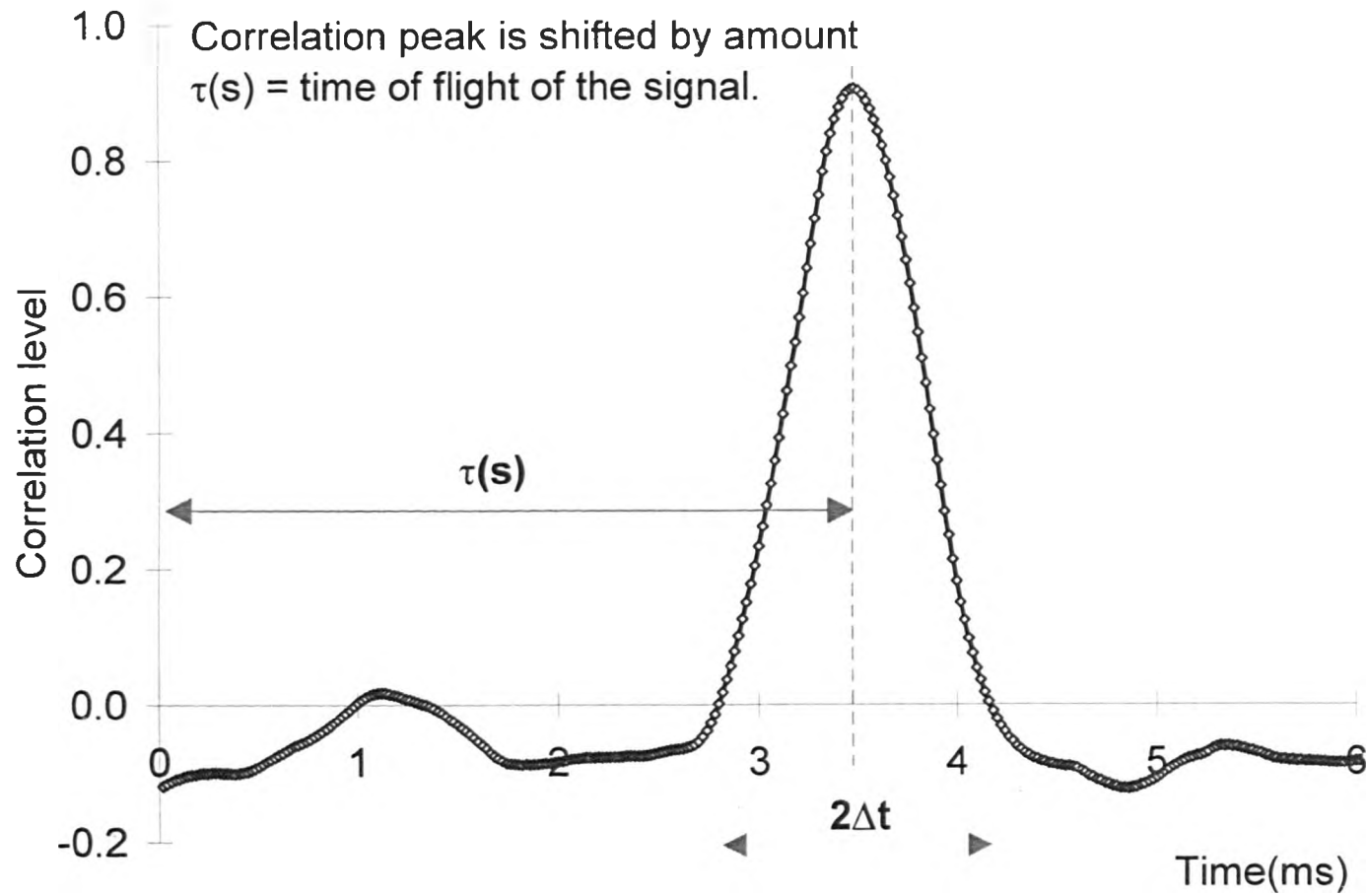


Figure 51: PRBS correlation profile.

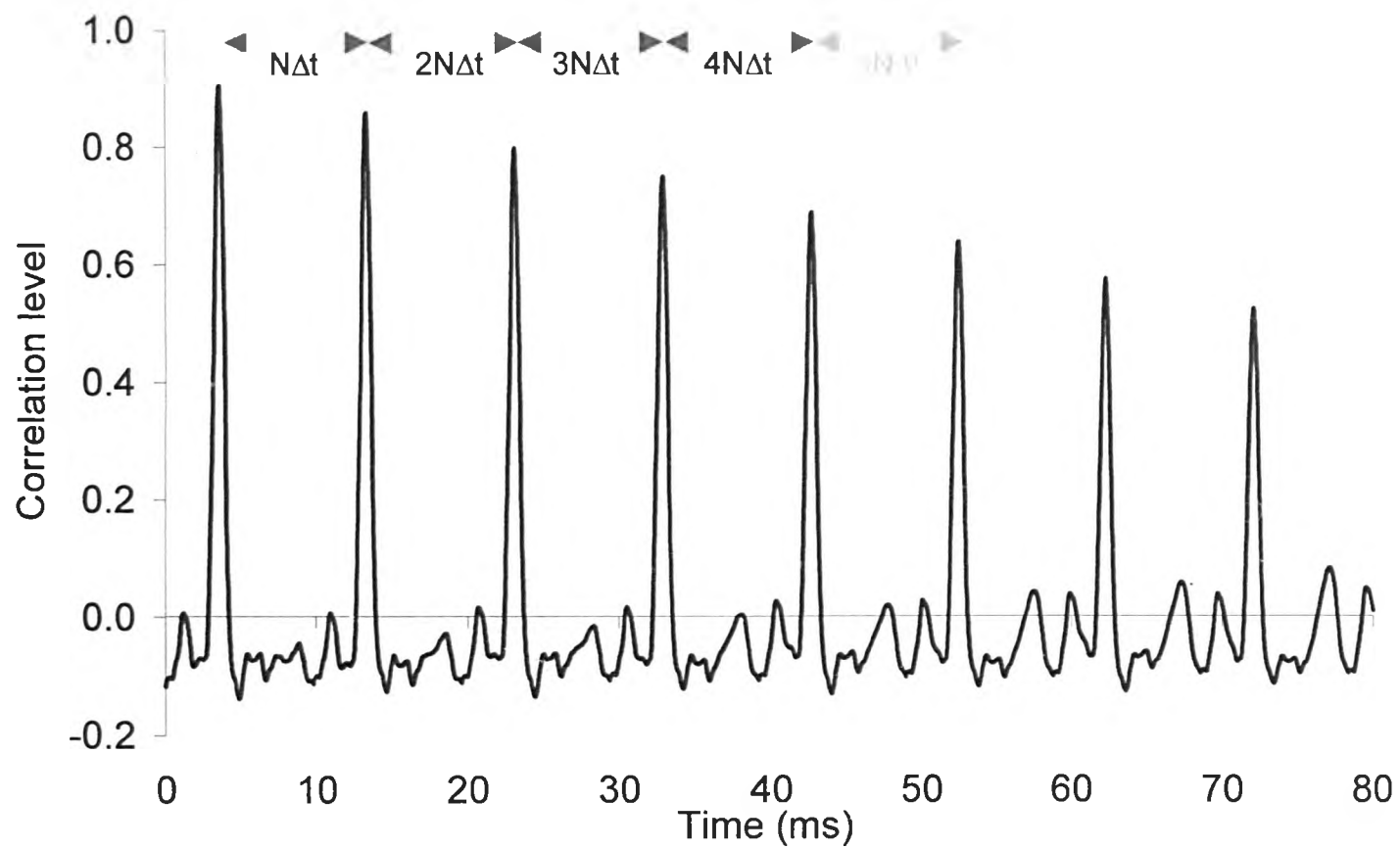


Figure 52: Correlation function of a PRBS signal of period  $N\Delta t$ .

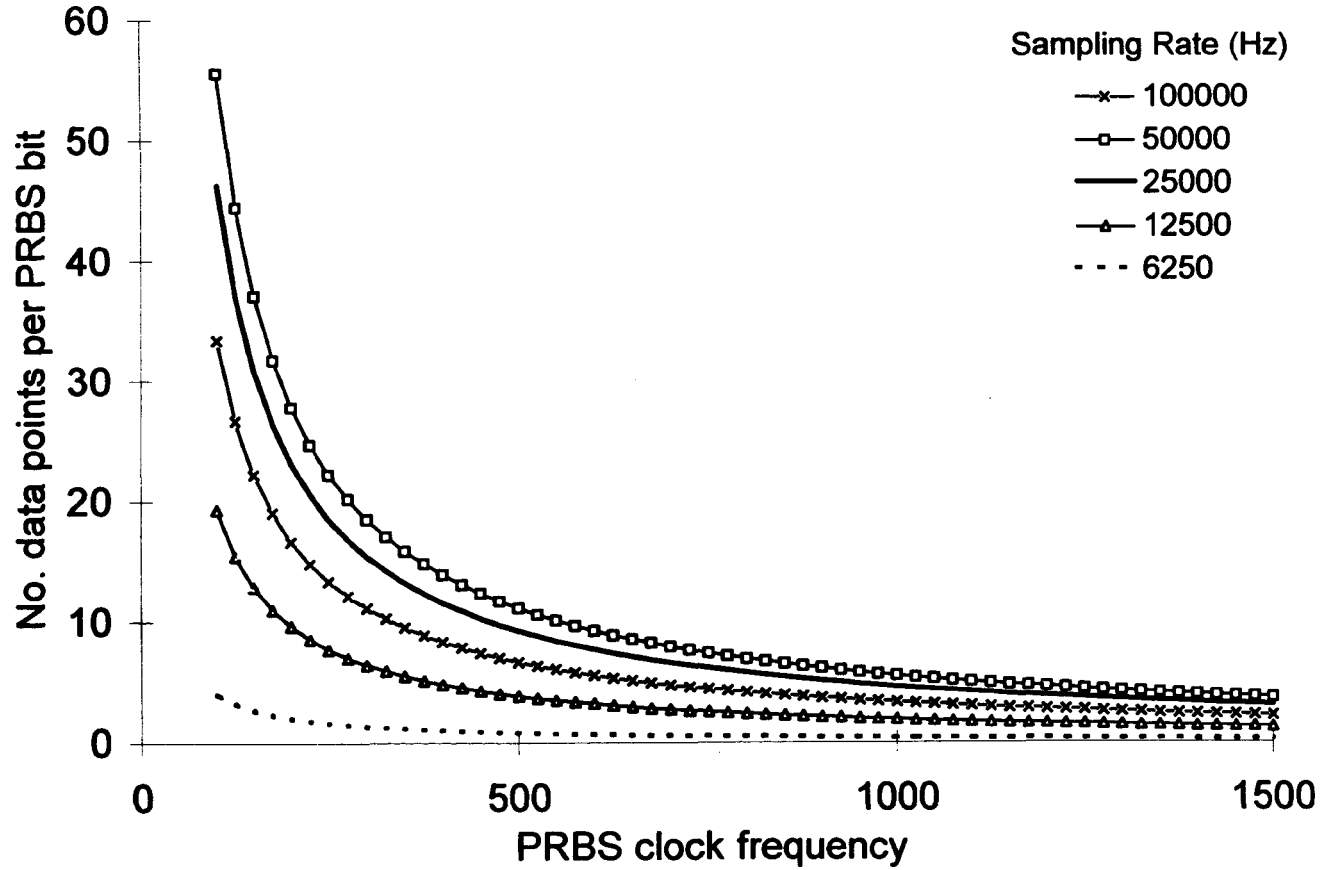


Figure 53: Sampling considerations for a 15 bit PRBS.

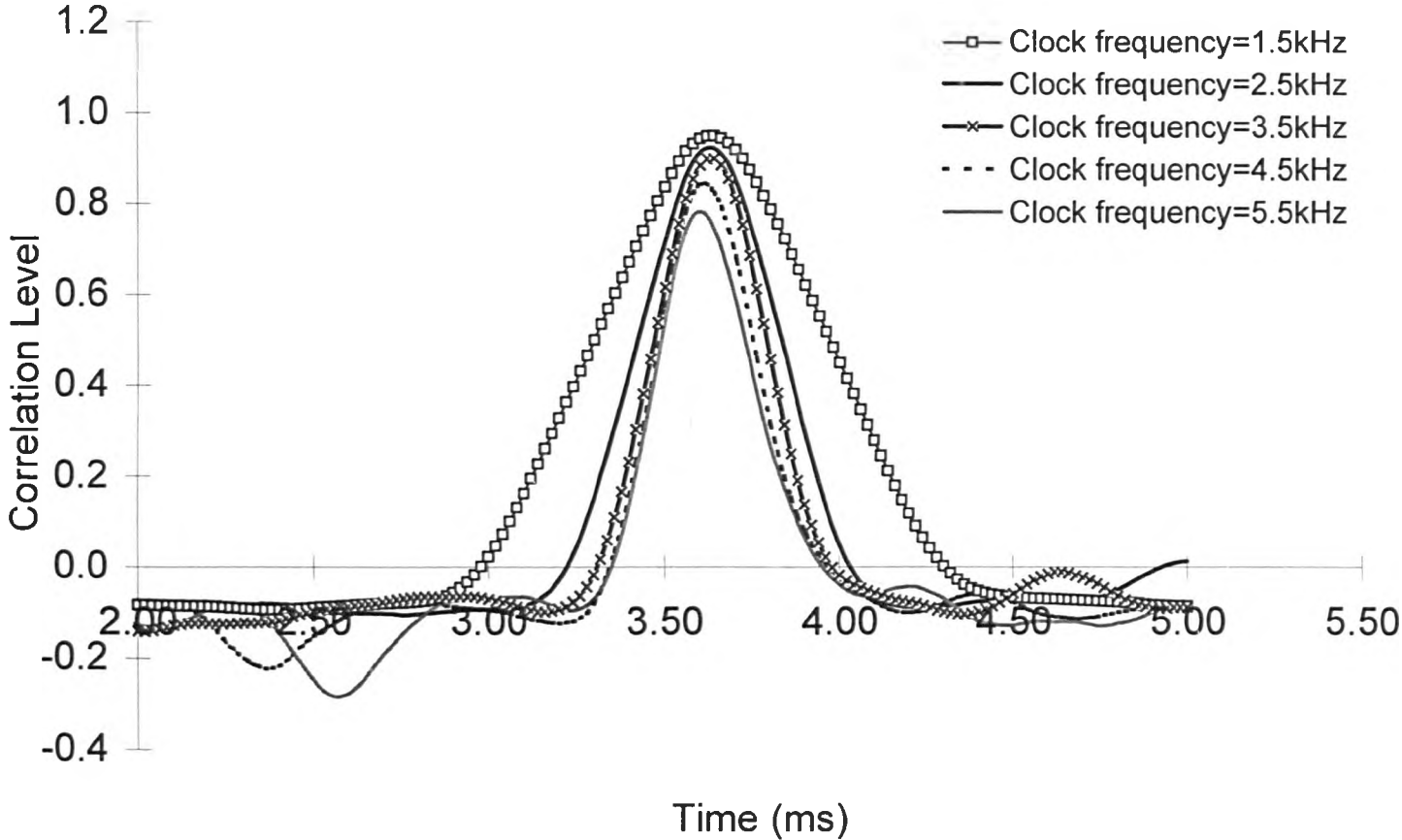


Figure 54: Effect of reducing the PRBS period on the correlation profile.

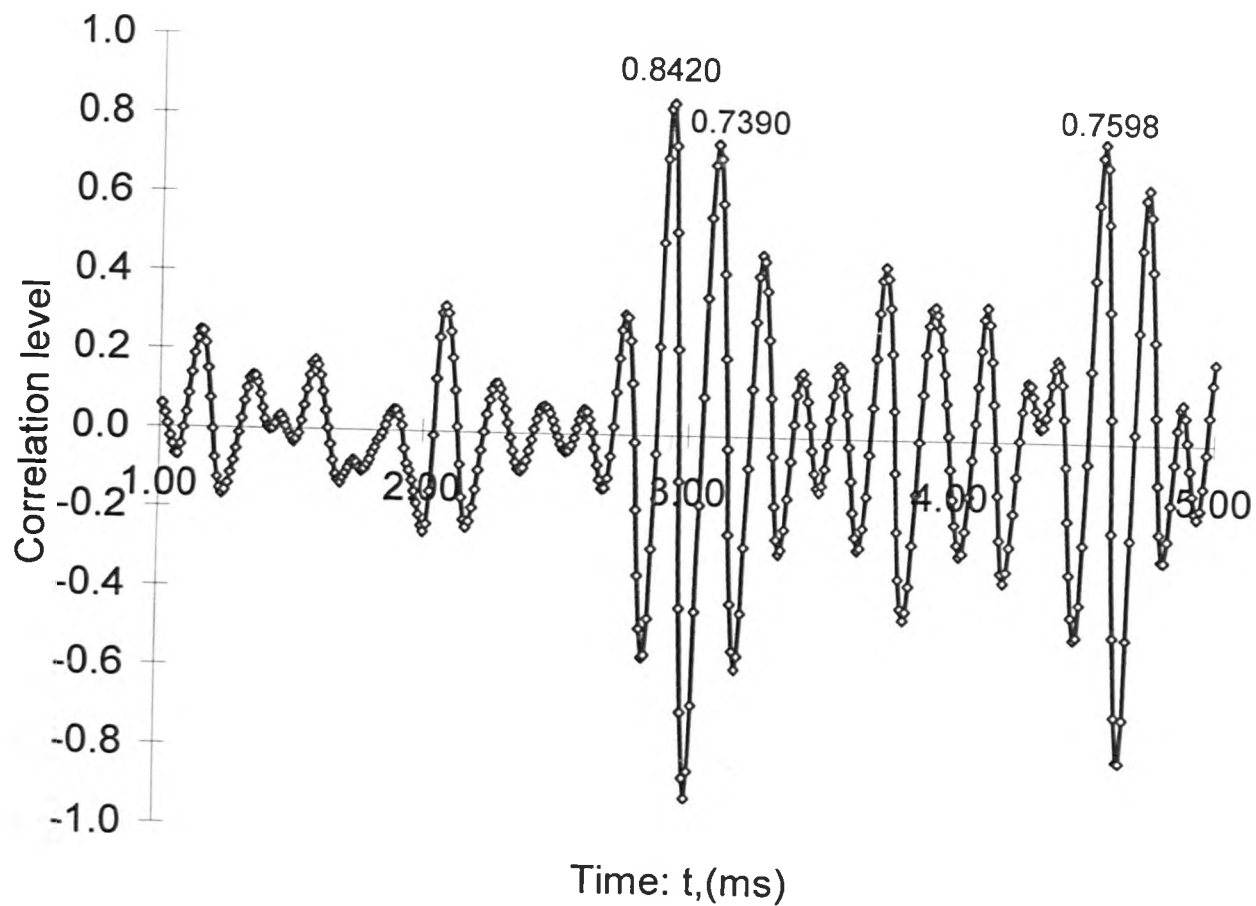
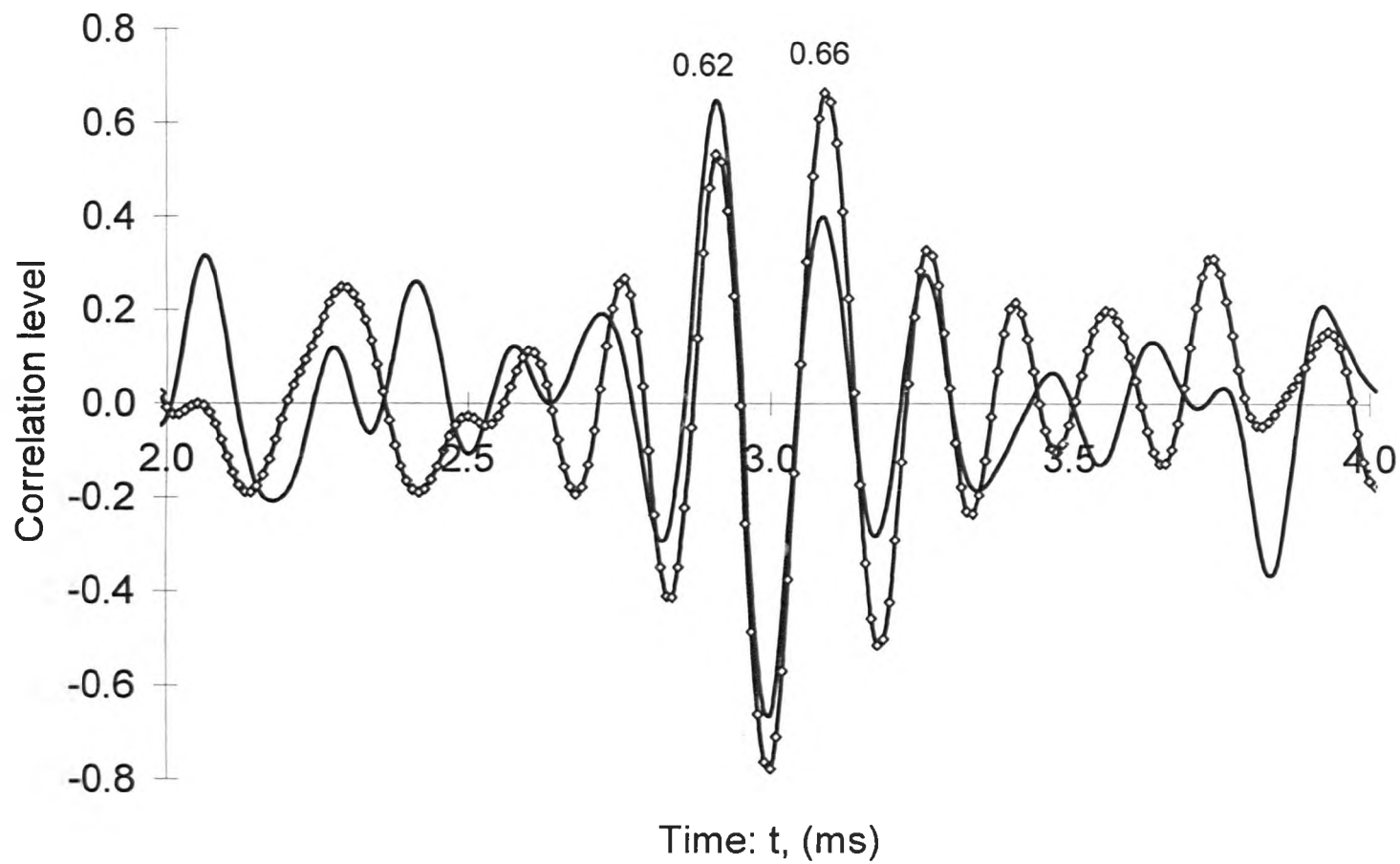


Figure 55: Chirp correlation profile for low noise conditions.



**Figure 56: Chirp correlation profiles of two signals under similar conditions.**

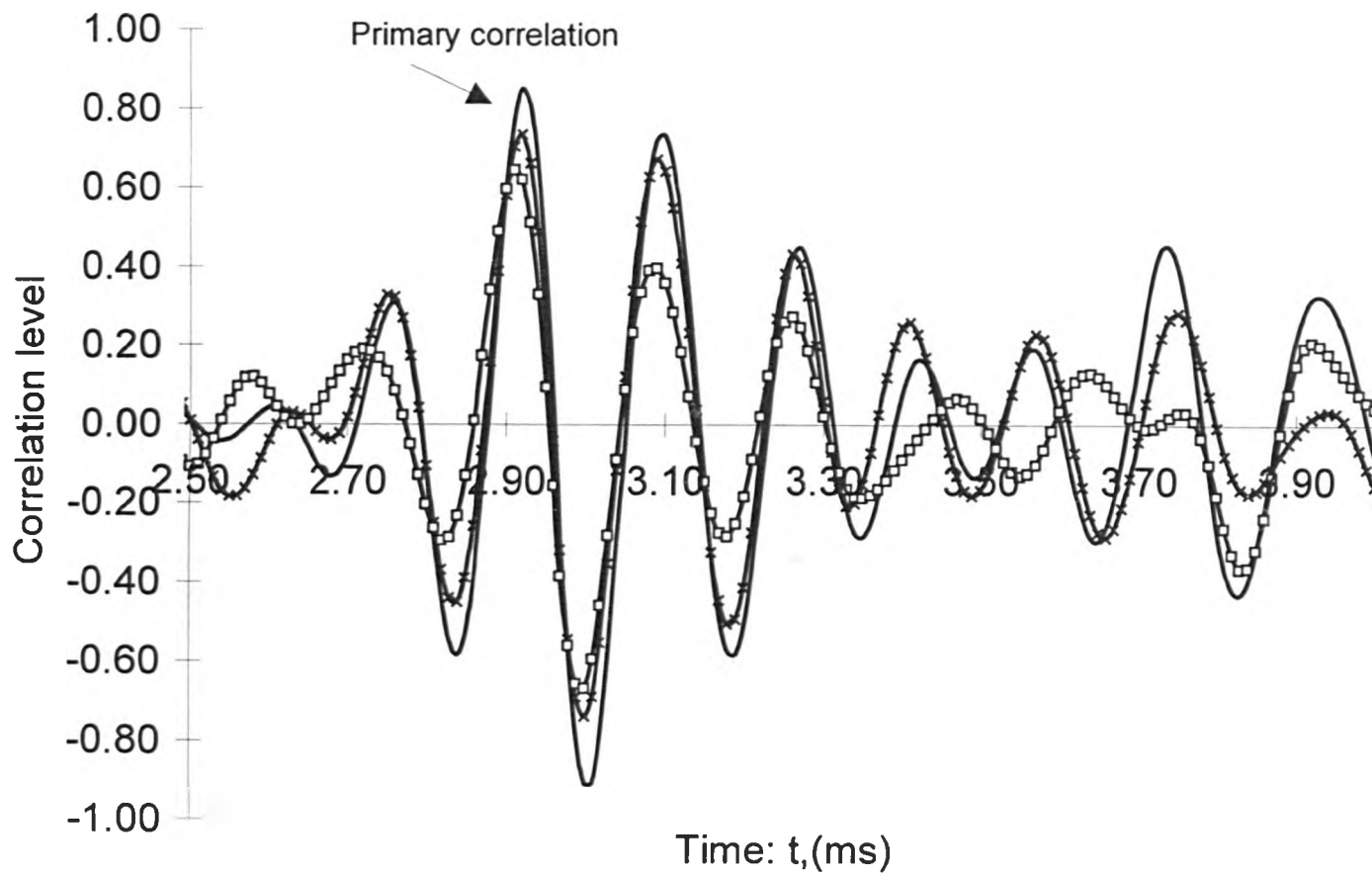


Figure 57: Chirp correlation profiles for increasing noise levels.

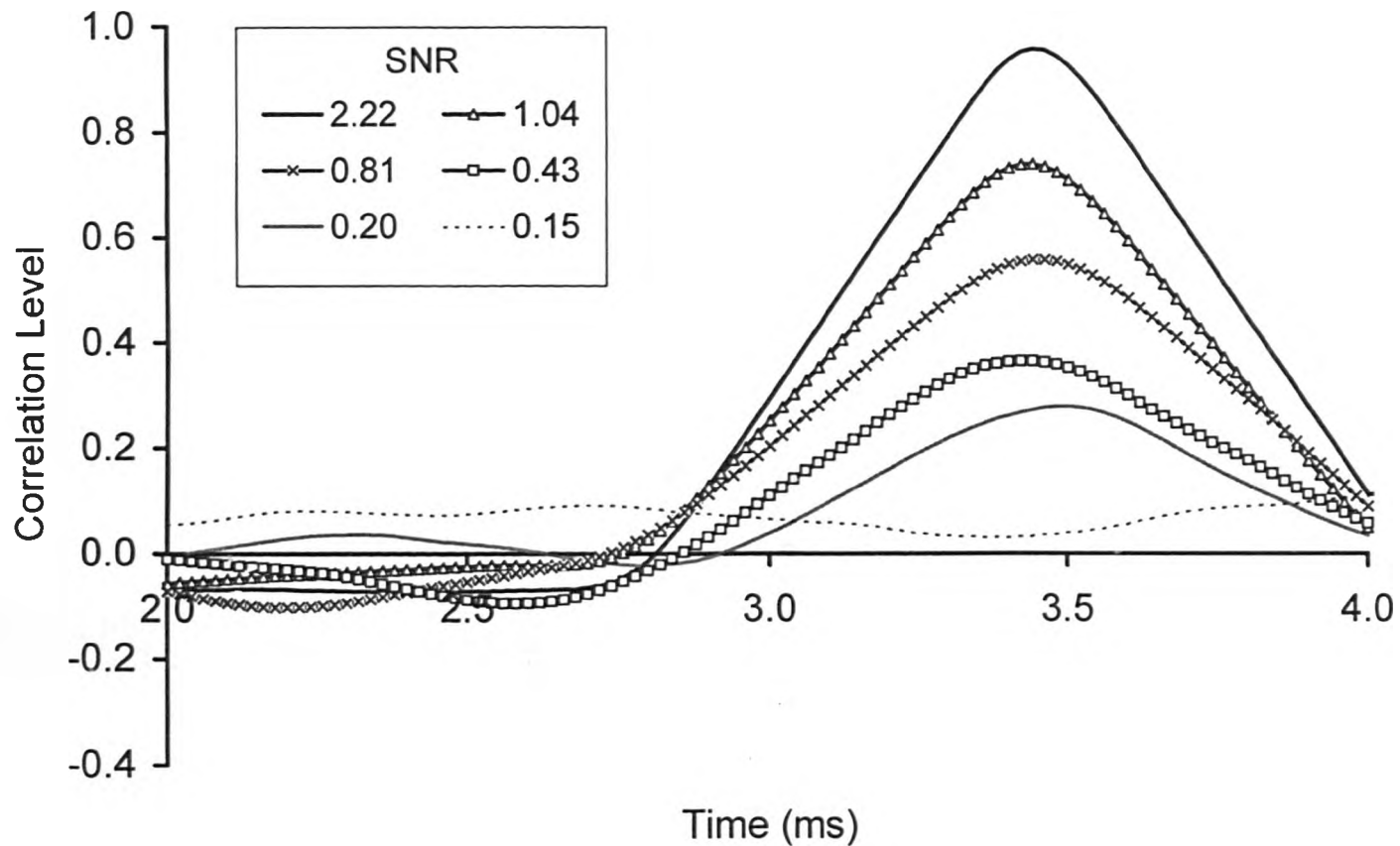


Figure 58: PRBS correlation profiles for various levels of SNR

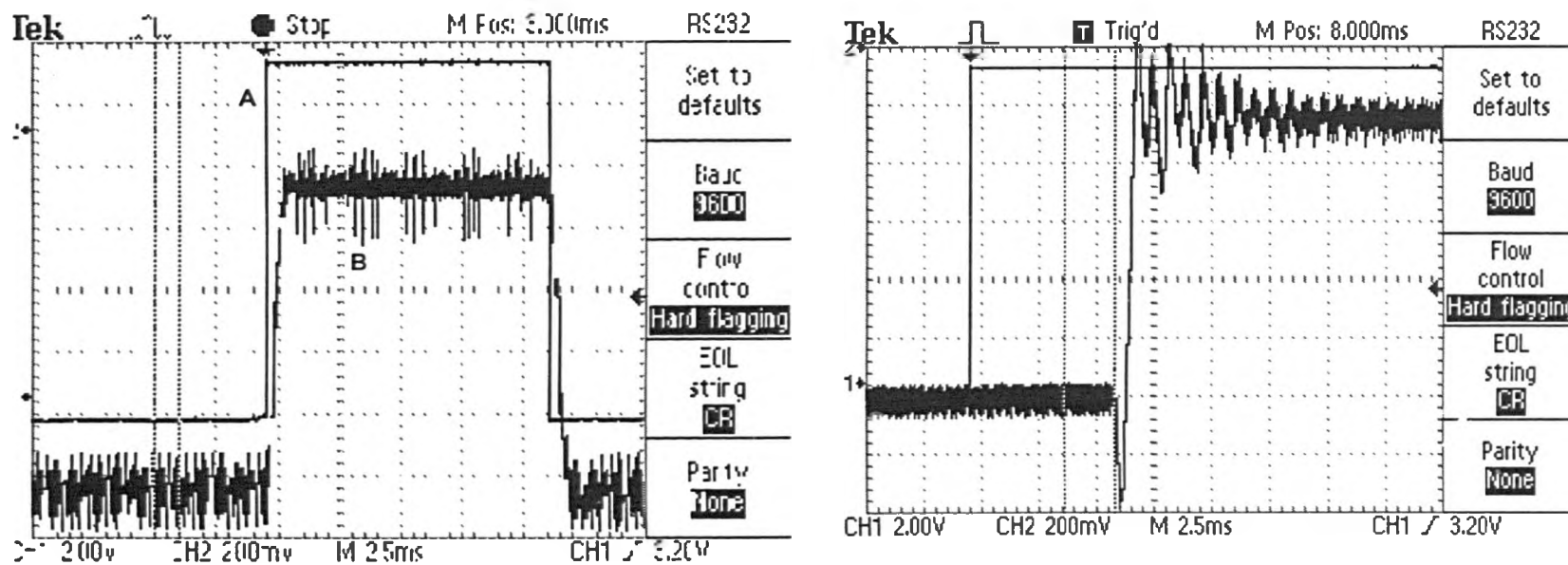
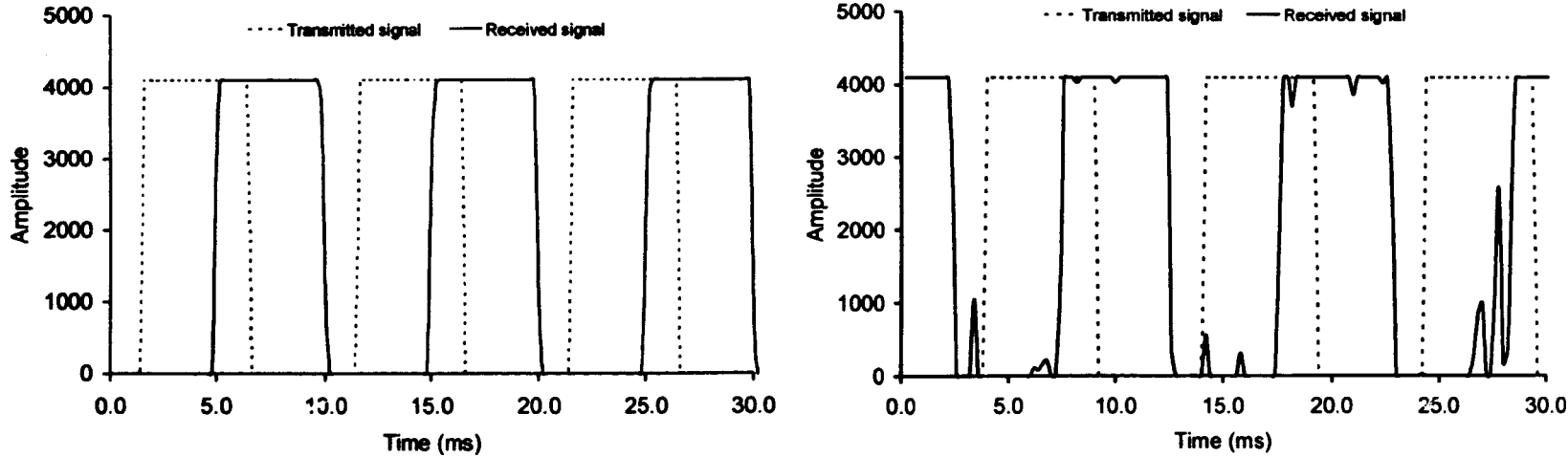
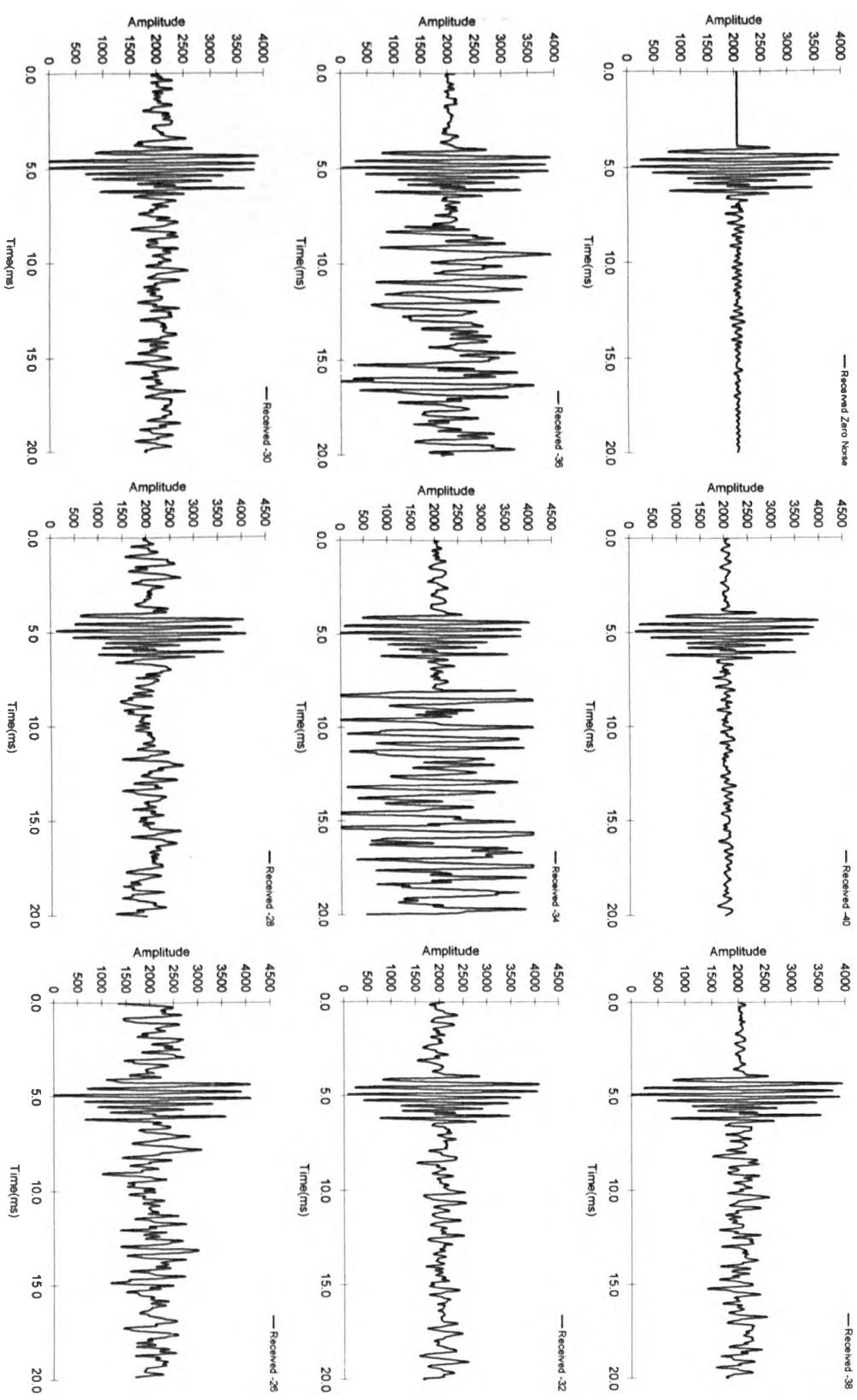
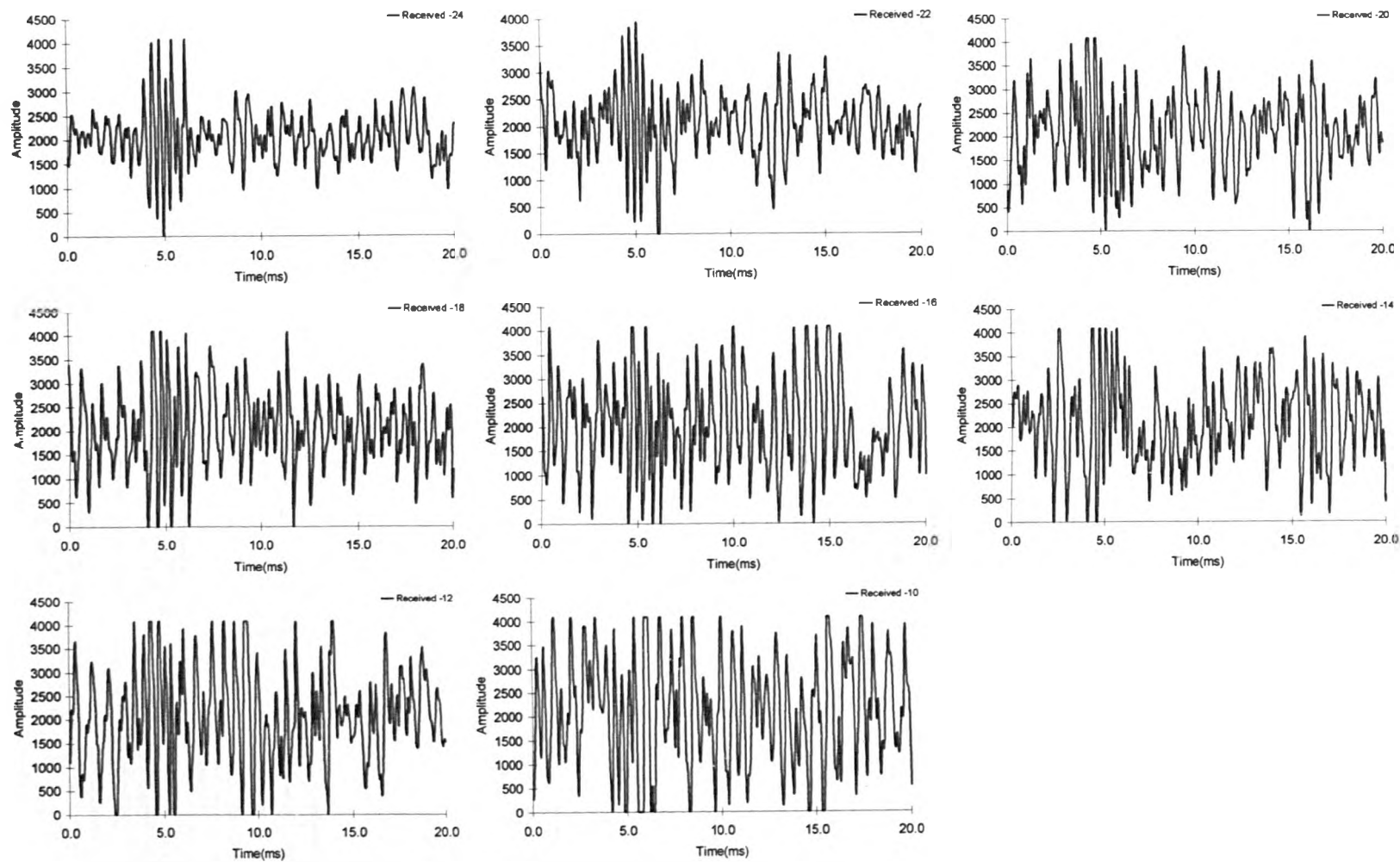


Figure 59(a,b): Oscilloscope traces of modulated and demodulated signals.

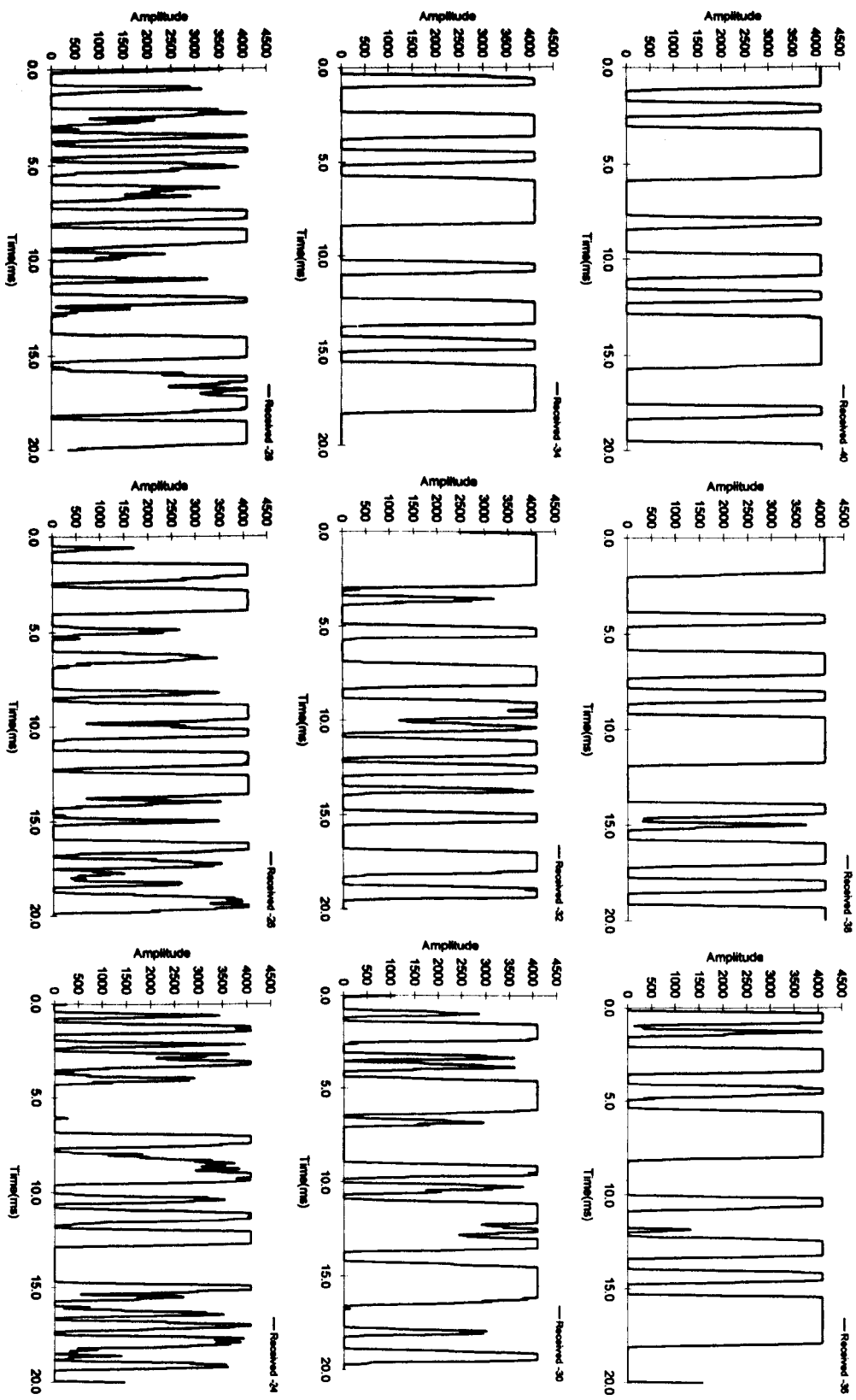


**Figure 60: a) FM signal in low noise & b) FM signal degradation for increasing noise**





**Figure 61: Received chirp signal profiles in the presence of increasing noise levels.**



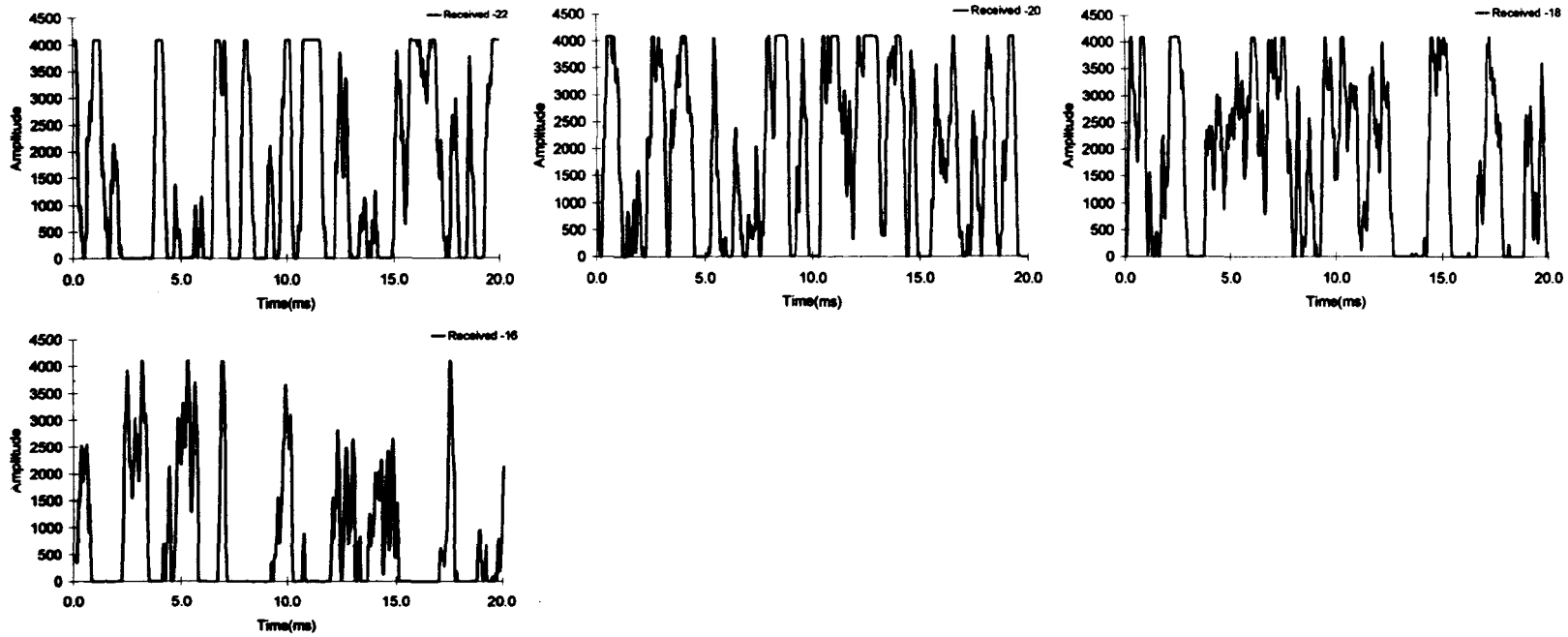


**Figure 62: PRBS received signal profiles in the presence of increasing noise levels.**

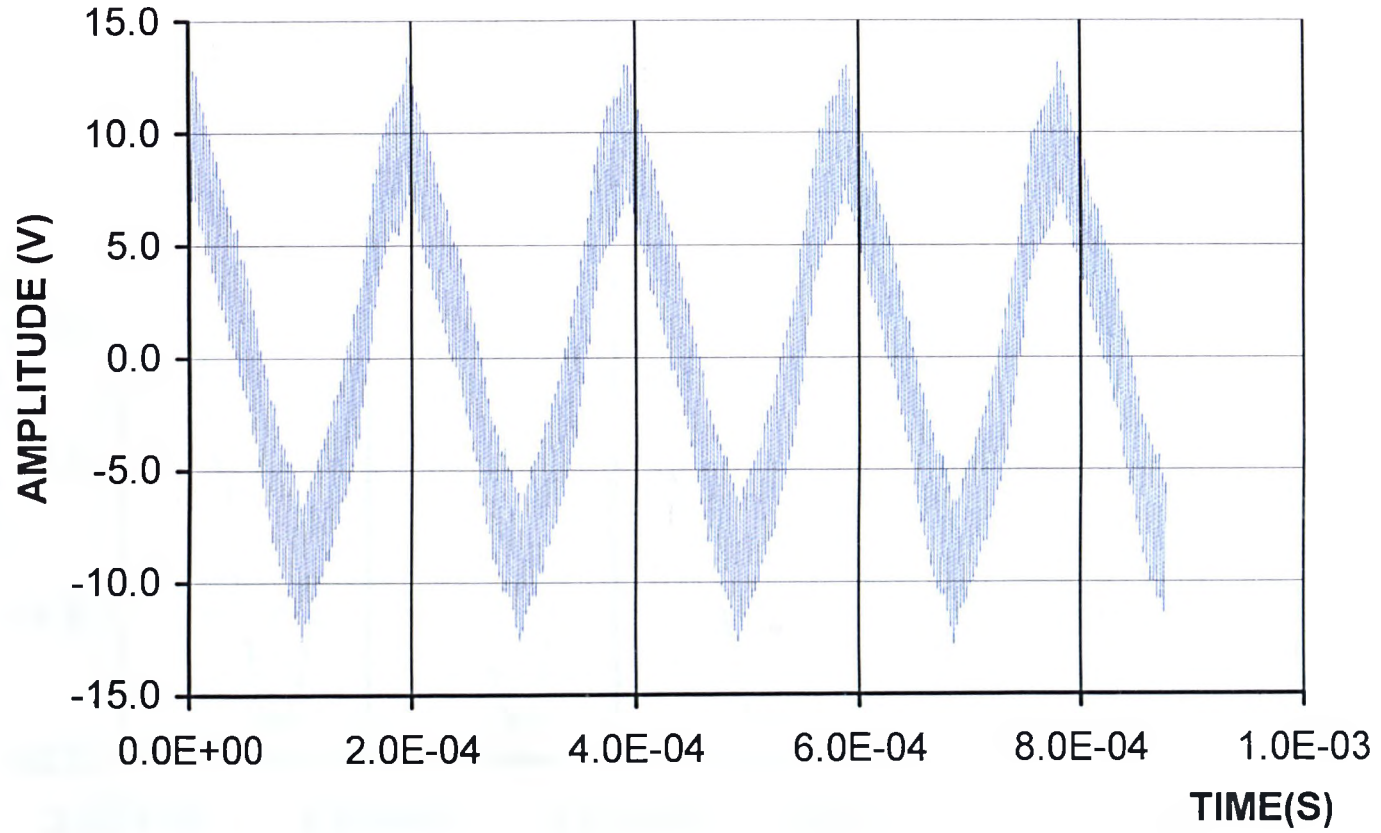


**Figure 63: Plot of the modulated signal at the amplifier output at maximum gain (zero modulation)**

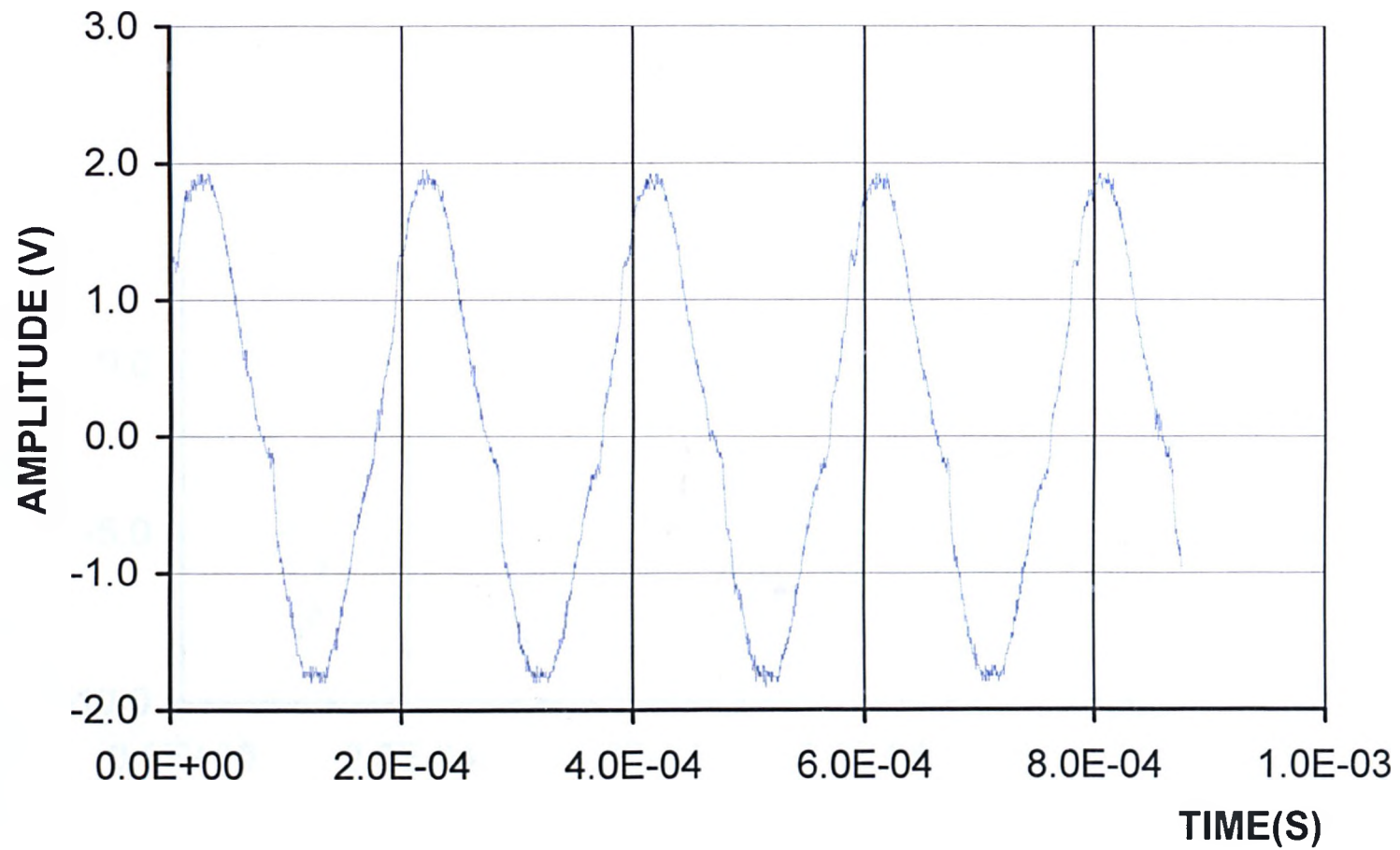


Figure 64: Plot of the modulated signal at the amplifier output at reduced gain (zero modulation)

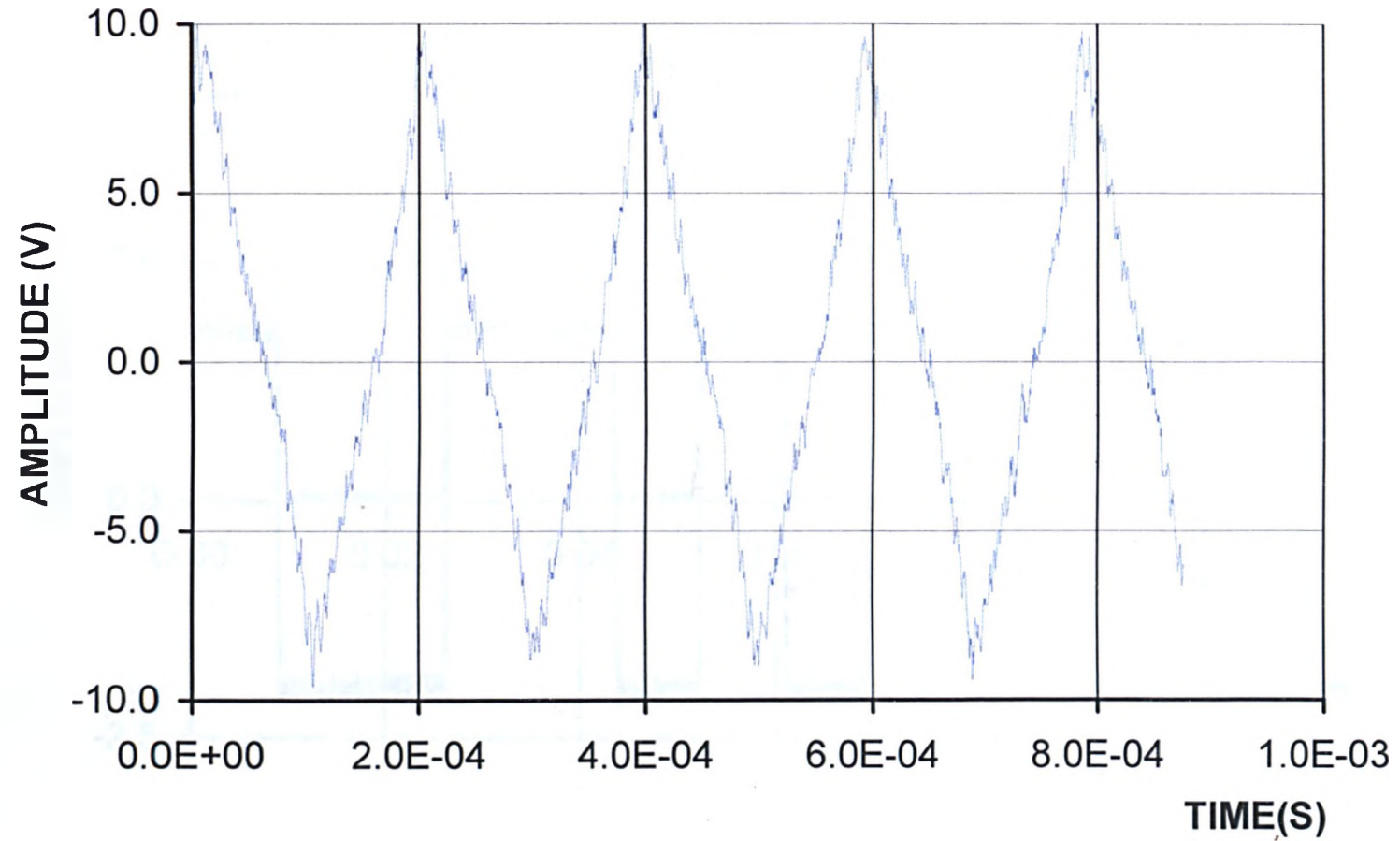


Figure 65: Plot of the modulated signal at the amplifier output at maximum gain (zero modulation) with filter

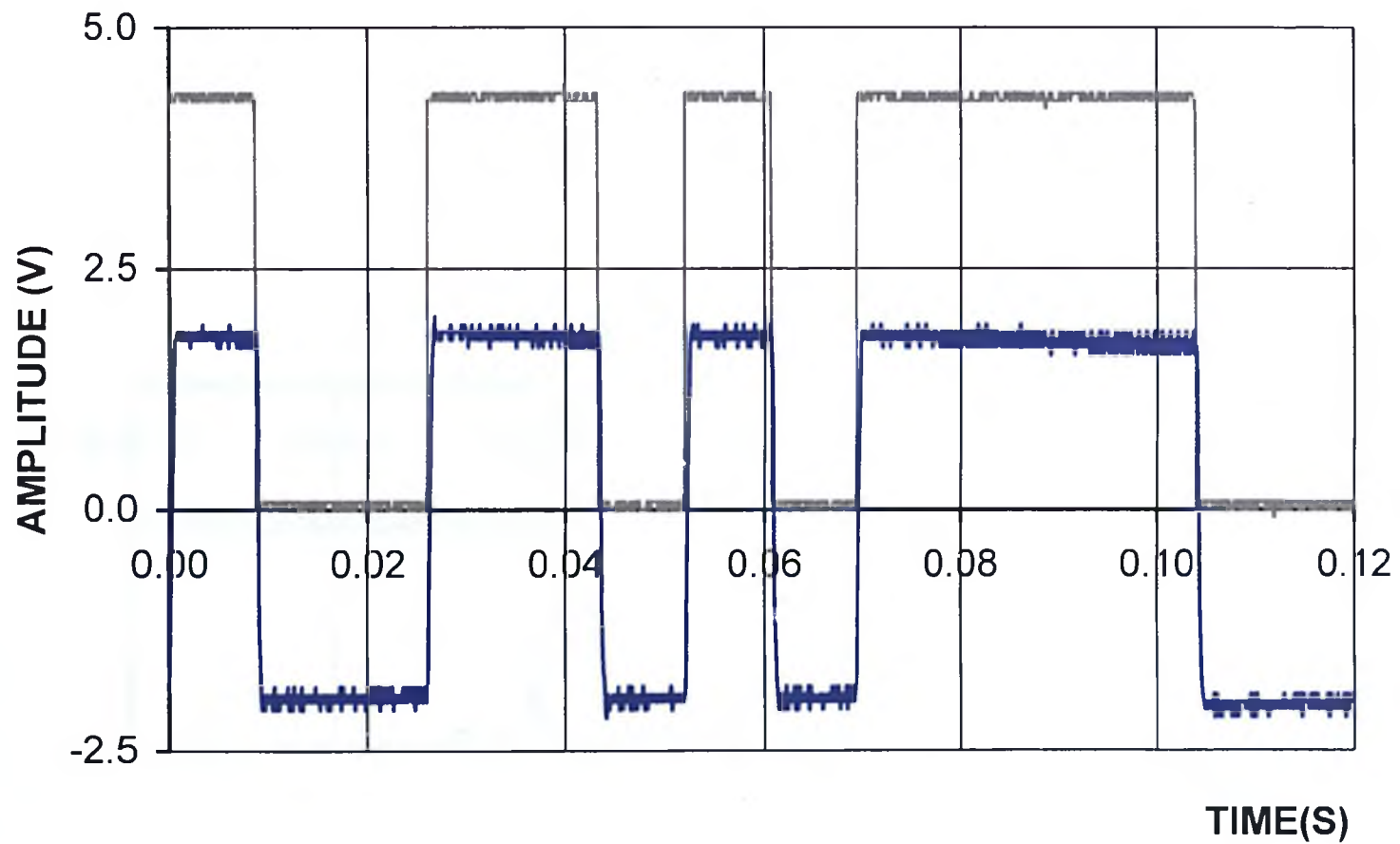


Figure 66: Direct input raw PRBS input signal with demodulated output signal (low clock frequency)

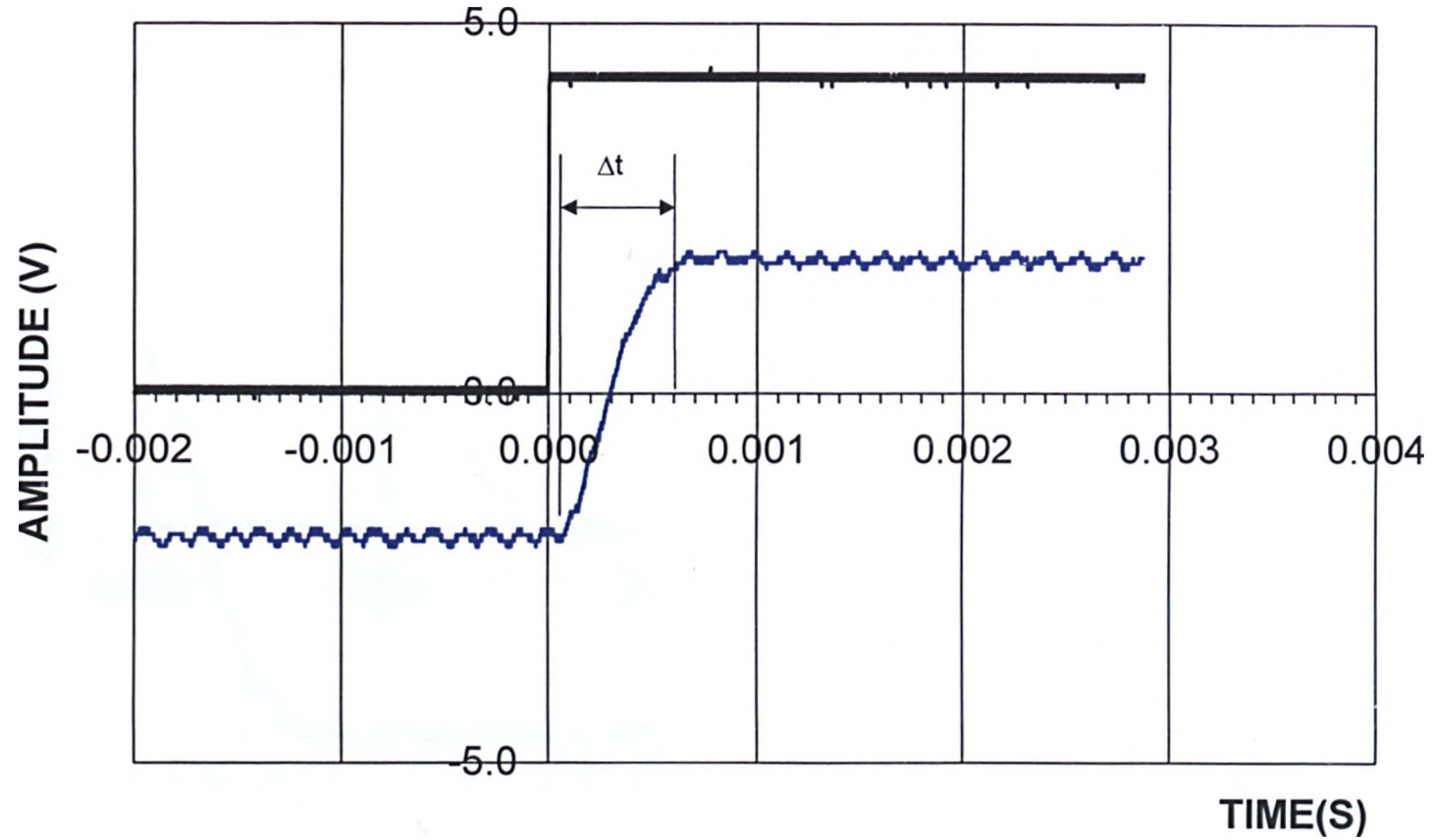


Figure 67: Direct input raw PRBS input signal with demodulated output signal to indicate circuit delay (low clock frequency)

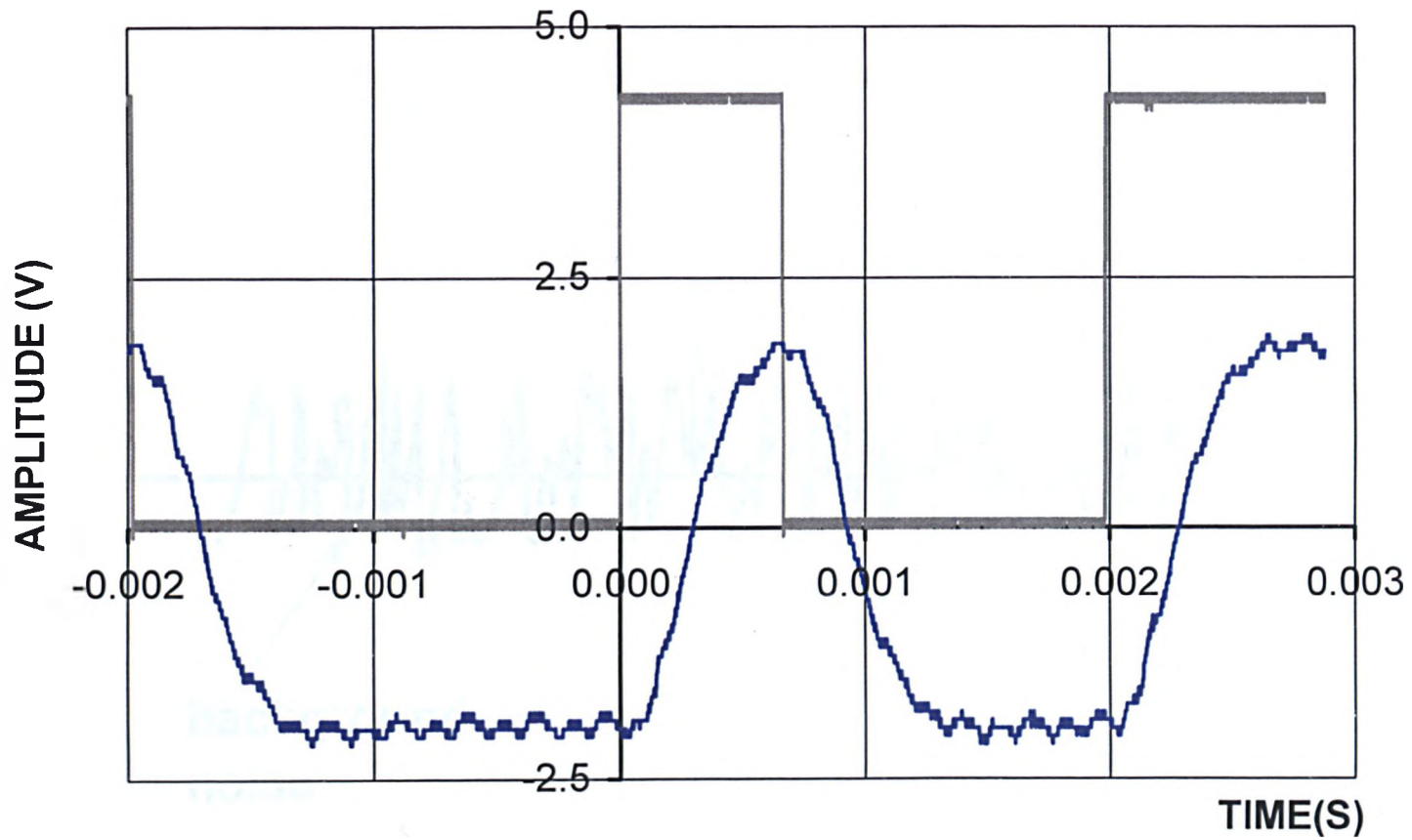
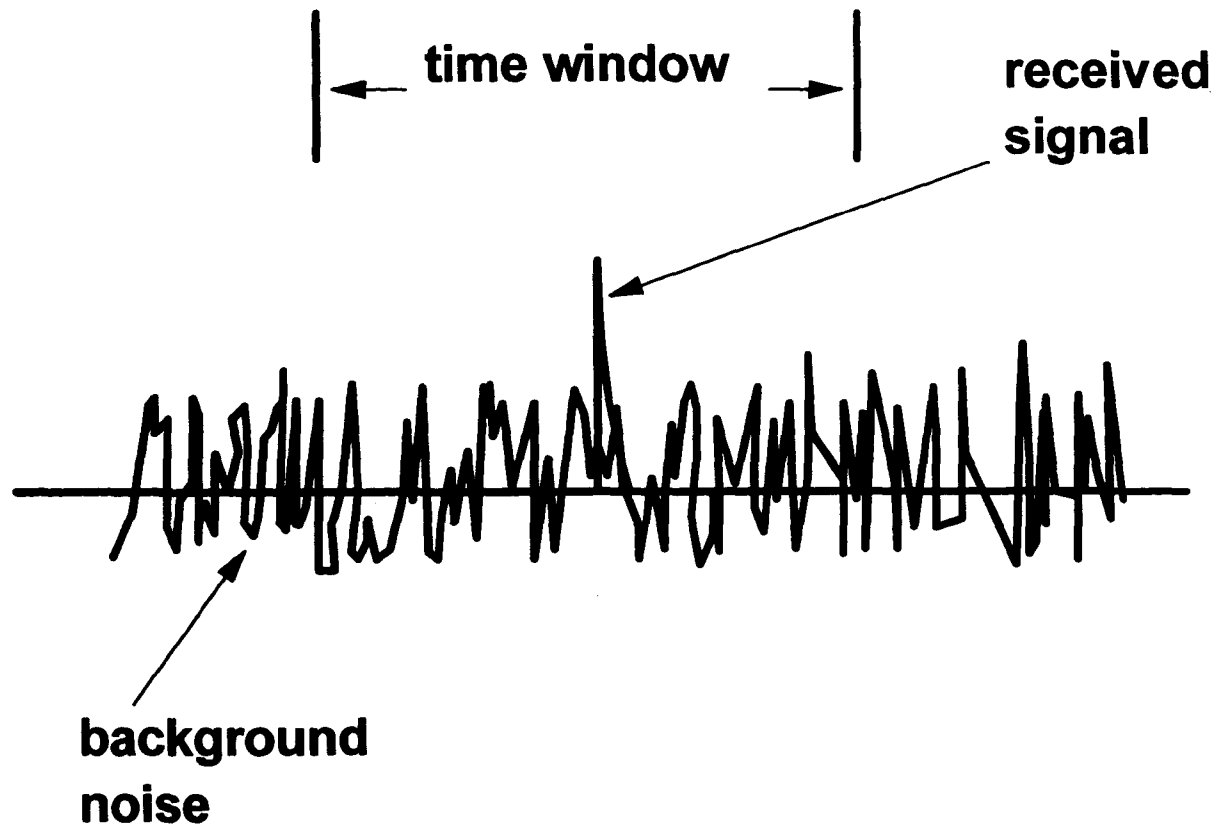
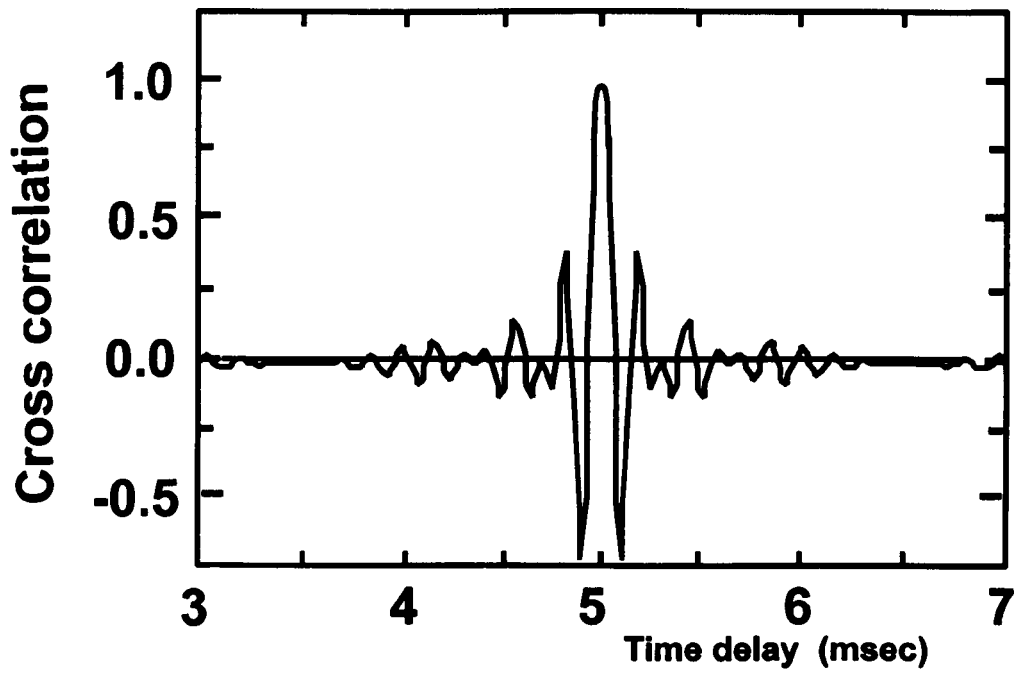


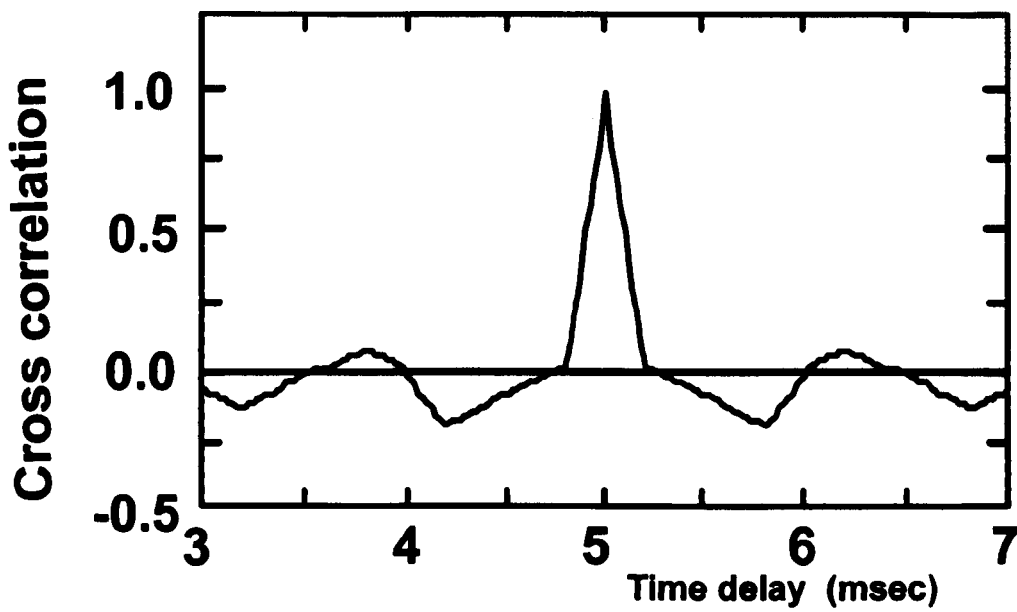
Figure 68: Direct input raw PRBS input signal with demodulated output signal (high clock frequency)



**Figure 69: Single shock pulse embedded in acoustic noise.**



a)



b)

**Figure 70: Noise free correlation functions of transmitted signals of 3ms duration and sampled at 150 points: (a) single sequence 15 bit PRBS, (b) chirp function with frequency from 4 to 6 kHz.**

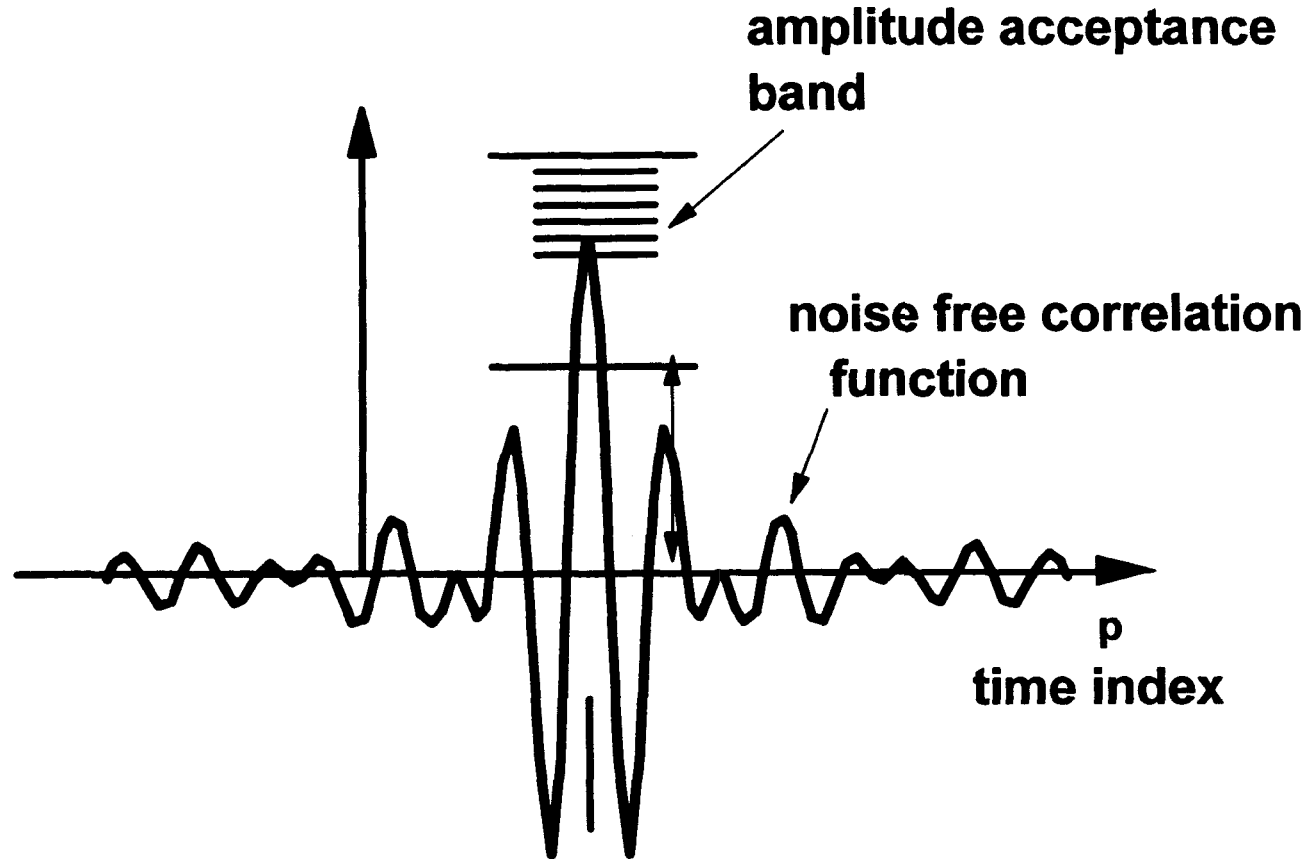


**Figure 71: Model used to estimate variance of the measured transit time due to background noise using the correlation method.**

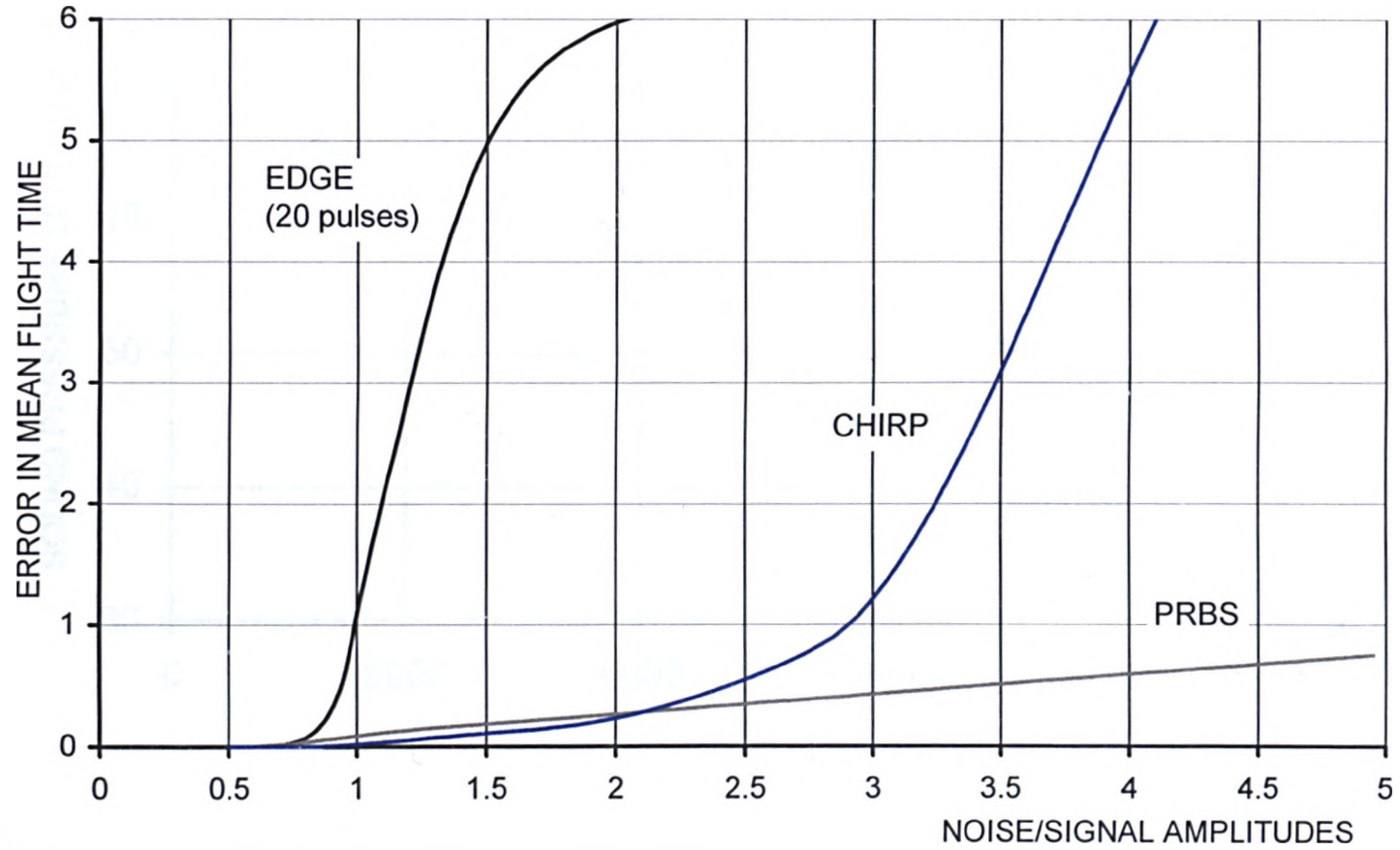
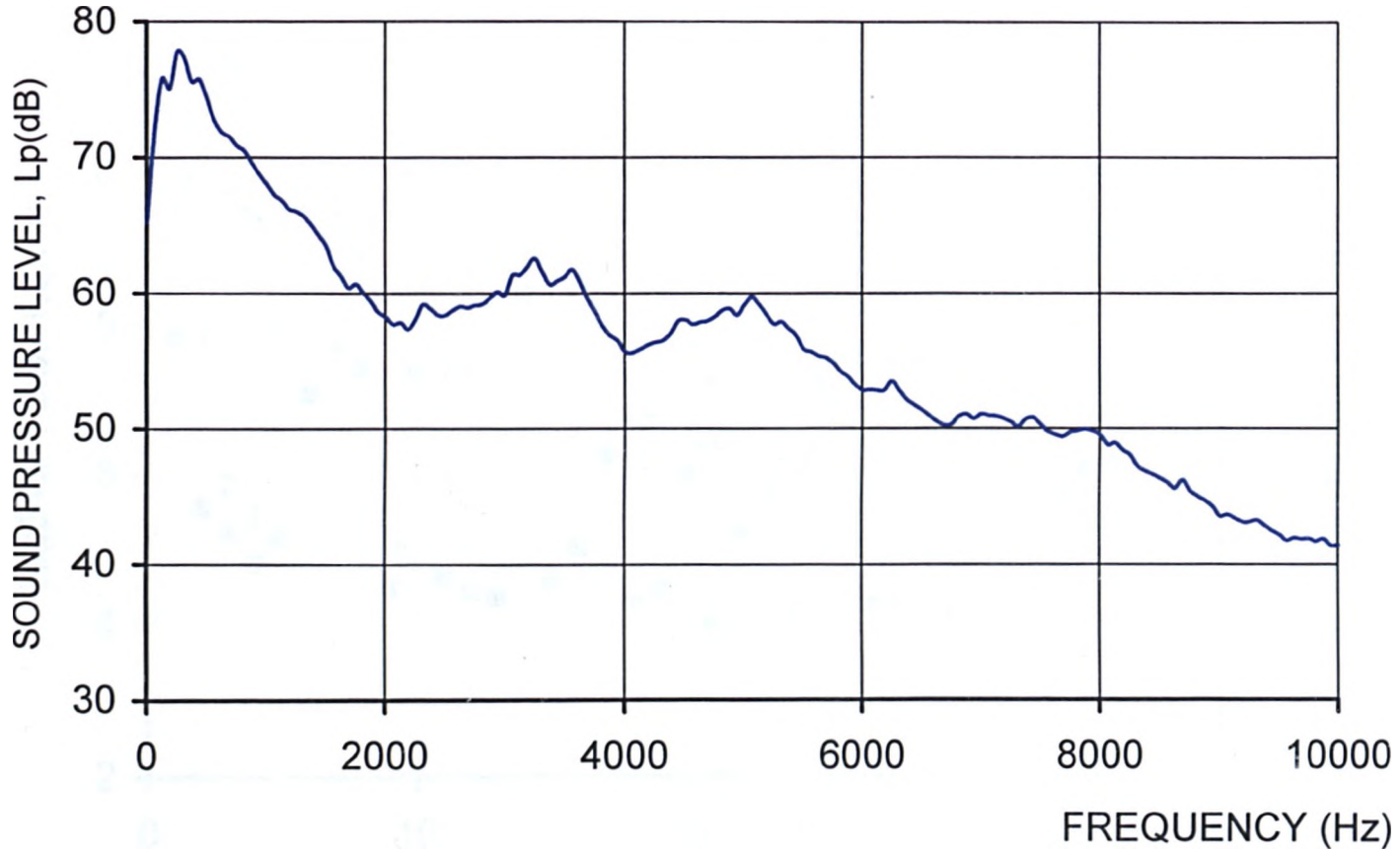


Figure 72: The relative performance error for edge, chirp and PRBS as function of noise/signal amplitude



**Figure 73: Average combustion and background noise levels for the combustion of 1.0 kg/s propane at the fire rig test facility.**

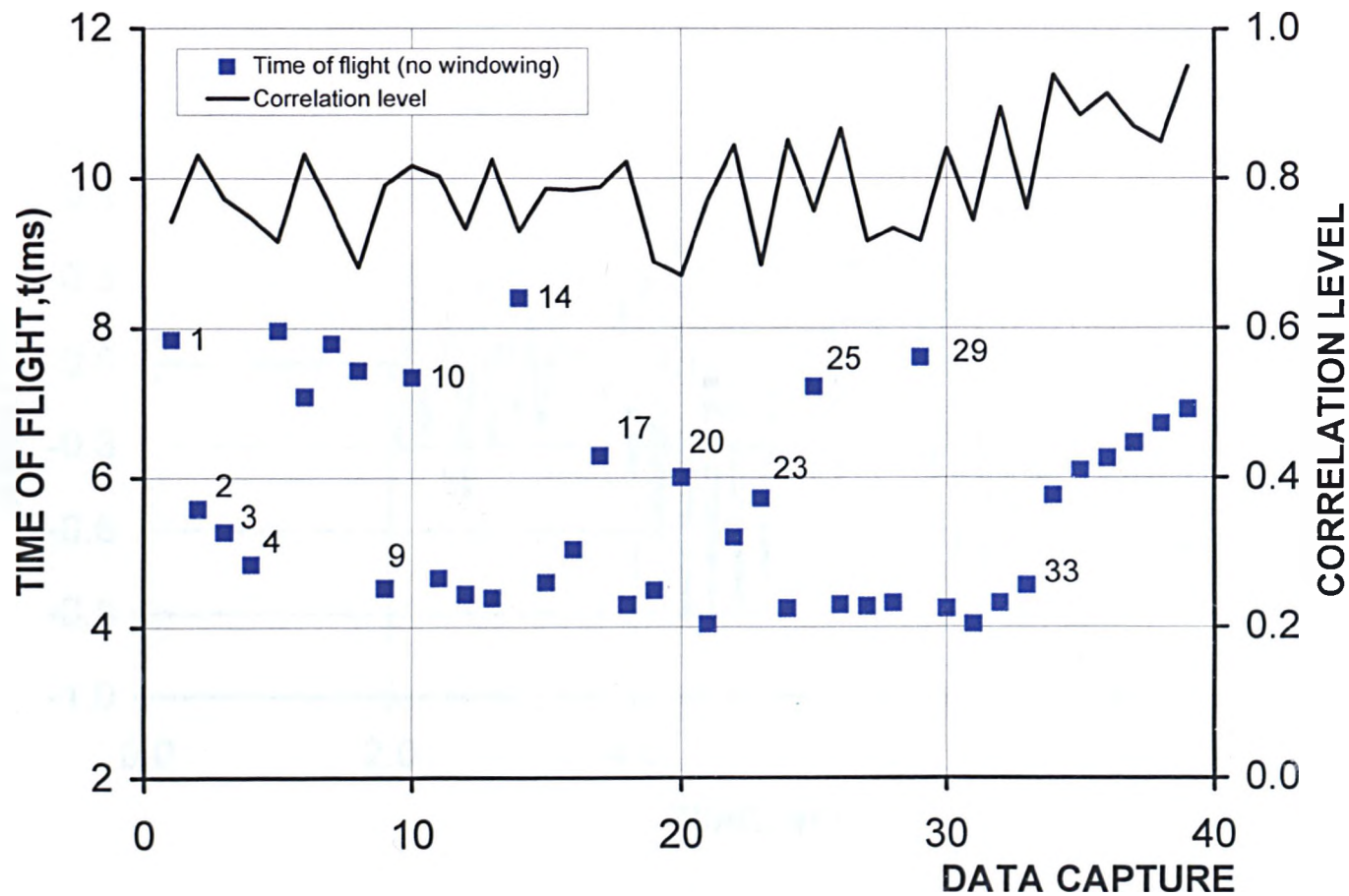
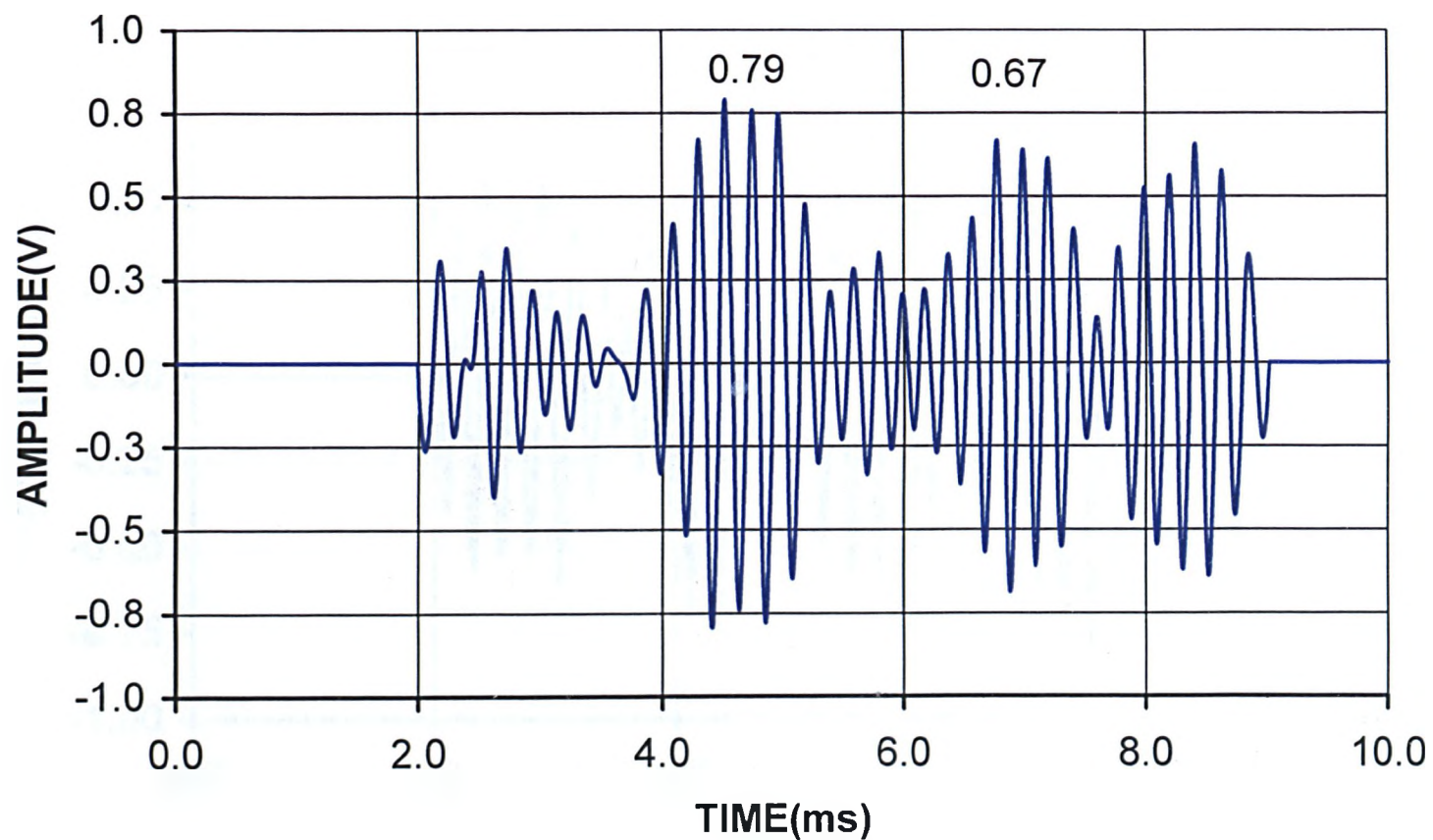
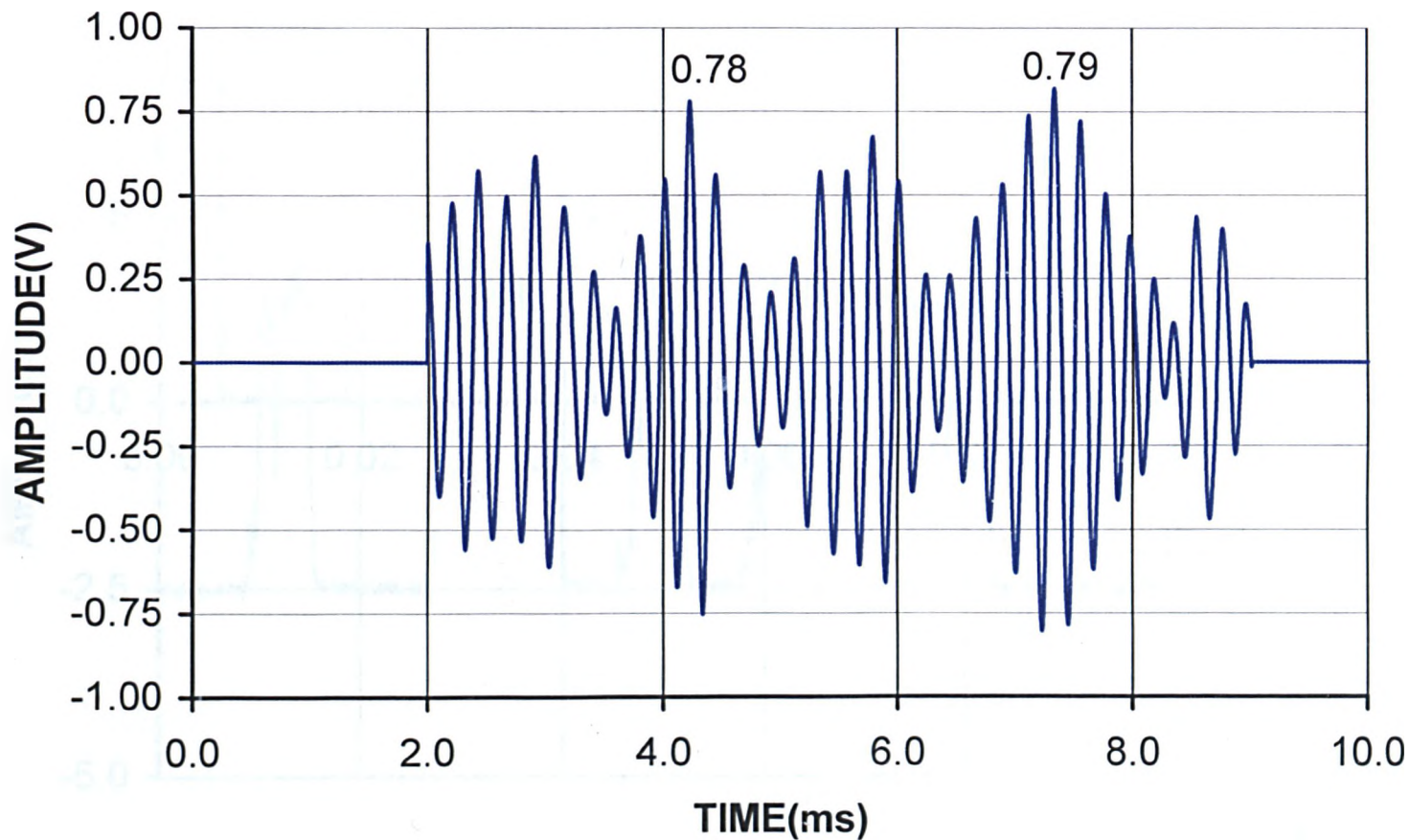


Figure 74: Chirp flight time and correlation values measured at the exit of the compartment fire rig with combustion of 0.1kg/s propane ( $x=3.465\text{m}$ )



**Figure 75: Successful chirp correlation profile recorded at the exit of the compartment fire rig with combustion of 0.1kg/s propane (x=3.465m)**



**Figure 76: Failure mode chirp correlation profile recorded at the exit of the compartment fire rig with combustion of 0.1kg/s propane ( $x=3.465\text{m}$ )**

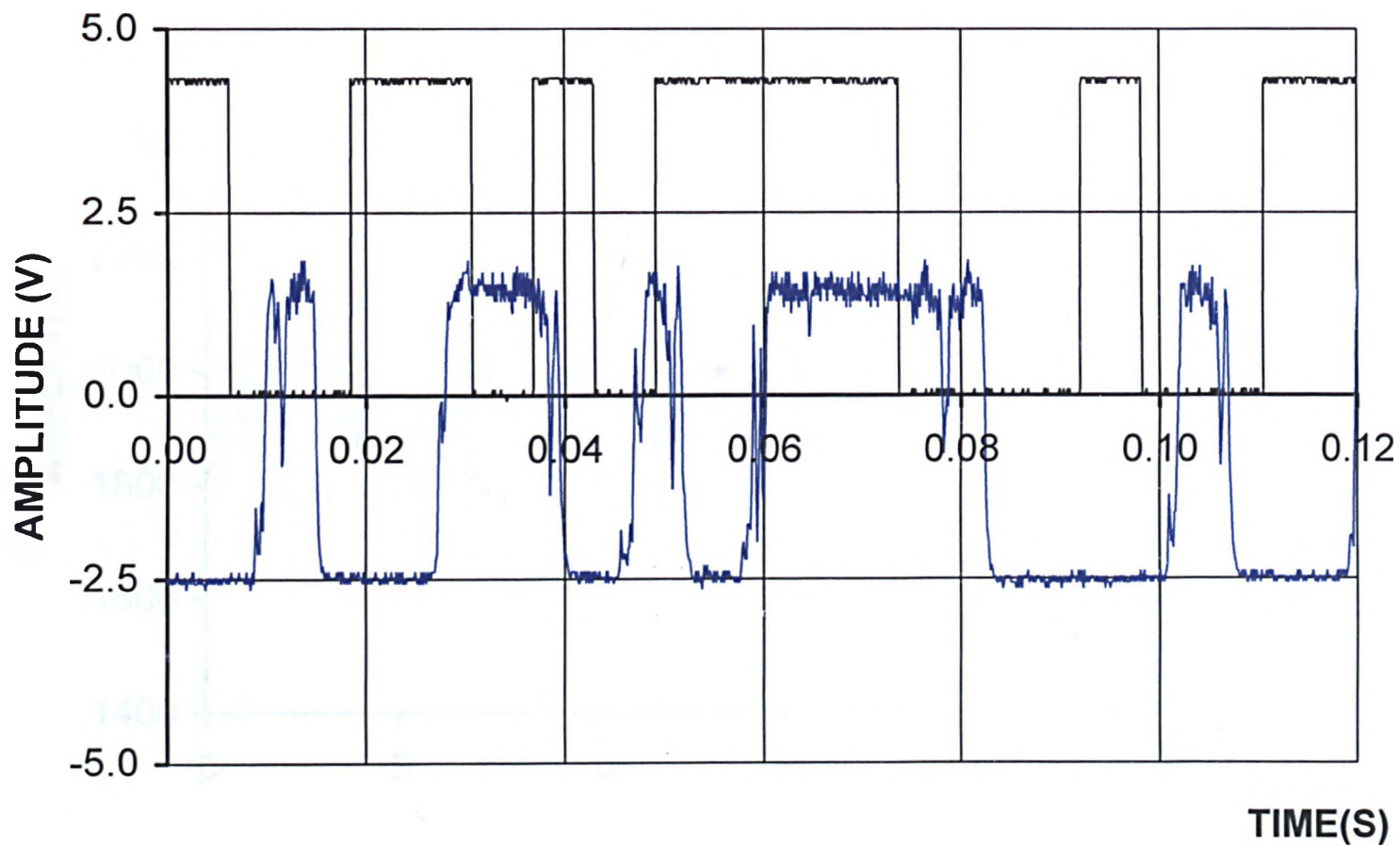


Figure 77: Raw input and demodulated output PRBS signals for ambient conditions ( $x=3.027m$ )

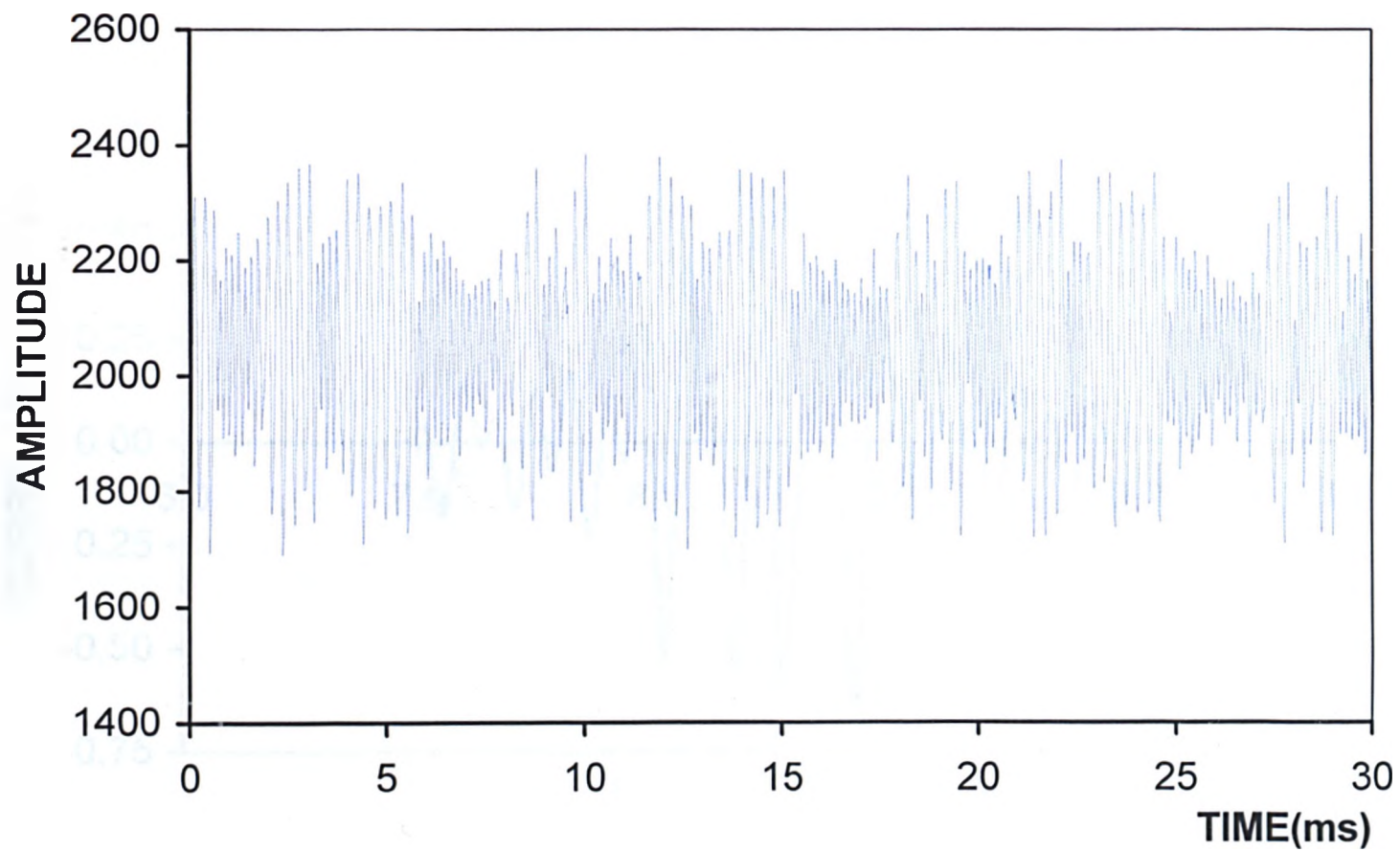
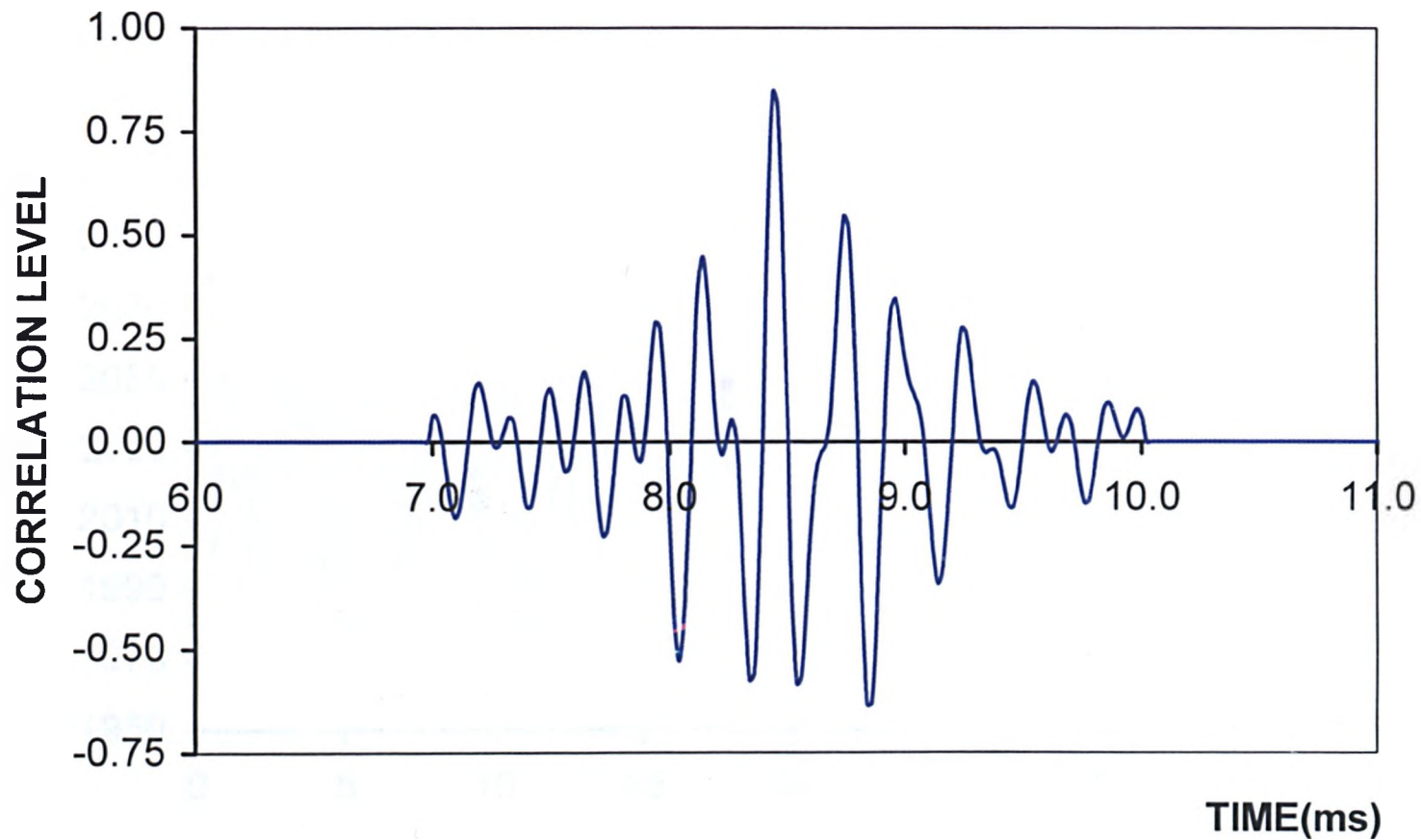
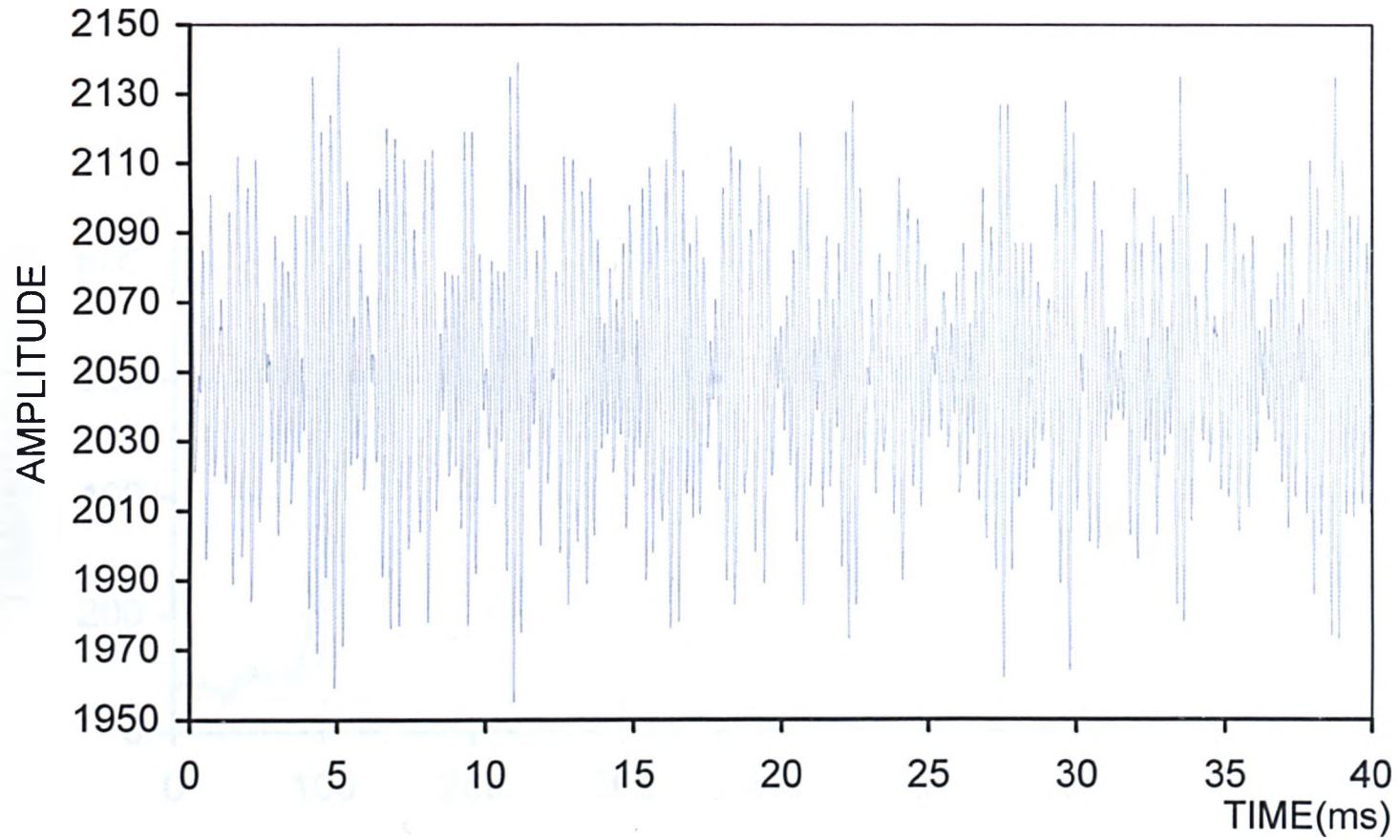


Figure 78: Raw modulated output PRBS signal for ambient conditions at a separation distance of 3.14m



**Figure 79: Correlation profile of raw modulated input and raw modulated output PRBS signals under ambient conditions  
(x=3.027m)**



**Figure 80: modulated PRBS output signal for combustion of 0.03kg/s mass flow rate of propane at a separation distance of 3.14m**

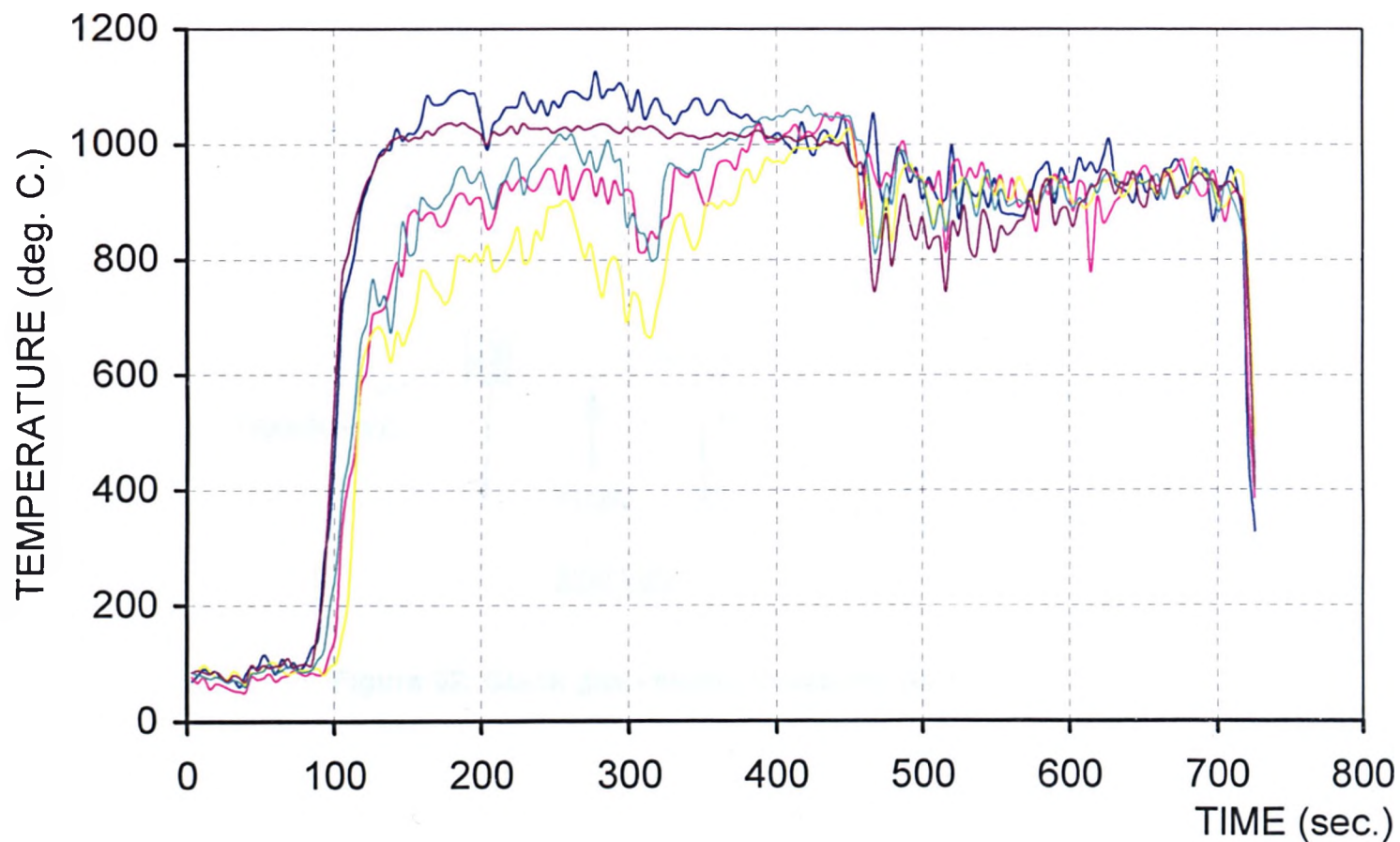


**Figure 81: Temperature measurements produced by thermocouples located at the compartment fire rig upper exit**

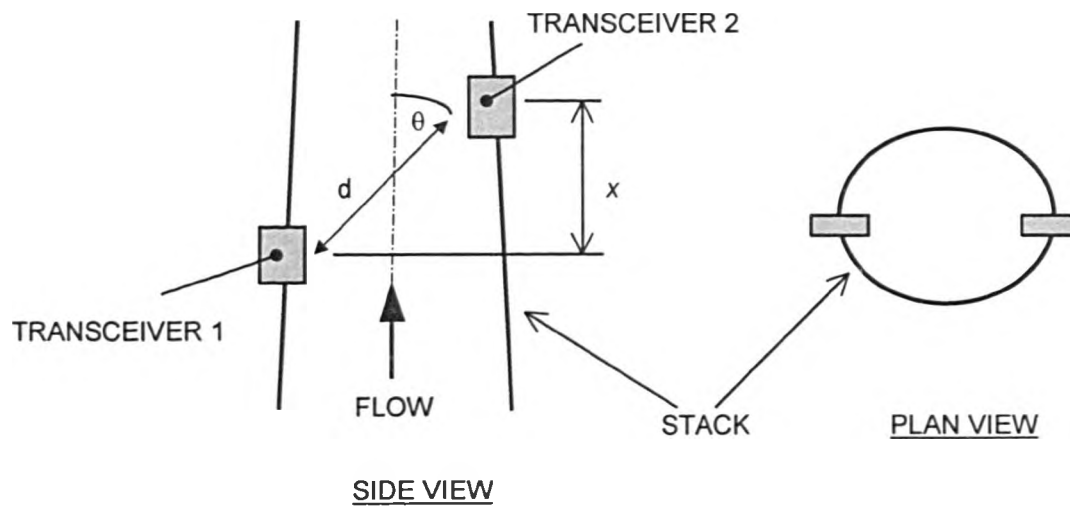


Figure 82: Stack gas velocity measurement system.

## Publications and Presentations

### Journal Paper

Ewan, B. and Ireland, S.N. "*Error reduction study employing a pseudo-random binary sequence for use in acoustic pyrometry of gases,*" Review of Scientific Instruments, Volume 71, No. 12, December 2000.

### Journal Paper

Young, K.J., Ireland, S.N., Melendez-Cervates, M.C. and Stones, R. "*On the Systematic Error Associated with the Measurement of Temperature Using Acoustic Pyrometry in Combustion Products of Unknown Mixture,*" Journal of Measurement Science and Technology, January 2000

### Conference Paper and Oral Presentation

Ireland, S.N., Young, K.J. and Swithenbank, J. "*Fundamental Design and Application of an Acoustically Based Temperature Measurement System,*" IFRF Joint Flame Days - 1998. "Control of Flames and Combustion Processes." Island of Guernsey, Channel Islands, U.K.

### Conference paper

Ireland, S.N., Young, K.J. "*Fundamental Design and Application of an Acoustic Temperature Measuring System*" 1998 IChemE Research Event, Newcastle, UK

# References

- <sup>1</sup> Office of Science and Technology, "Progress through partnership," 13 March 1995, Energy Panel Report, OST. HMSO. ISBN 0-11-430127-1
- <sup>2</sup> Doebelin, E.O., "Measurement Systems Application and Design." McGraw Hill, 3rd Ed. pp.575-673, 1986
- <sup>3</sup> Chedaille, J. & Braud, Y., "Measurements in Flames." Industrial Flames. Vol 1. IFRF 1972
- <sup>4</sup> Jones, J.C., "Combustion Science: Principles and Practice." Millenium Books, pp.292-299, 1993
- <sup>5</sup> Doebelin, E.O., "Measurement Systems Application and Design." McGraw Hill, 3rd Ed. pp.618-649, 1986
- <sup>6</sup> Darling, C.R. "Pyrometry: A Practical Treatise on the Measurement of High Temperatures." Pub. E.&F.N.Spon Ltd. London, 1911.
- <sup>7</sup> Harrison, T.R., "Radiation Pyrometry and Its Underlying Principles of Radiant Heat Transfer," Wiley, New York, 1960.
- <sup>8</sup> Vanzetti, R., "Practical Applications of Infrared Techniques." Wiley, New York, 1972
- <sup>9</sup> Copalle, A., & Vervisch, P., "The Total Emissivities of High Temperature Flames." Combustion and Flame 49: pp.101-108, 1983
- <sup>10</sup> Taylor et al. "Instrumentation For Flows With Combustion.", Academic Press Ltd, 1993.
- <sup>11</sup> Drain, L.E. "The Laser Doppler Technique," Wiley, Chichester, 1980.
- <sup>12</sup> Taran, J.P. & Pealat, M., "Temperature: Its Measurement and Control in Science and Industry," Vol. 5, 575, American Institute of Physics, New York, 1982.
- <sup>13</sup> White, F.M., "Fluid Mechanics." 3rd edition, McGraw-Hill Inc, 1994 pp.514-517
- <sup>14</sup> Mayer, A.M., "On Acoustic Pyrometer", Philisophical Magazine, 45 1873, pp. 18-22
- <sup>15</sup> Green, S.G., & Woodham, A.U., "Rapid Temperature Distributi n Measurement by Sonic Pyrometry." CEGB, Marchwood Engineering Laboriories, Marchwood, Southampton, England, 1983
- <sup>16</sup> Dadd, M.W., "Acoustic Thermometry in Gases Using Pulse Techniques" High.Temp.Tech., 6, 1983
- <sup>17</sup> Bramanti, M., Salerno, A., "An Acoustic Pyrometer System for Tomographic Thermal Imaging in Power Plant Boilers." IEEE Trans. Instr. & Meas. , 45 No.1, pp: 159-165, 1996.
- <sup>18</sup> Kleppe, J.A., Nuspl, S.P., Szmania, E.P. & Norton, P.R., "Applications of Digital Signal Processing to Sonic Measurements of Temperature in Large Power Plants," Proc.Iasted.Conf.on High Tech. in the Power Industry, Bozeman, 1986 pp. 50-54
- <sup>19</sup> Nuspl, S.P., Kleppe, J.A., Szmania, E.P. & Norton, P.R., "Acoustic Pyrometry applied to Utility Boilers." Proc. Joint ASME/IEEE Power Generation Conf., Portland, October 1986
- <sup>20</sup> Kleppe, J.A., "High Temperature Gas Measurement Using Acoustic Pyrometry", Sensors, 13, No.1, 1996 pp.17-22
- <sup>21</sup> Fendrock, C.F. & Varela, D.W., "Ultrasonic Thermometry for Industrial Furnace Temperature Measurement." Sensors, 23 1995
- <sup>22</sup> Bragg, S.L., "Combustion Noise." Journal of the Institute of Fuel, 36, No.264 pp.12-16
- <sup>23</sup> Kleppe, J.A., "High Temperature Gas Measurement Using Acoustic Pyrometry", Sensors, 13, No.1, 1996 pp.17-22
- <sup>24</sup> Harris, C.M., "Handbook of Noise Control," McGraw Hill Pub., 1<sup>st</sup> Ed., 1957.
- <sup>25</sup> JANNAF Thermochemical data , Dow Chemical Co. , Michigan. National Bureau of Standards Circ. C461 (1947).
- <sup>26</sup> Blitz, J., "Fundamentals of Ultrasonics." Pub. Butterworth & Co., London 1963 pp. 40-86

- <sup>27</sup> Stones R H, Webb P J, 1983, 'The Application of Acoustic Pyrometry to Gas Temperature Measurement and Mapping', *IEEE Colloquium on Ultrasonics in the Process Industry*
- <sup>28</sup> Watanabe, K. & Sato, H., "Vortex Whistle as a Flowmeter." *IEEE Instr. & Meas. Tech.* 3, pp: 1225-1228, 1994
- <sup>29</sup> Sato, H. et al., "Vortex whistle as a Flowmeter." *IEEE Instr. & Meas. Tech.* 2, pp: 804-807, 1996
- <sup>30</sup> Hartmann, J., "Construction, Performance and Design of the Acoustic Air-Jet Generator." *J. Sci. Instr.* 16, pp: 140-149, 1939.
- <sup>31</sup> Callister, D.W., "Materials and Science Engineering an Introduction." 3rd Ed. John Wiley & Sons Inc. Appendic C, 1994.
- <sup>32</sup> Energy Research Unit, Building R63, Rutherford Appleton Laboratory (RAL), Chilton, Didcot, Oxon, OX11 0QX, UK.
- <sup>33</sup> Doebelin, E.O., "Measurement Systems, Application and Design." 3rd Ed. McGraw-Hill Book Co. 1986 pp 775-778
- <sup>34</sup> Bragg, S.L. "Combustion Noise." *J. Inst. Fuel*, 36, 1963, pp. 12-16
- <sup>35</sup> Thring, M.W., Seventh Symposium (International) on Combustion, Page 659, Butterworth 1959.
- <sup>36</sup> Brown, A.M., "Combustion Oscillations." paper to course on Oil Firing at Sheffield University, 1960.
- <sup>37</sup> Giammer, R.D. and Putnam, A.A., "Noise generation by turbulent flames." A.G.A. Catalog No. 00080, 1971.
- <sup>38</sup> Gupta, A.K., Syred, N. & Beer, J.M., "Noise emission from swirl combustors." *Applied Acoustics*, 9, April, 1976, pp. 151-163.
- <sup>39</sup> Smith, T.J.B. & Kilham, J.K. "Noise generation by open turbulent flames." *J. Acous. Soc. America*, No.5, 35, 1963. pp. 715-23.
- <sup>40</sup> Gupta, A.K. & Beer, J.M., "Noise emissions from open turbulent methane-air diffusion flames."
- <sup>41</sup> Green, S.G., & Woodham, A.U., "Rapid Temperature Distribution Measurement by Sonic Pyrometry." CEGB, Marchwood Engineering Laboratories, Marchwood, Southampton, England, 1983
- <sup>42</sup> Kleppe, J.A., Nuspl, S.P., Szmania, E.P. & Norton, P.R., "Applications of Digital Signal Processing to Sonic Measurements of Temperature in Large Power Plants," *Proc. Iasted. Conf. on High Tech. in the Power Industry*, Bozeman, 1986 pp. 50-54
- <sup>43</sup> Young, K.J., Keer-Rendon, A. & Beet, S.W., "The development and application of a novel acoustic pyrometer with improved signal/noise ratio."
- <sup>44</sup> Ryzhov, A.P., Shandro, A.I. & Meshcheryakov, V.G., "Determining the gas temperature in the furnace of a type P-67 boiler by an acoustic method." *Thermal engineering*, Vol. 41, No. 11, 1994. pp. 902-906.
- <sup>45</sup> Ireland, S.N., Young, K.J., Stones, R. and Weston, C. (1998) "Design and Application of an Acoustically Based Temperature Measurement System." *ICHEME Research Event*, Newcastle, 7-8 April 1998.
- <sup>46</sup> Shapiro, A.H., "The dynamics and thermodynamics of compressible flow." Ronald Press.
- <sup>47</sup> Wallis, G.B., "One dimensional two phase flow." McGraw Hill, New York 1969.
- <sup>48</sup> NBS 1947 JANNAF Thermochemical data, Dow Chemical Co., Michigan (Washington DC: National Bureau of Standards) Circ. C461
- <sup>49</sup> Richardson, E.G., "Ultrasonic Physics." Elsevier Pub. Co. 4, pp 102:141, 1962.
- <sup>50</sup> Kinsler, L.E. & Frey, A.R., "Fundamentals of Acoustics." John Wiley & Sons Inc., 2nd ed. 9, pp: 217-233, 1962.
- <sup>51</sup> Herzfeld, K.F. & Litovitz, T.A. "Absorption and Dispersion of Ultrasonic Waves." Academic Press, 1959.
- <sup>52</sup> Bhatia, A.B., "Ultrasonic Absorption." Oxford University Press, Oxford, 1967
- <sup>53</sup> Herzfeld, K.F. & Rice, F.O., *Physics Review* 31, 691 (1928)
- <sup>54</sup> Markham, J.J., Beyer, R.T. & Lindsay, R.B., "Absorption of Sound in Fluids" *Revs. Mod. Phys.* 23, 353-411 (1951)
- <sup>55</sup> Harris, C.M., "Absorption of Sound in Air versus Humidity and Temperature" *J. Acoust. Soc. Amer.*, 40 pp. 148-159, 1966

- 
- <sup>56</sup> Harris, C.M., "Effects of Humidity on the Velocity of Sound in Air," J.Acoust.Soc.Amer., 49, pp.890-893,1971
- <sup>57</sup> Harris, C.M., "Normalised Curve of Molecular Absorption versus Humidity," J.Acoust.Soc.Amer., 57, pp.241-242, 1975
- <sup>58</sup> Shields, F.D. & Carney, G.P., "Sound Absorption in Pure CO<sub>2</sub>, D<sub>2</sub>S Mixtures." J.Acoust.Soc.Amer., 47 pp.1269-1273 (1970)
- <sup>59</sup> Brophy, J.J. "Basic Electronics For Scientists," McGraw-Hill International Editions, 5<sup>th</sup> Ed. 1990.
- <sup>60</sup> Yarmolik, V.N. & Demidenko, S.N., "Generation and Application of Pseudorandom Sequences for Random Testing.", John Wiley & Sons, 1988.
- <sup>61</sup> Godfrey, K.R. "The theory of the correlation method of dynamic analysis and its application to industrial processes and nuclear power plant." Measurement and Control, Vol. 2, May 1969.
- <sup>62</sup> Williams, B.J. & Clarke, D.W. "Plant modelling from p.r.b.s. experiments Pt.1." Control. Oct. 1968 pp.856-860 and "Plant modelling from p.r.b.s. experiments Pt.2." Control. Nov. 1968 pp.947-951.
- <sup>63</sup> Turan, A., Swithenbank, J.S. & Billings, S.A. "Pseudo-random stimulus response of combustion systems." Journal of the Institute of Energy, 18, Dec. 1980.
- <sup>64</sup> Betts, J.A. "Signal Processing Modulation and Noise." English Universities Press Ltd. 1st Ed. 1970.
- <sup>65</sup> Ewan, B.C.R. & Ireland, S.N., "Error reduction study employing a pseudo-random binary sequence for use in acoustic pyrometry of gases,," Review of Scientific Instruments, Vol. 71, No. 12, pp4658-4664.
- <sup>66</sup> Stones R H, Webb P J, 1983, 'The Application of Acoustic Pyrometry to Gas Temperature Measurement and Mapping', *IEEE Colloquium on Ultrasonics in the Process Industry*
- <sup>67</sup> Schueler, C.F., Lee, H. and Wade, G. "Fundamentals of Digital Ultrasonic Imaging." IEEE Transactions on Sonics and Ultrasonics, Vol. SU-31, No. 4, July 1984.
- <sup>68</sup> Wade, G. "Ultrasonic Imaging by Reconstructive Tomography." Acoustical Imaging, Vol. 9, K.Y.Wang, Ed. New York 1980, pp. 379-431
- <sup>69</sup> Ryzhov, A.P., Shandro, A.I. and Meshcheryakov, V.G. "Determining the Gas Temperature in the Furnace of a Type P-67 Boiler by an Acoustic Method." Thermal Engineering, Vol. 41, No. 11, 1994, pp. 902-906.
- <sup>70</sup> Bramanti, M., Salerno, A.T., Pasini, S. and Gray, A. "An Acoustic Pyrometer System for Tomographic Thermal Imaging in Power Plant Boilers." IEEE Transactions on Instrumentation and Measurement, Vol. 45, No. 1, February 1996.
- <sup>71</sup> Pollakowski, M. & Ermert, H. 1994 "Chirp signal matching and signal power optimisation in pulse-echo mode ultrasonic nondestructive testing." IEEE Transactions on ultrasonics, ferroelectrics and frequency control, Vol.41, no.5, September.
- <sup>72</sup> Schaffs, W., "Landolt-Börnst: Numerical Data and Functional Relationships in Science and Technology." Group 2: Atomic and Molecular Physics, Volume 5: Molecular Acoustics. Pub. Springer-Verlag, 1967.

# Appendix 1



# Calibration Chart

## Condenser Microphone Type 4135

Serial No: 2006949

### Calibration Data

Sensitivity,  $S_0$ : -48.6 dB re 1 V/Pa  
equivalent to: 3.72 mV/Pa  
Correction Factor,  $K_0$ : +22.6 dB  
Cartridge Capacitance: 6.4 pF

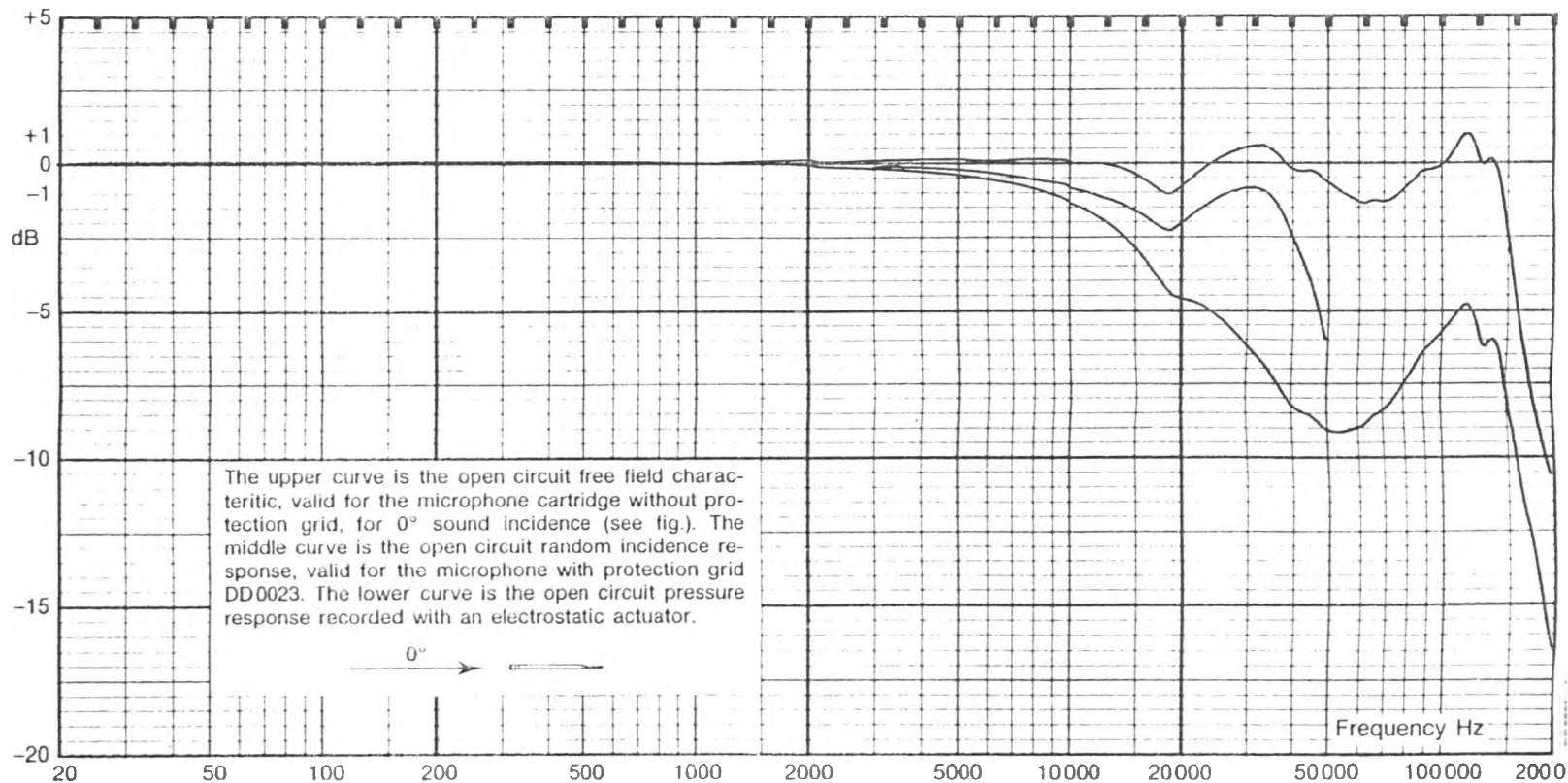
### Calibration Conditions

Polarization Voltage: 200 V  
Ambient Static Pressure: 1009 hPa  
Ambient Temperature: 24 °C  
Relative Humidity: 50 %

Date: 11.Sep.1997 Signature: BK

Calibration data valid at 1013 hPa, 23°C and 50% RH.  
For supplementary information, see reverse side of chart.

1 Pa = 1 N/m<sup>2</sup> = 10 dynes/cm<sup>2</sup> = 10 μbar  
1 Pa corresponds to a SPL of 94 dB re 20 μPa.



## **Appendix 2**

# CHIRP software program: MASTER7.BAS

```
DECLARE SUB ClearVariables ()
.....
.....
' MASTER7.BAS - PROGRAM TO SEND, RECEIVE AND PROCESS SOUND SIGNALS
' FOR AN ACOUSTIC PYROMETRY SYSTEM
' LAST UPDATED - 15 Oct 1997
.....
.....
.....

' Subroutine and Function Definition
  DECLARE SUB Correlation ()
  DECLARE SUB Threshold ()
  DECLARE SUB DummySetup ()
  DECLARE SUB das1600init ()
  DECLARE SUB refresh ()
  DECLARE SUB runprogram ()
  DECLARE SUB PlotData ()
  DECLARE SUB DrawRunScreen ()
  DECLARE SUB ReceiveSetup ()
  DECLARE SUB TransmitSetup ()
  DECLARE SUB ReadData ()
  DECLARE SUB WriteData ()
  DECLARE SUB DataCapture ()

' Include the datalogger files
' $INCLUDE: 'c:\das1600\QB4DECL.BI'
' $INCLUDE: 'c:\das1600\DASDECL.BI'
' $INCLUDE: 'c:\das1600\DAS1600.BI'

' VARIABLE LIST
' Variable used by driver functions.
  DIM SHARED nBoards AS INTEGER
  DIM SHARED DErr AS INTEGER          ' Error flag
  DIM SHARED szCfgName AS STRING      ' File name string
  DIM SHARED DAS1600 AS LONG, DAS1200 AS LONG

' DA Frame variables
  REM $DYNAMIC
  DIM SHARED OPData(4000) AS INTEGER
  DIM SHARED OPBufa(4000) AS INTEGER
  REM $STATIC
  DIM SHARED DAFrame AS LONG
  DIM SHARED OPSampleRate AS LONG
  DIM SHARED OPSampleNo AS LONG
  DIM SHARED OPChannel AS INTEGER
  DIM SHARED OLevel AS INTEGER

' AD Frame variables
  DIM SHARED IPData(4000) AS INTEGER
  DIM SHARED IStatus AS INTEGER
  DIM SHARED ICount AS LONG
  DIM SHARED ADMemLoc AS INTEGER
  DIM SHARED ADFrame AS LONG
  DIM SHARED ADBuf AS LONG
  DIM SHARED IPChannel AS INTEGER
  DIM SHARED IPGain AS INTEGER
  DIM SHARED IPSampleNo AS LONG
  DIM SHARED IPSampleRate AS LONG

' Signal Processing Variables
  DIM SHARED Pathlength AS SINGLE
  DIM SHARED ProbeLength AS SINGLE
  DIM SHARED TAmb AS SINGLE
  DIM SHARED ProcessOption AS INTEGER
  DIM SHARED Threshlev AS INTEGER
  DIM SHARED PulseDur AS SINGLE
```

```
DIM SHARED SWFreq AS LONG
DIM SHARED SWPulse AS INTEGER
DIM SHARED ChirpStart AS LONG
DIM SHARED Chirpstop AS LONG
DIM SHARED ChirpDur AS SINGLE
DIM SHARED OpType AS INTEGER
DIM SHARED Corr(4000) AS SINGLE
DIM SHARED CorrWindow AS INTEGER
DIM SHARED CorrRange AS INTEGER
DIM SHARED MaxCor AS SINGLE
DIM SHARED TransmitTime AS SINGLE
DIM SHARED MinTime AS SINGLE
DIM SHARED MaxTime AS SINGLE
DIM SHARED Temperature AS SINGLE
DIM SHARED LowerRange AS INTEGER
DIM SHARED UpperRange AS INTEGER
DIM SHARED CountMaxTP AS INTEGER
DIM SHARED MaxCorrRatio AS SINGLE
DIM SHARED MaxTP(100, 2) AS SINGLE
```

' Plot variables

```
DIM SHARED xorigin AS INTEGER
DIM SHARED yorigin AS INTEGER
DIM SHARED xrange AS INTEGER
DIM SHARED yrange AS INTEGER
DIM SHARED xmax AS INTEGER
DIM SHARED ymax AS INTEGER
DIM SHARED xmin AS INTEGER
DIM SHARED ymin AS INTEGER
```

' General Variables

```
DIM SHARED choice AS STRING * 1
DIM SHARED runtime AS STRING * 1
DIM SHARED hold AS STRING * 3
DIM SHARED logdata AS STRING * 3
DIM SHARED FlightTime AS SINGLE
DIM SHARED outputfile AS STRING
DIM SHARED InputFile AS STRING
DIM SHARED caption AS STRING
DIM SHARED delt AS SINGLE
DIM SHARED pi AS SINGLE
DIM SHARED temp AS LONG
DIM SHARED sample AS STRING
```

.....  
' DEFAULT VALUES OF CONSTANTS

```
pi = 4! * ATN(1!)
IPChannel = 5
IPGain = 1
IPSampleNo = 4000
IPSampleRate = 100000
Pathlength = 3.729
ProcessOption = 1: Threshlev = 3000
OPChannel = 0
OpType = 1
OPlevel = 2047
xmin = 1
ymax = 4095
ymin = 0
hold = "OFF"
```

.....  
' Configure the datalogger boards

```
nBoards = 2
szCfgName = "MASTER1.CFG" + CHR$(0)
DErr = DAS1600DEVOPEN%(SSEGADD(szCfgName), nBoards): IF DErr <> 0 THEN PRINT DErr: STOP
DErr = DAS1600GETDEVHANDLE%(0, DAS1600): IF DErr <> 0 THEN PRINT "getdevhandle"; DErr: STOP
DErr = DAS1600GETDEVHANDLE%(1, DAS1200): IF DErr <> 0 THEN PRINT "getdevhandle"; DErr: STOP
```

```
QBFarHeapSize& = SETMEM(0)
NewFarHeapSize& = SETMEM((-QBFarHeapSize& / 2)
PRINT " Driver's Far Heap Size: "; QBFarHeapSize& - NewFarHeapSize&
PRINT " QB's Far Heap Size: "; NewFarHeapSize&
PRINT
```

```
' .....
```

**MAIN PROGRAM**

```
CLS  
DO  
LOCATE 3, 22: PRINT "THE UNIVERSITY OF SHEFFIELD"  
LOCATE 4, 16: PRINT "ACOUSTIC PYROMETRY SOFTWARE: version 6"  
LOCATE 5, 16: PRINT "*****"  
LOCATE 6, 16: PRINT "Written by: Dr K J YOUNG / S.N.IRELAND: Last update: 10 Oct 1997"
```

```
LOCATE 9, 2: PRINT "PLEASE INPUT YOUR CHOICE"
```

```
LOCATE 10, 2: PRINT "1. TRANSMITTED SIGNAL"  
LOCATE 11, 2: PRINT "2. RECEIVED SIGNAL"  
LOCATE 12, 2: PRINT "3. RUN PROGRAM"  
LOCATE 13, 2: PRINT "4. EXIT PROGRAM"
```

```
choice = INKEY$  
IF choice = "1" THEN  
CLS  
CALL TransmitSetup
```

```
ELSEIF choice = "2" THEN  
CLS  
CALL ReceiveSetup
```

```
ELSEIF choice = "3" THEN  
CLS  
CALL runprogram
```

```
ELSEIF choice = "4" THEN  
STOP  
END IF  
LOOP  
END
```

**SUB ClearVariables STATIC**

```
FOR i = 1 TO 4000  
IPData(i) = 2047  
NEXT i
```

```
FOR i = 0 TO 4000  
Corr(i) = 0  
NEXT i
```

```
FOR i = 1 TO 100  
MaxTP(i, 1) = 0  
MaxTP(i, 2) = 0  
NEXT i
```

```
CountMaxTP = 0  
MaxCorr = 0!  
MaxCorrRatio = 0!  
Temperature = 0!
```

```
'Specify the initial max scale of the graph plotter  
xmax = IPSampleNo  
xmin = 1
```

END SUB

```
.....  
SUB Correlation STATIC  
.....
```

```
' ZERO THE CORRELATION ARRAY BEFORE CONTINUING  
FOR i = 0 TO 4000  
Corr(i) = 0!  
NEXT i
```

```
' Now set the correlation window and ranges
```

```

CorrWindow = OPSampleNo
IF (MinTime = 0 AND MaxTime = 0) THEN
  LowerRange = 0
  UpperRange = IPSampleNo - OPSampleNo
ELSE
  LowerRange = (MinTime - TransmitTime) * IPSampleRate
  UpperRange = (MaxTime - TransmitTime) * IPSampleRate
END IF

' Check that the correlation is feasible
IF (LowerRange < 0 OR (UpperRange + OPSampleNo) > IPSampleNo OR IPSampleRate <> OPSampleRate) THEN
  LOCATE 28, 30: COLOR 4: PRINT "WARNING: Correlation impossible ": EXIT SUB
END IF

' The input data is compared with the output, so meanop is constant
MeanIP = 0!
MeanOP = 0!
FOR i = 1 TO CorrWindow
  MeanIP = MeanIP + CSNG(IPData(i + LowerRange)) / CSNG(CorrWindow)
  MeanOP = MeanOP + CSNG(OPData(i)) / CSNG(CorrWindow)
NEXT i

' MAIN CORRELATION LOOP, VARIABLE TO DEFINE SHIFT IS delta
FOR Delta = LowerRange TO UpperRange

' CALCULATE meanf2 WHICH VARIES WITH TIME SHIFT
IF (Delta > LowerRange) THEN
  MeanIP = MeanIP + (-IPData(Delta) + IPData(CorrWindow + Delta)) / CorrWindow
END IF

' CALCULATE THE VARIOUS SUMMATIONS IN THE CORRELATION
denom1 = 0!
denom2 = 0!
numer = 0!
FOR i = 1 TO CorrWindow
  numer = numer + (OPData(i) - MeanOP) * (IPData(i + Delta) - MeanIP)
  denom1 = denom1 + (OPData(i) - MeanOP) ^ 2
  denom2 = denom2 + (IPData(i + Delta) - MeanIP) ^ 2
NEXT i

' COMBINE THE SUMMATIONS TO CALCULATE THE CORRELATION
Corr(Delta) = numer / SQR(denom1 * denom2)
NEXT Delta

' FIND THE MAXIMUM VALUE AND REPORT IT
MaxCor = 0!
FOR Delta = LowerRange TO UpperRange
  IF Corr(Delta) > MaxCor THEN
    MaxCor = Corr(Delta)
    FlightTime = i / IPSampleRate
  END IF
NEXT Delta

' FIND OUT WHERE THE TURNING POINTS ARE:
CountMaxTP = 0

FOR i = LowerRange + 2 TO UpperRange - 2
  IF (Corr(i) > Corr(i - 1) AND Corr(i) > Corr(i + 1)) THEN
    CountMaxTP = CountMaxTP + 1
    MaxTP(CountMaxTP, 1) = i / IPSampleRate
  END IF
NEXT i

' Now find the neighbouring minima
j = i + 1
DO UNTIL ((Corr(j) < Corr(j - 1) AND Corr(j) < Corr(j + 1)) OR j >= UpperRange - 1)
  j = j + 1
LOOP
IF j >= UpperRange - 1 THEN
  minima1 = 1E+20
ELSE
  minima1 = Corr(j) + 1
END IF

j = i - 1

```

```
DO UNTIL (Corr(j) < Corr(j - 1) AND Corr(j) < Corr(j + 1)) OR (j <= LowerRange + 1)
  j = j - 1
LOOP
```

```
IF j <= LowerRange + 1 THEN
  minima2 = 1E+20
ELSE
  minima2 = Corr(j) + 1
END IF
```

```
MaxTP(CountMaxTP, 2) = 2! * (Corr(i) + 1) / (minima1 + minima2)
```

```
END IF
```

```
NEXT i
```

```
MaxCorrRatio = 0
FOR i = 1 TO CountMaxTP
  IF MaxTP(i, 2) > MaxCorrRatio THEN
    MaxCorrRatio = MaxTP(i, 2)
    FlightTime = MaxTP(i, 1)
  END IF
NEXT i
```

```
END SUB
```

```
.....
SUB das1600init STATIC
.....
```

```
IF OpType <> 1 THEN ' set up DA frame unless it is just a trigger
' SET UP THE DA FRAME
  DErr = KGetDAFrame%(DAS1600, DAFrame)
  DErr = KSetBuf%(DAFrame, OPBufa(1), OPSampleNo)
  DErr = KSetChn%(DAFrame, OPChannel)
  DErr = KSetCikRate%(DAFrame, CLNG(1E+07 / OPSampleRate))
END IF
```

```
' SET UP THE AD FRAME
  DErr = KGetADFrame%(DAS1600, ADFRame): IF DErr <> 0 THEN PRINT "getadframe"; DErr: STOP
  DErr = KDMAAlloc%(ADFRame, IPSampleNo, ADBuf, ADMemLoc): IF DErr <> 0 THEN PRINT "KDMAAlloc"; DErr:
STOP
  DErr = KSetDMABuf%(ADFRame, ADBuf, IPSampleNo): IF DErr <> 0 THEN PRINT "KSetDMABuf"; DErr: STOP
  DErr = KSetChn(ADFRame, IPChannel)
  DErr = KSetG(ADFRame, IPGain)
  DErr = KSetCikRate%(ADFRame, CLNG(1E+07 / IPSampleRate)): IF DErr <> 0 THEN PRINT "clkrate"; DErr: STOP
  DErr = KSetADFreeRun(ADFRame): IF DErr <> 0 THEN PRINT "FreeRun"; DErr: STOP
```

```
END SUB
```

```
.....
SUB DataCapture STATIC
.....
```

```
IF OpType = 1 THEN
  now = TIMER
  DErr = KDAWrite%(DAS1600, OPChannel, CLNG(2048) * 16&)
  DErr = KDMAStart%(ADFRame): IF DErr <> 0 THEN PRINT "Syncstart"; HEX$(DErr): STOP
  DO: DErr = KDMAStatus%(ADFRame, Status, Count): LOOP UNTIL Status = 0
  DErr = KMoveBufToArray%(IPData(1), ADBuf, IPSampleNo)
  DO UNTIL TIMER > now + PulseDur: LOOP
  DErr = KDAWrite%(DAS1600, OPChannel, CLNG(3071) * 16&)
```

```
ELSE
```

```
  DErr = KSyncStart%(DAFrame): IF DErr <> 0 THEN PRINT "Syncstart", HEX$(DErr): STOP
  DErr = KDMAStart%(ADFRame): IF DErr <> 0 THEN PRINT "Syncstart"; HEX$(DErr): STOP
  DO: DErr = KDMAStatus%(ADFRame, Status, Count): LOOP UNTIL Status = 0
  DErr = KMoveBufToArray%(IPData(1), ADBuf, IPSampleNo)
```

END IF

```
' Reorder the data to the beginning of the array
FOR i = 1 TO IPSampleNo
  IPData(i) = IPData(i) / 16 AND &HFFF
NEXT i
```

END SUB

.....  
**SUB DrawRunScreen STATIC**  
.....

SCREEN 12  
xres = 640  
yres = 480

xorigin = xres \* .05  
yorigin = yres \* .4  
xrange = xres \* .9  
yrange = -yres \* .25

x1 = xorigin  
x2 = xorigin + xrange  
y1 = yorigin  
y2 = yorigin + yrange  
LINE (x1, y1)-(x2, y2), 8, BF  
LINE (x1 - 1, y1 + 2)-(x1 - 2, y2), 15, BF  
LINE (x1, y1 + 1)-(x2, y1 + 2), 15, BF

FOR i = 1 TO 5  
 x1 = xorigin - 1  
 x2 = xorigin - 4  
 y1 = yorigin + yrange \* (i - 1) / 4  
 y2 = y1  
 LINE (x1, y1)-(x2, y2), 15  
NEXT i

FOR i = 1 TO 11  
 y1 = yorigin + 1  
 y2 = yorigin + 4  
 x1 = xorigin + xrange \* (i - 1) / 10  
 x2 = x1  
 LINE (x1, y1)-(x2, y2), 15  
NEXT i

LOCATE 1, 2: COLOR 2: PRINT "C"; : COLOR 7: PRINT "APTURE"  
LOCATE 1, 14: COLOR 2: PRINT "L"; : COLOR 7: PRINT "OG DATA OFF"  
LOCATE 1, 30: COLOR 2: PRINT "H"; : COLOR 7: PRINT "OLD OFF"  
LOCATE 1, 45: COLOR 2: PRINT "M"; : COLOR 7: PRINT "AIN MENU"

COLOR 4: LOCATE 4, 20: PRINT "ACOUSTIC PYROMETER PROGRAM: MASTER SCREEN":

COLOR 4: LOCATE 16, 2: PRINT "TRANSMIT OPTIONS": COLOR 2

LOCATE 17, 2: PRINT " Channel number = "; OPChannel

LOCATE 18, 2: PRINT " Signal type = ";

IF OpType = 1 THEN

LOCATE 18, 20: PRINT "Trigger "

LOCATE 19, 1: PRINT " "

LOCATE 20, 2: PRINT " "

LOCATE 21, 2: PRINT " "

ELSEIF OpType = 2 THEN

LOCATE 18, 20: PRINT "Square wave burst"

LOCATE 19, 2: PRINT " Frequency = "; SWFreq; "Hz"

LOCATE 20, 2: PRINT " Number of pulses = "; SWPulse

LOCATE 21, 2: PRINT " "

ELSEIF OpType = 3 THEN

LOCATE 18, 20: PRINT "Chirp "

LOCATE 19, 2: PRINT " Start f = "; ChirpStart; "Hz"

LOCATE 20, 2: PRINT " Stop f = "; Chirpstop; "Hz"

LOCATE 21, 2: PRINT " Duration = "; ChirpDur; "ms"

END IF

COLOR 4: LOCATE 23, 2: PRINT "RECEIVE OPTIONS": COLOR 2  
LOCATE 24, 2: PRINT " Chan = "; IPChannel: " Gain = "; IPGain  
LOCATE 25, 2: PRINT " Sampling Rate = "; IPSampleRate  
LOCATE 26, 2: PRINT " Number of samples = "; IPSampleNo  
LOCATE 27, 2: PRINT " Path length = "; Pathlength  
LOCATE 28, 2: PRINT " Sig Proc = ";  
IF ProcessOption = 1 THEN  
LOCATE 28, 15: PRINT " Threshold"  
ELSEIF ProcessOption = 2 THEN  
LOCATE 28, 15: PRINT " Cross corr"  
END IF

END SUB

.....  
SUB DummySetup STATIC  
.....

' SOME SAMPLE DATA FOR THE SYSTEM TO CHEW ON

IF ProcessOption = 2 THEN  
IPSampleNo = OPSampleNo \* 2  
xmax = IPSampleNo  
FOR i = 1 TO 20  
IPData(i) = 2047!  
NEXT i  
FOR i = 1 TO OPSampleNo  
IPData(20 + i) = OPData(i)  
NEXT i  
FOR i = OPSampleNo + 21 TO IPSampleNo  
IPData(i) = 2047  
NEXT i

ELSE  
IPSampleNo = 400  
xmax = IPSampleNo  
FOR i = 1 TO 100  
IPData(i) = 2047  
NEXT i  
FOR i = 1 TO IPSampleNo  
IPData(i + 100) = 2047 + 2045 \* i \* SIN(i) \* EXP(-i / 15) / 10  
NEXT i

END IF  
END SUB

.....  
SUB PlotData STATIC  
.....

xdiff = xmax - xmin  
x1 = xorigin  
y1 = yorigin + CSNG(yrange) \* CSNG(IPData(xmin)) / CSNG(yrange)  
y1data = yorigin + CSNG(yrange) \* CSNG(OPData(1)) / 4095!

IF ProcessOption = 2 THEN y1cor = yorigin + yrange / 2 + CSNG(yrange) \* CSNG(Corr(xmin - 1)) / 2!

FOR i = 1 TO xdiff  
x2 = xorigin + xrange \* i / xdiff  
y2 = yorigin + CSNG(yrange) \* CSNG(IPData(i + xmin)) / CSNG(yrange)  
y2data = yorigin + CSNG(yrange) \* CSNG(OPData(i + 1)) / 4095!  
LINE (x1, y1)-(x2, y2), 14  
LINE (x1, y1data)-(x2, y2data), 3  
IF xdiff <= 70 THEN CIRCLE (x2, y2), 2, 14: CIRCLE (x2, y2data), 2, 3

' PLOT AN EXTRA LINE IF THIS IS A CORRELATION

IF ProcessOption = 2 THEN  
y2cor = yorigin + yrange / 2 + CSNG(yrange) \* CSNG(Corr(i - 1 + xmin)) / 2!  
LINE (x1, y1cor)-(x2, y2cor), 15  
IF xdiff <= 70 THEN CIRCLE (x2, y2cor), 2, 15  
y1cor = y2cor  
END IF  
x1 = x2  
y1 = y2  
y1data = y2data



```
PRINT ">"; sample
LINE INPUT #10, sample
PRINT ">"; sample
```

```
INPUT #10, OPChannelNo, OPGain, OPSampleRate, OPSampleNo, TransmitTime
PRINT OPChannelNo; TAB(15); OPGain; TAB(30); OPSampleRate; TAB(45); OPSampleNo; TAB(60); TransmitTime
```

```
LINE INPUT #10, sample
LINE INPUT #10, sample
PRINT ">"; sample
```

```
INPUT #10, OpType
PRINT OpType
LINE INPUT #10, sample
PRINT ">"; sample
```

```
IF OpType = 1 THEN INPUT #10, PulseDur: PRINT PulseDur
IF OpType = 2 THEN INPUT #10, SWFreq, SWPulse: PRINT SWFreq; TAB(15); SWFreq
IF OpType = 3 THEN INPUT #10, ChirpStart, Chirpstop, ChirpDur: PRINT ChirpStart; TAB(15); Chirpstop; TAB(30);
ChirpDur
```

```
LINE INPUT #10, sample
LINE INPUT #10, sample
PRINT ">"; sample
LINE INPUT #10, sample
PRINT ">"; sample
LINE INPUT #10, sample
PRINT ">"; sample
```

```
INPUT #10, IPChannelNo, IPGain, IPSampleRate, IPSampleNo, Pathlength
```

```
PRINT IPChannelNo; TAB(15); IPGain; TAB(30); IPSampleRate; TAB(45); IPSampleNo; TAB(60); Pathlength
```

```
LINE INPUT #10, sample
LINE INPUT #10, sample
PRINT ">"; sample
```

```
INPUT #10, ProcessOption
PRINT ProcessOption
LINE INPUT #10, sample
PRINT ">"; sample
```

```
IF ProcessOption = 1 THEN INPUT #10, MaxTime, MinTime: PRINT MaxTime; TAB(15); MinTime
IF ProcessOption = 2 THEN INPUT #10, Threshlev: PRINT Threshlev
```

```
LINE INPUT #10, sample
PRINT ">"; sample
LINE INPUT #10, sample
PRINT ">"; sample
LINE INPUT #10, sample
LINE INPUT #10, sample
IF IPSampleNo > OPSampleNo THEN
  Maxval = IPSampleNo
ELSE
  Maxval = OPSampleNo
END IF
```

```
IF ProcessOption = 1 THEN
  FOR i = 1 TO Maxval
    INPUT #10, OPData(i), IPData(i)
  NEXT i
ELSE
  FOR i = 1 TO Maxval
    INPUT #10, OPData(i), IPData(i), Corr(i)
  NEXT i
END IF
```

```
INPUT sample
```



```
LOCATE 13, 1: PRINT "           "
```

```
LOCATE 14, 1: PRINT "           "
```

```
LOCATE 15, 1: PRINT "           "
```

```
LOCATE 16, 1: PRINT "           "
```

LOOP

END SUB

```
.....  
SUB refresh  
.....
```

```
x1 = xorigin  
x2 = xorigin + xrange + 3  
y1 = yorigin  
y2 = yorigin + yrange - 3
```

```
LINE (x1, y1)-(x2, y2), 8, BF
```

END SUB

```
.....  
SUB runprogram STATIC  
.....
```

```
CALL ClearVariables
```

```
' INITIAL LOOP TO FIND OUT WHETHER THIS IS A DUMMY RUN OR FOR REAL
```

```
LOCATE 10, 1: PRINT "WHAT TYPE OF RUN IS THIS"
```

```
LOCATE 11, 5: PRINT "1. DUMMY RUN"
```

```
LOCATE 12, 5: PRINT "2. DATALOGGER RUN"
```

```
LOCATE 13, 5: PRINT "3. RECALL OLD DATA"
```

```
LOCATE 14, 5: PRINT "4. BACK TO MAIN MENU"
```

```
INPUT runtype
```

```
IF runtype = "1" THEN
```

```
CALL DummySetup
```

```
ELSEIF runtype = "2" THEN
```

```
CALL das1600init
```

```
ELSEIF runtype = "3" THEN
```

```
CALL ReadData
```

```
ELSEIF runtype = "4" THEN
```

```
CLS
```

```
EXIT SUB
```

```
END IF
```

```
' Draw the initial screen
```

```
CALL DrawRunScreen
```

```
.....  
' MAIN PROGRAM LOOP
```

```
DO
```

```
' START DATALOG SEQUENCE IF LIVE RUN
```

```
IF runtype = "2" AND hold = "OFF" THEN
```

```
CALL DataCapture
```

```
END IF
```

```
' ANALYSE THE DATA EITHER BY CORRELATION OR THRESHOLD IF HOLD IS OFF
```

```
IF hold = "OFF" THEN
```

```
IF ProcessOption = 1 THEN ' THRESHOLD DETECTION
```

```
CALL Threshold
```

```
ELSEIF ProcessOption = 2 THEN 'CORRELATION
```

```
CALL Correlation
```

```
END IF
```

```
' CALCULATE THE TEMPERATURE BASED ON THE FLIGHTTIME
```

```
IF FlightTime + TransmitTime > .00001 THEN
```

```
Temperature = ((Pathlength) / (FlightTime + TransmitTime)) ^ 2 / (1.4 * 287!)
```

```
END IF
```



```

' Free the frame ready for the next operations
  DErr = KFreeFrame%(ADFrame)
  DErr = KFreeFrame%(DAFrame)
  DErr = KDMAFree%(ADMemLoc)
  SCREEN 0
  EXIT SUB
END IF

LOOP

```

```

END SUB

```

```

*****
SUB Threshold STATIC
*****

```

```

' SUBROUTINE TO ESTIMATE THE ARRIVAL TIME OF THE PULSE BY ANALYSING THE
' FIRST OCCURENCE ABOVE A SET TRIGGER LEVEL

```

```

' FIND THE POINT AT WHICH THE DATA GOES ABOVE THRESHOLD
i = 1
DO WHILE IPData(i) < Threshlev AND i < IPSampleNo
  i = i + 1
LOOP

```

```

' IF THIS POINT IS IN THE PLOT RANGE THEN PLOT THE THRESHOLD VALUE

```

```

IF i < IPSampleNo THEN
  FlightTime = CSNG(i) / IPSampleRate
ELSE
  FlightTime = 0!
  LOCATE 28, 30: COLOR 4: PRINT " WARNING: Threshold never reached": COLOR 7
END IF

```

```

time = TIMER
DO WHILE (TIMER - time) < 2: LOOP

```

```

END SUB

```

```

*****
SUB TransmitSetup STATIC
*****

```

```

' INPUT SECTION

```

```

CLS

```

```

' FIRST CLEAR THE DATA THAT IS ALREADY IN THE OUTPUT BUFFERS
FOR i = 1 TO 4000
  OPData(i) = 2047
NEXT i

```

```

DO

```

```

  LOCATE 3, 22: PRINT "THE UNIVERSITY OF SHEFFIELD"
  LOCATE 4, 16: PRINT "OPTIONS FOR TRANSMITTED SIGNAL"
  LOCATE 5, 16: PRINT "*****"

```

```

  COLOR 14:

```

```

  LOCATE 17, 2: PRINT "CURRENT SETUP"
  LOCATE 18, 2: PRINT " Channel no = "; OPChannel; "OP level"; OPllevel
  LOCATE 19, 2: PRINT " Signal type = ";

```

```

  IF OpType = 1 THEN

```

```

    LOCATE 19, 27: PRINT "Trigger      "
    LOCATE 20, 1: PRINT "          "
    LOCATE 21, 2: PRINT "          "
    LOCATE 22, 2: PRINT "          "

```

```

  ELSEIF OpType = 2 THEN

```

```

    LOCATE 19, 27: PRINT "Square wave burst"
    LOCATE 20, 2: PRINT " Frequency = "; SWFreq; "Hz"
    LOCATE 21, 2: PRINT " Number of pulses = "; SWPulse
    LOCATE 22, 2: PRINT "          "

```

```

  ELSEIF OpType = 3 THEN

```

```

    LOCATE 19, 27: PRINT "Chirp          "
    LOCATE 20, 2: PRINT " Start f = "; ChirpStart; "Hz"

```

```

LOCATE 21, 2: PRINT " Stop f = "; Chirpstop; "Hz"
LOCATE 22, 2: PRINT " Duration = "; ChirpDur; "ms"
END IF
COLOR 7

```

```

LOCATE 6, 2: PRINT "PLEASE INPUT YOUR CHOICE"
LOCATE 7, 2: PRINT "1. CHANNEL NO"
LOCATE 8, 2: PRINT "2. SIGNAL TYPE"
LOCATE 9, 2: PRINT "3. SET OUTPUT LEVEL"
LOCATE 10, 2: PRINT "4. EXIT "

```

```

choice = INKEY$

```

```

IF choice = "1" THEN

```

```

    LOCATE 11, 2: PRINT "INPUT THE CHANNEL NO "
    INPUT OPChannel

```

```

ELSEIF choice = "2" THEN

```

```

    LOCATE 11, 2: PRINT "INPUT THE SIGNAL TYPE"
    LOCATE 12, 2: PRINT "1=trigger 2=burst 3=chirp"

```

```

    INPUT OpType

```

```

    IF OpType = 1 THEN

```

```

        LOCATE 12, 1: PRINT "INPUT THE PULSE DURATION (s)"
        INPUT PulseDur

```

```

    ELSEIF OpType = 2 THEN

```

```

        LOCATE 12, 1: PRINT "INPUT THE FREQUENCY AND NO OF pulses"
        INPUT ; SWFreq

```

```

        INPUT SWPulse

```

```

    ELSEIF OpType = 3 THEN

```

```

        LOCATE 12, 1: PRINT "INPUT THE START AND STOP FREQUENCY AND DURATION IN ms"
        INPUT ; ChirpStart
        INPUT ; Chirpstop
        INPUT ChirpDur

```

```

    END IF

```

```

ELSEIF choice = "3" THEN

```

```

    LOCATE 12, 1: PRINT "INPUT THE OUTPUT LEVEL (BINARY)"
    LOCATE 13, 1: INPUT OLevel

```

```

ELSEIF choice = "4" OR choice = CHR$(27) THEN

```

```

    CLS

```

```

    ' **** LOAD UP THE OUTPUT BUFFERS WITH THE DATA ****

```

```

    IF OpType = 3 THEN

```

```

        OPSampleRate = 100000

```

```

        OPSampleNo = OPSampleRate * ChirpDur / 1000

```

```

        delt = 1 / OPSampleRate

```

```

        FOR i = 1 TO OPSampleNo

```

```

            omega = 2! * pi * (ChirpStart + (i - 1) * (Chirpstop - ChirpStart) / (OPSampleNo - 1))

```

```

            OPData(i) = (2048 + 2047 * SIN(omega * (i - 1) * delt))

```

```

            temp = CLNG((2048 + OLevel * SIN(omega * (i - 1) * delt))) * 16&

```

```

            IF (temp > (2 ^ 15 - 1)) THEN temp = temp - 2 ^ 16

```

```

            OPBuffa(i) = CINT(temp)

```

```

        NEXT i

```

```

        TransmitTime = OPSampleNo / OPSampleRate

```

```

        OPBuffa(OPSampleNo) = 2047 * 16

```

```

    ELSEIF OpType = 2 THEN

```

```

        OPSampleRate = 2 * SWFreq

```

```

        OPSampleNo = 2 * SWPulse

```

```

        OPData(1) = 2047

```

```

        FOR i = 2 TO OPSampleNo STEP 2

```

```

            OPData(i) = 2047 + OLevel

```

```

            OPData(i + 1) = 2047 - OLevel

```

```

        NEXT i

```

```

        OPData(OPSampleNo) = 2047

```

```

        FOR i = 1 TO OPSampleNo

```

```

            temp = CLNG(OPData(i)) * 16&

```

```

    IF (temp > (2 ^ 15 - 1)) THEN temp = temp - 2 ^ 16
    OPBuffa(i) = CINT(temp)
NEXT i
    TransmitTime = (OPSampleNo) / OPSampleRate
    OPBuffa(OPSampleNo) = 2047 * 16
ELSEIF OpType = 3 THEN
    TransmitTime = 0!
END IF

```

```

EXIT SUB
END IF

```

```

LOCATE 11, 1: PRINT "
LOCATE 12, 1: PRINT "
LOCATE 13, 1: PRINT "
LOCATE 14, 1: PRINT "
LOCATE 15, 1: PRINT "
LOCATE 16, 1: PRINT "

```

```

LOOP

```

```

END SUB

```

```

.....
SUB WriteData
.....

```

```

' This subroutine outputs trace details to a file for later
' inspection

```

```

LOCATE 18, 35: COLOR 4: PRINT "TRACE CAPTURE": COLOR 7
LOCATE 19, 35: PRINT "Name the output file"
LOCATE 20, 35: INPUT outputfile
LOCATE 18, 35: PRINT "
LOCATE 19, 35: PRINT "What is the caption "
LOCATE 20, 35: PRINT "
LOCATE 20, 35: INPUT caption
LOCATE 18, 35: PRINT "
LOCATE 19, 35: PRINT "
LOCATE 20, 35: PRINT "

```

```

OPEN outputfile FOR OUTPUT AS #10

```

```

PRINT #10, "....."
PRINT #10, " TRACE OUTPUT DATA FILE FROM PROGRAM MASTER7"
PRINT #10, "....."
PRINT #10, "Filename : "; outputfile
PRINT #10, "Date : "; DATE$, " Time : "; TIME$
PRINT #10,
PRINT #10, "TRANSMIT VARIABLES"
PRINT #10, "....."
PRINT #10, "Channel No"; TAB(15); "OPGain"; TAB(30); "OPsampleRate"; TAB(45); "OPSampleNo"; TAB(60); "XmitTime";
PRINT #10, OPChannelNo; TAB(15); OPGain; TAB(30); OPSampleRate; TAB(45); OPSampleNo; TAB(60); TransmitTime
PRINT #10,
PRINT #10, "Output Type"
PRINT #10, OpType
IF OpType = 1 THEN
    PRINT #10, "Pulse Duration (s)"
    PRINT #10, PulseDur
ELSEIF OpType = 2 THEN
    PRINT #10, "Freq (Hz)"; TAB(15); "#pulses"
    PRINT #10, SWFreq; TAB(15); SWPulse
ELSEIF OpType = 3 THEN
    PRINT #10, "Start F(Hz)"; TAB(15); "Stop F(Hz)"; TAB(30); "Duration"
    PRINT #10, ChirpStart; TAB(15); Chirpstop; TAB(30); ChirpDur

```

```

END IF
PRINT #10,
PRINT #10, "RECEIVE VARIABLES"
PRINT #10, "....."

```

```

PRINT #10, "Channel No"; TAB(15); "IPGain"; TAB(30); "IPsamplerate"; TAB(45); "IPSampleNo"; TAB(60);
"Pathlength(m)"
PRINT #10, IPChannelNo; TAB(15); IPGain; TAB(30); IPSampleRate; TAB(45); IPSampleNo; TAB(60); Pathlength
PRINT #10,
PRINT #10, "Processing Option"
PRINT #10, ProcessOption
IF ProcessOption = 1 THEN
  PRINT #10, "Maxtime"; TAB(15); "Mintime (s)"
  PRINT #10, MaxTime; TAB(15); MinTime
ELSEIF ProcessOption = 2 THEN
  PRINT #10, "Threshold Level"
  PRINT #10, Threshlev
END IF
PRINT #10,
PRINT #10, "....."
PRINT #10, "          DATA TRACES"
PRINT #10, "....."
PRINT #10, "Max corr"; TAB(15); "Flight t (ms)"; TAB(30); "Temperature (K)"
PRINT #10, MaxCor; TAB(15); FlightTime; TAB(30); Temperature
PRINT #10,
IF IPSampleNo > OPSampleNo THEN
  Maxval = IPSampleNo
ELSE
  Maxval = OPSampleNo
END IF

PRINT #10, "Transmitted data"; TAB(20); "Received data"; TAB(40);
IF ProcessOption = 2 THEN
  PRINT #10, "Correlation"
  FOR i = 1 TO Maxval
    PRINT #10, OPData(i); TAB(20); IPData(i); TAB(40); Corr(i)
  NEXT i
ELSE
  PRINT #10,
  FOR i = 1 TO Maxval
    PRINT #10, OPData(i); TAB(20); IPData(i)
  NEXT i
END IF
CLOSE #10
END SUB

```

# PRBS Control Software: PRBS2.BAS

*(CHANGED SUBROUTINES FROM MASTER7 PROGRAM INCLUDED ONLY)*

```
*****
*****
*****
' PRBS2.BAS - PROGRAM TO SEND, RECEIVE AND PROCESS PRBS SOUND SIGNALS
' FOR AN ACOUSTIC PYROMETRY SYSTEM
' WRITTEN BY - STEPHEN IRELAND
' LAST UPDATED - AUGUST 1999
*****
*****
*****
```

' Subroutine and Function Definition

```
DECLARE SUB PRBS ()
DECLARE SUB ClearVariables ()
DECLARE SUB Correlation ()
DECLARE SUB Threshold ()
DECLARE SUB DummySetup ()
DECLARE SUB das1600init ()
DECLARE SUB refresh ()
DECLARE SUB runprogram ()
DECLARE SUB PlotData ()
DECLARE SUB DrawRunScreen ()
DECLARE SUB ReceiveSetup ()
DECLARE SUB TransmitSetup ()
DECLARE SUB ReadData ()
DECLARE SUB WriteData ()
DECLARE SUB DataCapture ()
```

' Include the datalogger files

```
$INCLUDE: 'c:\das1600\QB4DECL.BI'
$INCLUDE: 'c:\das1600\DASDECL.BI'
$INCLUDE: 'c:\das1600\DAS1600.BI'
```

' VARIABLE LIST

' Variable used by driver functions.

```
DIM SHARED nBoards AS INTEGER
DIM SHARED DErr AS INTEGER ' Error flag
DIM SHARED szCfgName AS STRING ' File name string
DIM SHARED DAS1600 AS LONG, DAS1200 AS LONG
```

' DA Frame variables

```
' REM $DYNAMIC
DIM SHARED OPData(8000) AS INTEGER
DIM SHARED OPBufa(8000) AS INTEGER
' REM $STATIC
DIM SHARED DAFrame AS LONG
DIM SHARED OPSampleRate AS LONG
DIM SHARED OPSampleNo AS LONG
DIM SHARED OPChannel AS INTEGER
DIM SHARED OLevel AS INTEGER
```

' AD Frame variables

```
DIM SHARED IPData(16000) AS INTEGER
DIM SHARED Status AS INTEGER
DIM SHARED Count AS LONG
DIM SHARED ADMemLoc AS INTEGER
DIM SHARED ADFrame AS LONG
DIM SHARED ADBuf AS LONG
DIM SHARED IPChannel AS INTEGER
DIM SHARED IPGain AS INTEGER
DIM SHARED IPSampleNo AS LONG
DIM SHARED IPSampleRate AS LONG
```

' Signal Processing Variables

```
DIM SHARED Pathlength AS SINGLE
DIM SHARED ProbeLength AS SINGLE
DIM SHARED TAmb AS SINGLE
DIM SHARED ProcessOption AS INTEGER
```

DIM SHARED ThreshLev AS INTEGER  
DIM SHARED PulseDur AS SINGLE  
DIM SHARED SWFreq AS LONG  
DIM SHARED SWPulse AS INTEGER  
DIM SHARED ChirpStart AS LONG  
DIM SHARED Chirpstop AS LONG  
DIM SHARED ChirpDur AS SINGLE  
DIM SHARED OpType AS INTEGER  
DIM SHARED Corr(8000) AS SINGLE  
DIM SHARED PRBSWindow AS INTEGER  
DIM SHARED CorrWindow AS INTEGER  
DIM SHARED CorrRange AS INTEGER  
DIM SHARED MaxCor AS SINGLE  
DIM SHARED TransmitTime AS SINGLE  
DIM SHARED MinTime AS SINGLE  
DIM SHARED MaxTime AS SINGLE  
DIM SHARED MaxCorrTime AS SINGLE  
DIM SHARED MinCorrTime AS SINGLE  
DIM SHARED Temperature AS SINGLE  
DIM SHARED LowerRange AS INTEGER  
DIM SHARED UpperRange AS INTEGER  
DIM SHARED CountMaxTP AS INTEGER  
DIM SHARED MaxCorrRatio AS SINGLE  
DIM SHARED MaxTP(100, 2) AS SINGLE  
DIM SHARED NFMCrossings AS INTEGER  
DIM SHARED StdDev AS SINGLE  
DIM SHARED Delay AS SINGLE  
DIM SHARED MeanIP AS SINGLE  
DIM SHARED MeanOP AS SINGLE  
DIM SHARED Delta AS INTEGER  
DIM SHARED denom1 AS SINGLE  
DIM SHARED denom2 AS SINGLE  
DIM SHARED numer AS SINGLE

' Plot variables

DIM SHARED xorigin AS INTEGER  
DIM SHARED yorigin AS INTEGER  
DIM SHARED xrange AS INTEGER  
DIM SHARED yrange AS INTEGER  
DIM SHARED xmax AS INTEGER  
DIM SHARED ymax AS INTEGER  
DIM SHARED xmin AS INTEGER  
DIM SHARED ymin AS INTEGER  
DIM SHARED y2data AS SINGLE  
DIM SHARED y1data AS SINGLE  
DIM SHARED x1cor AS SINGLE  
DIM SHARED x2cor AS SINGLE  
DIM SHARED MaxDelta AS SINGLE

' General Variables

DIM SHARED choice AS STRING \* 1  
DIM SHARED runtype AS STRING \* 1  
DIM SHARED hold AS STRING \* 3  
DIM SHARED logdata AS STRING \* 3  
DIM SHARED FlightTime AS SINGLE  
DIM SHARED outputfile AS STRING  
DIM SHARED InputFile AS STRING  
DIM SHARED caption AS STRING  
DIM SHARED Delt AS SINGLE  
DIM SHARED pi AS SINGLE  
DIM SHARED temp AS LONG  
DIM SHARED sample AS STRING

\*\*\*\*\*  
' DEFAULT VALUES OF CONSTANTS

pi = 4! \* ATN(1)  
IPChannel = 6  
IPGain = 0  
IPSampleNo = 16000  
IPSampleRate = 100000  
Pathlength = 3.718  
ProcessOption = 3: ThreshLev = 2200  
OPChannel = 7  
OpType = 1  
OPllevel = 200

```
xmin = 1
ymax = 4095
ymin = 0
hold = "OFF"
```

```
.....
' Configure the datalogger boards
```

```
  nBoards = 2
  szCfgName = "MASTER1.CFG" + CHR$(0)
  DErr = DAS1600DEVOPEN%(SSEGADD(szCfgName), nBoards): IF DErr <> 0 THEN PRINT DErr: STOP
  DErr = DAS1600GETDEVHANDLE%(0, DAS1600): IF DErr <> 0 THEN PRINT "getdevhandle"; DErr: STOP
  DErr = DAS1600GETDEVHANDLE%(1, DAS1200): IF DErr <> 0 THEN PRINT "getdevhandle"; DErr: STOP
```

```
  QBFarHeapSize& = SETMEM(0)
  NewFarHeapSize& = SETMEM(-QBFarHeapSize& / 2)
  PRINT " Driver's Far Heap Size: "; QBFarHeapSize& - NewFarHeapSize&
  PRINT " QB's Far Heap Size: "; NewFarHeapSize&
  PRINT
```

```
.....
SUB ClearVariables STATIC
```

```
.....
'   FOR i = 1 TO IPSampleNo
'     IPData(i) = 2047
'   NEXT i
```

```
'   FOR i = 1 TO 100
'     MaxTP(i, 1) = 0
'     MaxTP(i, 2) = 0
'   NEXT i
```

```
  CountMaxTP = 0
  MaxCorr = 0!
  MaxCorrRatio = 0!
  Temperature = 0!
```

```
END SUB
```

```
.....
SUB DataCapture STATIC
```

```
.....
  IF OpType = 1 THEN
    now = TIMER
    DErr = KDAWrite%(DAS1600, OPChannel, CLNG(2048) * 16&)
    DErr = KDMAStart%(ADFrame): IF DErr <> 0 THEN PRINT "Syncstart"; HEX$(DErr): STOP
    DO: DErr = KDMAStatus%(ADFrame, Status, Count): LOOP UNTIL Status = 0
    DErr = KMoveBufToArray%(IPData(1), ADBuf, IPSampleNo)
    DO UNTIL TIMER > now + PulseDur: LOOP
    DErr = KDAWrite%(DAS1600, OPChannel, CLNG(3071) * 16&)
```

```
  ELSE
```

```
    IF ProcessOption <> 3 THEN DErr = KSyncStart%(DAFrame): IF DErr <> 0 THEN PRINT "Syncstart", HEX$(DErr): STOP
    DErr = KDMAStart%(ADFrame): IF DErr <> 0 THEN PRINT "Syncstart"; HEX$(DErr): STOP
    DO: DErr = KDMAStatus%(ADFrame, Status, Count): LOOP UNTIL Status = 0
    DErr = KMoveBufToArray%(IPData(1), ADBuf, IPSampleNo)
```

```
  END IF
```

```
' Reorder the data to the beginning of the array
```

```
  FOR i = 1 TO IPSampleNo
    IPData(i) = IPData(i) / 16 AND &HFFF
  NEXT i
```

```
' Arrange the data into two separate arrays
```

```
  FOR i = 1 TO IPSampleNo / 2
    IPData(i) = IPData(i * 2 - 1)
    OPData(i) = IPData(i * 2)
  NEXT i
```

END SUB

```
*****  
SUB PlotData STATIC  
*****
```

'Specify the initial max scale of the graph plotter

```
xmax = IPSampleNo / 5  
xdiff = xmax - xmin  
x1 = xorigin  
y1 = yorigin + CSNG(yrange) * CSNG(IPData(xmin)) / CSNG(yrange)  
y1data = yorigin + CSNG(yrange) * CSNG(OPData(1)) / 4095!  
  
y1cor = yorigin + yrange / 2 + CSNG(yrange) * CSNG(Corr(xmin - 1)) / 2!
```

```
FOR i = 1 TO xdiff  
  x2 = xorigin + xrange * i / xdiff  
  y2 = yorigin + CSNG(yrange) * CSNG(IPData(i + xmin)) / CSNG(yrange)  
  y2data = yorigin + CSNG(yrange) * CSNG(OPData(i + 1)) / 4095!  
  LINE (x1, y1)-(x2, y2), 14  
  LINE (x1, y1data)-(x2, y2data), 3  
  IF xdiff <= 70 THEN CIRCLE (x2, y2), 2, 14: CIRCLE (x2, y2data), 2, 3
```

' PLOT AN EXTRA LINE IF THIS IS A CORRELATION

```
y2cor = yorigin + yrange / 2 + CSNG(yrange) * CSNG(Corr(i - 1 + xmin)) / 2!  
LINE (x1, y1cor)-(x2, y2cor), 15  
IF xdiff <= 70 THEN CIRCLE (x2, y2cor), 2, 15  
y1cor = y2cor
```

```
x1 = x2  
y1 = y2  
y1data = y2data  
NEXT i
```

' Cross hairs for FlightTime

```
i = FlightTime * IPSampleRate / 2  
IF i >= xmin AND i <= xmax - 1 THEN  
  x1 = xorigin + CSNG(i - xmin + 1) * CSNG(xrange) / CSNG(xdiff)  
  LINE (x1, yorigin)-(x1, yorigin + yrange), 0  
END IF
```

```
LOCATE 14, 3: PRINT USING "##.##"; 1000! * (TransmitTime + CSNG(xmin - 1) / CSNG(IPSampleRate)); : PRINT  
"ms"
```

```
LOCATE 14, 73: PRINT USING "##.##"; 1000! * (TransmitTime + CSNG(xmax - 1) / CSNG(IPSampleRate)); :  
PRINT "ms"
```

```
LOCATE 17, 55: COLOR 14: PRINT "Flight Time = ";  
PRINT USING "##.##"; 1000! * (FlightTime); : PRINT " ms ": COLOR 7  
LOCATE 18, 55: COLOR 14: PRINT "Temperature = ";  
PRINT USING "###.##"; Temperature - 273!; : PRINT " C ": COLOR 7  
LOCATE 19, 55: COLOR 14: PRINT "Max Corr = ";  
PRINT USING "#.###"; MaxCor: COLOR 7  
LOCATE 20, 55: COLOR 14: PRINT "Max Corr Ratio = ";  
PRINT USING "###"; MaxCorRatio: COLOR 7  
LOCATE 21, 55: COLOR 14: PRINT "LowerRange(l) = ";  
PRINT USING "###"; LowerRange: COLOR 7  
LOCATE 22, 55: COLOR 14: PRINT "UpperRange(l) = ";  
PRINT USING "###"; UpperRange: COLOR 7  
LOCATE 23, 55: COLOR 14: PRINT "MaxDelta(l) = ";  
PRINT USING "###"; MaxDelta: COLOR 7  
LOCATE 24, 55: COLOR 14: PRINT "CorrStart(l) = ";  
PRINT USING "###"; MinTime: COLOR 7  
LOCATE 25, 55: COLOR 14: PRINT "CorrStop(l) = ";  
PRINT USING "###"; MaxTime: COLOR 7  
LOCATE 26, 55: COLOR 14: PRINT "CorrStart(ms) = ";  
PRINT USING "###"; MinCorrTime: COLOR 7  
LOCATE 27, 55: COLOR 14: PRINT "CorrStop(ms) = ";  
PRINT USING "###"; MaxCorrTime: COLOR 7
```

' If Correlation then plot the CorrRatio line

```

' IF ProcessOption = 3 THEN
' FOR i = 1 TO CountMaxTP
'   x = MaxTP(i, 1) * IPSampleRate
'   y = MaxTP(i, 2)
'   IF x >= xmin + 1 AND x <= xmax - 3 AND y >= 1 THEN
'
'     x = xorigin + xrange * (x - xmin + 1) / xdiff
'     y = yorigin + yrange * y / MaxCorrRatio
'     CIRCLE (x, y), 3, 10
'     CIRCLE (x, y), 1, 10
'
'   END IF
' NEXT i
' END IF

```

END SUB

```

*****
SUB PRBS
*****

```

```

' ZERO THE CORRELATION ARRAY BEFORE CONTINUING
' FOR i = 1 TO IPSampleNo / 2
'   Corr(i) = 0!
' NEXT i

```

'Now set the correlation window and ranges  
'Remember to include Transmit Time in final version

```

PRBSWindow = IPSampleNo / 4
LowerRange = 0!
UpperRange = PRBSWindow - LowerRange

```

```

' Check that the correlation is feasible
' IF (LowerRange < 0) OR (UpperRange > IPSampleNo \ 2) THEN
'   LOCATE 28, 30: COLOR 4: PRINT "WARNING: Correlation impossible ": EXIT SUB
' END IF

```

```

' The input data is compared with the output, so meanop is constant
MeanIP = 0!
MeanOP = 0!
FOR i = 1 TO PRBSWindow
  MeanIP = MeanIP + CSNG(IPData(i)) / CSNG(PRBSWindow)
  MeanOP = MeanOP + CSNG(OPData(i)) / CSNG(PRBSWindow)
NEXT i

```

'MAIN CORRELATION LOOP, VARIABLE TO DEFINE SHIFT IS Delta

```

FOR Delta = MinTime TO MaxTime

```

' CALCULATE meanf2 WHICH VARIES WITH TIME SHIFT

```

IF (Delta > LowerRange) THEN
  MeanIP = MeanIP + (-IPData(Delta) + IPData(PRBSWindow + Delta)) / PRBSWindow
END IF

```

'CALULATE THE VARIOUS SUMMATIONS IN THE CORRELATION

```

denom1 = 0!
denom2 = 0!
numer = 0!

FOR i = 1 TO PRBSWindow
  numer = numer + (OPData(i) - MeanOP) * (IPData(i + Delta) - MeanIP)
  denom1 = denom1 + (OPData(i) - MeanOP) ^ 2
  denom2 = denom2 + (IPData(i + Delta) - MeanIP) ^ 2
NEXT i

```

' COMBINE THE SUMMATIONS TO CALCULATE THE CORRELATION

```

Corr(Delta) = numer / SQR(denom1 * denom2)

```

NEXT Delta

' FIND THE MAXIMUM VALUE AND REPORT IT

```
MaxCor = 0!
FOR Delta = 0 TO PRBSWindow
  IF Corr(Delta) > MaxCor THEN
    MaxCor = Corr(Delta)
    MaxDelta = Delta
    FlightTime = (MaxDelta / (IPSampleRate / 2))
  END IF
NEXT Delta
```

\*\*\*\*\*  
SUB ReceiveSetup STATIC  
\*\*\*\*\*

' INPUT SECTION

CLS

DO

```
LOCATE 3, 22: COLOR 1: PRINT "THE UNIVERSITY OF SHEFFIELD"
LOCATE 4, 22: COLOR 7: PRINT "OPTIONS FOR RECEIVED SIGNAL"
LOCATE 5, 16: PRINT "*****"
```

COLOR 4:

```
LOCATE 17, 6: PRINT "CURRENT SETUP": COLOR 2
LOCATE 18, 6: PRINT " Chan no= "; IPChannel; " Gain = "; IPGain; ""
LOCATE 19, 6: PRINT " Sampling Rate = "; IPSampleRate; " Number of samples = "; IPSampleNo
LOCATE 20, 6: PRINT " Path length = "; Pathlength
LOCATE 21, 6: PRINT " Processing option = ";
```

```
IF ProcessOption = 1 THEN
  LOCATE 21, 25: PRINT " Threshold detection"
  LOCATE 22, 2: PRINT " Threshold level = "; ThreshLev
ELSEIF ProcessOption = 2 THEN
  LOCATE 21, 25: PRINT " Cross correlation "
ELSEIF ProcessOption = 3 THEN
  LOCATE 21, 27: PRINT " PRBS Correlation  "
END IF
COLOR 7:
```

```
LOCATE 7, 6: PRINT "PLEASE INPUT YOUR CHOICE....?"
LOCATE 8, 6: PRINT "1. CHANNEL NO AND GAIN....."
LOCATE 9, 6: PRINT "2. SAMPLE SPEED AND RATE..."
LOCATE 10, 6: PRINT "3. PATH LENGTH....."
LOCATE 11, 6: PRINT "4. PROCESSING OPTION....."
LOCATE 12, 6: PRINT "5. RETURN TO MAIN MENU....."
```

choice = INKEY\$

IF choice = "1" THEN

```
LOCATE 13, 6: PRINT "INPUT THE CHANNEL NO AND GAIN  "
DO: LOCATE 14, 6: INPUT IPChannel: LOOP UNTIL IPChannel >= 0 AND IPChannel < 9
DO: LOCATE 15, 6: INPUT IPGain: LOOP UNTIL IPGain > -1 AND IPGain < 4
```

ELSEIF choice = "2" THEN

```
LOCATE 13, 6: PRINT "INPUT THE SAMPLE SPEED AND NUMBER"
PRINT
DO: LOCATE 14, 6: INPUT IPSampleRate: LOOP UNTIL IPSampleRate < 100000 OR IPSampleRate > 0
DO: LOCATE 15, 6: INPUT IPSampleNo: LOOP UNTIL IPSampleNo > 1
```

ELSEIF choice = "3" THEN

```
LOCATE 13, 6: PRINT "INPUT THE PATH LENGTH"
LOCATE 14, 6: INPUT Pathlength
```

ELSEIF choice = "4" THEN

```
LOCATE 13, 6: PRINT "INPUT THE PROCESSING OPTION"
LOCATE 14, 6: PRINT "1 = THRESHOLD, 2 = CROSS CORRELATION, 3 = PRBS Correlation"
DO: LOCATE 15, 6: INPUT ProcessOption: LOOP UNTIL ProcessOption = 1 OR ProcessOption = 2 OR ProcessOption
```

= 3

IF ProcessOption = 1 THEN

```
LOCATE 14, 6: PRINT "WHAT IS THE THRESHOLD LIMIT (1-4095)  "
DO: LOCATE 15, 6: INPUT ThreshLev: LOOP UNTIL ThreshLev > 0 AND ThreshLev < 4096
ELSEIF ProcessOption = 2 OR ProcessOption = 3 THEN
  LOCATE 14, 6: PRINT "ENTER THE EXPECTED TIME RANGE (ms) (0's for all) "
```

```

DO: LOCATE 15, 6: PRINT "          ": LOCATE 15, 2: INPUT ; MinCorrTime: INPUT ; MaxCorrTime: LOOP
UNTIL (MaxTime > MinTime OR MaxTime = 0)
  MinTime = MinCorrTime / ((1 / (IPSampleRate / 2)) * 1000)
  MaxTime = MaxCorrTime / ((1 / (IPSampleRate / 2)) * 1000)

END IF

ELSEIF choice = "5" OR choice = CHR$(27) THEN
  CLS
  EXIT SUB
END IF

LOCATE 13, 1: PRINT "          "
LOCATE 14, 1: PRINT "          "
LOCATE 15, 1: PRINT "          "
LOCATE 16, 1: PRINT "          "

LOOP

END SUB

```

## **Appendix 3**

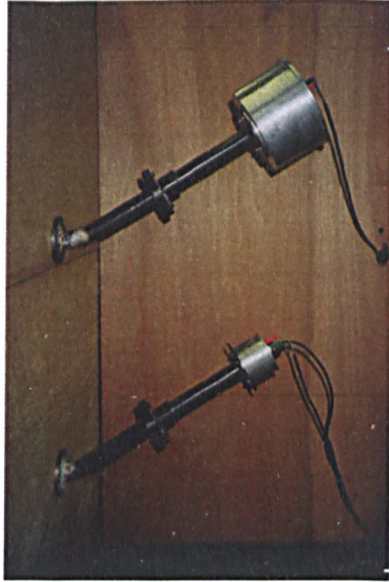


**Plate 1:** *Transmitter (top) and Receiver (bottom).*

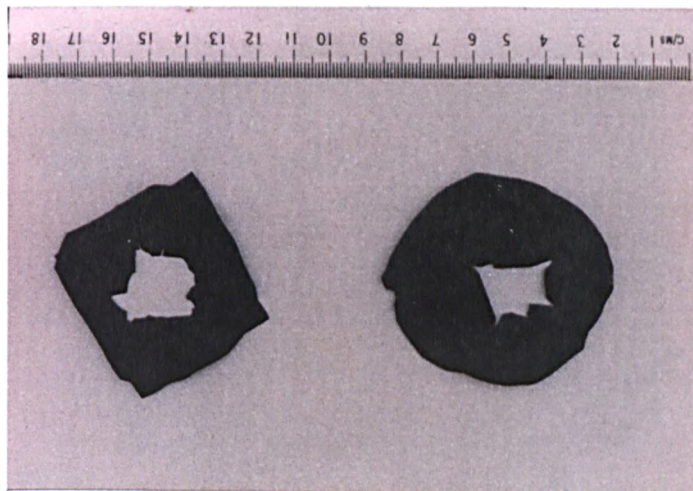


**Plate 2:** *Failed nylon nitile membranes due to direct radiation*

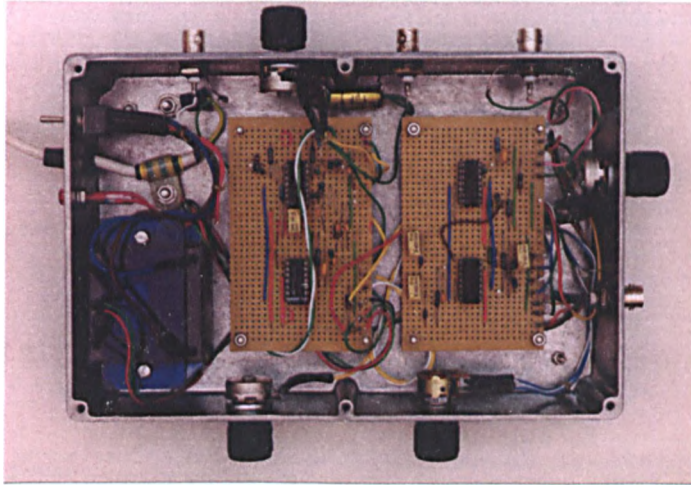


*Plate 3: Frequency Modulation Circuit c/o Kingfield Electronics*

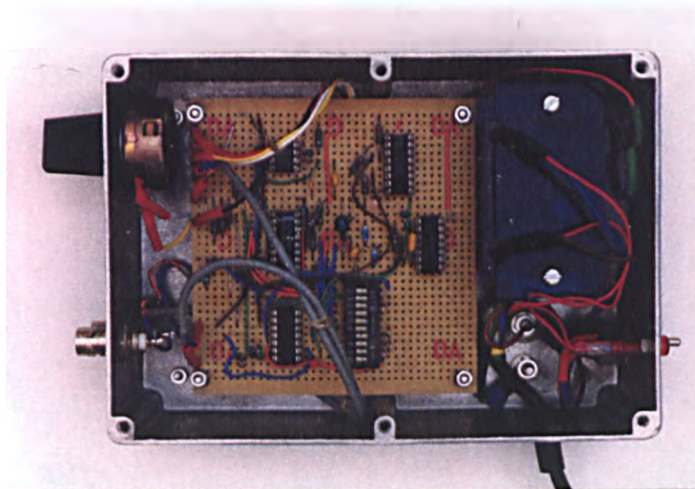


*Plate 4: PRBS Generation Circuit 1 c/o Kingfield Electronics*



*Plate 5: Control screen with in-house written software running.*



*Plate 6: Experimental fire-rig with 0.1kg/s combustion of Propane*